Mathematical modeling of the tumor-immune system interactions: equilibrium and escape phases

Kevin Kokou Atsou

UNIVERSITÉ CÔTE D'AZUR

ÉCOLE DOCTORALE
SCIENCES FONDAMENTALES ET APPLIQUÉES

THÈSE DE DOCTORAT

Modélisation mathématique des interactions tumeurs-système immunitaire: phase d'équilibre et d'échappement

Kokou Kevin ATSOU

Laboratoire Jean Alexandre Dieudonné (LJAD)

Présentée en vue de l'obtention du grade de docteur en
Mathématiques
d'Université Côte d'Azur

Dirigée par : *Thierry Goudon*

Soutenue le : 18 Décembre 2020

Devant le jury, composé de :
Véronique Braud, Dr, IPMC, UCA
Stephane Descombes, Pr, UCA
Magali Tournus, Mcf, Aix-Marseille Univ.
Magali Ribot, Pr, Univ. Orléans
Fabien Crauste, Dr, MAP5, Univ. de Paris
Marie Doumic, Dr, Inria Paris
Thierry Goudon, Dr, Inria Sophia Antipolis

canceropôle Provence-Alpes-Côte d'Azur — le propulseur régional des recherches et innovations anticancers
cnrs
Inserm — La science pour la santé / From science to health
FONDATION ARC POUR LA RECHERCHE SUR LE CANCER
RÉGION SUD PROVENCE ALPES CÔTE D'AZUR
Inria — inventeurs du monde numérique

UNIVERSITÉ CÔTE D'AZUR - UFR SCIENCES
École Doctorale de Sciences Fondamentales et Appliquées

THÈSE

pour obtenir le titre de
DOCTEUR EN SCIENCES de
l'Université Côte d'Azur

Discipline : Mathématiques

présentée et soutenue par
Kevin ATSOU

Modélisation mathématique des interactions tumeurs-système immunitaire : phase d'équilibre et d'échappement

Thèse dirigée par
Thierry Goudon
Soutenue le 18 Décembre
2020

devant le Jury composé de

Rapporteurs :		
Marie DOUMIC	HDR	Inria et Sorbonne Université
Fabien CRAUSTE	HDR	Université de Paris
Examinateurs :		
Magali TOURNUS	Maître de Conférence	Aix-Marseille Université
Magali RIBOT	Professeur	Université d'Orléans
Véronique BRAUD	HDR	Université Côte d'Azur
Stéphane DESCOMBES	Professeur	Université Côte d'Azur

Résumé : Les récents succès de l'immunothérapie pour le traitement du cancer ont mis en évidence l'importance des interactions entre les cellules tumorales et les cellules immunitaires. Cependant, ces interactions reposent sur des mécanismes extrêmement complexes, ce qui rend difficile la conception de traitements efficaces visant à renforcer la réponse immunitaire. Par conséquent, les modèles mathématiques décrivant la croissance tumorale sont nécessaires pour reproduire et prédire fidèlement la dynamique spatio-temporelle de ces interactions. Le but de cette thèse est de proposer un modèle mathématique de croissance tumorale, décrivant l'interaction de la tumeur avec les cellules immunitaires.

Pour ce faire, nous avons commencé par introduire un modèle mathématique destiné à décrire au moyen d'un système d'équations aux dérivées partielles les premières étapes des interactions entre les cellules immunitaires effectrices et les cellules tumorales. Le modèle est structuré en taille et en espace, et il prend en compte la migration des cellules effectrices cytotoxiques spécifiques de l'antigène tumoral vers le micro-environnement tumoral via un mécanisme chimiotactique. Nous avons étudié sur des bases numériques le rôle des paramètres clés du modèle tels que la division et les taux de croissance des cellules tumorales, ainsi que les taux de conversion et de mortalité des cellules immunitaires. Nos principales conclusions sont doubles. Premièrement, le modèle présente un contrôle possible de la croissance tumorale par la réponse immunitaire ; néanmoins, le contrôle n'est pas complet en ce sens que les états d'équilibre asymptotiques conservent des tumeurs résiduelles et des cellules immunitaires activées. Deuxièmement, les hétérogénéités spatiales de la source des cellules immunitaires peuvent réduire considérablement l'efficacité de la dynamique de contrôle, faisant apparaître des schémas de rémission-récurrence.

Par suite, nous avons développé des méthodes numériques pour prédire les paramètres des états d'équilibre sans exécuter des simulations du problème d'évolution. En utilisant des méthodes d'analyse de sensibilité globale, nous avons étudié le rôle des paramètres du modèle et identifié un impact prédominant du système immunitaire sur le taux de division des cellules tumorales. Nous avons montré que les meilleures stratégies thérapeutiques consistaient à augmenter la force de l'action létale des cellules immunitaires sur les cellules tumorales et le taux de conversion des cellules immunitaires naïves en cellules effectrices. Nous avons ensuite validé cette méthode à l'aide d'analyses rétrospectives expérimentales et cliniques. Ces résultats peuvent être utilisés dans le traitement du cancer pour concevoir des combinaisons thérapeutiques optimisées.

Enfin, nous avons introduit un modèle mathématique destiné à décrire la double nature de la réponse immunitaire, avec l'activation de mécanismes à la fois anti-tumoraux et pro-tumoraux. La compétition entre ces effets antagonistes conduit soit à des phases d'équilibre, soit à des phases d'échappement. Ce modèle est utilisé pour étudier l'efficacité des stratégies d'immunothérapie comparant l'effet des monothérapies à l'effet la combinaison de thérapies. Les résultats ont indiqué que la combinaison de stratégies d'immunothérapie est plus efficace pour contrôler la croissance tumorale mais le succès

du traitement est fortement conditionné par une combinaison appropriée entre la dose du traitement et le temps d'administration du traitement.

Mots clefs : Croissance tumorale. Système immunitaire. Phase d'équilibre. Phase d'évasion. Analyse de sensibilité. Stratégies d'immunothérapie.

Abstract: The recent successes of immunotherapy for the treatment of cancer has highlighted the importance of the interactions between tumor cells and immune cells. However, these interactions are based on extremely complex mechanisms, making it difficult to design an effective treatment aimed at strengthening the immune response. Therefore, the mathematical models of tumor growth are needed to faithfully reproduce and predict the spatio-temporal dynamics of tumor growth. The aim of this thesis is to propose a mathematical model for tumor growth, describing the interaction of the tumor with the immune cells.

We started by introducing a mathematical model intended to describe by means of a system of partial differential equations the earliest stages of the interactions between effector immune cells and tumor cells. The model is structured in size and space, and it takes into account the migration of the tumor antigen-specific cytotoxic effector cells towards the tumor micro-environment by a chemotactic mechanism. We investigated on numerical grounds the role of the key parameters of the model such as the division and growth rates of the tumor cells, and the conversion and death rates of the immune cells. Our main findings were two-fold. Firstly, the model exhibits a possible control of the tumor growth by the immune response; nevertheless, the control is not complete in the sense that the asymptotic equilibrium states keep residual tumors and activated immune cells. Secondly, space heterogeneities of the source of immune cells can significantly reduce the efficiency of the control dynamics, making patterns of remission-recurrence appear.

Next, we developed numerical methods to predict the parameters of the equilibrium states without running simulations of the evolution problem. By using global sensitivity analysis methods, we investigated the role of the parameters of the model and identified a predominant impact of the immune system over division rate of tumor cells. We showed that the best therapeutic strategies were to increase the strength of the lethal action of immune cells on tumor cells and the conversion rate of naive immune cells into effector cells. We then validated this method using retrospective experimental and clinical analyses. These findings can be used in cancer treatments to design optimized therapy combinations.

Finally, we introduced a mathematical model intended to describe the dual nature of the immune response, with the activation of both anti-tumor and pro-tumor mechanisms. The competition between these antagonistic effects leads to either equilibrium or escape phases. This model is used to investigate the efficacy of immotherapy strategies comparing the effect of monotherapies to the effect of combination of therapies. The findings indicated that combination of immunotherapy strategies are more efficient in controling tumor growth but the success of the treatment is strongly conditionned by the administrated dose and the time of the treatment administration.

Key words: Tumor growth. Immune system. Equilibrium phase. Escape phase. Sensitivity analysis. Immunotherapy strategies.

Remerciements

Mes pensées vont premièrement à mon directeur de thèse, Thierry Goudon. Je voudrais sincèrement te remercier de m'avoir donné cette opportunité, de m'avoir montré le chemin à suivre, de m'avoir supporté, d'avoir dirigé mes premiers pas dans l'univers de la recherche en mathématiques appliquées et de m'avoir accompagné de tes conseils jusqu'à la fin de ma thèse. J'ai énormément appris en travaillant sous ta direction. Tu as toujours su trouver les bons mots pour me guider sur la bonne voie et tu as toujours été patient vis-à-vis de ma propension au travail solitaire. Dans les moments difficiles, tu as toujours été là pour m'encourager. Merci pour tout. Merci aussi à Véronique. Je te remercie d'avoir accepté de faire partie de mon jury. Ce fut un très grand plaisir de collaborer avec toi. Nos nombreux échanges sur le volet biologique de ma thèse et ton enthousiasme (notamment sur le "papier de la mort qui tue") ont toujours attisé ma motivation.

Je suis également reconnaissant envers Fabien Crauste et Marie Doumic pour voir accepté d'être les rapporteurs de ma thèse. Je vous remercie pour votre lecture minutieuse de mon manuscrit et pour vos remarques très constructives. Je remercie aussi Stephane Descombes, Magali Tournus et Magali Ribot d'avoir accepté de prendre part au jury de cette thèse.

Le travail de recherche est parsemé de moments de doute et d'incertitude. Ce cheminement est comparable à un voyage solitaire en bateau. Quand la mer se déchaîne et qu'il n'y a personne à l'horizon, ce qui te permet de tenir, c'est le soutien de ceux qui ont toujours cru en toi. Ce travail est aussi le fruit du soutien inconditionnel de mon père durant tout mon cursus scolaire (paix à son âme). Papa, j'aurais vraiment aimé partager ma joie avec toi en ce jour. Merci à ma mère, merci de n'avoir jamais cessé de me remplir de force et de courage par tes encouragements et tes prières. Mes remerciements vont également à mes soeurs Déla, Anita et à mon beau-frère Gilles pour son aide et son soutien indéniable depuis mon arrivée en France. Je suis aussi très reconnaissant envers mes amis Elaud et Ornella (les Antibois) qui m'ont toujours soutenu. Merci à Elaud pour les visites guidées à Antibes, les bons plats et pour les pubs sur le "traitement anti-cancer" que "je suis censé créer" et merci à Nella pour tes messages d'encouragement et ton soutien.

J'ai passé trois magnifiques années de thèse au laboratoire. Pour cela, je tiens tout d'abord à remercier le personnel du labo qui a contribué de façon significative au bon déroulement de cette thèse. Merci Jean-Marc et Roland pour votre sollicitude. Merci aussi à Anita, Chiara et à Marie-Cécile pour votre diligence et votre patience. Je remercie également Maxime Ingremeau avec qui j'ai pu effectuer quelques séances de discussions et de travaux très enrichissants. J'adresse aussi mes sincères remerciements à mes collègues de bureau : Léo, Hadrien et Biao. Merci Léo, j'ai été très chanceux de t'avoir eu comme co-bureau et frère de thèse. J'ai une très grande admiration pour ta capacité d'analyse et de concentration. Travailler avec toi a été un vrai régal et les moments que nous avons passés ensemble à lire des papiers et à discuter de divers sujets mathématiques m'ont énormément édifiés. Je te souhaite vraiment le meilleur pour la suite de ta carrière de chercheur. Ne change jamais. Merci à toi, Mehdi pour nos discussions, pour ces moments d'échange entre passionnés de mangas, pour nos discussions cinéma, pour nos soirées jeu vidéo et pour les livres que tu m'as refilés, je te promets d'en faire bon usage. Merci Hadrien pour les soirées Mariokart, un jour, je viendrai prendre des cours particuliers.

Un grand merci à tous les doctorants et post-doctorants que j'ai rencontrés durant mon passage au labo. Merci Gaëtan, organiser le séminaire des doctorants avec toi a été très passionnant. Ton sens de l'organisation et ta passion pour les mathématiques m'ont toujours impressionné et je pense que tu as une très belle carrière de chercheur devant toi. Merci Afeintou pour tes conseils et ta bonne humeur toujours contagieuse. Merci Giulia L. pour ton aide et tes conseils et à Victor M. pour tous les moments de mots croisés et pour avoir si bien organisé le séminaire des doctorants. Un grand merci à Julie L. (pour tous tes conseils sur les formalités administratives), Haroune, Billel, Yash, Jonathan, Giulia M., Eliot, Marco, Joubine, Cécile, Samira, Laurence, Reine, Brett, Dahmane, Zakaria, Bochra, Maxime P., Ali, Bochra, Najwa, Nahla, Alekos. Merci à tous pour les moments inoubliables que nous avons passés ensemble.

Enfin, je ne te remercierai jamais assez Johanna. Mon amour, merci pour ton soutien, ton aide et pour m'avoir supporté durant toute cette thèse. Merci infiniment pour tes encouragements dans cette dernière ligne droite et merci pour les pauses forcées que tu m'obligeais à prendre. Je suis très chanceux et heureux de t'avoir à mes côtés.

Table des matières

Table des figures

Liste des tableaux

Première partie

Modélisation mathématique des interactions tumeurs-système immunitaire : phase d'équilibre et d'échappement

There are two possible outcomes : if the result confirms the hypothesis, then you've made a measurement. If the result is contrary to the hypothesis, then you've made a discovery

Enrico Fermi

The first lesson is what questions to ask.

Robert Jordan, Knife of Dreams.

CHAPITRE. 1

Introduction générale

Contents

Malgré l'évolution technologique et les avancées majeures dans la recherche contre les cancers, force est de constater que ce fléau reste toujours persistant. Les cancers demeurent de nos jours la première cause de mortalité chez l'homme et la deuxième chez la femme [1]. Toutefois, la découverte et la compréhension du rôle du système immunitaire dans la lutte contre les néoplasmes donne une lueur d'espoir. En effet, il ressort de plusieurs études cliniques et expérimentales ([27, 34, 65, 82, 86]) que le système immunitaire joue un role primordial et critique dans la prévention et l'éradication des tumeurs. L'argument de base repose sur le fait que la croissance tumorale est la conséquence de diverses mutations génétiques et épigénétiques qui confèrent à la tumeur des antigènes [2] non seulement identifiables par les cellules du système immunitaire mais aussi capables de déclencher une réponse immunitaire effective. Cette découverte sous-entend alors que les tumeurs observables cliniquement, et bien souvent agressives, sont celles qui ont échappé au contrôle du système immunitaire. Cette assertion est parfaitement corroborée par cette citation de M. Burtnet dans [14] : *It is by no means inconceivable that small accumulation of tumor cells may develop and because of their possession of new antigenic potentialities provoke an effective immunological reaction with regression of the tumor and no clinical hint of its existence* [3].

Cependant, les interactions entre les cellules du système immunitaire et les cellules tumorales reposent sur des mécanismes extrêmement complexes. Brièvement, dans une réponse immunitaire anti-tumorale efficace, les néo-antigènes exprimés par la tumeur sont capturés par les cellules présentatrices d'antigène (APC) telles que les cellules dendritiques (DC) qui activent les lymphocytes T naïfs dans les organes lymphoïdes secondaires drainant le site tumoral. En conséquence, les lymphocytes T $CD8^+$ effecteurs activés et proliférants migrent vers le micro-environnement tumoral où elles pourront éliminer les tumeurs. Cette boucle est connue sous le nom de *cycle immunitaire anti-tumoral*, voir [16]. Néanmoins, ce cycle est soumis à de nombreux obstacles. De manière succincte, les antigènes tumoraux peuvent être traités comme des auto-antigènes et conduire à l'amorçage d'une réponse immunosuppressive faisant intervenir des cellules protumorales capables d'inhiber les réponses immunitaires effectrices [81]. Aussi, les cellules tumorales peuvent produire des cytokines inhibitrices telles que IL-10 ou IL-4 (Interleukine 10 ou Interleukine 4) qui diminuent l'inflammation dans le microenvironnement tumoral et qui conduisent à des lymphocytes T anergiques et tolérants [43, 68]. Les tumeurs expriment également des protéines telles que PD-L1 qui peuvent se lier aux récepteurs PD-1 sur des lymphocytes T activés, inhibant ainsi leur activité cytotoxique [44].

Ces interactions se traduisent par trois phases distinctes englobées dans le concept

1. santé publique France.
2. Molécules capables de déclencher une réponse immunitaire
3. *Il n'est en aucun cas inconcevable qu'une petite accumulation de cellules tumorales puisse se développer et, en raison de leur possession de nouvelles potentialités antigéniques, provoquer une réaction immunologique efficace avec régression de la tumeur et aucun indice clinique de son existence.*

d'*immunoédition* du cancer (mise en évidence par les travaux de G. P. Dunn et al. dans [27] et [28]) : l'*élimination*, où le système immunitaire est capable de détecter et d'éradiquer purement et simplement les cellules tumorales qui ne peuvent donc pas proliférer, l'*équilibre*, où le système immunitaire est capable de maintenir l'expansion de la tumeur dans un état dormant et persistant et l'*échappement*, où les mécanismes protumoraux prennent le dessus et conduisent la tumeur à se développer de manière incontrôlée (voir Fig. 1.1).

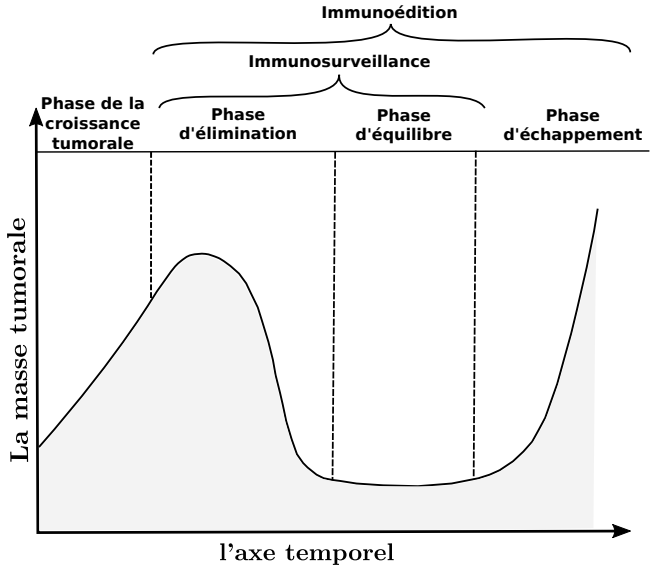

FIGURE 1.1 – illustration des phases de l'immunoédition

Une grande partie des phénomènes biologiques sous-jacents à ces interactions reste encore de nos jours incomprise. Et les causes de cette incompréhension sont diverses. Une première cause réside dans son caractère multiéchelle, par exemple elle fait intervenir diverses molécules, protéines et récepteurs qui réagissent à des échelles extrèmement petites comparées à l'échelle de taille des cellules tumorales et l'échelle spatiale de déplacement des cellules du système immunitaire. Une deuxième cause notable réside dans la difficulté d'acquisition de données due à diverses limitations techniques et expérimentales. En l'occurrence, dans le secteur de l'imagerie médicale, les scanners modernes de type PET ont une résolution limitée qui ne permet de détecter que des tumeurs de diamètre plus grands que $7\ mm$ [30]. Nous verrons dans cette thèse que la taille des tumeurs sous contrôle du système immunitaire peut être bien inférieure à ce seuil de détection. Aussi les tumeurs détectables au delà de cette taille sont probablement déjà dans une phase d'échappement.

Pour pallier ces problèmes, il est important de concevoir des modèles mathématiques capables de décrire et de synthétiser ces phénomènes complexes afin de procéder à

des expérimentations numériques (dites in silico). Les plus-values de la modélisation mathématique et des simulations informatiques résident en leur reproductibilité et en leur flexibilité. D'une part, leur reproductibilité permet de reproduire diverses expériences de façon non onéreuse et d'autre part, leur flexibilité nous permet d'ajouter à souhait divers phénomènes biologiques afin de décrire des mécanismes de plus en plus complexes ou de faire varier des paramètres méconnus. Cette dernière qualité nous permettra, dans cette thèse, de décrire des mécanismes de plus en plus riches et d'analyser non seulement la dualité de la réponse immunitaire (anti-)tumorale mais aussi les stratégies de traitement basées sur l'immunothérapie.

Somme toute, l'objectif de cette thèse est de proposer un modèle mathématique permettant de décrire la croissance tumorale tout en tenant compte de son interaction avec les cellules du système immunitaire. La particularité de notre approche peut se décliner en deux points. Tout d'abord, nous considérons la tumeur comme un amas de cellules structurées par leur taille et caractérisées par leur propension à une prolifération incontrôlée. Ainsi, sans réponse immunitaire, le modèle conduit à une croissance exponentielle de la tumeur. Puis nous incorporons une dimension spatiale décrivant l'évolution et le déplacement des différentes populations de cellules du système immunitaire spécifiques à l'antigène tumoral. Par conséquent, la taille des cellules tumorales étant infiniment petite comparée à l'échelle de déplacement des cellules du système immunitaire, les modèles que nous avons construits au cours de cette thèse s'inscrivent dans la gamme des modèles multiéchelles.

Dans ce manuscrit, nous reprenons des articles publiés ou des projets soumis pour publication. Ils peuvent être lus indépendamment, même si une progression logique motive l'ordre de la présentation. Cette raison explique aussi certaines répétitions, notamment dans les introductions de chaque chapitre. Le chapitre 2 a été publié dans *Journal of Theoretical Biology* (voir [3]), le chapitre 3 est soumis dans une revue spécialisée en oncologie, le chapitre 4 est soumis pour publication dans une revue de mathématiques appliquéees à la biologie. Ces travaux ont été rythmés par une forte collaboration avec des biologistes de l'Institut de Pharmacologie Moléculaire et Cellulaire (I.P.M.C), en l'occurrence V. Braud et F. Anjuère. Les chapitres 5 et 6 sont issus de projets CEMRACS (Centre d'Été Mathématique de Recherche Avancée en Calcul Scientifique), le premier avec L. Almeida [4], M. Marulli [5], D. Peurichard [6] et R. Tesson [7] a été publié dans *ESAIM procs* (voir [2]) et le second avec B. Al-Taki [8], J. J. Casanova [9], T. Goudon [10], F.

4. Sorbonne Université, CNRS, Lab. Jacques-Louis-Lions, 4 place Jussieu, 75005, Paris, France
5. LAGA, UMR 7539, CNRS, Université Paris 13, France, University of Bologna, Italy
6. Sorbonne Université, Inria, Mamba, Lab. Jacques-Louis Lions, 4 place Jussieu, 75005, Paris, France
7. Université Paris-saclay, CMLA, UMR 8536, CNRS, Paris, France
8. B.I.C.M.R, Peking University, Beijing, China
9. Ceremade, Université Paris Dauphine, PSL, CNRS
10. Université Côte d'Azur, Inria, CNRS, LJAD

Lagoutière [11], P. Lafitte [12], S. Minjeaud [10] a été soumis dans *ESAIM procs*

La complexité inhérente non seulement à l'interaction entre les tumeurs et le système immunitaire mais aussi à la modélisation mathématique de ce phénomène nous impose une définition claire du cadre biologique sous-jacent. Ainsi, dans ce chapitre, une première partie sera consacrée à la description du contexte biologique. Pour ce faire, après avoir posé les bases nécessaires à la compréhension du système immunitaire, nous décrirons les mécanismes régissant la croissance tumorale puis nous détaillerons son interaction avec les cellules du système immunitaire. Dans une deuxième partie, nous ferons un panorama des modèles existant dans la littérature puis finalement une troisième partie sera consacrée aux apports de la thèse.

1.1 Le contexte biologique

Les modèles mathématiques que nous avons développés au cours de cette thèse s'inscrivent dans le cadre biologique des *tumeurs solides* et du *cycle immunitaire tumoral*. Dans l'optique de comprendre ce cycle, nous allons tout d'abord introduire brièvement les propriétés générales des cellules cancéreuses, propriétés qui nous serviront plus tard de bases pour la modélisation de la croissance tumorale (voir les hypothèses retenues au Chap. 2, notamment les hypothèses **A.3**, **A.4** et la Partie 2.2.2). Dans un second temps, nous parlerons brièvement du cycle cellulaire anti-tumoral, puis, finalement nous détaillerons quelques mécanismes d'évasion souvent amorcés par la tumeur pour échapper au contrôle du système immunitaire.

1.1.1 La genèse des cellules cancéreuses

Le cycle cellulaire normal (des eucaryotes) est rythmé par plusieurs phases importantes qui se suivent de façon séquentielle. Ces phases sont généralement subdivisées en quatre, il s'agit dans l'ordre des phases G_1, S, G_2 puis M. Les phases les plus fondamentales du cycle sont les phases S et M. Au cours de la phase S dite de Synthèse, la cellule procède à la replication de l'ADN puis au cours de la phase M dite de Mitose, elle se divise en deux cellules filles identiques. Les phases G_1 et G_2 sont des phases de préparation, elles désignent des phases intermédiaires [13] au cours desquelles la cellule procède à sa croissance et se prépare à la phase suivante. Par conséquent, au cours de la phase G_1 la cellule se prépare à la réplication d'ADN puis au cours de la phase G_2, la cellule se met dans les bonnes conditions pour entamer la phase de division cellulaire. Toute cellule possède un certain nombre de points de contrôle permettant d'assurer le bon

11. Institut Camille Jordan, Université Claude Bernard, Lyon
12. CentraleSupelec, Labo. MICS
13. Gap en anglais

déroulement du cycle cellulaire. En effet, il existe deux types de systèmes de contrôle au sein d'une cellule,

— les systèmes en charge de la promotion de la croissance cellulaire, en d'autres termes, de la prolifération cellulaire,

— et, les systèmes protègeant contre la croissance cellulaire « erronée ».

Ces deux systèmes travaillent en symbiose afin d'assurer un bon équilibre non seulement dans le processus de morphogenèse des tissus mais aussi dans le processus de renouvellement des cellules. Toutefois, il arrive que des cellules prolifèrent de façon incontrollée due à l'altération de certains gènes, dit «proto-oncogènes». Ainsi, Durant le cycle cellulaire, une cellule doit résoudre un certain nombre de défis critiques. Succinctement, avant toute division cellulaire (phase M), elle met en oeuvre des mécanismes permettant de lire, d'éditer et de corriger l'ADN nouvellement synthétisé. En cas de défaillance dans la réparation de l'ADN, un autre système de contrôle se charge d'arrêter la prolifération de la cellule et dans des cas plus sévères d'enclencher un processus de mort cellulaire dit d'apoptose. Ce dernier point de contrôle s'avère très important et est régi par des gènes appelés « gènes suppresseurs de tumeur». Un des gènes suppresseur de tumeur le plus connu est le gène *p53*, les mutations altérants ce dernier étant à l'origine de la plupart des tumeurs humaines ([46, 66]).

L'apparition d'une cellule cancéreuse est, somme toute, le résultat de diverses mutations génétiques touchant non seulement les proto-oncogènes mais aussi les gènes suppresseurs de tumeur. Plus précisément, une cellule cancéreuse est une cellule qui prolifère de façon incontrolée et qui ne cesse d'accumuler diverses mutations génétiques (voir [88]).

Dans notre travail nous nous sommes limités à la description du phénomène de prolifération incontrolée. Pour ce faire, nous avons dégagé deux caractéristiques essentielles de la croissance d'une cellule tumorale. En l'occurrence, la croissance naturelle en taille de chaque cellule et le mécanisme de division des cellules tumorales matures en cellules filles identiques (voir Sect. 2.2.2). Le modèle mathématique est structuré en taille, plus particulièrement, l'état d'une cellule tumorale est entièrement caractérisé par sa taille ou de façon équivalente, par son volume ou par sa masse (voir Chap. 2, **A.3**, **A.4**). Non seulement cette caractérisation est pratique pour guider l'intuition, mais elle est aussi flexible. C'est-à-dire libre à d'autres interprétations. Notamment, une structuration des cellules par la quantité de complexes cyclines qu'elles contiennent conduirait aux mêmes équations, voir [7, 8]. Notons cependant que le phénotype des cellules tumorales peut s'étendre à plusieurs autres facteurs ou degrés de liberté, à savoir : le taux de mutation, l'âge, l'accès aux nutriments, etc. Toutefois, incorporer plus de paramètres soulèverait également le problème de l'accès à ceux-ci. L'accès aux données étant aussi très limité, il est fort probable que le problème d'estimation des paramètres soit mal posé diminuant ainsi la précision et la capacité prédictive du modèle. Cette difficulté doit être gardée à l'esprit pour proposer

une modélisation efficace. En particulier il convient d'hiérarchiser les phénomènes biologiques, d'accepter d'en négliger certains et d'être en mesure de mettre en oeuvre des méthodes d'identification de paramètres à partir de mesures indirectes.

Les questions que nous pouvons nous poser à ce stade sont les suivantes : les diverses mutations génétiques que subissent les cellules tumorales confèrent-elles à ces dernières le statut de "cellule étrangère" capable de déclencher une réponse immunitaire ? Si réponse immunitaire il y a, est-elle efficace pour contrôler la croissance tumorale ? Si cette réponse immunitaire est inefficace, pourrions-nous la modifier pour la rendre plus efficace ? Dans les parties qui vont suivre, nous allons répondre à ces questions.

1.1.2 L'immunoédition des cellules cancéreuses

La théorie de l'immunosurveillance, initialement proposée par M. Burnet et L. Thomas dans la seconde moitié du XXème siècle stipule que le système immunitaire possède les moyens nécessaires pour reconnaître, contrôler et éradiquer les néoplasmes (voir [31, 32]). Diverses expériences in vivo ont en effet corroboré cette théorie (nous pouvons citer à titre d'exemple [87, 58, 83, 84, 93, 39]) en prouvant que les souris immunodéprimées ont plus de chance de développer une tumeur que les souris normales. Le premier modèle que nous avons développé au cours de cette thèse (voir chap. 2 et 3) décrit bien la phase d'équilibre prédite par Dunn et al. dans [27]. Plus précisement, le modèle présente un contrôle de la croissance tumorale par la réponse immunitaire ; cependant, le contrôle n'est pas complet dans le sens où les états d'équilibre asymptotiques contiennent des cellules tumorales résiduelles et des cellules du système immunitaire activées (Nous renvoyons aux sec. 1.3.1 et 1.3.2 et au chap. 2 et 3 pour plus de détails).

Toutefois, l'immunosurveillance ne caractérise que les premières étapes de la croissance tumorale. La capacité du système immunitaire à fournir une défense efficace contre l'émergence des cellules cancéreuses est en réalité très limitée. En effet, le cycle immunitaire tumoral est jonché d'un grand nombre d'obstacles induits par la tumeur dans le but d'une part de désamorcer ou de désactiver la réponse immunitaire déjà établie et d'autre part d'éviter l'identification des cellules du système immunitaire. Ces obstacles favorisent à la fois l'échappement de la tumeur (voir Fig. 1.1) et la diminution de la réponse immunitaire. Dans la deuxième partie de cette thèse, nous avons enrichi notre modèle pour prendre en compte certains mécanismes d'échappement induits par la tumeur. Le modèle résultant nous a permis non seulement de reproduire la phase d'échappement caractéristique de l'immunoédition mais aussi d'analyser, sur des bases numériques, l'effet de diverses stratégies thérapeutiques qui peuvent restaurer la réponse immunitaire (Nous renvoyons aux parties 1.3.3 et 1.3.3 et au chap. 4 pour plus de détails).

Dans les parties qui vont suivre nous allons décrire (succintement) respectivement, les mécanismes qui gouvernent la surveillance immunitaire et certains mécanismes d'évasion amorcés par la tumeur pour échapper au contrôle du système immunitaire.

Le cycle immunitaire tumoral : la surveillance immunitaire

En général, la réponse immunitaire requiert la présence de molécules spécifiques appelés *antigènes*. Les antigènes, sont souvent exprimés sur des classes de molécules présentes à la surface des cellules appelées *Complexe Majeur d'Histocompatibilité* (CMH) de classe I. Ils sont, à l'origine, des fragments de protéines endogènes à la cellule témoignant des changements que cette dernière aurait subi par exemple lors d'une infection virale. Par conséquent, ils sont non seulement reconnaissables par les cellules du système immunitaire mais aussi capables d'amorcer une réponse immuntaire efficace. En effet, les mutations génétiques ayant conduit à la formation des cellules cancéreuses confèrent à ces dernières des antigènes qui sont reconnaissables par les cellules du système immunitaire (voir [92, 11, 12]).

Ainsi, pour que la réponse immunitaire anti-tumorale soit efficace, il faut qu'elle fasse intervenir les cellules du système immunitaire adaptatif. Ces dernières étant dotées d'un grand nombre de récepteurs sur leur membrane, sont capables d'amorcer une réponse immunitaire spécifique à un antigène. Plus précisément, les lymphocytes T dites Cytotoxiques (LTC ou CTL en anglais) en l'occurrence, les lymphocytes T $CD8^+$ dites cellules tueuses et $CD4^+$ dites cellules auxiliaires sont capables de reconnaître les antigènes spécifiques aux cellules cancéreuses (voir [11, 12]). Toutefois, ces derniers ont besoin d'une activation pour passer d'un état "naïf" à un état cytotoxique spécifique à l'antigène tumoral. L'éfficacité de cette réponse n'est pas immédiate car les cellules naïves sont "en réserve" dans les organes lymphoides secondaires qui peuvent être distants du site tumoral. Toutefois, il existe des cellules spécifiques du système immunitaire inné appelées Cellules Présentatrices d'Antigène (CPA), en l'ocurrence, les Cellules Dendritiques (CD) ou les macrophages, qui d'une part, circulent en permanence dans l'organisme à l'affut de cellules étrangères et d'autre part, possèdent sur leur membrane, l'arsenal qu'il faut pour activer les lymphocytes T naïfs. Ces cellules possèdent sur leur membrane, les molécules du Complexe Majeur d'Histocompatibilité (CMH) de classe II, qui leur permettent de capturer des antigènes et de les présenter aux lymphocytes T naïfs. Ils disposent aussi d'une protéine appelée B7 qui interagit avec une autre protéine située sur la membrane des lymphocytes T naïfs appelée CD28 pour une ultime stimulation nécessaire à l'activation de ces derniers.

Après l'étape d'activation, les lymphocytes T spécifiques à l'antigène tumoral prolifèrent et migrent vers le site tumoral. En effet, les cellules tumorales produisent des petites protéines solubles appelées *chimiokines* qui attirent les lymphocytes T vers le micro-environment tumoral (voir [36, 91, 42]). Ce mécanisme d'attraction appelé *chimiotaxie* est régit par la faculté des cellules possédant des récepteurs sensibles au signal chimique attractif (chimioattractant) à se déplacer suivant les directions de plus forts gradients du chimioattractant. Ce phénomène est bien compris mathématiquement et est souvent modèlisé par des systèmes d'Équations aux Dérivés Partielles (EDP) dite de chimiotaxie ou de Keller-Segel (voir [41, 47, 90, 89, 21]).

Suite à l'infiltration de la tumeur par les lymphocytes T $CD8^+$ cytotoxiques, ces derniers reconnaissent puis détruisent leurs cibles en se liant à celles ci à travers l'interaction entre des récepteurs présents sur leur membrame appelés *récepteurs de cellules* T (ou T Cell Receptor, TCR en anglais) et l'antigène (présent sur le CMH de classe I des cellules tumorales) qui a été reconnu dans l'étape d'activation. La destruction des cellules tumorales par les lymphocytes T cytotoxiques (appelée mort immunogénique) favorise la diffusion des antigènes tumoraux dans le micro-environnement tumoral augmentant ainsi la réponse immunitaire.

Notons qu'il a été mis en évidence que les cellules naturelles tueuses (NK cells en anglais), qui constituent un sous-ensemble de cellules du système immunitaire inné peuvent aussi reconnaitre et tuer les cellules tumorales (voir [60, 10, 83]). Ces cellules circulent en permanence à travers les vaisseaux sanguins et les tissus et peuvent amorcer une réponse immédiate en cas de reconnaissance des cellules tumorales. Ainsi, nous pouvons distinguer deux types de réponses immunitaires anti-tumorales : une réponse orchestrée par les cellules tueuses naturelles (NK cells) et une autre plus lente orchestrée par les lymphocytes T $CD8^+$.

Nous verrons que ces deux types de réponse immunitaire, que l'on décrira sous forme de sources homogènes ou hétérogènes en espace, ont des effets différents sur l'efficacité du contrôle de la croissance tumorale. En effet, dans le processus de modélisation mathématique, nous avons pris en compte l'hétérogénéité spatiale inhérent au déploiement de la réponse immunitaire en structurant spatialement les lymphocytes T spécifiques à l'antigène tumoral. En effet, les lymphocytes T naïfs sont décrits par un bain de cellules inactives (naïves) situées à une certaine distance du micro-environnement tumoral tandis que les cellules naturelles tueuses (NK cells) sont distribuées de façon homogène dans le microenvironnement tumoral. Par conséquent, le flux de lymphocyte T dans le microenvironnement tumoral découle du processus d'activation (orchestré par les CD) à distance des lymphocytes T naïfs. Cependant, nous avons résumé le processus de migration des cellules dendritiques vers les clusters de cellules naïves et le processus d'activation proprement dit par un taux d'activation qui dépend de la masse de la tumeur (voir la Partie. 2.2.2).

Les diverses étapes que nous venons de décrire forment une boucle appelée *cycle de l'immunité tumorale*. Toutefois, comme nous l'avons noté, ce cycle est sujet à divers obstacles.

L'échappement des cellules cancéreuses

Malgré le rôle important joué par le système immunitaire dans l'élimination de certaines tumeurs, il échoue dans la lutte contre beaucoup d'autres, principalement en raison de la mise en place de mécanismes immunosuppresseurs qui rompent l'équilibre établi lors de la phase d'immunosurveillance (voir [12, 17, 67, 71, 97]). En effet, les phases ultérieures de la croissance tumorale se déroulent sans restriction et sont

caractérisées par l'inhibition des fonctions protectrices du système immunitaire et par des effets qui favorisent le développement de la tumeur ([27, 28, 71]). Les antigènes exprimés par les cellules tumorales peuvent être vus par le système immunitaire comme des antigènes de différenciation qui sont aussi exprimés par les cellules normales (voir [71]) et par conséquent induire une tolérance des lymphocytes T. En d'autre termes la réponse immunitaire anti-tumorale peut être considérée comme une réponse auto-immune que l'organisme va devoir contrôler.

Les cellules protumorales Parmi les mécanismes engendrés par la tumeur pour échapper à l'immunosuppression, nous pouvons noter le recrutement et le basculement d'une partie des cellules du système immunitaire d'un état spécifique à l'antigène tumoral vers un état "anergique" et d'une autre partie vers des fonctions protumorales. Ce processus intervient en principe dans le mécanisme d'homéostase de la réponse immunitaire ([64]). En effet, les cellules tumorales peuvent produire des facteurs inhibiteurs (*cytokines anti-inflammatoires*) tels que l'IL-10, l'IL-4 (Interleukine 10 ou Interleukine 4) et le TGF-β (le facteur de croissance transformant - bêta ou Transforming Growth Factor-beta en anglais) qui favorisent la polarisation des cellules immunitaires anti-tumorales en cellules protumorales. Par conséquent, les neutrophiles N1 et les macrophages activés classiquement (M1), qui sont aussi connus pour leur contribution à l'immunité anti-tumorale, ainsi que les cellules T effectrices et les cellules tueuses naturelles (Natural Killer cells en anglais, NK), sont respectivement convertis en neutrophiles associés aux tumeurs (ou Tumeur Associated Neutrophils en anglais, TAN) N2 et macrophages associés aux tumeurs (Tumeur Associated Macrophages en anglais, TAM) M2 (voir [37]) qui possèdent des activités protumorales. Ils font partie d'un ensemble de cellules myéloïdes suppressives qui peuvent également être directement recrutées à partir de la moelle osseuse. De plus, les cellules dendritiques deviennent tolérogènes, ce qui conduit à des cellules T anergiques et tolérantes, en plus de l'amorçage et de la prolifération des cellules T régulatrices (Treg). Le mode opératoire des cellules protumorales repose principalement sur la suppression des cellules anti-tumorales par contact direct et la secrétion de cytokines inhibitrices. Notons que compte tenu de l'importance de cette activité protumorale, le rapport cellules immunitaires effectrices/cellules immunitaires protumorales est considéré comme un indicateur pertinent de la survie du patient (voir [80]) : plus le rapport est élevé, meilleurs sont les pronostics vitaux du patient.

Outre les mécanismes immunosuppresseurs, les cellules immunitaires à fonctions protumorales contribuent également directement à la croissance de la tumeur, notamment par leur contribution à l'angiogenèse. En effet, sous la pression de l'hypoxie, des Facteurs de Croissance Endothéliale Vasculaire (Vascular Endothelial Growth Factor, VEGF en anglais) sont sécrétés. Ces facteurs de croissance induisent à leur tour la formation de nouveau vaisseaux sanguins qui vont alimenter la tumeur.

Les points de contrôle immunitaire Les lymphocytes T activés possèdent sur leur membrane des protéines de contrôle (checkpoint) appelées CTLA-4 et PD-1, qui ont pour rôle d'empêcher une prolifération excessive de la réponse immunitaire. D'une part les protéines de contrôle CTLA-4 interragissent avec le récepteur d'activation B7 exprimé par les cellules dendritiques (voir la Partie 1.1.2) empêchant ainsi l'activation des lymphocytes T dans les organes lymphoïdes secondaires. D'autre part les cellules tumorales expriment souvent sur leur surface, un ligand appelé PD-L1 qui se lie à la protéine de contrôle PD-1 et supprime non seulement la fonction effectrice des lymphocytes T mais aussi leur capacité à proliférer.

1.1.3 L'immunothérapie

Diverses stratégies d'immunothérapie ont été développé dans l'optique de booster la réponse immunitaire anti-tumorale. Ces stratégies se basent sur la compréhension du microenvironnement tumoral et du système immunitaire. Parmi les stratégies utilisées nous pouvons distinguer les stratégies utilisant des anticorps monoclonaux et les stratégies basées sur le transfert de lymphocytes T.

Les anticorps monoclonaux les anticorps monoclonaux sont des anticorps conçus pour s'attacher à des protéines spécifiques. L'objectif des thérapies basées sur ces anticorps est de bloquer les points de contrôle immunitaire (ils sont aussi appelés *inhibiteurs de point de contrôle*). comme nous l'avons mentionné dans la Partie 1.1.2, la surexpression des protéines de controle CTLA-4 et PD-1 par les lymphocytes T de même que la surexpression des ligands PD-L1 par les cellules tumorales est un facteur favorisant considérablement la suppression de la réponse immunitaire anti-tumorale. Ainsi, les cellules effectrices ayant été en contact avec des cellules tumorales possédant des ligands PD-L1. sont inhibées et deviennent *anergiques* c'est-à-dire tolérante à la présence de la tumeur. Par conséquent, les traitements capables de bloquer les interactions PD-1 et PD-L1 sont capables de restaurer l'activité effectrice des lymphocytes T anergiques. De même, les anticorps monoclonaux capables de bloquer les interactions entre les protéines de contrôle CTLA-4 et B7 sont capables de restaurer le mécanisme de conversion des lymphocyte T dans les ganglions lymphactiques secondaires. Divers anticorps monoclonaux ont été conçu, nous pouvons citer à titre d'exemple, l'*ipilimumab* qui peut s'attacher à la protéine CTLA-4 et empêcher les liaisons CTLA-4/B7. Toutefois, les anticorps bloquant les liaisons PD-1/PD-L1 ont connu plus de succès (voir [59]) notamment en ce qui concerne le traitement du Lymphome de Hodgkin et du cancer du poumon. Cependant, en général seul 15-18% des patients atteints de cancer répondent positivement à cette thérapie.

Le transfert de lymphocytes T L'efficacité des thérapies basées sur les anticorps monoclonaux reposent sur le fait que le système immunitaire produit déjà en quantité suffisante des lymphocytes T spécifiques à l'antigène tumoral. Cependant, dans de nombreux cas de tumeurs la quantité de ces lymphocytes T est très limitée. Deux stratégies d'immunothérapie permettent de s'attaquer à ce problème, il s'agit d'une part des thérapies basées sur le *transfert cellulaire adoptive* et d'autre part des thérapies basées sur le *transfert de cellules modifiées*. Le transfert cellulaire adoptive consiste à prélever des lymphocytes T du patient ayant infilitrées la tumeur et qui sont spécifiques à l'antigène tumoral puis à les cultiver en présence d'IL-2 enfin de provoquer leur prolifération. Une fois que le nombre necessaire de lymphocyte T est atteint, les cellules cultivées sont ensuite réinjectées aux patients. Dans certains cas plus graves, il est très difficiles d'isoler des cellules spécifiques à l'antigène tumoral. Par conséquent, la thérapie basée sur le tranfert de cellules modifiées consiste à modifier génétiquement les lymphocytes T du patient de façon à ce qu'il puisse reconnaitre facilement l'antigène tumoral. L'une des thérapies basée sur le tranfert de cellules modifiées la plus connue de nos jours est celle des cellules CAR-T (voir [15])

1.2 Vue d'ensemble sur l'état de l'art

Plusieurs modèles mathématiques ont été construits dans le but de mieux comprendre les paramètres clés qui dictent l'évolution en temps des interactions entre tumeur et système immunitaire. Nous pouvons citer à titre d'exemples [85, 35, 57, 19, 51, 50, 53, 76, 22, 72, 72, 73, 23, 97, 96, 54, 55, 38, 61, 77, 1, 45]. La majorité des modèles existants est souvent basée sur des systèmes d'Équations Différentielles Ordinaires (ODE) (voir [85, 35, 57, 19, 51, 50, 53, 76, 22, 72, 73, 23, 97, 96]), toutefois une partie du travail de modélisation a aussi été consacrée à des systèmes d'Équations aux Dérivées Partielles (EDP) (voir [54, 55, 38, 61, 77, 1]) décrivant la dimension spatiale inhérente à ces interactions. La particularité des différents modèles existants se situe d'abord dans le nombre d'espèces ou de compartiments décrits puis dans le système de couplage utilisé pour décrire les différentes interactions et enfin dans la modélisation de la croissance tumorale. L'interaction avec le système immunitaire repose principalement sur des équations de type proies-prédateurs. L'objectif de cette partie est non seulement de dresser un panorama de l'état de l'art mais aussi de comprendre les principales dynamiques apparaissant dans la modélisation des interactions entre tumeur et système immunitaire. Pour ce faire, nous nous focaliserons plus sur la description des modèles homogènes en espaces (sytèmes d'ODE) existants dans la littérature.

1.2.1 Les systèmes d'Équations Différentielles Ordinaires (EDO)

Les modèles à deux espèces

Les premiers modèles conçus pour décrire les interactions tumeur-système immunitaire sont des modèles à deux espèces essentiellement motivés par la théorie de l'immunosurveillance. S'inspirant du caractère proies-prédateurs de ces interactions, ils décrivent la tumeur comme une proie dont les prédateurs sont des cellules du système immunitaire (en particulier, les lymphocytes T $CD8^+$ ou les cellules naturelles tueuses NK). Tous les modèles à deux espèces découlent du cadre général défini par d'Onofrio dans [22]. En effet, les systèmes d'EDO à deux espèces existants peuvent se réduire au système général suivant :

$$N' = Ng(N) - M_N(N, C), \tag{1.1a}$$

$$C' = \Pi_C(N, C) - M_C(N, C) - \gamma(C) + \psi_C(t) \tag{1.1b}$$

où N désigne la densité de la population de cellules tumorales et C, la densité de cellules effectrices du système immunitaire. La fonction $g(N)$ représente le taux de croissance de la tumeur, les fonctions M_N et M_C qui dépendent à la fois de C et de N représentent respectivement la mortalité des cellules tumorales et la mortalité des cellules effectrices dues à l'interaction entre les deux populations de cellules. La fonction Π_C représente le terme de croissance ou de prolifération de la population des cellules effectrices. Il dépend à la fois de la densité de la population de cellules tumorales et de la densité des cellules effectrices ; γ représente la mortalité naturelle des cellules effectrices qui peut dépendre de la densité de ces dernières et finalement ψ_C représente un apport ou un flux entrant de cellules effectrices qui dépend du temps. Il peut décrire soit l'effet d'un traitement d'immunothérapie où l'activation continue de lymphocytes T spécifiques à l'antigène tumoral. Les modèles de types proies-prédateurs sont souvent représentés sous forme de diagrammes montrant les interactions entre les divers espèces ou compartiments en jeu (voir Fig. 1.2).

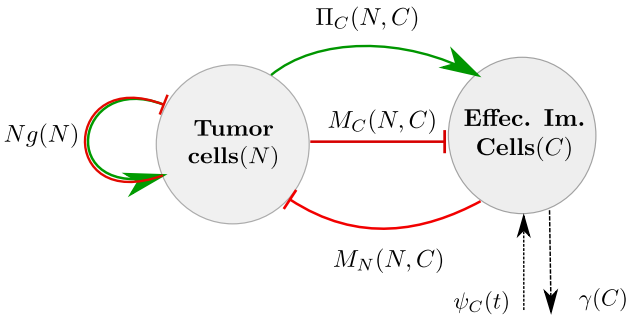

FIGURE 1.2 – modèle compartimental de l'interaction tumeur-système immunitaire

Comme exemples de modèles à deux espèces, nous pouvons citer :

Le modèle de Sotolongo-Costa et al. Dans [85], Sotolongo-Costa et al. proposent un modèle dans lequel

$$g(N) = p, \quad M_N(N, C) = qCN$$
$$\Pi_C = vNC, \quad M_C(N, C) = d_1 N, \quad \gamma(C) = d_2 C, \quad \psi_C(t) = s$$

où les constantes s, d_2, v, p, $q > 0$ et $d_1 \geq 0$ représentent respectivement, le taux constant de production des cellules du système immunitaire inné qui sont capables de reconnaître la tumeur, le taux de mortalité naturel des cellules du système immunitaire, le taux de prolifération de la réponse immunitaire dû aux antigènes tumoraux, le taux de croissance de la tumeur, le taux de mortalité de la tumeur dû à l'interaction avec le système immunitaire et enfin le taux de mortalité naturel des cellules du système immunitaire.

En étudiant analytiquement la stabilité linéaire du modèle, les auteurs ont pu explorer les valeurs de paramètre qui impactent l'équilibre du système. Ils ont pu ainsi identifier divers comportements clés en ce qui concerne la croissance tumorale et l'état d'équilibre résultant des interactions entre la tumeur et le système immunitaire. De façon succinte, deux configurations se dégagent de leurs analyses :

1. soit la masse tumorale évolue en oscillant vers un état incontrôlable,
2. soit les oscillations de la masse tumorale sont amorties et le système tend vers un équilibre où la tumeur est soit maintenue dans un état dormant, soit complètement éradiquée. Dans les deux cas il reste des résidus de cellules immunitaires à l'équilibre.

Le modèle de Forys et al. Dans [35] Forys et al. proposent un modèle qui décrit les mêmes dynamiques que [85] à l'exception du terme de prolifération de la réponse immunitaire et du terme de mortalité des cellules du système immunitaire dû à leur interaction avec la tumeur. En l'occurrence,

$$\Pi_C = vF(C, N)C, \quad M_C(N, C) = d_1 CN,$$

où deux exemples de fonctionnelles F sont étudiés, à savoir :

$$F_a(C, N) = \frac{(N/C)^\beta}{u^\beta + (N/C)^\beta},$$

$$F_b(C, N) = \frac{C^\beta}{w^\beta + C^\beta},$$

avec $u, v > 0$ et $\beta \geq 1$. Les fonctionnelles F_a et F_b représentent la fraction des cellules du système immunitaire qui ont été activé par les antigènes tumoraux. Pour $\beta = 1$, vF_b représente la fonctionnelle de Michaelis-Menten. Dans le cas général, où

$0 < \beta \leq 1$, F_a et F_b modélisent une certaine saturation dans la prolifération des cellules du système immunitaire spécifiques à l'antigène tumoral. Dans leurs analyses du modèle, les auteurs ont utilisé le critère de Dulac pour montrer que le système d'équations n'admet pas d'orbite fermé, autrement dit, il n'admet pas de solution périodique. Toutefois, il admet divers états d'équilibres localement ou globalement stables selon la valeur de certains paramètres. En l'occurrence, si le mécanisme immunosuppresseur est inexistant ($d_1 = 0$) et que la source de cellule du système immunitaire inné (s) est relativement faible ($s < d_2$), alors il existe un équilibre globalement stable qui contient des résidus de cellules tumorales et de cellules du système immunitaire. Par contre, si les mécanismes immunosuppresseurs sont actifs ($d_1 > 0$), deux cas se présentent : (1) si la réponse immunitaire innée est relativement faible ($s < d_2$), soit le système n'admet pas d'équilibre et dans ce cas la masse tumorale explose, soit il admet deux points d'équilibre dont un est stable. (2) Si la réponse immunitaire innée est relativement forte ($s > d_2$), soit la tumeur échappe au contrôle du système immunitaire et le système n'admet pas d'équilibre, soit il admet trois points d'équilibre dont un seul est stable, les autres étant des point-selles. Les auteurs ont aussi noté que le choix de la fonctionnelle (F_a, F_b) n'impacte pas la dynamique asymptotique.

ils indiquent en se basant sur les états d'équilibre que les paramètres les plus importants en ce qui concerne les traitements d'immunothérapie sont d'une part le taux de croissance tumorale p de la tumeur et d'autre part le flux entrant de cellule du système immunitaire, s.

En utilisant des données in vivo, et en estimant l'état d'équilibre de notre modèle, nous verrons plus tard dans cette thèse (voir chapitre 3), que ces paramètres font effectivement partie des paramètres les plus importants. Toutefois, nous allons plus loin dans notre analyse en indiquant d'autres paramètres et aussi les combinaisons entre paramètres les plus importants pour guider les stratégies d'immunothérapie.

En raison de leur simplicité conceptuelle, les modèles à deux espèces disposent d'un large éventail de méthodes mathématiques rendant relativement accessible leur analyse. Même, s'ils sont aussi capables de reproduire certains phénomènes biologiques qui caractérisent les interactions entre tumeur et système immunitaire, leur capacité à expliquer des phénomènes plus riches reste limitée.

Les modèles à trois espèces

En dehors des modèles à deux espèces, les modèles à plusieurs espèces permettent de décrire des phénomènes biologiques plus riches. On peut citer par exemple :

le modèle de Kirschner-Panetta Dans [51], D. Kirschner et J. C. Panetta ont conçu un modèle à trois espèces dans le but d'étudier non seulement le rôle des cytokines (en l'occurrence l'IL-2) dans la dynamique des interactions entre les tumeurs et le système immunitaire mais aussi de comprendre l'origine des oscillations de la masse tumorale à

court terme. Les interactions typiques du modèle sont illustrées dans la figure 1.3 et le modèle prend la forme générale suivante :

$$N' = Ng(N) - M_N(N, C, I), \tag{1.2a}$$

$$C' = \Pi_C^{(1)}(N, C) - M_C(N, C, I) - \gamma(C) + \Pi_C^{(2)}(N, C, I) + \psi_C(t), \tag{1.2b}$$

$$I' = \Pi_I^{(3)}(N, C, I) - \gamma_I(I) + \psi_I(t), \tag{1.2c}$$

où la croissance tumorale est modélisée par une fonction logistique, $g(N) = r(1 - \frac{N}{K})$, avec r le taux de croissance intrinsèque de la tumeur et K la taille maximale de la tumeur (*carrying capacity* en anglais) due à un acccès limité aux nutriments. Les termes de prolifération vérifient respectivement :

$$\Pi_C^{(1)}(N, C) = \alpha_1 N, \quad \Pi_C^{(2)}(N, C, I) = \alpha_2 \frac{CI}{\beta_1 + I}, \quad \Pi_C^{(3)}(N, C, I) = \alpha_3 \frac{CN}{\beta_2 + N},$$

le terme ψ_C est constant et représente l'effet des traitements capables d'améliorer le flux entrant de cellules effectrices, puis le ψ_I aussi constant représente l'effet des traitements capables d'améliorer le flux entrant de cytokines (IL-2). Sans traitement, le modèle admet deux types d'états stationnaires, le premier qui correspond à l'état sain c'est-à-dire avec absence de tumeur et de cellules du système immunitaire est inconditionnellement localement instable, le second qui correspond à l'état non sain, c'est-à-dire qui contient des résidus de cellules issues des espèces étudiées est conditionnellement stable. En effet la stabilité de ce dernier dépend du paramètre α_1 qui réprésente l'antigénicité de la tumeur. Ce paramètre s'avère très important dans leurs analyses et détermine les transitions de phase du système. Plus précisement, en fonction de la valeur de α_1, le système présente des oscillations et aussi un cycle limite dont la période diminue quand on augmente ce dernier (nous renvoyons à [51] pour plus de détails sur ce point).

Ce paramètre d'antigénicité peut être relié au taux d'activation des cellules effectrices que nous avons introduit dans notre modèle (voir chapitre 2, Partie 2.2.2). Nous verrons que ce taux fait partie des paramètres qui influencent le plus la dynamique du système. Plus précisement, plus ce taux sera relativement petit plus le modèle présentera des oscillations et voire même un comportement que l'on peut qualifier de périodique.

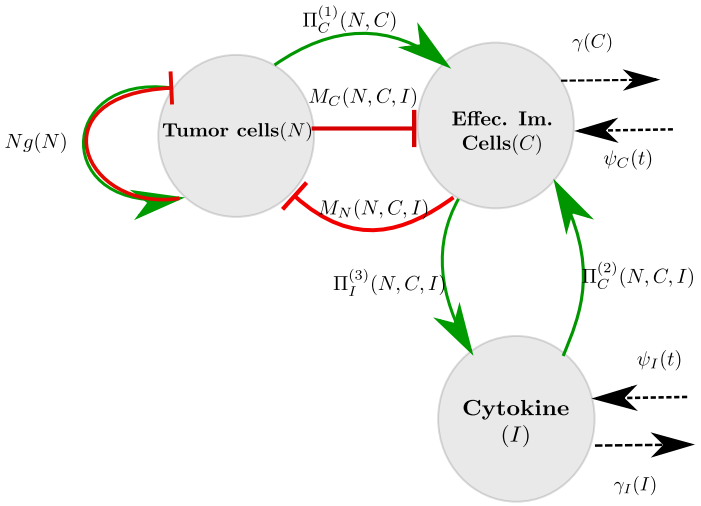

FIGURE 1.3 – modèle compartimental de l'interaction tumeur-système immunitaire-$IL-2$

L'analyse de l'effet des traitements d'immunothérapies conduit à des conclusions intéressantes mais limitées. D'une part, l'analyse de l'effet des traitements basés sur l'injection de cellules immunitaires cultivées spécifiques à l'antigène tumoral indique une meilleure efficacité de cette dernière par rapport aux traitements augmentant la concentration d'IL-2 dans le microenvironnement tumoral et d'autre part, l'analyse des thérapies combinant les deux traitements s'avère plus efficace que les monothérapies. Toutefois, ces résultats sont difficilement applicables cliniquement car l'effet des divers traitements est supposé constant dans le temps. Dans le chapitre 4, nous analyserons les effets de diverses stratégies d'immunothérapie en étudiant des thérapies administrées de façon périodique. Nous verrons que les contraintes sur la date de début des thérapies et leurs doses ont un impact important sur l'efficacité de ces dernières.

Notons que les oscillations observées dans le modèle de Sotolongo-Costa et al. et dans le modèle de Kirschner-Panetta sont en effet prépondérantes dans la dynamique des modèles à plusieurs espèces (ou multi-compartimentaux) (voir [50, 53, 22, 23]). En outre, certains cas d'oscillations amorties ou périodiques ont été observés biologiquement, nous pouvons citer à titre d'exemple, [48, 95]. Ainsi, dans [29], les auteurs distinguent quatre comportements caractéristiques des modèles à plusieurs espèces à savoir, une croissance ou une décroissance exponentielle, et une croissance ou décroissance oscillante (voir [51]). Toutefois, certains modèles incorporant (de façon artificielle) un certain retard (τ) dans la réponse immunitaire jouissent d'une cinquième dynamique dans laquelle la densité des deux populations présente des oscillations périodiques (ou avec un taux d'amortissement très faible, voir [9, 24, 4, 75, 49]). En effet, l'introduction d'un retard dans la modélisation de la réponse immunitaire est une tentative de décrire le décalage temporel dû à l'activation distante des cellules effectrices. Nous verrons

dans le chapitre 2 de cette thèse que notre modèle non seulement reproduit bien ces oscillations mais donne aussi des explications plus naturelles sur l'origine de ces dernières. Particulièrement, lorsque la source de cellules inactives du système immunitaire est distante du micro-environnement tumoral (ou hétérogène), l'efficacité du système immunitaire est considérablement réduite et on observe des oscillations que l'on peut considérer comme périodiques sur des temps d'observation assez longs. Nous verrons aussi que les paramètres jouant sur l'aggressivité de la tumeur d'une part et l'efficacité du système immunitaire d'autre part, peuvent amplifier ces oscillations.

1.2.2 Les systèmes d'Équations aux Dérivées Partielles (EDP)

La croissance tumorale Dans des stades avancés les tumeurs présentent un aspect géométrique particulier. En l'occurrence les tumeurs solides sphéroides possèdent un noyau hypoxique dû à l'absence de nutriments dans le microenvironnement tumoral (plus accentué en leur centre) et une couche de cellules proliférantes. Divers modèles d'EDP ont été construits dans le but de décrire les divers stades ou aspects de la croissance tumorale. Par exemple les modèles inspirés de la mécanique des fluides peuvent décrire les aspects géométriques de la croissance tumorale (voir [13, 74]). Le modèle que nous décrivons dans ce manuscrit (voir (1.3a), et (2.4)) ne se place pas à cette échelle. Une alternative au modèle de croissance division que nous avons utilisé pour les cellules tumorales pourrait être le système de K. Iwata et al. [45]. Ce modèle présente un comportement asymptotique proche (voir [20, 5]).

L'interaction avec le système immunitaire Notons que l'une des limites des modèles d'EDO réside dans le fait qu'ils ne prennent pas en compte les hétérogénéités spatiales sous-jacentes aux interactions entre les tumeurs et le système immunitaire. Diverses études montrent que la capacité des cellules effectrices à se déplacer sans encombre vers la tumeur est un facteur déterminant dans la réponse immunitaire anti-tumorale (voir [79, 78, 52]). Ainsi, dans [52] par exemple les auteurs observent que la densité de la matrice extracellulaire du microenvironnement tumoral influence de manière significative le taux d'infiltration de la tumeur par les lymphocytes T $CD8^+$. En effet, la densité de la matrice extracellulaire peut modifier le taux de diffusion des cellules effectrices dans le microenvironnement tumoral et par conséquent réduire ou augmenter l'efficacité de ces dernières. Il s'agit là non seulement d'une des conclusions du chapitre 2 (Partie 2.3.1) de cette thèse mais aussi d'un des obstacles de la réponse immunitaire anti-tumorale. Notons aussi que la quantité de chimiokine (substance chimioattractante) émise par la tumeur représente un facteur déterminant (voir [94]). Divers modèles mathématiques ont été concus pour comprendre ces dynamiques. Par exemple dans [61] A. Matzavinos et al. ont utilisé un modèle de type Fisher-Kolmogorov pour modéliser la croissance tumorale qu'ils ont couplé avec un modèle de chimiotaxis pour modéliser le déplacement des lymphocytes T cytotoxiques vers le microenvironnement tumoral et un modèle décrivant

la dynamique des complexes cellule tumorale-Lymphocyte T. Nous pouvons aussi citer le modèle de X. Lai et A. Friedmann dans [55] basé sur une approche "free boundary" pour la modélisation de la croissance tumorale et sur une approche inspirée de la mécanique des fluides pour modéliser le déplacement des cellules du système immunitaire.

1.3 Apports de la thèse et perspectives

Les travaux effectués au cours de cette thèse ont suivi une évolution progressive. Les apports non seulement au niveau mathématique mais aussi au niveau biologique sont divers.

Dans un premier temps, nous avons développé un modèle mathématique destiné à décrire les premières étapes des interactions entre cellules immunitaires effectrices et cellules tumorales. Le modèle est structuré en taille et en espace, et il prend en compte la migration des cellules effectrices cytotoxiques spécifiques à l'antigène tumoral vers le micro-environnement tumoral par un mécanisme chimiotactique. Nous avons étudié sur des bases numériques le rôle des paramètres clés du modèle tels que le taux de division, le taux de croissance des cellules tumorales, ainsi que les taux de conversion et de mortalité des cellules du système immunitaires. Nos principales conclusions sont doubles. Premièrement, le modèle décrit bien les phases de l'immunosurveillance, en l'occurrence, les états d'équilibre asymptotique conservent des tumeurs résiduelles et des cellules immunitaires activées. Ce fait est remarquable dans la mesure où l'état d'équilibre n'a pas été pris en compte dans la construction du modèle. Deuxièmement, l'hétérogénéité spatiale de la source des cellules du système immunitaire peut réduire considérablement l'efficacité de la dynamique de contrôle, faisant apparaître des schémas que l'on peut interpréter comme périodiques sur des temps d'observation assez longs caractérisés par une alternance entre phases de croissance tumorale et de rémission.

Dans un second temps nous avons développé des méthodes numériques pour prédire l'état d'équilibre sans effectuer des simulations du problème d'évolution. En utilisant des méthodes d'analyse de sensibilité globale, nous avons étudié simultanément l'influence des paramètres de la réponse immunitaire et de la croissance tumorale sur la masse tumorale à l'équilibre. Cette analyse nous a permis d'identifier un impact prédominant du système immunitaire sur la taille de la tumeur à l'équilibre. Les résultats obtenus dans cette partie soutiennent non seulement l'utilisation de combinaisons de thérapies qui maintiennent et renforcent la réponse immunitaire afin de contrôler la masse tumorale mais fournissent aussi des indications en ce qui concerne la conception et l'optimisation des traitements contre le cancer.

Dans un troisième temps nous avons enrichi le premier modèle en décrivant en plus des cellules effectrices, le processus d'activation des cellules protumorales. Le modèle résultant décrit bien les phases de l'immunoédition (voir Fig. 1.1). en l'occurrence, les effets antagonistes entre cellules protumorales et cellules effectrices conduisent soit à un

équilibre, soit à l'échappement de la tumeur.

Finalement, nous avons étudié sur des bases numériques l'effet de diverses stratégies thérapeutiques qui peuvent soit restaurer le rôle effecteur des cellules anergiques anti-tumorales, soit limiter les activités protumorales. L'étude démontre l'intérêt de combiner les deux approches comme stratégie d'immunothérapie.

1.3.1 Un modèle structuré en taille et en espace pour la croissance tumorale et son interaction avec les cellules T effectrices

Dans le chapitre 2, nous nous sommes focalisés sur la modélisation des premières étapes de la croissance tumorale. Pour ce faire, nous avons considéré deux populations de cellules :

— les cellules du système immunitaire qui regroupent les cellules tueuses du système immunitaire inné et les cellules cytotoxiques spécifiques à l'antigène tumoral (En l'occurrence, les cellules naturelles tueuses (NK) et les lymphocytes T $CD8^+$. Par la suite, nous désignerons par cellule effectrice, toute cellule qui s'attaque à la tumeur).

— les cellules tumorales.

La construction du modèle mathématique est basée sur un ensemble d'hypothèses simplificatrices qui résument le contexte biologique sous-jacent aux interactions entre les cellules effectrices et une tumeur naissante (voir la sec. 1.1.2). Ces hypothèses peuvent être discutables, mais elles visent à garder les mécanismes les plus pertinents avec un système d'équations aussi simple que possible. Nous renvoyons au chapitre 2, Partie 2.2.1 pour plus de détails sur ces questions. Le modèle prend en compte deux échelles distinctes dont la première, l'échelle spatiale, associée au déplacement des cellules effectrices est "infiniment grande" par rapport à la deuxième, l'échelle de la taille des cellules tumorales [14]. Nous considérons donc d'une part, la tumeur comme une masse ponctuelle, structurée par la taille z des cellules qui la contiennent et située au centre d'un domaine Ω et d'autre part les cellules effectrices activées situées à une certaine position $x \in \Omega$ et se déplaçant de façon erratique vers le site tumoral (le centre du domaine) dû à la combinaison d'un processus de diffusion naturelle et d' un processus de convection chimiotactique induit par la présence de la tumeur (voir Fig. 1.4).

14. Cette hypothèse rend négligeable les effets dû à la géométrie de la tumeur comparativement à l'échelle de déplacement des cellules effectrices

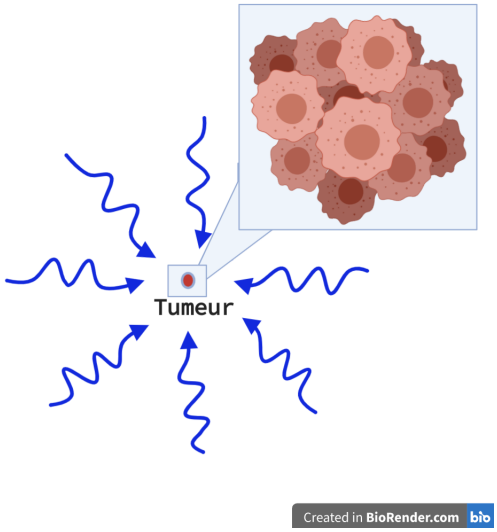

FIGURE 1.4 – illustration de l'interaction tumeur-système immunitaire modélisé par (1.3a)-(1.3e)

Les inconnues du modèle sont :

— la distribution des cellules tumorales structurées par leur volume, $(t, z) \mapsto n(t, z)$ de sorte que l'intégrale $\int_a^b zn(t, z)dz$ donne la taille de la tumeur occupé au temps t par des cellules tumorales ayant leur taille z dans l'intervalle (a, b) ;

— la concentration des cellules effectrices $(t, x) \mapsto c(t, x)$;

— la concentration du signal chimique (chimioattractant) qui attire les cellules effectrices vers le microenvironnement tumoral $(t, x) \mapsto \phi(t, x)$.

La force de la vitesse de déplacement de même que le taux d'activation des cellules effectrices dépendent directement de la masse totale de la tumeur, qui est proportionnelle à la quantité :

$$\mu_1 = \int_0^\infty zn(t, z)dz.$$

Nous modélisons ainsi la compétition entre le système immunitaire et la tumeur par l'EDP suivante (nous renvoyons au chapitre 2 pour plus de détails sur la construction du

système d'équations) :

$$\partial_t n + \partial_z(Vn) = Q(n) - m(n,c), \tag{1.3a}$$

$$\partial_t c + \nabla_x \cdot (c\chi\nabla_x\phi - D\nabla_x c) + \gamma c = pg(\mu_1)S, \tag{1.3b}$$

$$-\mathcal{K}\Delta_x\phi = \mu_1\left(\sigma(x) - \int_\Omega \sigma(y)\,\mathrm{d}y\right), \tag{1.3c}$$

$$n(t,0) = 0,\ c\Big|_{\partial\Omega} = 0,\ \mathcal{K}\nabla_x\phi\cdot\nu(\cdot)\Big|_{\partial\Omega} = 0, \tag{1.3d}$$

$$n(t=0,z) = n_0(z),\ c(t=0,x) = c_0(x). \tag{1.3e}$$

l'équation (1.3a) modélise l'évolution en temps de la distribution de cellules tumorales. En effet la dynamique de croissance-division propre aux cellules tumorales impliques d'une part une croissance en volume ou en taille dictée par le taux de croissance $z \mapsto V(z) \geq 0$ et le processus de division cellulaire décrit par l'opérateur $Q(n)$. Notons que le processus de division cellulaire ne change pas la masse totale de la tumeur. Par conséquent l'opérateur Q satisfait :

$$\int_0^\infty zQ(n)dz = 0.$$

Toutefois, le nombre de cellules dans la tumeur évolue sous l'effet de la division cellulaire, par conséquent,

$$\int_0^\infty Q(n)dz \geq 0.$$

Dans notre travail nous nous sommes souvent restreints au cas simple de l'opérateur de division binaire symétrique

$$Q(n)(t,z) = 4a(2z)n(t,2z) - a(z)n(t,z), \tag{1.4}$$

où $z \mapsto a(z)$ représente le taux de division d'une cellule de volume ou de taille z. L'équation (1.3a) est bien connue sous le nom d'équation de croissance-fragmentation ([62]). Ce type d'équation non-locale est assez courant en biologie (voir [25, 26, 69] et nous pouvons aussi citer à titre d'exemple certaines applications à la croissance tumorale : [7, 8]). L'equation (1.3a) est complétée par une distribution initiale de cellules tumorales (1.3e) et une condition au bord (1.3d) qui exclut la création de cellules de volume 0.

Dans le second membre de (1.3b), $x \mapsto S(x)$ représente la distribution spatiale de la source de cellules inactives du système immunitaire, à savoir les lymphocytes T cytotoxiques qui sont activés dans les ganglions lymphatiques drainants le site tumoral ou les cellules NK qui sont activées dans le microenvironnement tumoral. p, représente le taux d'activation des cellules effectrices (il peut être structuré spatialement) et le facteur adimensionnelle $\mu_1 \mapsto g(\mu_1)$ décrit comment la présence de cellules tumorales stimule la

production de nouvelles cellules effectrices et la conversion des cellules naïves en cellules effectrices ou leur recrutement. Par conséquent, il vérifie naturellement les hypothèses suivantes : (1) $g(0) = 0$ (2) $\forall \mu_1 \geq 0$, $g'(\mu_1) > 0$. Dans l'optique d'étudier les stades précoces de la croissance tumorale, nous avons utilisé une simple relation linéaire. par conséquent, dans cette partie, $g(\mu_1) = \mu_1$. La condition au bord de Dirichlet pour c dans (1.3d) indique que les cellules effectrices éloignées de la tumeur sont considérées comme inactives.

L'équation (1.3c) décrit le potentiel chimiotactique qui est induit par la présence de la tumeur. Le second membre de (1.3c) indique que la force du signal attractif est proportionnelle à la masse totale de la tumeur et est façonnée par une fonction de forme $x \mapsto \sigma(x)$. Enfin, les cellules effectrices sont capables de détruire les cellules tumorales. Ce processus est décrit par le terme de mort dans (1.3a). Typiquement,

$$m(c,n)(t,z) = \int_\Omega \delta(y)c(t,y)\,\mathrm{d}y \times n(t,z), \tag{1.5}$$

où $\delta \geq 0$ est une autre fonction de forme. Dans la suite, les paramètres $z \mapsto a(z)$ et $z \mapsto V(z)$ sont supposés constants ($a(z) \equiv a$ et $V(z) \equiv V$)

Le modèle (1.3a)-(1.3e) conduit à des observations pertinentes et en accord avec les observations biologiques relatives aux interactions en jeu.

Existence de phases d'équilibre : l'immunosurveillance Le système immunitaire est capable de contrôler la croissance tumorale et de maintenir la tumeur dans un état dormant, c'est-à-dire contenant des cellules tumorales non proliférantes, où le microenvironnement tumoral contient de cellules effectrices activées spécifiques à l'antigène tumoral. En effet, d'une part, la solution de l'équation de croissance-fragmentation converge vers un profil spécifique de distribution des cellules tumorales caractérisé par les éléments propres de l'opérateur de croissance-fragementation. Plus précisement, la solution $(t,z) \mapsto n(t,z)$ de l'équation (1.3a) converge vers une distribution de la forme $(t,z) \mapsto e^{\lambda t}\rho N(z)$ où ρ est entièrement déterminé par la condition initiale (nous renvoyons à [70] où ce résultat est établi avec des valeurs de paramètre constant, à [63] où ce résultat est établi avec des techniques d'entropie relative et à [20] pour une application à la croissance tumorale) [15] et la fonction $z \in \mathbb{R}^+ \mapsto N(z) \geq 0$ de même que la valeur $\lambda > 0$ (souvent appelé au taux de croissance malthusien de la tumeur) vérifient :

$$\begin{cases} \partial_z(VN) - Q(N) + \lambda N = 0 & \text{for } z \geq 0 \\ N(0) = 0, \qquad N(z) > 0 & \text{for } z > 0, \qquad \int_0^{+\infty} N(z)\,\mathrm{d}z = 1. \end{cases} \tag{1.6}$$

15. Notons que ce phénomène de convergence vers un profil de distribution stationnaire est bien connu en biologie sous le nom de *désynchronisation* des cellules ([25, 18]).

Nous renvoyons à [26] pour une preuve de l'existence des éléments propres (λ, N) avec des hypothèses générales sur les paramètres du modèle. Par conséquent l'etat d'équilibre représentant le contrôle de la tumeur dans un état dormant correspond au cas où la force du système immunitaire représentée par le facteur $\int_\Omega \delta(y)c(t,y)\,\mathrm{d}y$ dans (1.5) (que nous noterons $t \mapsto \mu_c(t)$) converge vers le taux de croissance malthusien de la tumeur, en d'autre terme, vers la valeur propre λ de l'opérateur de croissance-fragmentation. Par conséquent, la concentration de cellule effectrice à l'équilibre est déterminée par :

$$\int_\Omega \delta(y)c(t,y)\,\mathrm{d}y = \lambda. \tag{1.7}$$

Ce constat est assez robuste car il a été non seulement prédit pour des cas de tumeur non aggressive (avec un taux de division faible) par le théorème suivant (voir chapitre 2 pour plus de détails)

Theorem 1.3.1. *Soit Φ la solution de l'équation*

$$-\nabla_x \cdot (\mathcal{K}\nabla_x \Phi) = \sigma - \frac{1}{|\Omega|}\int_\Omega \sigma(y)\,\mathrm{d}y, \tag{1.8}$$

munie aux bords de la condition de Neumann homogène. si $\ell > 0$ est suffisamment petit, il existe un unique $\bar{\mu}_1(\ell) > 0$ tel que la solution $C_{\bar{\mu}_1(\ell)}$ de l'équation stationnaire

$$\gamma C - \nabla_x \cdot (D\nabla_x C) - \bar{\mu}_1 \nabla_x \cdot (C\nabla_x \Phi) = g(\bar{\mu}_1)pS, \qquad C\big|_{\partial\Omega=0} = 0, \tag{1.9}$$

vérifie la condition $\int_\Omega \delta C\,\mathrm{d}x = \ell$,

mais aussi observé numériquement pour des cas de tumeur aggressive (voir chapitre 2, Partie 2.3.1). Cependant, les simulations numériques (voir chapitre 2) ont aussi montré la présence d'oscillations dans l'évolution non seulement de la masse tumorale mais aussi de la concentration des cellules effectrices dans le microenvironnement tumoral. Ces oscillations sont influencées par les paramètres du modèle et peuvent ralentir la convergence vers l'état d'équilibre (nous verrons dans le chapitre 2 Partie 3.3.3 que ces oscillations décroissent de façon polynomiale). Ainsi, plus la tumeur est aggressive, c'est-à-dire le taux de division des cellules tumorales, a est élévé, et moins le système immunitaire est efficace (par exemple $x \mapsto \delta(x)$ a une faible amplitude, le taux d'activation p est petit), plus la masse tumorale oscille et plus le contrôle de la croissance tumorale est lent (nous renvoyons au chapitre 2, Partie 2.3.1). En conclusion, l'aggressivité de la tumeur et l'efficacité du système immunitaire constituent des facteurs déterminants dans le mécanisme de contrôle de la croissance tumorale.

Hétérogénéité spatiales et oscillations périodiques De façon remarquable, l'hétérogénéité spatiale de la distribution des cellules naïves avant le processus d'activation réduit

considérablement la capacité des cellules effectrices à contrôler la tumeur. Ce comportement s'explique par le fait que l'activation distante des cellules du système immunitaire laisse le temps à la tumeur de croître. La tumeur étant assez évoluée avant l'arrivée des cellules effectrices, il s'ensuit alors une alternance périodique de phases de rémission et de rechute (nous renvoyons au chapitre 3, Partie 2.3.2 pour une illustration de ce phénomène). Toutefois, nous verrons grâce à la méthode numérique développée dans le chapitre 2 que les oscillations qui apparaissent comme périodique dans ce cadre (distribution hétérogène) convergent en effet vers un état stationnaire, mais le taux d'amortissement de ces oscillations étant très petit il est difficile d'observer cet état dans des temps de simulation raisonnables.

1.3.2 Analyse de la phase d'équilibre dans une tumeur contrôlée par le système immunitaire

Dans le chapitre 3, nous nous sommes interessés à l'analyse de la phase d'équilibre caractérisée par le contrôle de la croisance tumorale par les cellules effectrices. Sachant qu'une tumeur devient de plus en plus maligne quand sa masse atteint certains seuils (voir [33, 56], nous renvoyons aussi au chapitre 4), il est préférable que cette masse soit la plus petite possible pour assurer la survie du patient. Le but principal de cette partie est d'identifier les paramètres biologiques clés sur lesquels il faut agir pour maintenir l'état d'équilibre et empêcher l'échappement de la tumeur. Pour ce faire, nous avons dans un premier temps estimé les intervalles dans lesquels vivent les paramètres du modèle (1.3a-1.3e). Cette estimation s'est effectuée en deux temps. Dans un premier temps, une recherche avancée dans la litérature a permis de retrouver la plupart des paramètres du modèle. Dans un deuxième temps, le modèle a été confronté à des données in vivo (fourni par les biologistes avec lesquelles nous collaborons) pour estimer les intervalles de confiance des paramètres restants (nous renvoyons au chapitre 2 pour plus de détails sur la procédure et les paramètres en jeu). Ensuite, nous avons estimé la masse de la tumeur à l'équilibre en nous basant sur le théorème 1.3.1. En effet ce dernier définit de façon implicite la masse de la tumeur à l'équilibre (noté μ_1), mais un obstacle de cette partie se situe dans l'estimation de la valeur propre (λ, voir les équations (1.6) et (1.7)) de l'opérateur de croissance-fragmentation. En effet, l'opérateur de croissance-fragmentation, au préalable défini sur l'espace $L^1(\mathbb{R}^+)$, est numériquement, tronqué et discrétisé sur $L^1([0, R])$ avec R la borne supérieure de la variable de taille des cellules tumorales. Par conséquent, le problème d'estimation de la valeur propre de plus grand module se redéfinit comme la recherche de la valeur propre principale d'une version décalée de la matrice sous-jacente au problème discret, qui peut être résolue par la méthode de la puissance ([40, Partie 1.2.5]). L'estimation de ce décalage est un préalable nécéssaire à la simulation numérique. Elle est fournie par l'énoncé suivant

Theorem 1.3.2. *Supposons que*

i) $z \mapsto V(z)$ *est une fonction continue appartenant à* L^∞ *et est inférieurement bornée par une constante positive,*

ii) $h\sum_{j=1}^{I} a(z_j)k(z_i|z_j)$ *reste uniformément borné par rapport à* h*,*

iii) pour tout $i \in \{1, ..., I-1\}$*, il existe* $j \in \{i+1, ..., I\}$ *tel que* $a(z_j)k(z_i|z_j) > 0$*,*

iv) il existe $Z_0 \in (0, \infty)$ *tel que, en posant* $\bar{\mathcal{N}}(z) = h\sum_{j=2}^{I} k(z_j|z)$*, nous avons* $a(z)(\bar{\mathcal{N}}(z) - 1) \geq \nu_0 > 0$ *pour tout* $z \geq Z_0$*.*

soit

$$\Lambda > \frac{\|V\|_{L^\infty}}{\min_{j\in\{1,...,I\}} |V_{j+1/2}|} \max_{k\in\{1,...,I\}} \left(h \sum_{j=k}^{I} a_j k(z_k|z_j) \right) - \min_{j\in\{1,...,I\}} |a_j|, \tag{1.10}$$

et supposons que $R > Z_0$ *est assez grand. ALors,* $\mathscr{T}_\Lambda^h$ *est inversible et il existe une paire* $\mu > 0$*,* $N \in \mathbb{R}^I$ *avec des composants positive, telle que* $\mathrm{Ker}\left((\mathscr{T}_\Lambda^h)^{-1} - \mu\right) = \mathrm{Span}\{N\}$*. De plus* $\lambda = \Lambda - \frac{1}{\mu} > 0$*.*

Ce résultat est une version discrète du théorème de Doumic-Gabriel (voir [26]) pour le problème continu. Le point crucial est de vérifier que le décalage à opérer n'est pas fondamentalement modifié par la discrétisation. Nous renvoyons au chapitre 3 pour plus de détails sur l'analyse de ce problème et plus précisement à la Partie 3.5.3 du dit chapitre pour une application de la méthode d'estimation sur des cas particuliers de division cellulaire dont les éléments propres (λ, N) sont connus. Pour l'estimation de la masse tumorale nous avons appliqué un algorithme de dichotomie au problème stationnaire défini par les équations (1.8) et (1.9) (nous renvoyons au chapitre 3, Partie 3.3.2 pour plus de détails sur les étapes de l'algorithme). Nous avons appelé par la suite l'algorithme qui permet d'estimer la masse tumorale à l'équilibre, algorithme de *puissance-dichotomie*.

Pour déterminer les paramètres les plus influents du modèle, nous avons effectué une analyse de sensibilité globale sur la masse tumorale à l'équilibre. Cette analyse nous a permis de calculer les *indices de Sobol*, qui permettent de mesurer à quel point la variance totale de la sortie de l'algorithme de puissance-dichotomie (la masse tumorale) peut être influencée par des sous-ensembles $i_1, \cdots, i_p$ de l'ensemble des paramètres $i_1, \cdots, i_k$ (avec $k > p$ le nombre de paramètres d'entrée incertain). Nous renvoyons aux Parties 3.3.4 et 3.5.4 pour plus de détails sur la méthode. Les conclusions de cette analyse sont diverses. Les paramètres les plus influents identifiés par la méthode sont dans l'ordre, la force du système immunitaire (l'amplitude de la fonction $x \mapsto \delta(x)$), le taux de mortalité naturel des cellues effectrices γ, le taux de division des cellules tumorales a et le flux entrant de cellules effectrices dans le microenvironnement tumoral (représenté par le produit pS). Ce classement indique non seulement l'importance de l'efficacité du sytème immunitaire mais aussi l'importance de l'immunothérapie. Les indices de Sobol indiquent aussi les paires de paramètres les plus influents. Ainsi, la paire (taux de division des cellules tumorales, force du système immunitaire) représente l'une des paires les plus

importantes. Cette dernière indique les thérapies basées sur la combinaison de traitements capables d'augmenter la réponse immunitaire anti-tumorale et de diminuer l'aggressivité de la tumeur ont de bonnes chances de réussir. Nous renvoyons à la Partie 3.4 du chapitre 3 pour plus de détails sur les résultats de cette analyse.

1.3.3 Un modèle structuré en taille et en espace pour la croissance tumorale et son interaction avec les cellules T effectrices et protumorales

Dans le chapitre 4, nous avons enrichi le modèle (1.3a)-(1.3e) en introduisant les mécanismes immunosuppresseurs engendrés par la tumeur pour contrecarrer la réponse immunitaire. Les étapes de construction du modèle constituent un prolongement naturel des étapes définies dans le chapitre 2. Le modèle prend en compte une population de cellules supplémentaires : Il s'agit des cellules "protumorales". Dans cette famille de cellules nous regroupons les lymphocytes T dites régulatrices ou facilitatrices (Tregs), les cellules suppressives dérivées de myéloïdes (MDSCs), les neutrophiles associés à la tumeur (TAN N2) et les macrophages associés à la tumeur (TAM M2) favorisant la croissance tumorale. Nous renvoyons au chapitre 4 pour plus de détails sur les hypothèses biologiques prises en compte dans le processus de modélisation. Le modèle que nous avons construit se présente comme suit :

$$\partial_t n + \partial_z \left(V(z) \left(1 + \int_\Omega b_1(y) c_r(t,y) \right) n \right) = Q(n) - m(n,c), \tag{1.11a}$$

$$\partial_t c + \nabla_x \cdot (c\chi \nabla_x \phi - D \nabla_x c) = g(\mu_1) S - \gamma c - k_r I \theta_1 c - k_c c c_r, \tag{1.11b}$$

$$\partial_t c_r + \nabla_x \cdot (c_r \chi \nabla_x \phi - D \nabla_x c_r) = I(p_r S_r + k_r \theta_1 c) - \gamma_r c_r, \tag{1.11c}$$

$$\partial_t I = \psi(\mu_1) - \tau I, \tag{1.11d}$$

$$-\nabla_x \cdot (\mathcal{K} \nabla_x \phi) = f(\mu_1)\sigma, \tag{1.11e}$$

$$n(t,0) = 0,\ c\big|_{\partial\Omega} = 0,\ c_r\big|_{\partial\Omega} = 0,\ \mathcal{K}\nabla_x\phi \cdot \nu(\cdot)\big|_{\partial\Omega} = 0, \tag{1.11f}$$

$$n(t=0,z) = n_0(z),\ c(t=0,x) = c_0(x),\ c(t=0,x) = c_r^0(x),\ I(t=0) = I_0. \tag{1.11g}$$

où $(t,x) \mapsto c_r(t,x)$ réprésente la concentration de cellules protumorales favorisant la croissance tumorale. l'activation des cellules protumorales dépend de la concentration de cytokines dans le microenvironnement tumoral, cette concentration est décrite par le signal $t \mapsto I(t)$. Ce signal s'active quand la masse tumorale dépasse une certaine masse critique $m > 0$ à travers la fonction de seuil ψ définie par :

$$\psi(\mu_1) = \bar{\psi} \begin{cases} (\mu_1 - m), & \mu_1 > m \\ 0, & \mu_1 \leq m \end{cases} \tag{1.12}$$

où $\bar{\psi} > 0$ et ψ vérifie : $\psi(0) = \psi'(0) = 0$. Les mécanismes immunosuppresseurs interviennent dans des phases ultérieures de la croissance tumorale, par conséquent, nous avons utilisé une loi de Gompertz pour modéliser la croissance en taille des cellules tumorales :

$$V(z) = rz\ln(b/z), \tag{1.13}$$

où $r > 0$ réprésente le taux de croissance intrinsèque des cellules tumorales et $b > 0$ représente la taille maximale que peut atteindre une cellule tumorale. Les cellules protumorales favorisent la croissance tumorale en agissant sur le taux de croissance des cellules tumorales à travers le terme :

$$V(z)\left(1 + \int_\Omega b_1(y)c_r(t,y)\,\mathrm{d}y\right)$$

où b_1 est une fonction de forme non-negative, à support compacte et à symmétrie radiale.

Existence de phases d'équilibre et d'échappement : immunoédition Le modèle reproduit bien les phases de l'immunoédition. Plus précisement, quand la masse critique m est positive, soit la croissance tumorale est immédiatement contrôlée par la réponse immunitaire anti-tumorale et par conséquent l'état d'équilibre contient un résidu de cellules tumorales dormant, des cellules effectrices activées et aucune cellule protumorale ($c_r \equiv 0$), soit la masse tumorale μ_1 et la concentration de cellules protumorale c_r explosent. Le premier cas se produit pour des taux de division faibles et le second (explosion de la masse tumorale) résulte des tumeurs plus aggressives. De plus, lorsque la croissance tumorale est contrôlée, la concentration des cellules effectrices ($x \mapsto c(x)$) vérifie (1.7) (nous renvoyons au chaptire 4, Partie 4.3 pour une illustration numérique de ces phénomènes). Cependant, si la masse critique est nulle ($m = 0$), soit l'état d'équilibre contient aussi des cellules protumorales résiduelles, soit la masse tumorale et la concentration de cellules protumorales (c_r) explosent.

Exploration des stratégies d'immunothérapie pour le traitement du cancer L'objectif principal de ce chapitre est l'exploration de diverses stratégies d'immunothérapie dans l'optique de restaurer le contrôle du système immunitaire. Pour ce faire, nous avons comparé les effets de deux stratégies d'immunothérapie. En effet, une certaine proportion de cellules effectrices ayant été en contact avec les cellules protumorales est dans un état anergique c'est-à-dire tolérant à la tumeur. Toutefois, les cellules anergiques peuvent être réactivées par des traitements spécifiques. Les traitements capables de restaurer de la réponse anti-tumorale font parties de la famille des traitements inhibiteurs de point de contrôle (Immune Checkpoint Inhibitors) tels que les anti-PD1 ou les anti-CTLA4. D'autres stratégies de traitement sont basées sur la réduction du recrutement des cellules protumorales. Dans un premier temps, nous avons discuté des effets de ces deux approches pris séparément puis nous avons analysé les effets de la combinaison de ces deux thérapies (Nous renvoyons à la Partie 4.4 du chapitre 4 pour plus de détails sur la construction des

protocoles de traitement). Les résultats de cette analyse s'avèrent très intéressants. Il en ressort que pour que les monothérapies soient efficaces, il faut respecter un bon compromis entre le temps de début de l'administration et la dose administrée. Ainsi un traitement administré plus tôt nécessite des doses relativement faibles pour être efficace. Toutefois, administrées tardivement, les monothérapies sont inefficaces ou requièrent d'augmenter les doses, au risque de créer un toxicité. Cependant, les traitements basés sur la combinaison des deux thérapies sont très efficaces. Administrés tardivement, ils sont capables de restaurer le contrôle de la tumeur à des doses relativement faibles.

1.4 Centre d'Été Mathématique de Recherche Avancée en Calcul Scientifique

Les travaux présentés dans cette partie sont indépendants du sujet traité au cours de cette thèse. Comme nous l'avons mentionné dans l'introduction de ce chapitre, ils sont issus de diverses collaborations lors de projets CEMRACS (Centre d'Été Mathématiques de Recherche Avancée en Calcul Scientifique) basés sur des thématiques différentes.

1.4.1 Les transitions de phase dans un modèle à deux espèces pour la ségrégation de cellule et la croissance logistique

Dans le chapitre 5, nous étudions un modèle de ségrégation cellulaire dans une population composée de deux types de cellules (A et B). En partant d'un modèle initialement proposé dans [6], nous cherchons à comprendre l'impact d'un processus de division cellulaire sur les capacités de ségrégation du système. Le modèle original décrit une population de cellules sphériques interagissantes avec leurs voisins proches au moyen d'un potentiel de répulsion et soumises à un mouvement brownien :

$$\begin{cases} dX_i^A = -\mu \nabla_{X_i^A} W^A(X^A, X^B)dt + \sqrt{2D_A}dB_i, \quad \forall\, i \in \{1, \dots, N_A\} \\ dX_i^B = -\mu \nabla_{X_\ell^A} W^B(X^A, X^B)dt + \sqrt{2D_B}dB_\ell, \quad \forall\, \ell \in \{1, \dots, N_B\}. \end{cases} \tag{1.14}$$

où les points $(X_i^A, X_l^B) \in \mathbb{R}^2 \times \mathbb{R}^2, i \in \{1, \cdots, N_A\}, l \in \{1, \cdots, N_B\}$ représentent respectivement les positions des centres des cellules A et des cellules B. μ représente un coefficient de mobilité donné et B_i est un mouvement brownien en dimension 2 $B_i = (B_i^1; B_i^2)$ avec une intensité $D_A > 0$ pour les espèces A et $D_B > 0$ pour les espèces B. W^S représente le potentiel répulsif des particules de type $S \in \{A, B\}$ (nous renvoyons au chapitre 5 pour plus de détails sur la formulation de ce potentiel). Nous ajoutons à ce modèle, un processus stochastique de naissance-mort :

$$\beta_S(X_i^S) = b_0^S - (b_0^S - \theta_S)\left(\frac{\mathcal{N}_{R_0}(X_i^S)}{N^*}\right), \qquad \delta_S(X_i^S) = d_0^S + (\theta_S - d_0^S)\left(\frac{\mathcal{N}_{R_0}(X_i^S)}{N^*}\right). \tag{1.15}$$

où le coefficient $\mathcal{N}_{R_0}(X_i^S)$ représente le nombre de cellules (des deux populations) dont les centres sont situés à une distance R_0 de X_i^S et N^* est le nombre maximal de cellules dans une boule de rayon R_0. Les paramètres b_0^S et d_0^S représentent respectivement le taux de naissance intrinsèque et le taux de mortalité d'un individus, le paramètre θ_S représente le taux de naissance limite quand la population aura atteint la capacité locale maximale N^*. Ce processus se rapproche d'un terme de croissance logistique quand le nombre de cellules devient grand. Nous avons abordé dans un premier temps le passage du modèle microscopique (1.14) vers un modèle macroscopique. Puis dans un second temps nous avons étudié la stabilité linéaire des états stationnaires spatialement homogènes du modèle macroscopique et obtenu un critère précis pour la transition de phase, qui relie la capacité de ségrégation du système aux paramètres du modèle. En comparant le critère avec celui obtenu sans croissance logistique, nous montrons que la capacité de ségrégation du système est le résultat d'une interaction complexe entre croissance logistique, diffusion et interactions mécaniques répulsives. Des simulations numériques sont présentées pour illustrer les résultats obtenus à l'échelle microscopique.

1.4.2 Explorations numériques de l'équation de Navier-Stokes compressible et barotrope

Dans le chapitre 6, nous nous intéressons à la simulation numérique du système de Navier-Stokes compressible suivant

$$\begin{aligned} \partial_t \rho + \partial_x(\rho u) &= 0, \\ \partial_t(\rho u) + \partial_x(\rho u^2) + \partial_x p - \partial_x(\mu(\rho)\partial_x u) &= f. \end{aligned} \tag{1.16}$$

Dans (1.16), les inconnues $(t,x) \mapsto \rho(t,x)$ et $(t,x) \mapsto u(t,x)$ représentent respectivement la densité et la vitesse d'un fluide. La quantité $\mu : \rho \in (0,\infty) \mapsto \mu(\rho) > 0$ est la viscosité du fluide. On se limite au cas isentropique, où la pression est une simple fonction de la densité, à savoir on fixe $p(\rho) = a\rho^\gamma$, avec $a > 0$ et $\gamma > 1$. Le fluide est soumis à la force extérieure f. Ce travail est particulièrement motivé par le travail de pionnier de D. Hoff. qui, au-delà de l'existence de solutions faibles, établit plusieurs faits sur les *solutions discontinues* de (1), qui, à première vue, sont assez surprenants. En effet, les discontinuités possibles de la vitesse initiale sont instantanément lissées : u devient continue, tandis que la densité ρ peut présenter des discontinuités, qui sont simplement transportées par le champ de vitesse u. En termes de méthodes numériques, l'idée de base consiste à utiliser des méthodes établies pour l'équation d'Euler, couplées à une discrétisation appropriée du terme de diffusion que nous allons comparer à des approches sur grilles décalées. La propriété de D. Hoff est vérifiée numériquement en utilisant notamment un schémas Lagrangien.

Bibliographie

[1] M. Al-Tameemi, M. Chaplain, and A. D'Onofrio. Evasion of tumours from the control of the immune system : Consequences of brief encounters. *Biology Direct*, 7, sep 2012.

[2] Almeida, Luis, Atsou, Kevin, Marulli, Marta, Peurichard, Diane, and Tesson, Rémi. Phase transitions in a two-species model for cell segregation and logistic growth. *ESAIM : ProcS*, 67 :1–15, 2020.

[3] K. Atsou, F. Anjuère, V. M. Braud, and T. Goudon. A size and space structured model describing interactions of tumor cells with immune cells reveals cancer persistent equilibrium states in tumorigenesis. *J. Theor. Biol.*, 490 :110163, 2020.

[4] S. Banerjee and R. R. Sarkar. Delay-induced model for tumor–immune interaction and control of malignant tumor growth. *Biosystems*, 91(1) :268 – 288, 2008.

[5] D. Barbolosi, A. Benabdallah, F. Hubert, and F. Verga. Mathematical and numerical analysis for a model of growing metastatic tumors. *Mathematical Biosciences*, 218(1) :1 – 14, 2009.

[6] J. Barré, P. Degond, D. Peurichard, and E. Zatorska. Modelling pattern formation through differential repulsion, 2019.

[7] B. Basse, B. C. Baguley, E. Marshall, W. R. Joseph, B. van Brunt, G. Wake, and D. J. N. Wall. A mathematical model for analysis of the cell cycle in cell lines derived from human tumors. *J. Math. Biol.*, 47(4) :295–312, 2003.

[8] F. Bekkal Brikci, J. Clairambault, B. Ribba, and B. Perthame. An age-and-cyclin-structured cell population model for healthy and tumoral tissues. *J. Math. Biol.*, 57(1) :91–110, 2008.

[9] P. Bi, S. Ruan, and X. Zhang. Periodic and chaotic oscillations in a tumor and immune system interactionmodel with three delays. *Chaos*, 24 :023101, 2014.

[10] F. Bihl, C. Germain, C. Luci, and V. M. Braud. Mechanisms of NK cell activation : CD4 + T cells enter the scene. *Cellular and Molecular Life Sciences*, 68(21) :3457–3467, 2011.

[11] T. Boon, J.-C. Cerottini, B. V. den Eynde, P. van der Bruggen, and A. V. Pel. Tumor antigens recognized by T lymphocytes. *Annual Review of Immunology*, 12(1) :337–365, 1994. PMID : 8011285.

[12] T. Boon, P. G. Coulie, B. J. V. den Eynde, and P. van der Bruggen. Human T-cell responses against melanoma. *Annual Review of Immunology*, 24(1) :175–208, 2006. PMID : 16551247.

[13] D. Bresch, T. Colin, E. Grenier, B. Ribba, D. Bresch, T. Colin, E. Grenier, B. Ribba, O. Saut, T. Colin, T. Cedex, and E. Grenier. A viscoelastic model for avascular tumor growth. *AIMS journals*, 2009.

[14] M. Burnet. *Immunological surveillance*. Elsevier, 2014.

[15] M. Cazaux, C. L. Grandjean, F. Lemaître, Z. Garcia, R. J. Beck, I. Milo, J. Postat, J. B. Beltman, E. J. Cheadle, and P. Bousso. Single-cell imaging of CAR T-cell activity in vivo reveals extensive functional and anatomical heterogeneity. *J. Experimental Medicine*, 216(5) :1038–1049, 2019.

[16] D. A. Chen and I. Mellman. Oncology meets immunology : The cancer immunity cycle. *Immunity*, 39(1) :1–10, 2013.

[17] D. A. Chen and I. Mellman. Elements of cancer immunity and the cancer-immune set point. *Nature*, 541 :321–330, 2017.

[18] G. Chiorino, J. A. Metz, D. Tomasoni, and P. Ubezio. Desynchronization rate in cell populations : Mathematical modeling and experimental data. *Journal of Theoretical Biology*, 208(2) :185–199, 2001.

[19] L. G. de Pillis, A. E. Radunskaya, and C. L. Wiseman. A validated mathematical model of cell-mediated immune response to tumor growth. *Cancer Res.*, 65(17) :7950–7958, 2005.

[20] A. Devys, T. Goudon, and P. Lafitte. A model describing the growth and size distribution of multiple metastatic tumors. *Disc. Cont. Dyn. Syst.-B*, 12 :731–767, 2009.

[21] H. Dirk. From 1970 until present : the keller-segel model in chemotaxis and its consequences, 2003.

[22] A. d'Onofrio. A general framework for modeling tumor-immune system competition and immunotherapy : mathematical analysis and biomedical inferences. *Physica D*, 208(3-4) :220–235, 2005.

[23] A. d'Onofrio and A. Ciancio. Simple biophysical model of tumor evasion from immune system control. *Phys. Rev. E*, 84 :031910, Sep 2011.

[24] A. d'Onofrio, G. F., P. Cerrai, and L. Fresch. Delay-induced oscillatory dynamics of tumour-immune system interaction. *Math. Comput. Model.*, 51 :572–591, 2010.

[25] M. Doumic. *Growth-fragmentation equations in biology*. Habilitation à diriger des recherches, Université Pierre et Marie Curie - Paris VI, June 2013.

[26] M. Doumic-Jauffret and P. Gabriel. Eigenelements of a general aggregation-fragmentation model. *Math. Models Methods Appl. Sci.*, 20(5) :757–783, 2010.

[27] G. P. Dunn, A. T. Bruce, H. Ikeda, L. J. Old, and R. D. Schreiber. Cancer immunoediting : from immunosurveillance to tumor escape. *Nat. Immunol.*, 3 :991–998, 2002.

[28] G. P. Dunn, L. J. Old, and R. D. Schreiber. The immunobiology review of cancer immunosurveillance and immunoediting. *Immunity*, 21 :137–148, 2004.

[29] R. Eftimie, J. L. Bramson, and D. J. D. Earn. Interactions between the immune system and cancer : A brief review of non-spatial mathematical models. *Bull. Math. Biol.*, 73(1) :2–32, Jan 2011.

[30] Y. E. Erdi. Limits of tumor detectability in nuclear medicine and PET. *Molecular imaging and radionuclide therapy*, 21(1) :23–28, 2012.

[31] B. F M. The concept of immunological surveillance. *Prog Exp Tumor Res.*, 13 :1–27, 1970.

[32] B. F M. Immunological surveillance in neoplasia. *Transplant Rev.*, 7 :2–25, 1971.

[33] J. Faget, S. Groeneveld, G. Boivin, M. Sankar, N. Zangger, M. Garcia, N. Guex, I. Zlobec, L. Steiner, A. Piersigilli, I. Xenarios, and E. Meylan. Neutrophils and snail orchestrate the establishmentof a pro-tumor microenvironment in lung cancer. *Cell Report*, 21 :3190–3204, 2017.

[34] J. D. Farrar, K. H. Katz, J. Windsor, G. Thrush, R. H. Scheuermann, J. W. Uhr, and N. E. Street. Cancer dormancy. VII. a regulatory role for $CD8+$ t-cells and $IFN-\gamma$ in establishing and maintaining the tumor-dormant state. *J. Immunol.*, 162(5) :2842–2849, 1999.

[35] U. Foryś, J. Waniewski, and P. Zhivkov. Anti-tumor immunity and tumor anti-immunity in a mathematical model of tumor immunotherapy. *Journal of Biological Systems*, 14(1) :13–30, 2006.

[36] M. J. Frederick and G. L. Clayman. Chemokines in cancer. *Expert Reviews in Molecular Medicine*, 3(19) :1–18, 2001.

[37] Z. G. Fridlender, J. Sun, S. Kim, V. Kapoor, G. Cheng, L. Ling, G. S. Worthen, and S. M. Albelda. Polarization of tumor-associated neutrophil phenotype by TGF-beta : "N1" versus "N2" TAN. *Cancer Cell*, 16(3) :183–194, 2009.

[38] A. Friedman and W. Hao. The role of exosomes in pancreatic cancer microenvironment. *Bull. Math. Biol.*, 80(5) :1111–1133, May 2018.

[39] M. Girardi, D. E. Oppenheim, C. R. Steele, J. M. Lewis, E. Glusac, R. Filler, P. Hobby, B. Sutton, R. E. Tigelaar, and A. C. Hayday. Regulation of cutaneous malignancy by $\gamma\delta$ t cells. *Science*, 294(5542) :605–609, 2001.

[40] T. Goudon. *Mathematics for Modeling and Scientific Computing*. Mathematics and Statistics. Wiley-ISTE, 2016.

[41] T. Hillen and K. J. Painter. A user's guide to PDE models for chemotaxis. *Journal of Mathematical Biology*, 58(1) :183, Jul 2008.

[42] B. Homey, A. Müller, and A. Zlotnik. Chemokines : Agents for the immunotherapy of cancer ? *Nature Reviews Immunology*, 2(3) :175–184, 2002.

[43] E. Itakura, R.-R. Huang, D.-R. Wen, E. Paul, P. H. Wünsch, and A. J. Cochran. IL-10 expression by primary tumor cells correlates with melanoma progression from radial to vertical growth phase and development of metastatic competence. *Mod. Pathol.*, 24(6) :801–809, 2011.

[44] Y. Iwai, M. Ishida, Y. Tanaka, T. Okazaki, T. Honjo, and N. Minato. Involvement of PD-L1 on tumor cells in the escape from host immune system and tumorimmunotherapy by PD-L1 blockade. *Proc. Natl. Acad. Sci.*, 99(19) :12293–12297, 2002.

[45] K. Iwata, K. Kawasaki, and N. Shigesada. A dynamical model for the growth and size distribution of multiple metastatic tumors. *J. Theor. Biol.*, 203 :177–186, 2000.

[46] Z. Jack T. and L. Scott W. Tumor suppressive functions of p53. *Cold Spring Harb Perspective Biol.*, 5, 2009.

[47] E. F. Keller and L. A. Segel. Model for chemotaxis. *J. Theor. Biol.*, 30(2) :225 – 234, 1971.

[48] B. J. KENNEDY. Cyclic Leukocyte Oscillations in Chronic Myelogenous Leukemia During Hydroxyurea Therapy. *Blood*, 35(6) :751–760, 06 1970.

[49] S. Khajanchi and J. J. Nieto. Mathematical modeling of tumor-immune competitive system, considering the role of time delay. *Applied Mathematics and Computation*, 340 :180–205, 2019.

[50] D. Kirschner, T. Jackson, and J. Arciero. A mathematical model of tumor-immune evasion and siRNA treatment. *Disc. Cont. Dyn. Syst.-B*, 4(1) :39–58, 2008.

[51] D. Kirschner and J. C. Panetta. Modeling immunotherapy of the tumor-immune interaction. *J. Math. Biol.*, 37 :235–252, 1998.

[52] D. E. Kuczek, A. M. H. Larsen, M. L. Thorseth, M. Carretta, A. Kalvisa, M. S. Siersbæk, A. M. C. Simões, A. Roslind, L. H. Engelholm, E. Noessner, M. Donia, I. M. Svane, P. T. Straten, L. Grøntved, and D. H. Madsen. Collagen density regulates the activity of tumor-infiltrating T cells. *Journal for ImmunoTherapy of Cancer*, 7(1) :1–15, 2019.

[53] V. A. Kuznetsov, I. A. Makalkin, M. A. Taylor, and A. S. Perelson. Nonlinear dynamics of immunogenic tumors : Parameter estimation and global bifurcation analysis. *Bull. Math. Biol.*, 56(2) :295–321, Mar 1994.

[54] X. Lai, W. E. Carson, A. Stiff, A. Friedman, R. Wesolowski, and M. Duggan. Modeling combination therapy for breast cancer with BET and immune checkpoint inhibitors. *Proc. Nat. Acad. Sc.*, 115(21) :5534–5539, 2018.

[55] X. Lai and A. Friedman. Combination therapy of cancer with cancer vaccine and immune checkpoint inhibitors : A mathematical model. *PLoS ONE*, 12(5) :1–24, 2017.

[56] C.-Y. Li, S. Shan, Q. Huang, R. D. Braun, J. Lanzen, K. Hu, P. Lin, and M. W. Dewhirst. Initial stages of tumor cell-induced angiogenesis : evaluation via skin window chambers in rodent models. *J. Nat. Cancer Institute*, 92(2) :143–147, 01 2000.

[57] H. Li, S. Wang, and F. Xu. Dynamical analysis of tumor-immune-help T cells system. *International Journal of Biomathematics*, 12(7), 2019.

[58] v. d. B. Maries F., K. David, O. Ferry, T. René, V. Spiros, L. Werner K., M. Cornelis J.M., Z. Rolf M., and H. Hans. Decreased tumor surveillance in perforin-deficient mice. *Journal of Experimental Medicine*, 184(5) :1781–1790, 1996.

[59] A. Martín-Ruiz, C. Fiuza-Luces, E. Martínez-Martínez, C. F. Arias, L. Gutiérrez, M. Ramírez, P. Martín-Acosta, M. J. Coronado, A. Lucia, and M. Provencio. Effects of anti-PD-1 immunotherapy on tumor regression : insights from a patient-derived xenograft model. *Scientific Reports*, 10(1) :1–14, 2020.

[60] L. Martínez-Lostao, A. Anel, and J. Pardo. How Do Cytotoxic Lymphocytes Kill Cancer Cells ? *Clinical Cancer Research*, 21(22) :5047–5056, 2015.

[61] A. Matzavinos, M. A. J. Chaplain, and V. A. Kuznetsov. Mathematical modelling of the spatio-temporal response of cytotoxic T-lymphocytes to a solid tumour. *Mathematical Medicine and Biology*, 21(1) :1–34, 2004.

[62] E. D. McGrady and R. M. Ziff. "shattering" transition in fragmentation. *Phys. Rev. Lett.*, 58 :892–895, Mar 1987.

[63] P. Michel, S. Mischler, and B. Perthame. General relative entropy inequality : an illustration on growth models. *J. Math. Pures et Appl.*, 84(9) :1235–1260, 2005.

[64] D. Mougiakakos, A. Choudhury, A. Lladser, R. Kiessling, and C. C. Johansson. Regulatory T Cells in Cancer. In G. F. V. Woude and G. Klein, editors, *Advances in Cancer Research*, volume 107, pages 57–117. Academic Press, 2010.

[65] M. Müller, F. Gounari, S. Prifti, H. J. Hacker, V. Schirrmacher, and K. Khazaie. Eblacz tumor dormancy in bone marrow and lymph nodes : Active control of proliferating tumor cells by $CD8+$ immune t-cells. *Cancer Res.*, 58(23) :5439–5446, 1998.

[66] R. Noa, B. Ran, O. Moshe, and R. Varda. Mutations in the p53 tumor suppressor gene. *Genes Cancer.*, 2, 2011.

[67] K. J. O'Byrne, A. G. Dalgleish, M. J. Browning, W. P. Steward, and A. L. Harris. The relationship between angiogenesis and the immune response in carcinogenesis and the progression of malignant disease. *European J. Cancer*, 36(2) :151–169, Jan 2000.

[68] S. Olver, P. . Groves, K. Buttigieg, E. S. Morris, M. L. Janas, A. Kelso, and N. Kienzle. Tumor-derived Interleukin-4 reduces tumor clearance and deviates the cytokine and granzyme profile of tumor-induced $CD8^+$ T-cells. *Cancer Res.*, 66(1) :571–580, 2009.

[69] B. Perthame. *Transport equations in biology*. Frontiers in Math. Birkhauser, 2007.

[70] B. Perthame and L. Ryzhik. Exponential decay for the fragmentation or cell-division equation. *J. Differ. Eq.*, 210 :155–177, 2005.

[71] G. A. Rabinovich, D. Gabrilovich, and E. M. Sotomayor. Immunosuppressive strategies that are mediated by tumor cells. *Ann. Rev. Immunol.*, 25(1) :267–296, 2007. PMID : 17134371.

[72] A. Rescigno and C. DeLisi. Immune surveillance and neoplasia-1 a minimal mathematical model. *Bulletin of Mathematical Biology*, 39(2) :201–221, 1977.

[73] A. Rescigno and C. DeLisi. Immune surveillance and neoplasia—ii a two-stage mathematical model. *Bulletin of Mathematical Biology*, 39(4) :487 – 497, 1977.

[74] B. Ribba, O. Saut, T. Colin, D. Bresch, E. Grenier, and J. Boissel. A multiscale mathematical model of avascular tumor growth to investigate the therapeutic benefit of anti-invasive agents. *Journal of Theoretical Biology*, 243(4) :532 – 541, 2006.

[75] F. Rihan, D. Abdel Rahman, S. Lakshmanan, and A. Alkhajeh. A time delay model of tumour–immune system interactions : Global dynamics, parameter estimation, sensitivity analysis. *Applied Mathematics and Computation*, 232 :606 – 623, 2014.

[76] M. Robertson-Tessi, A. El-Kareh, and A. Goriely. A mathematical model of tumor–immune interactions. *J. Theor. Biol.*, 294 :56 – 73, 2012.

[77] T. Roose, S. J. Chapman, and P. K. Maini. Mathematical models of avascular tumor growth. *SIAM Review*, 49(2) :179–208, 2007.

[78] H. Salmon and E. Donnadieu. Within tumors, interactions between T cells and tumor cells are impeded by the extracellular matrix. *OncoImmunology*, 1(6) :992–994, 2012.

[79] H. Salmon, K. Franciszkiewicz, D. Damotte, P. Validire, A. Trautmann, F. Mami-Chouaib, and E. Donnadieu. Matrix architecture defines the preferential localization and migration of T-cells into the stroma of human lung tumors. *J. Clinical Investigation*, 122(3) :899–910, 2012.

[80] E. Sato, S. H. Olson, J. Ahn, B. Bundy, H. Nishikawa, F. Qian, A. A. Jungbluth, D. Frosina, S. Gnjatic, C. Ambrosone, J. Kepner, T. Odunsi, G. Ritter, S. Lele, Y.-T. Chen, H. Ohtani, L. J. Old, and K. Odunsi. Intraepithelial CD8+ tumor-infiltrating lymphocytes and a high CD8+/regulatory T cell ratio are associated with favorable prognosis in ovarian cancer. *Proc. Nat. Acad. Sc.*, 102(51) :18538–18543, 2005.

[81] J. Shimizu, S. Yamazaki, and S. Sakaguchi. Induction of tumor immunity by removing $CD25^+$ $CD4^+$ t-cells : A common basis between tumor immunity and autoimmunity. *J. Immunol.*, 163 :5211–5218, 1999.

[82] M. J. Smyth, D. I. Godfrey, and J. A. Trapani. A fresh look at tumor immunosurveillance and immunotherapy. *Nat. Immunol.*, 2, 2001.

[83] M. J. Smyth, K. Y. Thia, S. E. Street, E. Cretney, J. A. Trapani, M. Taniguchi, T. Kawano, S. B. Pelikan, N. Y. Crowe, and D. I. Godfrey. Differential tumor surveillance by natural killer (NK) and NKT cells. *Journal of Experimental Medicine*, 191(4) :661–668, 2000.

[84] M. J. Smyth, K. Y. Thia, S. E. Street, D. MacGregor, D. I. Godfrey, and J. A. Trapani. Perforin-mediated cytotoxicity is critical for surveillance of spontaneous lymphoma. *Journal of Experimental Medicine*, 192(5) :755–760, 2000.

[85] O. Sotolongo-Costa, L. M. Molina, D. R. Perez, J. C. Antoranz, and M. C. Reyes. Behavior of tumors under nonstationary therapy. *Physica D : Nonlinear Phenomena*, 178(3-4) :242–253, 2003.

[86] T. H. Stewart. Immune mechanisms and tumor dormancy. *Medicina (B Aires)*, 56(Suppl. 1) :74–82, 1996.

[87] S. E. A. Street, E. Cretney, and M. J. Smyth. Perforin and interferon-γ activities independently control tumor initiation, growth, and metastasis. *Blood*, 97(1) :192–197, 01 2001.

[88] T. Tianhai, O. Sarah, W. James M, and H. Angus. The origins of cancer robustness and evolvability . *Integr. Biol. (Camb)*, 1, 2011.

[89] M. J. Tindall, P. K. Maini, S. L. Porter, and J. P. Armitage. Overview of mathematical approaches used to model bacterial chemotaxis II : Bacterial populations. *Bulletin of Mathematical Biology*, 70(6) :1570–1607, 2008.

[90] M. J. Tindall, S. L. Porter, P. K. Maini, G. Gaglia, and J. P. Armitage. Overview of mathematical approaches used to model bacterial chemotaxis I : The single cell. *Bulletin of Mathematical Biology*, 70(6) :1525–1569, 2008.

[91] A. P. Vicari and C. Caux. Chemokines in cancer. *Cytokine & Growth Factor Reviews*, 13(2) :143 – 154, 2002. Cytokines in Tumor Immunity and Immunotherapy.

[92] N. Vigneron. Human Tumor Antigens and Cancer Immunotherapy. *BioMed Research International*, 2015, 2015.

[93] S. Vijay, I. Hiroaki, B. Allen T., W. J. Michael, S. Paul E., O. Lloyd J., and S. Robert D. IFNgamma and lympohcytes prevent primary tomour development and shape tumour immunogenicity. *Nature*, 410(6832) :1107–1111, 2001.

[94] A. E. Vilgelm and A. Richmond. Chemokins modulate immune surveillance in tumorignesis, metastatsis, and response to immunotherapy. *Frontiers in Immunology*, 10(FEB) :6–8, 2019.

[95] H. Vodopick, E. Rupp, C. Edwards, F. Goswitz, and J. Beauchamp. Spontaneous cyclic leukocytosis and thrombocytosis in chronic granulocytic leukemia. *The New England journal of medicine*, 286(6) :284—290, February 1972.

[96] K. P. Wilkie and P. Hahnfeldt. Tumor–immune dynamics regulated in the microenvironment inform the transient nature of immune-induced tumor dormancy. *Cancer Research*, 73(12) :3534–3544, 2013.

[97] K. P. Wilkie and P. Hahnfeldt. Modeling the dichotomy of the immune response to cancer : Cytotoxic effects and tumor-promoting inflammation. *Bull. Math. Biol.*, 79 :1426–1448, 2017.

CHAPITRE. 2

A size and space structured model describing interactions of tumor cells with immune cells reveals cancer persistent equilibrium states in tumorigenesis

Contents

Abstract : The recent success of immunotherapies for the treatment of cancer has highlighted the importance of the interactions between tumor and immune cells. Mathematical models of tumor growth are needed to faithfully reproduce and predict the spatiotemporal dynamics of tumor growth. In this chapter, we introduce a mathematical model intended to describe by means of a system of partial differential equations the early stages of the interactions between effector immune cells and tumor cells. The model is structured in size and space, and it takes into account the migration of the tumor antigen-specific cytotoxic effector cells to- wards the tumor micro-environment by a chemotactic mechanism. We investigate on numerical grounds the role of the key parameters of the model such as the division and growth rates of the tumor cells, and the conversion and death rates of the immune cells. Our main findings are two-fold. Firstly, the model exhibits a possible control of the tumor growth by the immune response ; nevertheless, the control is not complete in the sense that the asymptotic equilibrium states keep residual tumors and activated immune cells. Secondly, space heterogeneities of the source of immune cells can significantly reduce the efficiency of the control dynamics, making patterns of remission-recurrence appear.

Keywords. Tumor growth. Immune system. Equilibrium phase.

2.1 Introduction

Cancer development is the consequence of an accumulation of mutations that leads to the deregulation of a relatively restricted number of key pathways, enough for tumor formation and progression. Tumors grow not only because of the genetic and epigenetic changes that confer a growth advantage, but also under the control of immune cells within the tumor microenvironment [18, 28]. Experimental and clinical evidences indicate that the immune system plays a critical role in the prevention and the eradication of tumors, see e. g. [18, 23, 43, 53, 54].

The genetic alterations in the tumor trigger the expression of neoantigens and upregulation of ligands of activating natural killer (NK) cell receptors which provides the immune system a basis to engage an immune response. In an efficient anti-tumor immune response, neoantigens are captured by Antigen Presenting Cells (APCs) such as Dendritic Cells (DCs) which activate naive/resting T-cells in secondary lymphoid organs draining the tumor site. As a result, activated and proliferating $CD8^+$ and $CD4^+$ effector T-cells will migrate towards the tumor micro-environment where they can eliminate tumors. This loop is known as the cancer immunity cycle, see [8]. Nonetheless, this cycle is subjected to many impediments. Succinctly, tumor antigens can be treated as self-antigens and lead to the priming of regulatory T-cells responses inhibiting effector responses [51] ; tumor cells can produce inhibitory cytokines such as IL-10 or IL-4 (Interleukin 10 or Interleukin 4) which diminish the inflammation and lead to anergic and tolerant T-cells [32, 45] ; tumors also express proteins such as PD-L1 which can bind to the PD-1 receptors on activated T-cells, inhibiting their cytotoxic activity [33]. Effective immune responses are thus counterbalanced by the activation of a myriad of immunosuppressive strategies [48]. The interactions between tumor cells and the

immune cells rely on highly complex mechanisms, that lead to divide the immune response to cancer into three different phases : elimination, equilibrium, and escape (see Fig. 1.1 and [18]). In this context, the design of an efficient treatment by enhancing the immune response, also called immunotherapy, is challenging.

Mathematical models might help to understand the interplay between tumor growth and the immune response [11, 14, 19, 36, 49]. These models can even be completed in order to also describe and optimize the action of chemotherapy treatments and strategies to boost immune responses [2, 56]. However, most of these models are based on quite sophisticated ordinary differential equations (ODEs) systems, and do not take into account space heterogeneities, and the displacement capabilities of the immune cells. Many models also do not consider in details the uncontrolled cellular division at the origin of the tumor growth. These are the questions we address, by proposing a description based on size and space structured interacting cell populations. In this model, more specifically intended to describe the early stages of the tumor growth, the displacement of the immune cells is governed by chemotaxis, according to signals emitted by the tumor. The construction of the coupled partial differential equations (PDEs) system is based on a set of modeling assumptions, detailed in Section 2.2.1 below. These simplifying assumptions can be questionable, but they are intended to keep the most relevant mechanisms with a system of equations as simple as possible. The modeling discussion is particularly driven by the following concerns : (1) to have at hand a model affordable for numerical simulation without a too important computational cost, (2) to reduce the number of parameters : considering more intricate phenomena would require to introduce further parameters, but their role can make the discussion more obscure, due to a lack of knowledge of their effective value, and difficulty in having access to measurements [20].

The chapter is organized as follows. In Section 2.2.1, we collect the modeling assumptions and in Section 2.2.2 we set up the model, which couples a convection-diffusion equation for the immune cells to a growth-fragmentation equation for the tumor cells. An overview of the main questions that are addressed with the model can be find in Section 2.2.3. Section 2.2.4 presents the mathematical insights on the equations, bringing out the capability of controlling the tumor growth, through an interpretation by means of identification of eigen-elements. The main result means that the tumor stops expanding, but it does not disappear entirely : a cancer-persistent equilibrium is reached between the tumor and the immune system, a phenomenon which has been clinically observed [9, 18, 37]. The theoretical statement assumes certain technical conditions, say on the smallness of the rate of tumor cell division, but we are not able to decide whether or not this technical restriction is necessary. Next, we investigate the features of the model on numerical grounds in Section 2.3. We check numerically the ability of the immune system to control tumor growth, in agreement with the theoretical result. We pay a specific attention in identifying the leading parameters that govern the immune response efficiency, which could be important to guide therapeutic strategies. Our simulations also reveal the importance of space-structuration : space heterogeneities of the sources of naive immune cells, that provide, once activated, the tumor-specific cytotoxic effector cells eliminating the tumor, dramatically influences the immune response efficiency. Replacing the homogeneous distribution of immune cells by a few spots makes the immune response less efficient. Instead of the control of the tumor, that would be kept at a fixed mass, what we can observe is a periodic succession of rapid growth and remission phases.

2.2 Mathematical model

2.2.1 Modeling assumptions

We take into account two populations of interacting cells :

— the tumor antigen-specific cytotoxic effector cells including $CD8^+$ T-cells and natural killer (NK) cells,

— the tumor cells.

The specific biological assumptions we consider to construct the model are based on the behavior of the effector cells in the micro-environment of a growing tumor and on the key phenomena governing tumor cell growth :

A.1 environmental constraints such as nutrient concentrations, temperature, etc. are assumed to be constant ;

A.2 the states of the tumor cells are characterized by their size (or, equivalently, their volume or their mass) ;

A.3 the growth rate of a tumor cell is a deterministic process : in absence of an immune response, each tumor cell grows with a certain rate which might depend on its size ;

A.4 when a tumor cell reaches a certain size, the so-called "fission size", it divides into daughter cells, usually two identical cells, at a certain rate ;

A.5 each tumor cell induces a signal, for instance of chemical nature, which is related to the tumor antigenicity : the higher the mass of the tumor and the higher the antigenicity, the higher the amplitude of the signal ;

A.6 the tumor antigen-specific $CD8^+$ T-cells are recruited and activated by APCs and the NK cells are recruited and activated by tumor cells from a bath of non-activated immune cells ; the recruitment is characterized by a certain rate driven by the presence of tumor cells ;

A.7 the activated tumor antigen-specific $CD8^+$ T-cells and the NK cells migrate towards the tumor micro-environment by chemotaxis : they follow the gradient of a potential induced by the overall tumor-derived signals ;

A.8 activated tumor antigen-specific $CD8^+$ T-cells and NK cells which reach the tumor induce the death of the targeted tumor cells ;

A.9 the tumor microenvironment is not immunosuppressive.

Let us discuss these assumptions, with possible hints for future developments of the modeling :

— assumption **A.1** makes sense as far as we model very early stages of tumor development. For the same reason, hypoxia effects are neglected.

— assumption **A.2** is quite restrictive. As it will be detailed below, we completely neglect any geometrical effect. It is likely that such a modeling only makes sense in the early stages of the tumor growth, when the size of the tumor remains small. Reasoning with the size of the cell is convenient to guide the intuition, but we can similarly work by characterizing the cells by the amount of cyclin complexes they contain ; this leads to the same kind of

equations, see [4, 5]. Moreover, many other factors can be relevant to characterize the state of a tumor cell : mutation rate, weight, age and access to nutrients, etc. It would be possible to incorporate more degrees of freedom, but it would also raise the issue of the access to the corresponding governing parameters. For this reason, it is unclear that incorporating further details will make the model more accurate.

— assumption **A.3** can be modified by introducing some stochasticity in the growth process.

— similar considerations apply to assumption **A.4**, which can take into account random effects, or depend on further variables.

— assumptions **A.5**, **A.6** and **A.9** are restrictive too : the model is set to be in the most favorable situation to eliminate tumors but other immune cells are also involved. An important role is played by activated $CD4^+$ T cells, mostly by the IFN-γ they secrete. $CD4^+$ T-cells participate to the activation of NK cells and $CD8^+$ T-cells. But, if on the one hand the activated $CD4^+$ T-cells are stimulating the proliferation of $CD8^+$ effector T-cells, on the other hand, they can be converted into regulatory T-cells and thus limit antitumor immunity. Consequently, the immune system not only act to suppress tumor growth, but it has both stimulatory and inhibitory effects and it might fail in controlling some growing tumors, due to immunosuppressive mechanisms triggered by the tumor [9, 48, 57]. The modeling of such immunosuppressive mechanisms is addressed in the chapter 4. Moreover, as the tumor grow, it itself becomes more heterogeneous under the mutation dynamics, which, in turn, activates various cytotoxic responses.

2.2.2 Construction of the model

The model uses two distinct length scales :

— the length scale of the displacement of the immune cells. Let us denote $[L]$ the corresponding unit (typically in mm). Immune cells thus occupy a certain position, denoted by x and measured with $[L]$.

— the length scale of the tumor cells. Let us denote $[l]$ its unit (typically in μm). Tumor cells have a certain volume, hereafter denoted by z, measured with the unit $[l]^3$ (typically μm^3).

This modeling assumes that the length scale associated to the displacement of the immune cells is "infinitely large" compared to the length scale associated to the size of the tumor cells. It is consistent with the fact that we neglect any effects due to the geometry of the tumor, which is not sensitive at the scale of the displacement of the immune cells. The interactions between the tumor and the immune system are described by the evolution of the following unknowns :

Tumor cell density. The population of tumor cells is structured by the volume variable : $(t, z) \mapsto n(t, z)$ stands for the volumic density of tumor cells. Let $[cell_n]$ denote the unit measuring the number of tumor cells. The density n is then measured in $[cell_n] \cdot [l]^{-3}$. Given two volumes $z_2 > z_1 > 0$, the integral $\int_{z_1}^{z_2} n(t, z)\,\mathrm{d}z$ gives the number of tumor cells having a volume in the interval $[z_1, z_2]$ at time t.

The cytotoxic effector cell concentration. We denote $(t,x) \mapsto c(t,x)$ the concentration of immune cells that are actively fighting against the tumor (it thus includes $CD8^+$ T-cells and NK cells) at time t and position x. Let $[cell_c]$ be the unit measuring the number of immune cells. Then c is measured in $[cell_c] \cdot [L]^{-3}$. (We will perform the simulations by restricting to the two dimensional framework, assuming homogeneity in the third direction; the necessary adaptation are left to the reader.)

The tumor growth and division

At the macroscopic scale, the tumor is seen as a punctual mass, located, say, at the center of the region of interest ($x = 0$). The model can be easily extended to take into account multiple tumor sites. Tumor cells proliferate in an uncontrolled manner due to a loss of checkpoints of the cell cycle and they proliferate massively by staying in the mitosis phase of the cell cycle. Neglecting for the time being the interaction with the cytotoxic cells, the evolution of the tumor results from two phenomena : a natural growth and the division of mature tumor cells into daughter cells.

Let $z \mapsto V(z) \geq 0$ be the natural, possibly size-dependent, growth rate of the tumor cells. With the time variable t measured in $[t]$ (typically in day), V is measured in $[l]^3 \cdot [t]^{-1}$. At the early stages of tumor growth, see assumption **A.1**, V can be assumed constant. More intricate growth laws are presented in Appendix, section 2.5.1.

The cell division mechanism is embodied into an operator

$$Q(n)(t,z) = -a(z)n(t,z) + \int_z^\infty a(z')k(z|z')n(t,z')\,\mathrm{d}z'. \tag{2.1}$$

where the gain term accounts for cells with size z produced by the division of larger cells, and the loss term is related to the division of cells with size z. The division process is governed by two quantities : the frequency $a(z')$ of division of cells having size z', thus measured in $[t]^{-1}$, and the distribution in size $k(z|z')$ of products from the division of a tumor cell with size z'. It is likely that the parameter of the division process depends on the size variable. For instance, division frequency might vanish for the smallest cells, which means $a(z) = 0$ for $0 \leq z \leq z_0$, and then be a non decreasing function of the size. The kernel k satisfies the fundamental identity [40]

$$\int_0^z z'k(z'|z)\,\mathrm{d}z' = z. \tag{2.2}$$

It implies the following mass conservation property

$$\int_0^\infty zQ(n)(t,z)\,\mathrm{d}z = -\int_0^\infty za(z)n(t,z)\,\mathrm{d}z + \int_0^\infty a(z')\left(\int_0^{z'} zk(z|z')\,\mathrm{d}z\right)n(t,z')\,\mathrm{d}z' = 0.$$

For further purposes, let us introduce the expected number of cells with size z, defined by

$$\bar{\mathcal{N}}(z) = \int_0^z k(z'|z)\,\mathrm{d}z'. \tag{2.3}$$

It is supposed to be larger to 1. Then, cell division changes the total number of cells by an amount given by

$$\int_0^\infty Q(n)(t,z)\,\mathrm{d}z = \int_0^\infty (\bar{\mathcal{N}}(z) - 1)a(z)n(t,z)\,\mathrm{d}z \geq 0.$$

Finally, the evolution of the population of tumor cells is driven by the PDE

$$\frac{\partial}{\partial t}n(t,z) + \frac{\partial}{\partial z}(V(z)n(t,z)) = Q(n)(t,z). \tag{2.4}$$

referred to as a growth-fragmentation equation [40]. This type of integro-differential equation is quite common in material science and in biology [16, 17, 26, 46] ; see also for specific applications to tumor growth, possibly taking into account several compartments, [4, 5]. Equation (2.4) is completed by the initial distribution of tumor cells

$$n|_{t=0} = n_0, \tag{2.5}$$

and a boundary condition. Hereafter, we assume that the size variable ranges over the whole interval $(0, +\infty)$, and the boundary condition excludes the creation of cells with volume 0 :

$$n(t,0) = 0. \tag{2.6}$$

Division and growth can be seen as competing mechanisms : the latter increases the size of the cells, while the break-up described by the former creates new smaller cells from the large ones. This can be understood by considering the evolution of the total number of tumor cells in the tumor $\mu_0(t)$ and the total volume of the tumor $\mu_1(t)$, respectively given by

$$\mu_0(t) = \int_0^\infty n(t,z)\,\mathrm{d}z, \qquad \mu_1(t) = \int_0^\infty zn(t,z)\,\mathrm{d}z. \tag{2.7}$$

Integrating (2.4) and using the boundary condition (2.6) yields

$$\frac{\mathrm{d}}{\mathrm{d}t}\mu_0(t) = \int_0^\infty (\bar{\mathcal{N}}(z) - 1)a(z)n(t,z)\,\mathrm{d}z \geq 0, \tag{2.8}$$

and

$$\frac{\mathrm{d}}{\mathrm{d}t}\mu_1(t) = \int_0^\infty V(z)n(t,z)\,\mathrm{d}z \geq 0. \tag{2.9}$$

Equation (2.8) tells us that the total number of cells in the tumor increases due to cellular division processes. However, division does not influence the total volume of the tumor : we see with equation (2.9) that the increase of the total volume of the tumor is only due to the growth rate $V > 0$. We refer the reader to Appendix, section 2.5.2 (Table 2.2) for details about units and parameters for the tumor growth model.

Binary Division. A relevant example is provided by the case of binary division, where a cell with volume z splits into two cells, with respective volumes αz and $(1-\alpha)z$, $\alpha \in (0, 1/2]$ being a division parameter. The corresponding kernel reads

$$k(z'|z) = \frac{1}{\alpha}\delta_{z'=\frac{z}{\alpha}} + \frac{1}{(1-\alpha)}\delta_{z'=\frac{z}{1-\alpha}}$$

and the division operator becomes

$$Q(n)(t,z) = -a(z)n(t,z) + \frac{1}{\alpha}a\Big(\frac{z}{\alpha}\Big)n\Big(t,\frac{z}{\alpha}\Big) + \frac{1}{1-\alpha}a\Big(\frac{z}{1-\alpha}\Big)n\Big(t,\frac{z}{1-\alpha}\Big). \tag{2.10}$$

Assuming the symmetry of the division process imposes $\alpha = 1/2$ in (2.10), and the division operator is given by

$$Q(n)(t,z) = 4a(2z)n(t,2z) - a(z)n(t,z). \tag{2.11}$$

Further relevant examples of division kernels can be found in [17].

Evolution of the cytotoxic effector cell population

The immune cells occupy the space domain $\Omega \subset \mathbb{R}^3$. The evolution of the tumor antigen-specific cytotoxic effector cell population is driven by the mass balance principle, which leads to the local balance law

$$\partial_t c + \nabla \cdot J = \mathcal{S}.$$

Gains and losses of cytotoxic effector cells result from two phenomena, which shape the expression of the flux J and the source $\mathcal{S}$:

- activated cytotoxic NK and T-cells, which can eliminate tumor cells, are extracted from a bath of non-activated immune cells. According to assumption **A.6**, the conversion of these immune cells into tumor antigen-specific effector cells depends on the mass of the tumor cells, the quantity we have already denoted $\mu_1(t)$. The description of the recruitment process involves
  - $(t,x) \mapsto S(t,x)$, the space distribution of the source of immune cells (measured in $[cell_c] \cdot [L]^{-3}$). We shall observe different behaviors of the system depending whether the source S is constant or space-inhomogeneous.
  - p, the, possibly space-dependent, rate at which NK and T-cells are activated (measured in $[t]^{-1}$). It takes into account the antigenicity of the tumor cells.
  - a dimensionless factor $\mu_1 \mapsto g(\mu_1)$ that describes how the presence of tumor cells stimulates the production of new effector cells and the conversion of immune cells into effector cells or their recruitment. Hence, we naturally have $g(0) = 0$. Since we are treating early stages of tumor growth, we can use a mere linear relation. However, it can be relevant for longer term interaction to impose a threshold on the recruitment process [57]. Such a saturation effect is usually taken into account with a Michaelis-Menten law [11, 38, 36], which leads to

    $$g(\mu_1) = \frac{\mu_1}{\beta + \mu_1}, \tag{2.12}$$

    where β is the steepness coefficient of the immune cell recruitment, measured in $[cell_n]$ like μ_1.
- the tumor antigen-specific cytotoxic effector cells die at a certain rate, denoted by γ. This rate can be space-dependent, or μ_1-dependent; it is measured in $[t]^{-1}$. In what follows, we will always assume that $\gamma > 0$ is constant.

Therefore, we get

$$\mathcal{S} = g(\mu_1)pS - \gamma c.$$

We turn to the description of the tumor antigen-specific cytotoxic effector cells displacement. The motion of the cytotoxic effector cells results from two distinct phenomena :

— a natural diffusion that makes the population of activated immune cells spread in the whole domain. It is characterized by the diffusion coefficient $x \mapsto D(x)$, measured in $[L]^2 \cdot [t]^{-1}$. It can be space dependent and matrix-valued, in order to describe for instance different tissues or tissues where the displacement is easier in certain directions than in others. The details of the migration process can play a critical role in the anti-tumor immune surveillance. For instance in [50], it is reported that the fibers of the extracellular matrix control the trajectories of the cytotoxic effector cells in human lung tumors and the geometrical effects can restrict the amount of these cells infiltrating the tumor.

— a displacement towards the tumor governed by the tumor cells antigenicity : according to assumptions **A.5** and **A.7**, the activated NK and T-cells follow the gradient of a potential, that we denote $\phi(t,x)$, induced by the tumor antigens. The directed movement of the NK and T-cells in response to the signal induced by the tumor is conditioned by the sensitivity of their membrane receptor, embodied into a factor denoted χ. It might be possible to assume that χ depends on the attractive potential ϕ, for instance to model the fact that cells do not detect signals that are too weak or too high. We can find more details about such chemotactic mechanisms in [29, 30, 31, 35] ; the role of such effects in the immune response to tumor growth is already pointed out in [39].

Gathering these information, we have

$$J = \underbrace{c\chi\nabla_x\phi}_{\text{convection by chemotaxis}} - \underbrace{D\nabla_x c}_{\text{diffusion}}, \tag{2.13}$$

where the chemotactic velocity $\chi\nabla_x\phi$ is measured in $[L] \cdot [t]^{-1}$.

Finally, the concentration of tumor antigen-specific cytotoxic effector cells obeys the PDE

$$\partial_t c + \nabla_x \cdot (c\chi\nabla_x\phi - D\nabla_x c) = g(\mu_1)pS - \gamma c. \tag{2.14}$$

It is endowed by the initial data

$$c\big|_{t=0} = c_0, \tag{2.15}$$

and the homogeneous Dirichlet condition

$$c\big|_{\partial\Omega} = 0, \tag{2.16}$$

which means that the immune cells far from the tumor are non-activated.

The tumor-induced attractive potential

The attractive potential ϕ is induced by the presence of tumor cells. Every tumor cell with size z produces a certain chemical signal, according to a form function $\sigma(x,z)$. Having in mind the chemical nature of the signal, the attractive potential can be measured in number of chemoattractant molecules, with a unit denoted by $[mol]$. Accordingly, the coefficient χ will be measured in $[L]^2 \cdot [t]^{-1} \cdot [mol]$ and σ in $[mol] \cdot [cell_n]^{-1} \cdot [l]^{-3}[t]^{-1}$. The chemoattractant molecules are subjected to a natural diffusion, depending on a coefficient $\mathcal{K}$ (measured in $[L]^2 \cdot [t]^{-1}$). We

can simply assume that $\mathcal{K} > 0$ is a scalar constant, but it could be a matrix-valued function of the space variable as well. The source of the attractive potential is given by the sum of all the chemical contributions of the tumor cells, which leads to the equation

$$-\nabla \cdot (\mathcal{K}\nabla\phi)(x) = \int_0^\infty zn(t,z)\sigma(x,z)\,\mathrm{d}z, \tag{2.17}$$

with a given matrix-valued function $x \in \Omega \mapsto \mathcal{K}(x)$ (verifying $0 < \kappa_\star \leq \mathcal{K}(x)\xi \cdot \xi \leq \kappa^\star < \infty$ for any $x \in \Omega$, $\xi \in \mathbb{S}^2$). If the form function σ does not depend on the size variable, this becomes

$$-\nabla \cdot (\mathcal{K}\nabla\phi)(x) = \sigma(x)\mu_1(t). \tag{2.18}$$

The equation is set on the domain Ω and needs to be completed by boundary conditions. We can choose Dirichlet boundary conditions $\phi|_{\partial\Omega} = 0$. However, it is more relevant to consider instead the homogeneous Neumann condition, which tells us that the flux of chemoattractant vanishes on the boundaries of the domain

$$\mathcal{K}\nabla_x\phi \cdot \nu|_{\partial\Omega} = 0. \tag{2.19}$$

In this case, (2.17), or (2.18), is not consistent with the boundary condition : the right hand side should be replaced by

$$\int_0^\infty zn(t,z)\sigma(x,z)\,\mathrm{d}z - \frac{1}{|\Omega|}\int_\Omega\int_0^\infty zn(t,z)\sigma(x,z)\,\mathrm{d}z\,\mathrm{d}x$$

the mean of which vanishes.

Effect of the immune system on the tumor

According to assumption **A.8**, when the tumor antigen-specific cytotoxic effector cells reach the tumor micro-environment, they release cytotoxic substances which eventually leads to the death of the tumor cells. This effect is described by adding a death term in the tumor growth model (2.4), which becomes

$$\partial_t n + \partial_z(Vn) = Q(n) - m(c,n). \tag{2.20}$$

It is natural to suppose that $m(c,n)$ vanishes if either c or n vanishes. The expression of the death term involves a non negative space-dependent weight $x \mapsto \delta(x)$, measured in $[cell_n] \cdot [cell_c]^{-1} \cdot [t]^{-1} \cdot [l]^{-3}$, which incorporates both the strength of the immune response and a radius of interaction. This weight might equally depend on the tumor volume $t \mapsto \mu_1(t)$. Inspired from [36] the death term can be modeled by Michealis-Menten kinetics :

$$m(c,n)(t,z) = \int_\Omega \delta(y)c(t,y)\,\mathrm{d}y \times \frac{1}{\alpha} \times \frac{n(t,z)}{1+\alpha' n(t,z)}, \tag{2.21}$$

with $\alpha, \alpha' > 0$, but we shall also work with a linear expression (which amounts to set $\alpha' = 0$). Further details on the units of the parameters of the equations can be found in Appendix, section 2.5.2 (Table 2.3).

2.2.3 Summary and workplan

The general interaction model we are dealing with thus reads

$$\begin{cases} \partial_t n + \partial_z(Vn) = Q(n) - m(c,n), & \text{for } t \geq 0,\ z \geq 0, \\ \partial_t c + \nabla_x \cdot (c\chi\nabla_x\phi - D\nabla_x c) = pg(\mu_1)S - \gamma c, & \text{for } t \geq 0,\ x \in \Omega, \\ -\nabla \cdot (\mathcal{K}\nabla\phi) = \int_0^\infty zn(t,z)\sigma(x,z)\,\mathrm{d}z & \\ \qquad\qquad -\frac{1}{|\Omega|}\int_\Omega \int_0^\infty zn(t,z)\sigma(x,z)\,\mathrm{d}z\,\mathrm{d}x, & \text{for } t \geq 0,\ x \in \Omega, \\ n(t,0) = 0, & \text{for } t \geq 0, \\ n(t=0,z) = n_0(z), & \text{for } z \geq 0, \\ c(t,x) = 0, & \text{for } x \in \partial\Omega, \\ c(t=0,x) = c_0(x), & \text{for } x \in \Omega, \\ \mathcal{K}\nabla\phi \cdot \nu = 0, & \text{for } x \in \partial\Omega. \end{cases} \tag{2.22}$$

We remind the reader that the cell division operator $Q(n)$ and the immune cell-tumor interaction term $m(c,n)$ are defined in (2.1) and (2.21) respectively. We refer the reader to Tables 2.2 and 2.3 where the biological meaning of the unknowns and of the parameters is recapitulated.
We shall see that the model (2.22) is able to reproduce equilibrium states, where the tumor and the effector cells are in a dynamic balance, and we will provide a mathematical justification of this fact (see Theorem 2.2.2 below). In the equilibrium phase, as pointed out in [18], tumor cell proliferation appears to be controlled by the immune system and we address on numerical grounds the effects that influence this control. In particular, the mass of the residual tumor and the speed of convergence to the equilibrium state can vary significantly with the parameters of the model. Accordingly, we particularly challenge the following effects :

— dealing with a space-structured model gives access to new phenomena : we will compare the homogeneous distribution of the source of naive immune cells to the case where the cells are heterogeneously distributed at a certain distance of the micro-environment of the tumor.

— it is important to determine how the parameters influence the dynamics, not only through their strength, but also depending whether or not they depend on the size or space variables : On the one hand, the aggressiveness of the tumor can be tested by acting on the growth rate V and on the division rate a of the tumor cells. On the other hand, the efficiency of the host immune system depends on the activation rate p, the death rate γ, the immune strength δ and the migration of NK and T-cells towards the tumor microenvironment. Note also that immunotherapy can modify these parameters, for instance by improving tumor elimination through increasing cytotoxic strength (that can be achieved by acting on anti-immune checkpoint like PD-1) [57], by fostering T-cells enrichment, as a consequence of the depletion of $\mathrm{Gr1}^+$ cells, or by blocking myeloid suppressor cell recruitment to the tumor site [22, 27, 34].

— as said above, saturation effects can be taken into account in both the conversion process of immune cells into tumor antigen-specific cytotoxic effector cells and the death of tumor cells by these cytotoxic cells. We will discuss the role of these saturation effects on the dynamics, comparing the saturated and non-saturated models in Appendix, section 2.5.4.

2.2.4 A few mathematical comments

This Section aims at providing at intuition on the behavior of the solutions of (2.22), based on mathematical arguments. First, with some simplifying assumptions, the equations can be reduced to a mere ODEs system, which admits stationary solutions. The stability analysis helps in understanding the role of the parameters of the model. Second, by means of eigen-elements of the cell division equation, we identify a scenario which reproduces the equilibrium phase of the tumor-immune interaction [18].

A simplified model : damping and oscillations

Under some restrictive assumptions, we can obtain a closed set of ODEs by integrating (2.22) oer the size and space variables. This (oversimplified) situation shed some light on the role of the parameters. Let us consider the very specific case where

— the source S of immune cell is constant,

— all parameters V, δ, p, $\mathcal{K}$ are constant,

— σ does not depend on the size variable,

— the interactions are non saturated : $m(c,n) = \delta n \int_\Omega c\,\mathrm{d}y$, and $g(\mu_1) = \mu_1$,

— we consider the binary division model, as described in (2.11), with a constant frequency a.

Moreover, we replace the homogeneous Dirichlet boundary condition (2.16) for the NK and T-cells by the Neumann boundary condition

$$\nabla c \cdot \nu\big|_{\partial\Omega} = 0. \tag{2.23}$$

These assumptions clearly lack of biological relevance. For instance, assuming that a and δ are constant means that any tumor cell has the same division rate a, irrespective of its size, and any effector cell acts the same way on the tumor, irrespective of its position in the domain Ω. The resulting model reads

$$\begin{cases} \big(\partial_t n + \partial_z(Vn)\big)(t,z) = -an(t,z) + 4an(t,2z) - \delta n(t,z)\int_\Omega c(t,y)\,\mathrm{d}y, \\ \partial_t c + \nabla_x \cdot (c\chi\nabla_x\phi - D\nabla_x c) = p\mu_1 S - \gamma c, \\ -\mathcal{K}\Delta_x\phi = \mu_1\langle\sigma\rangle, \\ n(t=0,z) = n_0(z),\ c(t=0,x) = c_0(x), \\ n(t,0) = 0,\ \nabla_x c\cdot\nu(t,\cdot)\big|_{\partial\Omega} = 0,\ \nabla_x\phi\cdot\nu(t,\cdot)\big|_{\partial\Omega} = 0, \end{cases} \tag{2.24}$$

where we use the shorthand notation $\langle\sigma\rangle = \sigma - \frac{1}{|\Omega|}\int_\Omega \sigma \,\mathrm{d}x$. As simple as it appears, this model can provide useful hints on the qualitative features of the original PDEs system. In this simple framework, the dynamics can be understood by considering a reduced system of ODEs. Indeed, we obtain a closed system of equations for μ_0, μ_1, given by (2.7), and the total number of active immune cells

$$\mu_c(t) = \int_\Omega c(t,x)\,\mathrm{d}x.$$

We get

$$\begin{cases} \frac{\mathrm{d}}{\mathrm{d}t}\mu_0 = \mu_0\left(a - \delta\mu_c\right), \\ \frac{\mathrm{d}}{\mathrm{d}t}\mu_1 = V\mu_0 - \delta\mu_1\mu_c, \\ \frac{\mathrm{d}}{\mathrm{d}t}\mu_c = \pi pS\mu_1 - \gamma\mu_c. \end{cases} \tag{2.25}$$

The states

$$\begin{pmatrix}\mu_0^H\\ \mu_1^H\\ \mu_c^H\end{pmatrix} = \begin{pmatrix}0\\0\\0\end{pmatrix}, \qquad \begin{pmatrix}\mu_0^{UH}\\ \mu_1^{UH}\\ \mu_c^{UH}\end{pmatrix} = \begin{pmatrix}\frac{\gamma a^2}{\pi\delta VpS}\\ \frac{\gamma a}{\pi\delta pS}\\ \frac{a}{\delta}\end{pmatrix}$$

are equilibrium solutions of (2.25). The former corresponds to an healthy state, the latter to a stationary state with residual tumors and immune cells. For the unhealthy state, the more important the bath of immune cells or the recruitment probability, the lesser the tumor mass; the more agressive the tumor (with a higher division rate a) or the weaker the immune system, the higher the tumor mass.

The Jacobian matrix evaluated at the equilibrium points reads

$$J^H = \begin{pmatrix} a & 0 & 0\\ V & 0 & 0\\ 0 & \pi pS & -\gamma\end{pmatrix}, \qquad J^{UH} = \begin{pmatrix} 0 & 0 & -\frac{\gamma a^2}{\pi VpS}\\ V & -a & -\frac{\gamma a}{\pi pS}\\ 0 & \pi pS & -\gamma\end{pmatrix},$$

respectively. Therefore, as far as the cell division is active ($a > 0$), J^H has a positive eigenvalue and the healthy state is unstable. For the unhealthy state, the characteristic polynomial is $p(\lambda) = -\lambda^3 - (a+\gamma)\lambda^2 - 2a\gamma\lambda - \gamma a^2$. We distinguish two cases, driven by the ratio $\frac{\gamma}{a}$ ($=\frac{\text{death rate of immune cells}}{\text{tumor cells division rate}}$)

— if $\gamma > 4a$, the eigenvalues are real; they are given by

$$\lambda_1 = -a, \quad \lambda_2 = \frac{1}{2}\left(-\sqrt{\gamma(\gamma-4a)} - \gamma\right), \quad \lambda_3 = \frac{1}{2}\left(\sqrt{\gamma(\gamma-4a)} - \gamma\right),$$

and they are all negative.

— if $\gamma < 4a$, the eigenvalues have an imaginary part :

$$\lambda_1 = -a, \quad \lambda_2 = \frac{1}{2}\left(-i\sqrt{\gamma(4a-\gamma)} - \gamma\right), \quad \lambda_3 = \frac{1}{2}\left(i\sqrt{\gamma(4a-\gamma)} - \gamma\right),$$

but all the real parts are negative : $\lambda_1 < 0$, $\mathrm{Re}(\lambda_2) = \mathrm{Re}(\lambda_3) = -\frac{\gamma}{2} < 0$.

Therefore, the unhealthy state is always stable. The asymptotic behavior of the solution depends only the ratio γ/a : $\gamma = 4a$ is a threshold between a purely damped behavior, see Fig. 2.1 and 2.2-(a), (b), (c), and an oscillatory behavior (the greater the cell division, the faster the oscillations), see Fig. 2.1 and 2.2-(d), (e), (f). These oscillations thus appear when the tumor is more aggressive, while the damping rate is driven by the immune efficiency.

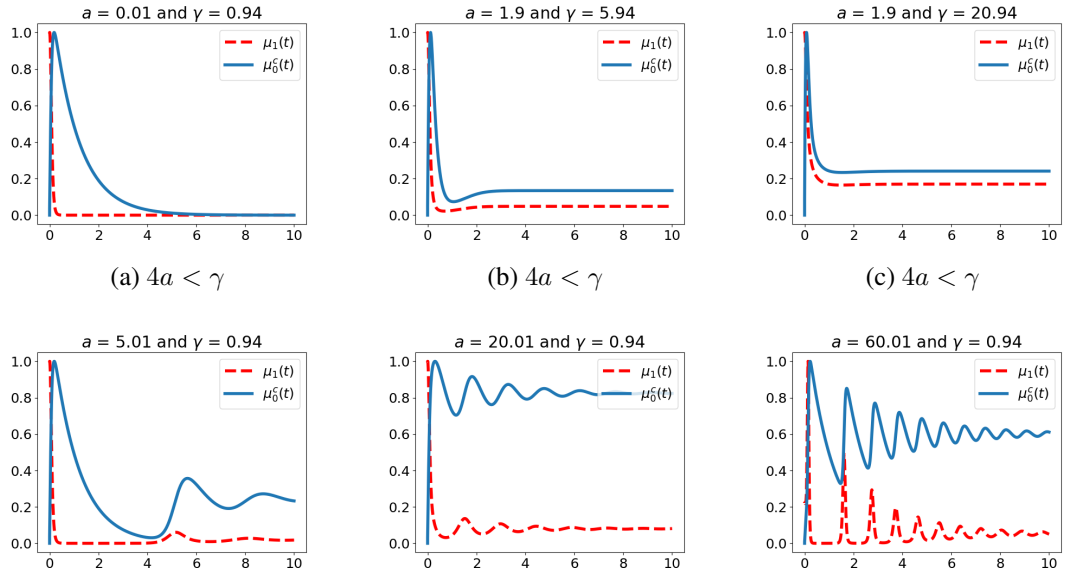

(a) $4a < \gamma$ (b) $4a < \gamma$ (c) $4a < \gamma$

(d) $4a > \gamma$ (e) $4a > \gamma$ (f) $4a > \gamma$

FIGURE 2.1 – Typical behavior of the solutions of (2.25). The data are : $V = 0.616$, $\delta = 0.5$, $p = 4.66$, $S = 6.38$ (x-axis : time, y-axis : μ_1, mass of the tumor, and μ_c, the total number of active immune cells).

Existence of equilibrium phases

Let us go back to the growth-fragmentation equation (2.4), with a general division process described by (2.1), with possibly size-dependent division frequency $z \mapsto a(z)$ and growth rate $z \mapsto V(z)$, respectively, neglecting for a while the immune response. The large time behavior of the cell division equation is described by means of eigen-elements of the transport-division operator. Namely, we seek a positive function $z \geq 0 \mapsto N(z) \geq 0$ and a positive number $\lambda > 0$ such that

$$\begin{cases} \partial_z(VN) - Q(N) + \lambda N = 0 & \text{for } z \geq 0 \\ N(0) = 0, \qquad N(z) > 0 & \text{for } z > 0, \qquad \int_0^{+\infty} N(z)\,\mathrm{d}z = 1. \end{cases} \tag{2.26}$$

The analysis of this eigen-problem requires some technical assumptions. For instance, when the growth rate V is constant, we suppose :

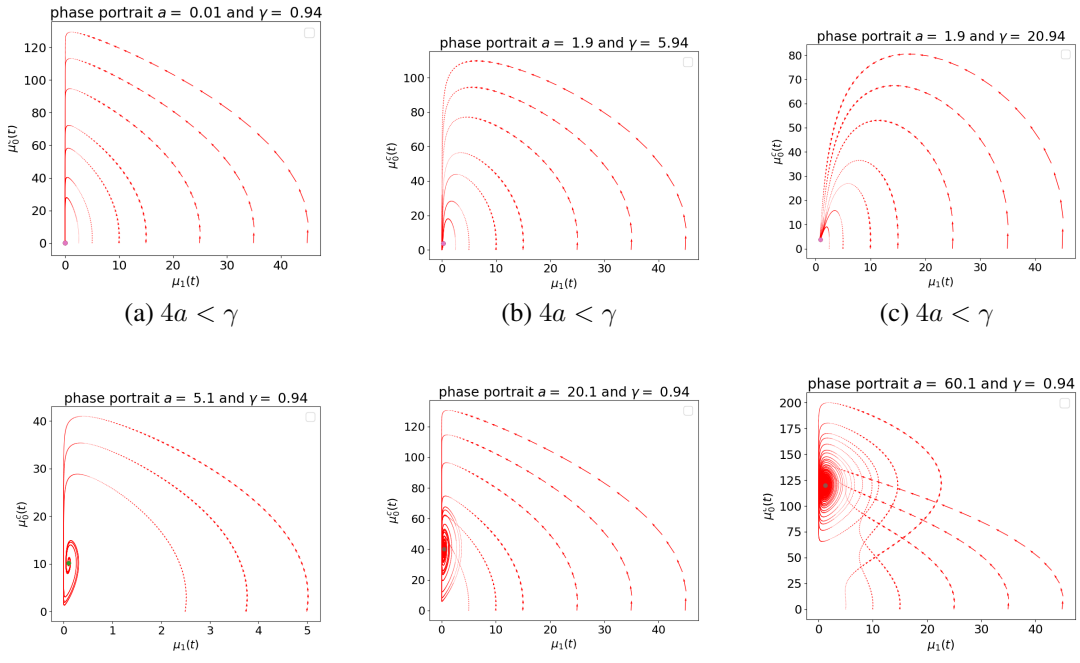

(a) $4a < \gamma$ (b) $4a < \gamma$ (c) $4a < \gamma$

(d) $4a > \gamma$ (e) $4a > \gamma$ (f) $4a > \gamma$

FIGURE 2.2 – Typical phase portraits (μ_1, μ_c) of (2.25) for different initial tumor mass. The data are : $V = 0.616$, $\delta = 0.5$, $p = 4.66$, $S = 6.38$

(H1) $a \in L^\infty((0,\infty))$ and there exists $z_\star \geq 0$, $\alpha^\star \geq \alpha_\star > 0$ such that $0 \leq a(z) \leq \alpha^\star$ for any $z \geq 0$, $0 < \alpha_\star \leq a(z)$ for any $z \geq z_\star$,

(H2) $k(z|z') \geq 0$, $k(z|z') = 0$ when $z' < z$ and $\int_0^\infty z k(z|z')\,\mathrm{d}z = z'$.

These assumptions ensure the existence-uniqueness of the eigenpair (λ, N), satisfying (2.26), see [41] and the textbook [46, Theorem 4.6] which indicates further connections with the renewal equation. The case where the growth rate V is non-constant is addressed in [17] ; the assumptions necessary for the analysis are collected in Appendix, section 2.5.1. Then, it can be shown that $n(t,z)$ behaves as time becomes large like $e^{\lambda t}\rho N(z)$, where $\rho > 0$ is entirely determined by the initial condition n_0 : see [42] where this result is established by using relative entropy techniques (and [13] for a very similar problem arising in tumor growth modeling too).

The precise expression of the eigen-function N is not explicitly known in general. Nevertheless, for the specific kernel of symmetric binary division, see (2.11), with a constant division rate we have detailed information, as shown in [3], see also [47] and [46, Lemma 4.1].

Lemma 2.2.1. *Let Q be defined by (2.11) with a constant division rate $a > 0$. Let V be a positive*

constant. Let $(\alpha_n)_{n\in\mathbb{N}}$ *be the sequence defined by the recursion*

$$\alpha_0 = 1, \qquad \alpha_n = \frac{2}{2^n - 1}\alpha_{n-1}.$$

Then the function

$$N(z) = \bar{N}\sum_{n=0}^{\infty}(-1)^n\alpha_n \exp\left(-2^{n+1}\frac{a}{V}z\right),$$

with $\bar{N} > 0$ *an appropriate normalizing constant, belongs to the Schwartz class* $\mathscr{S}(\mathbb{R}^+)$ *and is the unique solution of* (2.26)*, where* $\lambda = a$*.*

The shape of the profile is governed by the ratio $\frac{a}{V}$ $(= \frac{\text{division rate}}{\text{growth rate}})$, as illustrated by Fig. 2.3 : the smaller the division rate (resp. the higher the growth rate), the more spread the profile. According to the intuition a large growth rate promotes the formation of large tumor, a large division rate favors the proliferation of small cells.

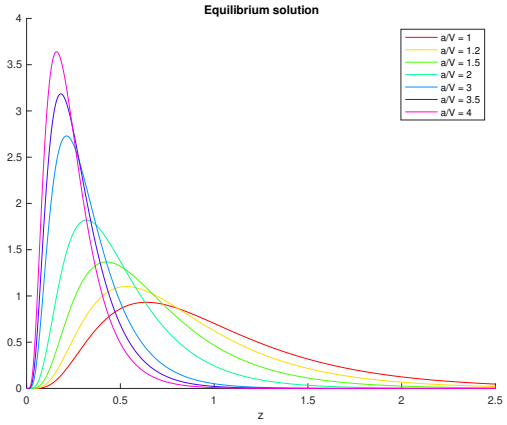

FIGURE 2.3 – Shape of the leading eigen-function of the growth-division equation for several values of $\frac{a}{V}$ (x-axis : z, size of the tumor cells, y-axis : number of tumor cells at the final time)

This (semi-)explicit formula will be used to check numerically the behavior of the coupled problem when it tends to a stationary state. For general fragmentation kernels, we can obtain the following relation : integrating (2.26) over $z \in (0, \infty)$ yields

$$\lambda = \int_0^\infty Q(N)\,\mathrm{d}z = \int_0^\infty (\bar{\mathcal{N}}(z) - 1)a(z)N(z)\,\mathrm{d}z$$

with $\bar{\mathcal{N}}$ defined in (2.3) (which tells us that $\lambda = a$ for (2.11) with a constant division rate). Similarly, considering the first order moment of the equation, we get

$$\lambda = \frac{\int_0^\infty VN(z)\,\mathrm{d}z}{\int_0^\infty zN(z)\,\mathrm{d}z}. \tag{2.27}$$

Now, we turn back to the coupled system (2.22) : these considerations will be crucial to discuss the large time behavior of the system. Precisely, we consider the version where

— there is no saturation in the death rate induced by the interaction,

— σ depends only on the space variable x.

Namely, we have

$$\begin{cases} \partial_t n + \partial_z(Vn) = Q(n) - n\int_\Omega \delta(x)c(t,x)\,\mathrm{d}x \\ \partial_t c + \nabla_x \cdot (\chi c \nabla_x \phi - D\nabla_x c) = pg(\mu_1)S - \gamma c, \\ -\nabla_x \cdot (\mathcal{K}\nabla_x \phi) = \mu_1 \langle \sigma \rangle \\ n(t=0,z) = n_0(z),\ c(t=0,x) = c_0(x) \\ n(t,0) = 0,\ c(t,\cdot)\big|_{\partial\Omega} = 0,\ \mathcal{K}\nabla_x\phi(t,\cdot)\big|_{\partial\Omega} = 0. \end{cases}$$

Here, we assume

— $\mathcal{K}$, D are bounded matrix-valued functions defined on Ω, that verify a uniformly elliptic condition,

— V, a and k are such that (2.26) admits a unique solution,

— $g : [0,\infty) \mapsto [0,\infty)$ is a C^1 increasing function such that $g(0) = 0$,

— $x \mapsto pS(x)$ and $x \mapsto \sigma(x)$ are non negative functions that belong to $L^2(\Omega)$.

We observe in the numerical experiments that in many situations, a non proliferation state can be reached and the integral $\int_\Omega \delta(y)c(t,y)\,\mathrm{d}y$ tends to a constant. We wish to provide a mathematical explanation of this phenomenon, which corresponds to the equilibrium phase clinically observed [9, 18, 37], with residual tumors and active immune cells. A natural candidate for the tumor size-distribution is an equilibrium $\bar{\mu}_0 N(z)$, with N the eigen-function defined by (2.26). Thus, we wish to identify a stationary solution of (2.22) under the form $(\bar{\mu_0} N(z), \bar{C})$. This leads to the relation

$$\underbrace{(\partial_z(V\bar{\mu}_0 N) - Q(\bar{\mu_0}N))(z)}_{=-\lambda\bar{\mu}_0 N(z)} = -\bar{\mu}_0 N(z)\int_\Omega \delta(x)\bar{C}(x)\,\mathrm{d}x.$$

Hence, the concentration of cytotoxic effector cells should satisfy

$$\int_\Omega \delta(x)\bar{C}(x)\,\mathrm{d}x = \lambda,$$

the leading eigenvalue of the (free-)fragmentation equation. This can be checked on the numerical simulations, for the simplified division model (2.11) with a constant division rate $a > 0$, and working with a constant growth rate V : we find that $\int_\Omega \delta(y)c(t,y)\,\mathrm{d}y$ tends to a, and $n(t,z)$ becomes proportional to the profile given in Lemma 2.2.1. Therefore, we expect that the immune system organizes so that the death rate induced by the action of the cytotoxic effector cells counterbalances the natural Malthusian behavior of the cell division equation. That the death rate can, in certain circumstances, reaches the leading eigenvalue of the cell division equation is justified by the following statement.

Theorem 2.2.2. *Let Φ be the solution of*

$$-\nabla_x \cdot (\mathcal{K}\nabla_x \Phi) = \sigma - \frac{1}{|\Omega|}\int_\Omega \sigma(y)\,\mathrm{d}y,$$

endowed with the homogeneous Neumann boundary condition. If $\ell > 0$ is small enough, there exists a unique $\bar{\mu}_1(\ell) > 0$ such that $C_{\bar{\mu}_1(\ell)}$, solution of the stationary equation

$$\gamma C - \nabla_x \cdot (D\nabla_x C) - \bar{\mu}_1 \nabla_x \cdot (C\nabla_x \Phi) = g(\bar{\mu}_1) pS, \qquad C\big|_{\partial\Omega=0} = 0, \tag{2.28}$$

satisfies $\int_\Omega \delta C\,\mathrm{d}x = \ell$.

Proof. We introduce the mapping

$$\mathscr{F} : (\ell, \mu_1) \in [0,\infty) \times [0,\infty) \longmapsto \int_\Omega \delta C_{\mu_1}\,\mathrm{d}x - \ell$$

where C_{μ_1} is the solution of (2.28) associated to μ_1. We are searching for the zeroes of $\mathscr{F}$. Of course $\mathscr{F}(0,0) = 0$, with $C_0 = 0$. Next, we have $\partial_{\mu_1}\mathscr{F}(\ell,\mu_1) = \int_\Omega \delta C'_{\mu_1}\,\mathrm{d}x$, with C'_{μ_1} the solution of

$$\gamma C' - \nabla_x \cdot (D\nabla_x C') - \mu_1 \nabla_x \cdot (C'\nabla_x \Phi) = g'(\mu_1) pS + \nabla_x \cdot (C_{\mu_1}\nabla_x \Phi), \qquad C'\big|_{\partial\Omega=0} = 0.$$

In particular, since $g'(0)pS \neq 0$ is non negative and $C_0 = 0$, the maximum principle for elliptic equations tells us that $C'_0 > 0$. It follows that $\partial_{\mu_1}\mathscr{F}(0,0) = \int_\Omega a C'_0\,\mathrm{d}x > 0$. We can thus apply the implicit function theorem : there exists $\ell_\star > 0$ and a mapping $\bar{\mu}_1 : \ell \in [0,\ell_\star) \mapsto \bar{\mu}_1(\ell)$ such that for any $\mathscr{F}(\ell, \bar{\mu}_1(\ell)) = 0$ holds for any $\ell \in [0,\ell_\star)$. We have

$$\partial_\ell \mathscr{F}(\ell,\bar{\mu}_1(\ell)) + \bar{\mu}_1'(\ell)\partial_{\mu_1}\mathscr{F}(\ell,\bar{\mu}_1(\ell)) = -1 + \bar{\mu}_1'(\ell)\partial_{\mu_1}\mathscr{F}(\ell,\bar{\mu}_1(\ell)) = 0$$

with $\partial_{\mu_1}\mathscr{F}(0,0) > 0$. Hence, $\ell \mapsto \bar{\mu}_1(\ell)$ is increasing on the neighborood of $\ell = 0$, and it thus takes positive values. ∎

We remind the reader that the asymptotic behavior for the tumor population is expected to be described by an eigen-function associated to the leading eigenvalue λ, thus proportional to $z \mapsto N(z)$. Theorem 2.2.2 defines implicitly the corresponding value $\bar{\mu}_1$ of the total mass, and we can find $\bar{\mu}_0$ accordingly (for instance, when V is constant, by going back to (2.27) we get $\lambda = V\frac{\bar{\mu}_0}{\bar{\mu}_1}$). Theorem 2.2.2 applies when the leading eigenvalue is small enough. For the simple binary division model (2.11) with a constant division rate a, according to Lemma 2.2.1, this is a smallness assumption on a. Therefore this statement raises the following questions that will be investigated numerically : (1) is this condition only a technical requirement ? how small should be a to observe a control and what happens as a becomes large ? (2) how μ_1, the total mass of the persistent tumor, behaves with respect to the parameters ? These issues can be interpreted as indicators of the efficiency of the immune response. In the next chapter, we investigate how this approach permits us to compute *a priori* the equilibrium state and the mass of the residual tumor that can be predicted for a given set of parameters (see chapter 3).

2.3 Results of the numerical experiments

In what follows, the tumor is always located at the origin of the computational domain Ω. The simplification discussed in Section 2.2.4 is very specific : it does not hold when changing the boundary condition for c and taking into account the fact that the action of the cytotoxic cells is localized. To this end, we use a weight δ, which is a Gaussian centred at $x = 0$ with a fixed variance θ and an amplitude A :

$$\delta(x) = \frac{A}{\theta\sqrt{2\pi}} \exp\left(-\frac{|x|^2}{2\theta^2}\right). \tag{2.29}$$

For defining the source term of the chemoattractant potential, we also use a Gaussian profile

$$\sigma(x) = \frac{A_\sigma}{\theta_\sigma\sqrt{2\pi}} \exp\left(-\frac{|x|^2}{2\theta_\sigma^2}\right). \tag{2.30}$$

Throughout this Section, we assume that the interaction term has the form :

$$m(c,n)(t,z) = n(t,z)\int_\Omega \delta(y)c(t,y)\,\mathrm{d}y$$

and $g(\mu_1) = \mu_1$. In order to ease comparison, we make use of the binary division operator, so that we will compare the asymptotic size-distributions of tumors with the profile given by Lemma 2.2.1. Appendix, section 2.5.3 provides details about the numerical method used to perform the simulations. For the simulations, we shall use the following data, otherwise explicitly stated : the initial data are $c_0(x) = 0$ and $n_0(z) = \mathbf{1}_{0\leq z\leq 750}$ and the parameters are given in Table 2.1.

R	A	θ^2	A_σ	θ_σ^2	a	V	p	χ	S	γ
1	1	0.02	0.002	0.05	0.8	0.616	0.25	0.864	20	0.18

TABLE 2.1 – Data for the simulations

2.3.1 Homogeneous distribution of the source of immune cells : an equilibrium state with persistent tumors establishes

We start by considering the case where the source of immune cells is homogeneously distributed which means that S is constant over the domain Ω. This assumption is relevant for the NK cells.

The fundamental observation is that the size-distribution of tumors tends to the profile given in Lemma 2.2.1, see Fig. 2.4. The chemotactic potential, and the concentration of activated cytotoxic cells also tend to stationary states : the former points towards the center of the domain where the tumor is located, see Fig. 2.5, the latter is more concentrated at the center of the domain, see

Fig. 2.6. In Fig. 2.7–2.11, we show the evolution of the mass μ_1 of the tumor compared to the immune strength $\bar{\mu}_c(t) = \int_\Omega \delta(x)c(t,x)\,\mathrm{d}x$, for different values of the parameters. Depending on the values of the parameters, we observe some damped oscillations in the tumor mass and in the concentration of immune cells. We observe that, when the tumor mass decreases, the tumor antigen-specific cytotoxic effector cells take more time to leave the tumor micro-environment. This latter phenomenon is converted into a slight delay in the time evolution of the cytotoxic effector cells concentration in the tumor micro-environment with respect to the evolution of the tumor mass when both of them are decreasing. According to what is expected from Theorem 2.2.2, $\bar{\mu}_c(t)$ tends to a, the leading eigenvalue of the free-growth/division equation; this is a robust observation of the numerical investigation.

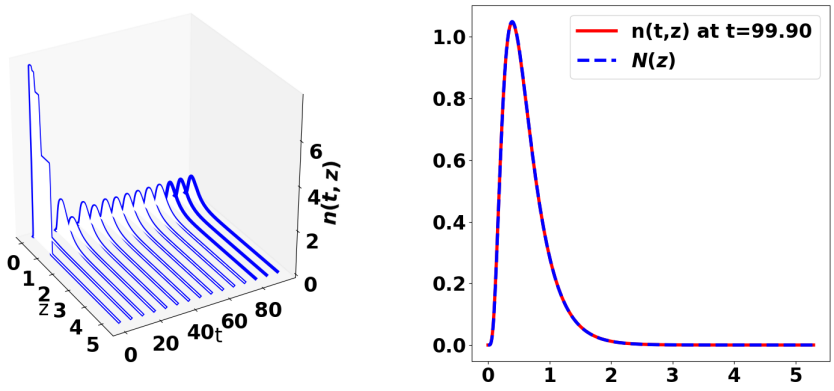

(a) Time evolution of the tumor profile

(b) Comparison of the tumor size-distribution at $T = 99.90$ with the exact asymptotic state (x-axis : z, size of the tumor cells, y-axis : number of tumor cells at the final time)

FIGURE 2.4 – Convergence to the asymptotic profile

Next, we make the parameters vary in order to discuss the influence of their value on the behavior of the system. We only modify one quantity at a time, the others being kept as in Table 2.1.

— *Tumor aggressiveness.* By increasing the rate division a we make the tumor more aggressive, see Fig. 2.7. We recover a qualitative behavior observed in Section 2.2.4 : for small a's the mass of the tumor is rapidly damped, and oscillation-free. An oscillatory behavior can be observed as a increases : the higher a, the higher the frequency. For the tested parameters, the damping always occurs, with a convergence towards the expected asymptotic profile. The asymptotic mass of tumor is significantly positive for large a. We observe that the tumor mass reaches higher values when a is larger, both during the transient states and for the equilibrium value. Note also that the profile of the time evolution becomes sharper, especially for the reaction of the immune system, see (d) : $\bar{\mu}_c$ increases rapidly in

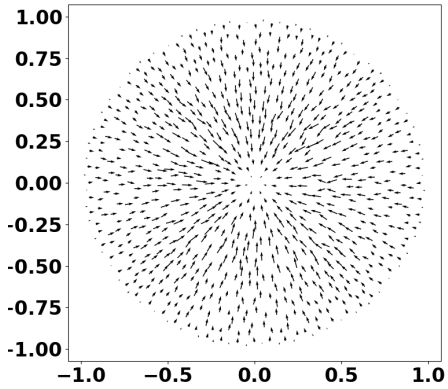

FIGURE 2.5 – Non saturated interactions, homogeneous source of immune cells : the gradient of the chemotactic potential at $t = 50.0$ (x,y-axis correspond to the space coordinates)

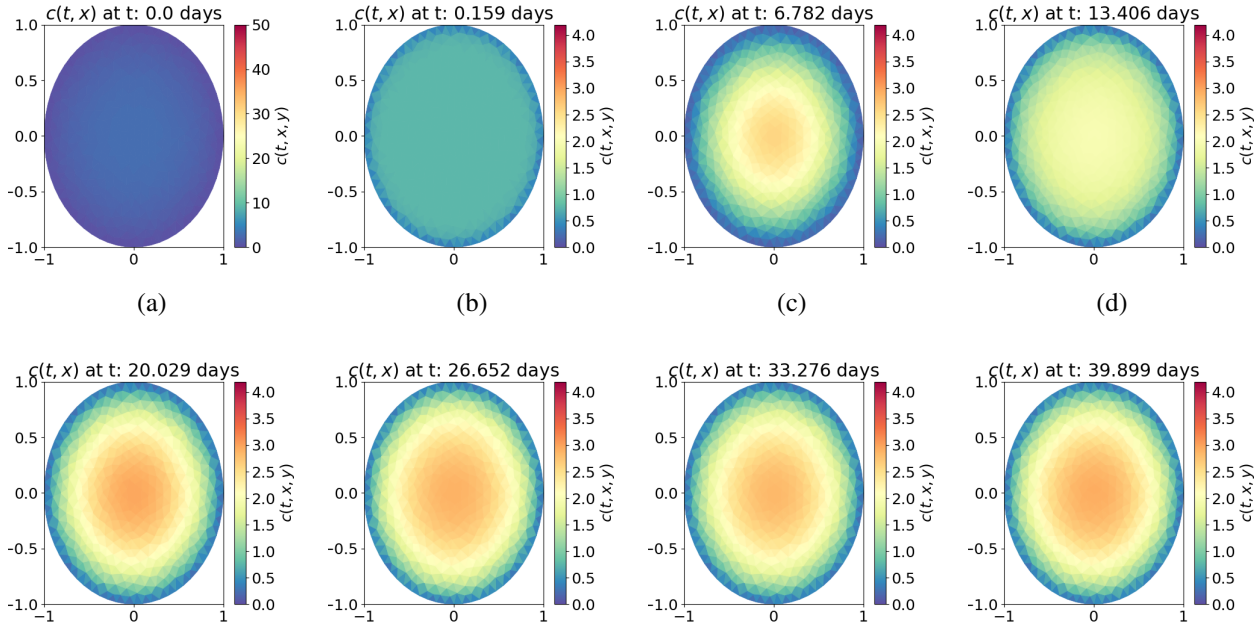

(a) (b) (c) (d)

(e) (f) (g) (h)

FIGURE 2.6 – Non saturated interactions, homogeneous source of immune cells : time evolution of the cytotoxic effector cells concentration c (x,y-axis correspond to the space coordinates)

response to a growth of the tumor mass, and, once the tumor controlled, it relaxes gently.

Consistently with Section 2.2.4, as the immune cell death rate γ decreases, oscillations appear. Note also that the value of γ impacts significantly the asymptotic value of the mass of the tumor : the higher γ, the higher the tumor mass, see Fig. 2.8.

— *Efficiency of the immune response.* The immune response is enhanced by increasing either A, the amplitude of the death term in the tumor growth equation (it measures the strength of the immune cells against the tumor cells), see (2.29), or the conversion rate p : this sensitively reduces the final amount of tumors, and slightly accelerates the damping, see Fig. 2.9.

The immune response is also influenced by playing on the strength of the chemoattractive effect (by increasing χ or A_σ). The amplitude A_σ represents the amplitude of the tumor antigenicity, see (2.30). It is well known that the more antigenic a tumor, the more effective the immune response. Quite surprisingly, the effect is not that sensitive : by increasing A_σ oscillations are slightly smoothed out and the convergence to the asymptotic profile is a bit faster, see Fig. 2.10. What is much more important is the diffusion coefficient D : increasing D dramatically reduces the efficiency of the immune system : an asymptotic profile is still reached, but the equilibrium tumor mass can be significantly higher, see Fig. 2.11 (note it it is not monotone with respect to D). This observation raises the issue of considering space dependent diffusion coefficients, possibly matrix valued, describing more or less favorable spreading conditions depending on the tissues surrounding the tumor.

2.3.2 Influence of space-heterogeneities : equilibrium states vs. periodic behavior

In this Section, we keep the same model and data as in Table 2.1, but we deal with a non homogenous source of immune cells, see Fig. 2.12. This situation is biologically related to the action of the T-cells. It describes the fact that non-activated T-cells are retained in the draining lymph nodes where they are activated by the dendritic cells presenting the tumor antigens and they proliferate. Once activated they migrate from the lymph nodes towards the tumor site. However, space-inhomogeneities of the source S dramatically impacts the dynamics : in many situations, with the same data as in homogeneous case but the source [1], we observe an oscillatory behavior and there is no sensitive damping at all, at least on the time scale of observation. This observation should be considered with caution (it is not excluded that the control occurs on a very long time scale and that the damping is so weak that it cannot be observed on the time scale of the simulation), bearing in mind both its mathematical signification and its practical relevance. In particular, there are cases where the asymptotic profile does not establish. In fact, what we observe is a control of a different nature : the tumor mass does not blow up, nor stabilize ; instead it seems to oscillate, alternating spikes and remissions. Fig. 2.13 shows the space-repartition of the cytotoxic effector cells : we clearly observe the reproduction of patterns, where the concentration of active immune cells is always higher in the source sites, but can be significantly weak at the center of the domain, where the tumor stands. Meanwhile, see Fig. 2.14-(c) and (d), we observe a rapid

1. the comparison makes sense since the source has in the two cases the same total mass $\int S \, \mathrm{d}x$.

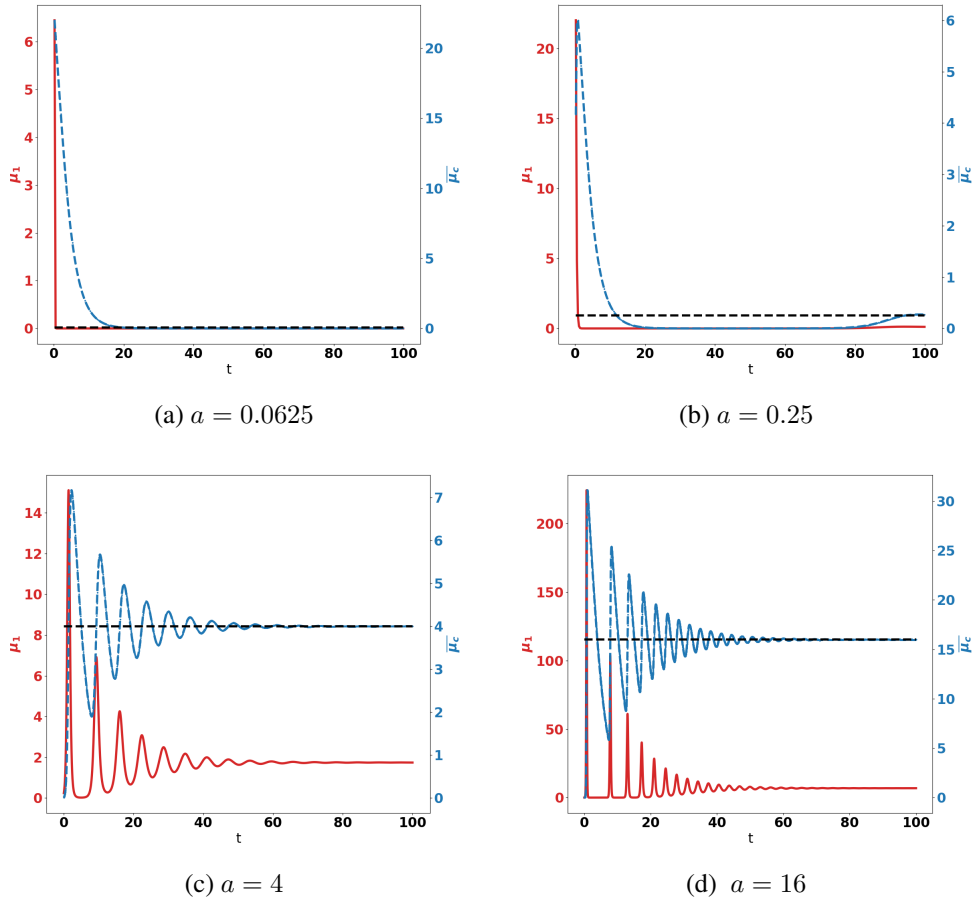

(a) $a = 0.0625$ (b) $a = 0.25$

(c) $a = 4$ (d) $a = 16$

FIGURE 2.7 – Non saturated interactions, homogeneous source of immune cells. Evolution of the tumor mass μ_1 (red curves, left axis), and of $\bar{\mu}_c$ (blue curve, right axis) for several values of the division rate a

growth of the tumor mass, which next shrinks significantly under the action of the immune system and then remains in a dormant state for a while, as time evolves, see [1, 9, 37] for comments on such oscillations. It is remarkable that these oscillations result only from space heterogeneities, while the model does not take into account anti-immune reactions or inflammatory mechanisms. The relevance of such oscillatory behavior has been pointed out in several modeling works, see for instance [36], where they are reproduced by introducing delays in ODEs [6, 15], or stochastic effects [7] ; here they naturally emerge in the dynamic of the PDEs system.

— *Tumor aggressiveness.* There is no indication, on the time of simulation of trend to an equilibrium when the division rate is large. Reducing the division rate a restores the damping, see Fig. 2.14, which agrees with the guess from Section 2.2.4. For larger a we observe peaks of tumor mass and immune cells, which appear regularly. The period (about 27 time units) of the oscillations does not change substantially with a. The tumor mass

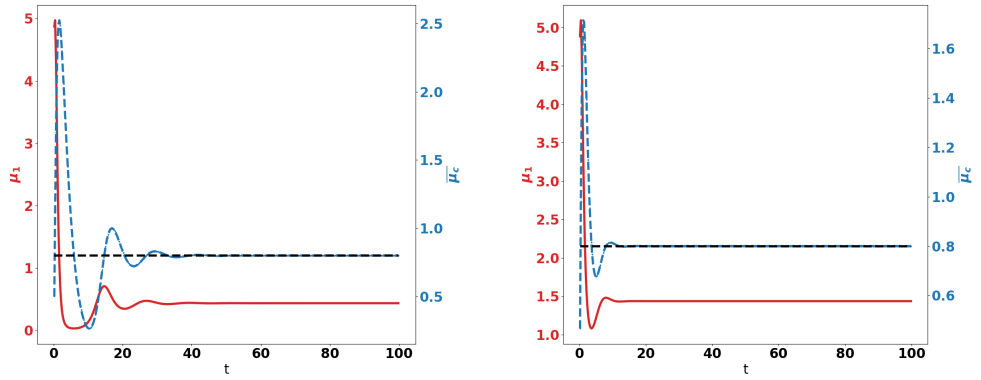

(a) $\gamma = 0.0625$ (b) $\gamma = 0.25$

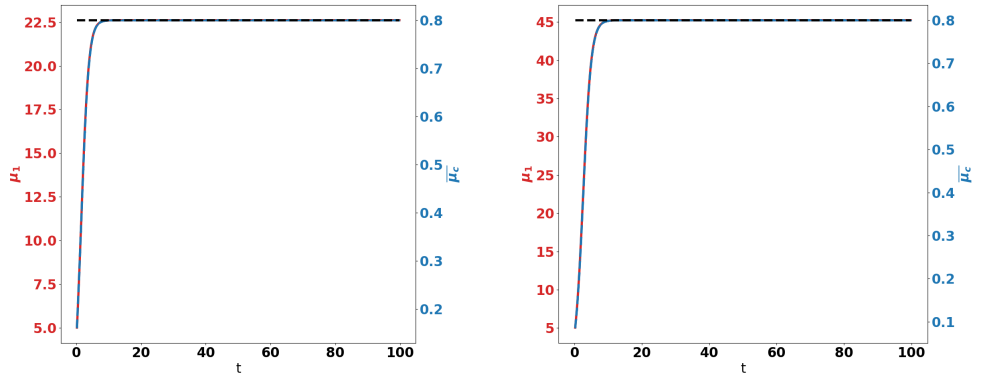

(c) $\gamma = 1$ (d) $\gamma = 16$

FIGURE 2.8 – Non saturated interactions, homogeneous source of immune cells. Evolution of the tumor mass μ_1 (red curves, left axis), and of $\bar{\mu}_c$ (blue curve, right axis) for several values of the immune cells death rate γ

reaches also higher values as a increases.

We make the immune cell death rate γ vary, for a relatively small value of a (given in Table 2.1). As γ increases, the equilibrium is reached faster, with less oscillations but it leads to an asymptotic state with a larger tumor mass, see Fig. 2.15.

— *Efficiency of the immune response.* Strengthening the immune response A or the conversion rate p damps the tumor growth, and reduces the oscillations, see Fig. 2.16. On the figure, we observe the delay of the immune system compared to the tumor growth. Influence of the chemoattractant effect is stronger than in the homogeneous case : increasing A_σ improves significantly the damping, see Fig. 2.17.

What is remarkable is the fact that the equilibrium phase can be recovered by strengthening the chemoattractant effect : this is illustrated in Fig. 2.18, where the data are the same as in Fig. 2.14-(c), but the chemotactic strength χ has been increased.

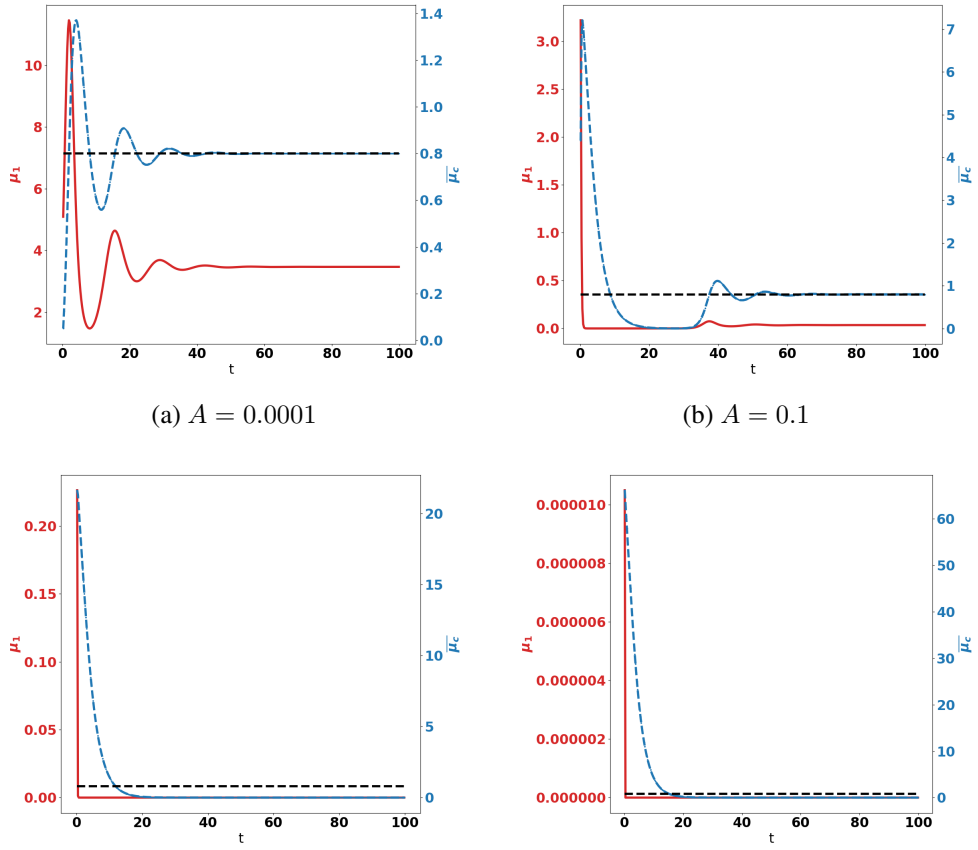

(a) $A = 0.0001$ (b) $A = 0.1$

(c) $A = 10$ (d) $A = 100$

FIGURE 2.9 – Non saturated interactions, homogeneous source of immune cells. Evolution of the tumor mass μ_1 (red curves, left axis), and of $\bar{\mu}_c$ (blue curve, right axis) for several values of A

2.4 Conclusive discussion

We have set up a new model intended to describe the interaction between the immune system and tumors. Based on size and space structured densities, the system of PDEs is able to take into account the displacement of tumor antigen-specific cytotoxic immune cells and the size variation of the tumor cells. Despite its simplicity the model allows us to bring out some relevant observations.

In particular, it is able to reproduce the formation of equilibrium phases, characterizing the ability of the immune system to restrain cancer growth for extended time periods. This effect, which leads to persistent tumors at a controlled level, was inferred from clinical observations and demonstrations using mouse models [18, 37]. Here, it is predicted mathematically and it has been checked numerically. This observation has important practical consequences. For instance,

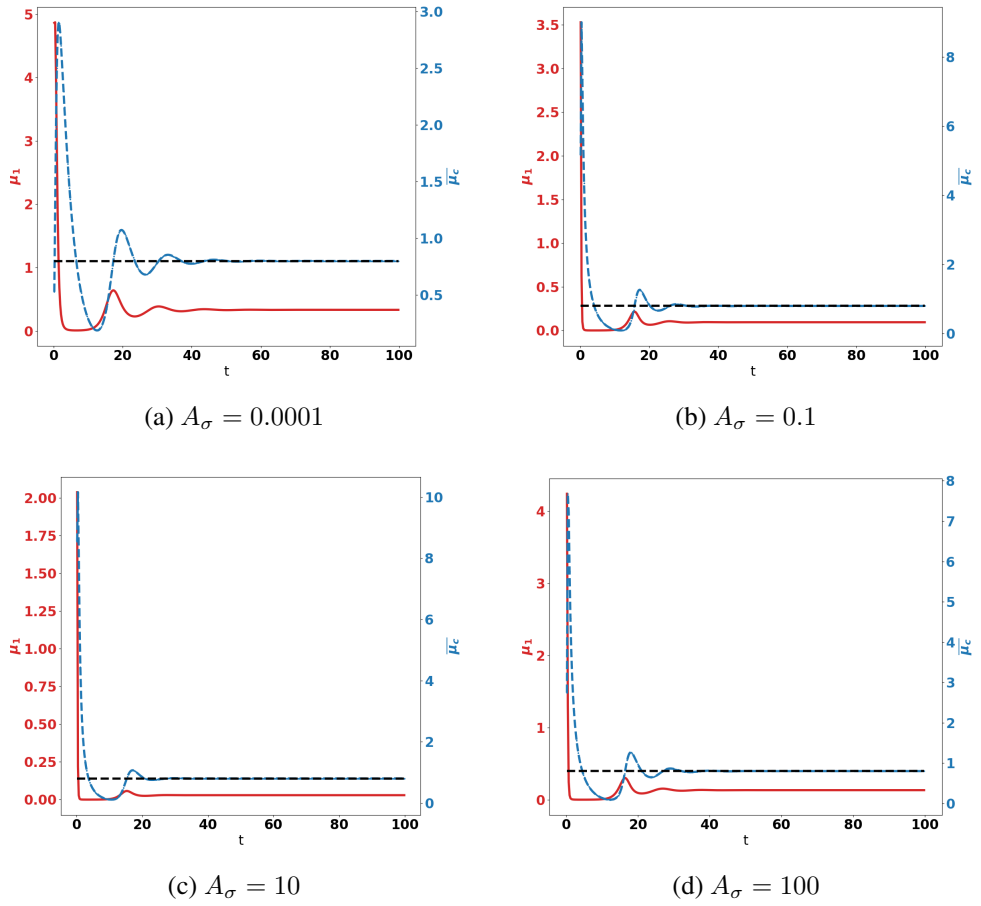

(a) $A_\sigma = 0.0001$ (b) $A_\sigma = 0.1$

(c) $A_\sigma = 10$ (d) $A_\sigma = 100$

FIGURE 2.10 – Non saturated interactions, homogeneous source of immune cells. Evolution of the tumor mass μ_1 (red curves, left axis), and of $\bar{\mu}_c$ (blue curve, right axis) for several values of A_σ.

it is possible that this dormant state is constituted of tumors with size below the measurement capacities of the current imaging methods. However, a change in the tumor environment such as a modification of the immune system efficiency can break the control over the tumor. This is in agreement with reports on transplantation of undetected cancer from organ donor into immunosuppressed recipients [37]. Maintaining cancer in a viable equilibrium state represents a relevant goal of cancer immunotherapy. It is therefore important to understand the parameters that govern the efficiency of the immune response and the parameters to target to improve tumor control.

Moreover, the numerical experiments also show the crucial role of space organization and reveal phenomena that cannot be captured by non spatially structured models. In particular controlling the tumor with a low total mass is much more difficult when the source of immune cells is non homogeneously distributed. In such a situation, periodic patterns can be observed with the

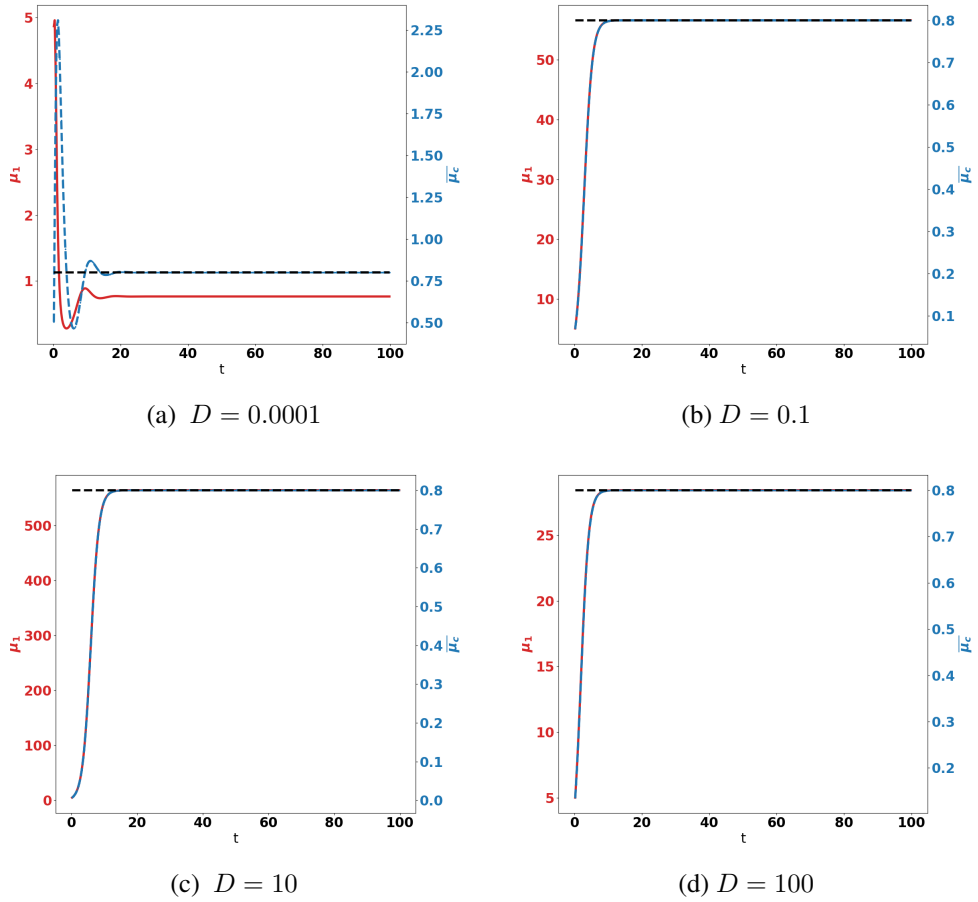

(a) $D = 0.0001$ (b) $D = 0.1$

(c) $D = 10$ (d) $D = 100$

FIGURE 2.11 – Non saturated interactions, homogeneous source of immune cells. Evolution of the tumor mass μ_1 (red curves, left axis), and of $\bar{\mu}_c$ (blue curve, right axis) for several values of the diffusion coefficient D.

chronic formation of tumors having a significantly high mass, alternating with remission periods. Having a homogeneous source of immune cells in the peripheral environment of the tumor makes the immune response much more efficient, since it promotes an immediate contact between the tumor and the cytotoxic effector cells. Otherwise, the capacity in draining the activated immune cells towards the tumor, expressed through the strength of the chemotaxis potential, is a critical parameter of the immune response. Biologically, the role of the spatial distribution of the source of immune cells can be related to the types of cytotoxic cells considered in the modeling. The source of NK cells could be assumed to be homogenously distributed at the early stage of tumor growth. In contrast, T-cells need an efficient priming which occurs in the draining lymph nodes, and their sources is therefore non-homogeneously distributed. Hence, as shown in [22], both NK and $CD8^+$ T-cells cooperate to the anti-tumor immune response and our results can illustrate the complimentary role of NK and $CD8^+$ T-cells. Moreover, our study shows that enhancing

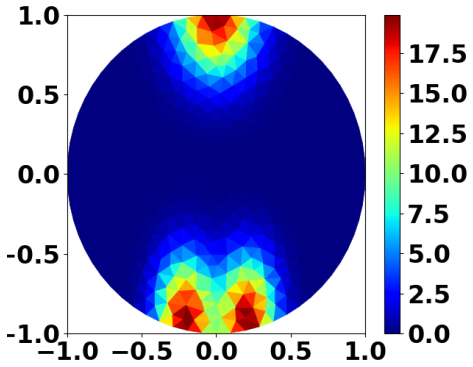

FIGURE 2.12 – Heterogeneous source of immune cells S (x,y-axis correspond to the space coordinates)

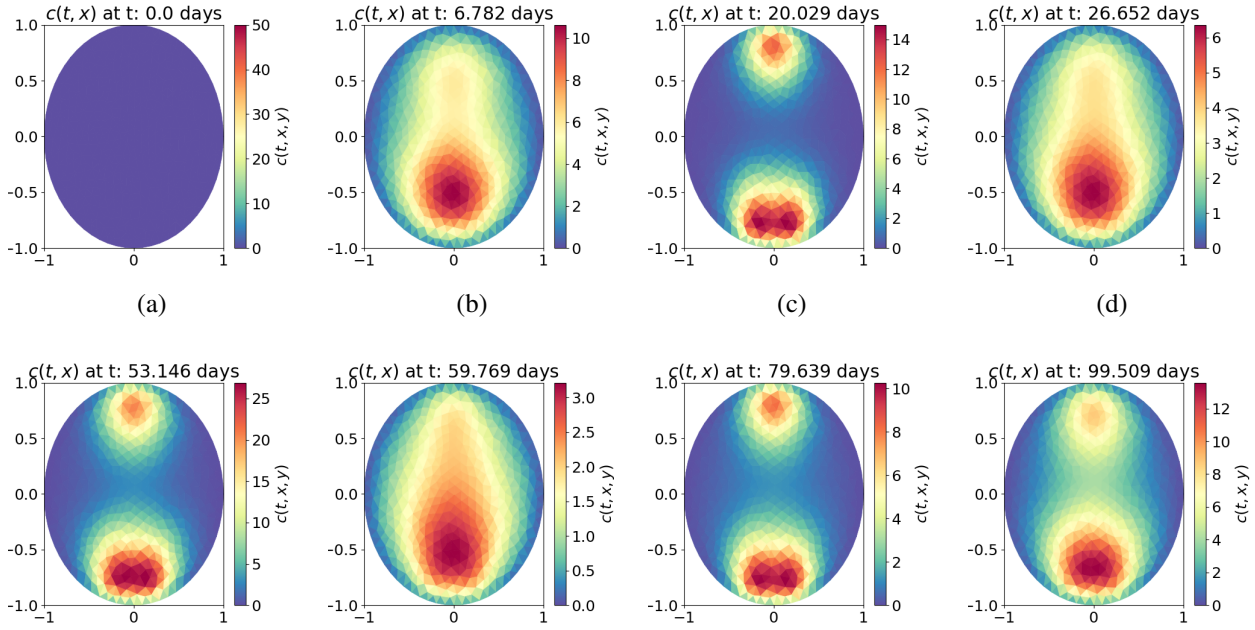

(a) (b) (c) (d)

(e) (f) (g) (h)

FIGURE 2.13 – Time evolution of the cytotoxic effector cells concentration $c(t, x)$ (x,y-axis correspond to the space coordinates)

the chemoattractant effects is crucial in the immune response. Promoting the migration of T-cells towards the tumor microenvironment has indeed been identified as a possible strategy for immunotherapy [52], for instance by increasing the level of Th1 chemokines like CXCL9 and CXCL10, which increases the level of tumor-infiltrating $CD8^+$ T cells [44]. Our findings are

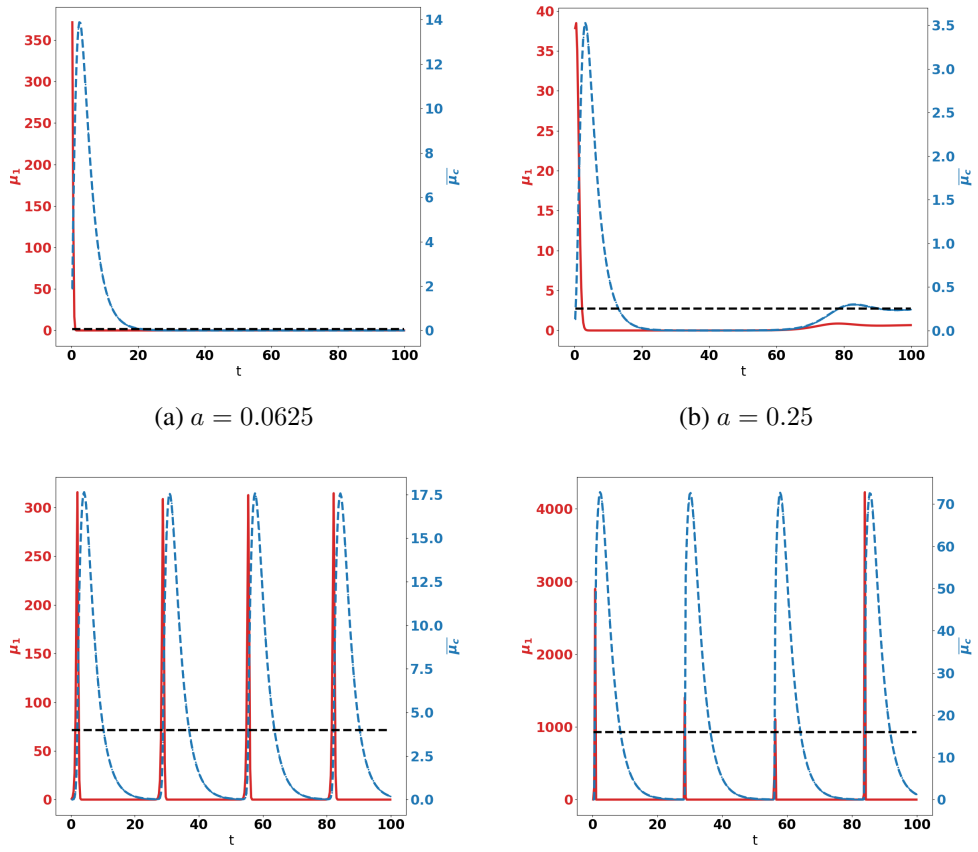

(a) $a = 0.0625$ (b) $a = 0.25$

(c) $a = 4$ (d) $a = 16$

FIGURE 2.14 – Non saturated interactions, heterogeneous source of immune cells. Evolution of the tumor mass μ_1 (red curves, left axis), and of $\bar{\mu}_c$ (blue curve, right axis) for several values of the division rate a.

equally consistent with current experimental and clinical data which show the role of immune check-point in immunosuppressing T-cell responses. Indeed, T-cells express PD-1 after being activated as a mechanism of retro-control; using anti-PD-1 antibodies restores the activation of these cells (cytotoxicity and secretion of IFN-γ). A greater clearance of tumors has been observed when anti-PD-1 therapy is combined with anti-CTLA4 therapy, possibly because of the removal of a checkpoint for T-cell proliferation and priming [9]. These effects appear in the model by playing with the parameters p or A so that the immune cells are more activated or more efficient at killing tumors.

The current version of the model however misses several phenomena, which require further modeling efforts. In particular, it does not address numerous immunosuppressive mechanisms that establish as the tumor grows. For instance, in well-developed tumors, stromal activity can develop signaling modalities which inhibit T-cell activity and favor the recruitment of myeloid-derived

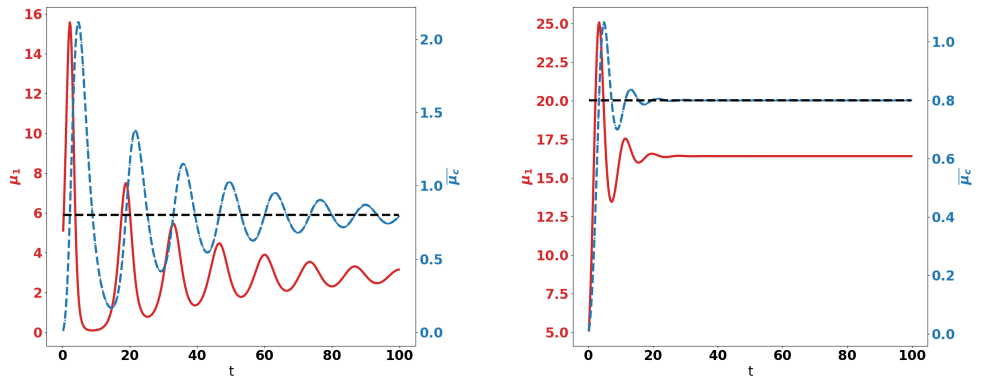

(a) $\gamma = 0.0625$ (b) $\gamma = 0.25$

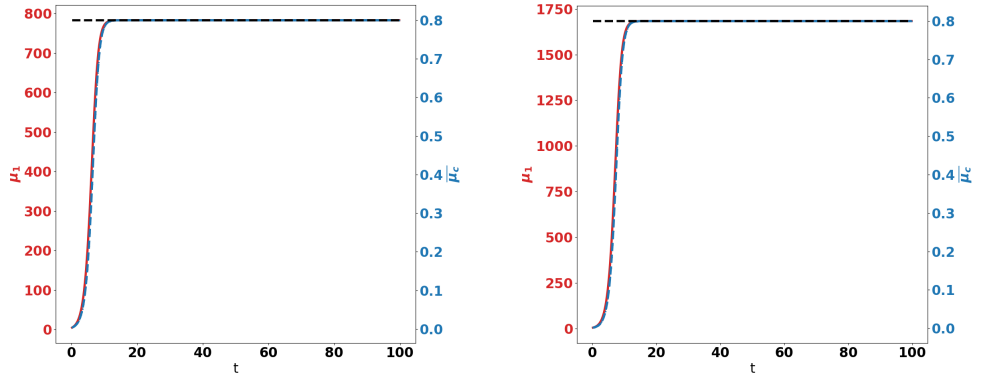

(c) $\gamma = 1$ (d) $\gamma = 16$

FIGURE 2.15 – Non saturated interactions, heterogeneous source of immune cells. Evolution of the tumor mass μ_1 (red curves, left axis), and of $\bar{\mu}_c$ (blue curve, right axis) for several values of the immune cells death rate γ

suppressors cells, which have T-cell suppressive capacity. These effects contribute to the chronic development of tumors ; they will be investigated in the chapter 4.

2.5 Appendix

2.5.1 Tumor growth

The growth rate $z \mapsto V(z)$ can incorporate some mechanisms describing that the growth becomes more difficult for larger tumors. Relevant examples, depicted in Fig. 2.19, are :

— Exponential law : $V(z) = V_0 \exp(-\tau z)$ where τ is a relaxation parameter,

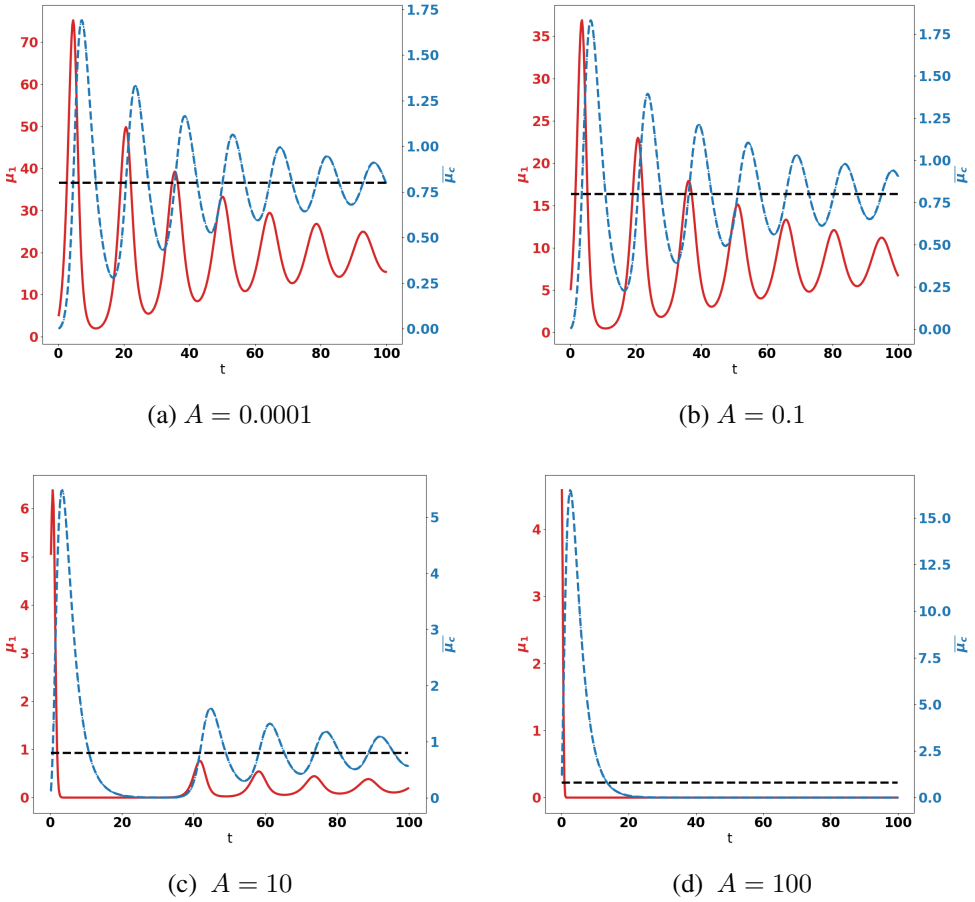

(a) $A = 0.0001$ (b) $A = 0.1$

(c) $A = 10$ (d) $A = 100$

FIGURE 2.16 – Non saturated interactions, heterogeneous source of immune cells. Evolution of the tumor mass μ_1 (red curves, left axis), and of $\bar{\mu}_c$ (blue curve, right axis) for several values of A

— Logistic law : $V(z) = V_0 \left(\dfrac{\exp(-(z-s))}{1+\exp(-(z-s))} \right)$,

— Gompertz' law : $V(z) = V_0 \exp(-b(\exp(cz)))$.

Further examples and details on the modeling of the growth rate can be found in the review [55].

In order to establish the existence of a leading eigen-element, as discussed in Section 2.2.4, the following assumptions should be fulfilled [17] :

— $\int |z'|^2 k(z'|z)\,\mathrm{d}z' < z^2$;

— $a \in L^1_{\mathrm{loc}}((0,\infty)) \cap \mathcal{F}$, where $\mathcal{F}$ is the set of non negative functions f such that we can find $p, q \geq 0$ verifying $\limsup_{z\to\infty} z^{-p} f(z) < \infty$ and $\liminf_{z\to\infty} z^q f(z) > 0$;

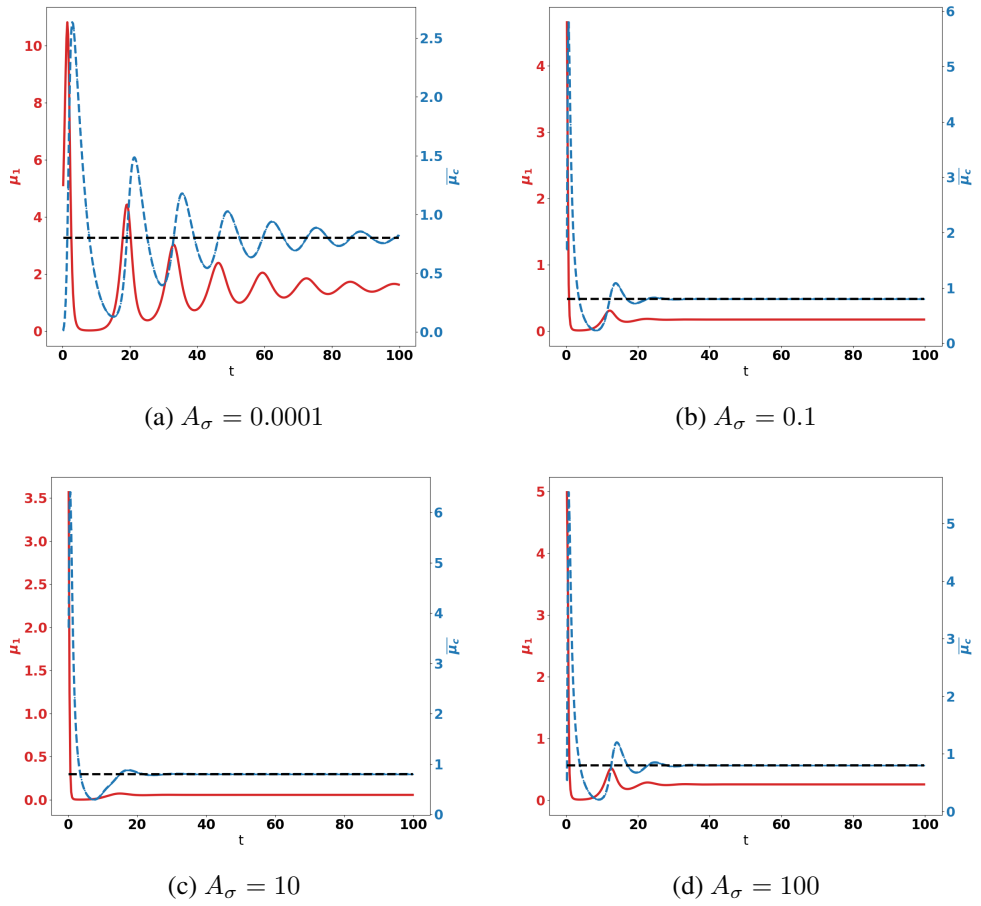

(a) $A_\sigma = 0.0001$ (b) $A_\sigma = 0.1$

(c) $A_\sigma = 10$ (d) $A_\sigma = 100$

FIGURE 2.17 – Non saturated interactions, heterogeneous source of immune cells. Evolution of the tumor mass μ_1 (red curves, left axis), and of $\bar{\mu}_c$ (blue curve, right axis) for several values of A_σ

— there exists $r \geq 0$ such that $\mathrm{supp}(a) \subset [r, \infty)$;

— there exists $\alpha_1 \geq 0$ such that $z^{\alpha_1} V(z) \in L^\infty_{\mathrm{loc}}$ and for any compact $K \subset (0, \infty)$ we can find $c_K > 0$ such that $V(z) \geq c_K$ a.e. on K ;

— for a certain $\gamma \geq 0$, $z \mapsto \frac{z^\gamma}{V(z)}$ lies in the set L^1_0 of functions f for which there exists $d > 0$ such that $f \in L^1((0, d))$;

— there exists $M \geq 0, \gamma \geq 0$ such that $\int_0^s k(z'|z)\,\mathrm{d}z' \leq \min(1, M(s/z)^\gamma)$;

— $\frac{a}{V}$ also lies in L^1_0 and it verifies $\lim_{z\to\infty} \frac{za(z)}{V(z)} = \infty$.

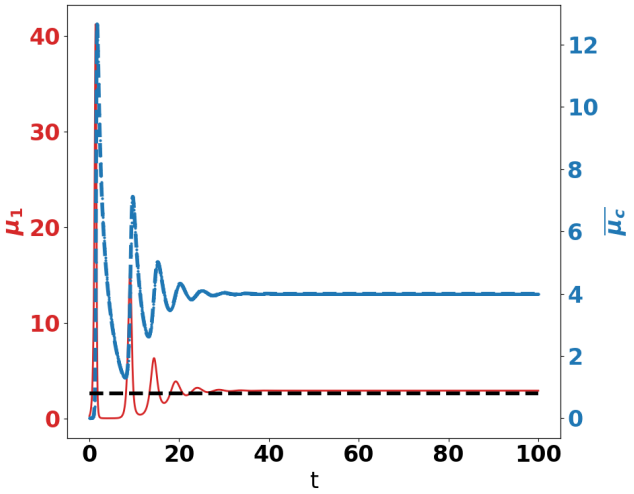

FIGURE 2.18 – Non saturated interactions, heterogeneous source of immune cells. Evolution of the tumor mass μ_1 (red curves, left axis), and of $\bar{\mu}_c$ (blue curve, right axis) with $a = 4$ and $\chi = 100$

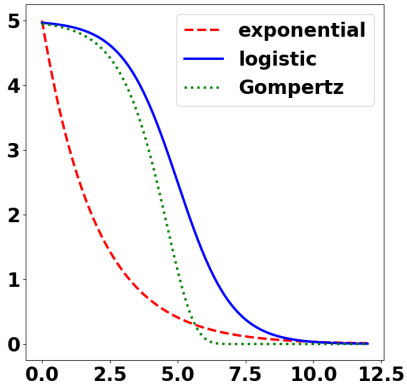

FIGURE 2.19 – Shape of several growth laws $z \mapsto V(z)$ (x-axis : z, size of the tumor cells, y-axis : growth rate of the cells)

We refer the reader to [17] for further comments and interpretations on the these assumptions, which guaranty existence-uniqueness for (2.26).

2.5.2 Model parameters

Table 2.2 collects the information about variables, parameters and units for the tumor growth model, and Table 2.3 details the units of the parameters of the equations for the immune system.

variables	descriptions	units	example of units	Estimated values examples	Source
z	volume of tumor cells	$[l]^3$	μm^3	$\sim 10^3 \mu m^3$ (in average)	
t	time variable	$[t]$	day		
n	density of tumor cells with a volume z	$[cell_n] \cdot [l]^3$	$cell_n \cdot \mu m^{-3}$	A tumor reaching the size of $1cm^3$ (approximately $1g$ wet weight) is commonly assumed to contain 1×10^9cells ($10^{-3} cell_n \cdot \mu m^{-3}$)	[12]
V	tumor cells growth rate	$[l]^3 \cdot [t]$	$\mu m^3 \cdot day^{-1}$	$0.985 \cdot 10^3 \mu m^3 \cdot day^{-1}$ (Breast tumor)	
a	rate at which a cell of size z divides	$[l]^{-1}$	day^{-1}		
k	distribution of cells from a cell of size z dividing	$[l]^{-3}$	μm^{-1}		
μ_0	total number of tumor cells in the tumor	$[cell_n]$	$cell_n$		
μ_1	total volume of the tumor	$[cell_n] \cdot [l]^3$	$cell_n \cdot \mu m^3$		

TABLE 2.2 – Recap of the main definitions and notations for the tumor growth model

Remark 2.5.1. *The model can take into account two distinct saturation effects : the former in the expression of the recruitment term of the cytotoxic effector cells, through the function g, the latter in the expression of the death term describing the action of the activated immune cells on the tumor. We also work with saturationless models, which means*

$$g(\mu_1) = \mu_1, \qquad m(c, n) = n \int_\Omega \delta(y) c(t, y) \, \mathrm{d}y.$$

We leave the reader adapt the definition of the units to such cases.

2.5.3 Numerical method

For the numerical simulation of the model, we use the so-called finite volume approach, for which we refer the reader to [21].

The growth-division equation. The computational domain for the size variable is the interval $[0, z_\star]$ where $z_\star$ is chosen large enough : due to the division processes, we expect the the solution remains essentially on a bounded interval, and the cut-off should not perturb too much the solution. For the simplified binary division model, a guess is provided by using the profile given by

variables	descriptions	units	example of units	Estimated values examples	Source
x	space variable	$[L]$	mm		
c	concentration of activated cytotoxic effector cells	$[cell_c] \cdot [L]^{-3}$	$cell_c \cdot mm^{-3}$		
χ	chemotactic coefficient	$[L]^2 \cdot [t]^{-1} \cdot [mol]^{-1}$	$mm^2 \cdot mmol^{-1} \cdot day^{-1}$	$10^{-2} - 10^3 cm^2 s^{-1} mol^{-1}$ or $8.64 \times 10^1 - 8.64 \times 10^6 mm^2 \cdot mmol^{-1} \cdot day^{-1}$ (Macrophages)	Farell and al. 1990 [24]
ϕ	attractive potential	$[mol]$	$mmol$		
D	natural space diffusion coef. of the cytotoxic effector cells population	$[L]^2 \cdot [t]^{-1}$	$mm^2 \cdot day^{-1}$	$8.64 \times 10^{-7} cm^2 \cdot s^{-1}$ or $8.64 \times 10^{-5} mm^2 \cdot day^{-1}$ (cytotoxic effector cells) (or $0.025 mm^2 \cdot day^{-1}$ for effector T-cells)	A. Friedman et al. [25], (A.K. Cooper et al. [10])
p	conversion rate of immune cell into tumor antigen-specific cytotoxic effector cells	$[t]^{-1}$	day^{-1}	$0.25 \ day^{-1}$ (IL-2 induced activation)	A. Friedman et al. [25]
S	density of the source of immune cells	$[cell_c] \cdot [L]^{-3}$	$cell_c \cdot mm^{-3}$		
β	steepness coefficient of the immune cell recruitment	$[cell_n]$	$cell_n$		
γ	natural death rate of the tumor antigen-specific cytotoxic effector cells	$[t]^{-1}$	day^{-1}	$0.18 \ day^{-1}$	A. Friedman et al. [25]
$\mathcal{K}$	natural space diffusion of the attractive potential ϕ	$[L]^2 \cdot [t]^{-1}$	$mm^2 \cdot day^{-1}$	$2.16 \ mm^2 \cdot day^{-1}$	
σ	chemical signal induced by each tumor cell	$[mol] \cdot n^{-1} \cdot [l]^{-3} [t]^{-1}$	$mmol \cdot cell_n^{-1} \cdot \mu m^{-3} \cdot day^{-1}$	$200 \cdot 10^{-3} \ mmol \cdot -_A^{-1} \cdot day^{-1}$	
δ	strength of the immune response	$\frac{[cell_n]}{[cell_c] \cdot [t] \cdot [l]^3}$	$cell_n \cdot cell_c^{-1} \cdot \mu m^{-3} \cdot day^{-1}$	$1 \ day^{-1}$, average rate at which effector T-cells kill tumor cells	A. K. Cooper et al. [10]
α	steepness coefficient of the tumor cell death term	$[cell_n] \cdot [l]^3$	$cell_n \cdot \mu m^{-3}$		

TABLE 2.3 – Recap of the main definitions and notations for the immune system model

Lemma 2.2.1. This domain is split into cells $M_i = (z_{i-1/2}, z_{i+1/2})$, centered on $z_i = \frac{z_{i-1/2}+z_{i+1/2}}{2}$ where

$$z_0 = z_{1/2} = 0 < ... < z_{i-1/2} < z_i < z_{i+1/2} < ... < z_{N+1/2} = z_{N+1} = z_\star.$$

In what follows, the step $\Delta z = z_{i+1/2} - z_{i-1/2}$ is assumed to be constant. We denote by Δt the time step and $t^\kappa = \kappa \Delta t$. The discrete unknowns n_i^κ, with $i \in \{1, ..., I\}$ and $\kappa \in \{1, ..., N_t\}$ are intended to be approximation of the mean value $\frac{1}{\Delta z} \int_{M_i} n(t^\kappa, z) \, \mathrm{d}z$. The integral that defines the gain term of the division operator is approximated by a simple quadrature rule. For the operator (2.11) the kernel involves Dirac masses which are approached by peaked Gaussian. The scheme reads

$$\Delta z \frac{n_i^{\kappa+1} - n_i^\kappa}{\Delta t} + F_{i+\frac{1}{2}}^\kappa - F_{i-\frac{1}{2}}^\kappa = -a_i \Delta z n_i^\kappa + \Delta z^2 \sum_{j=1}^{I} a(z_j) k(z_i|z_j) n_j^\kappa - m_i^\kappa, \tag{2.31}$$

where $F^{\kappa}_{i+\frac{1}{2}} = V_{i+\frac{1}{2}} n^{\kappa}_i$ represents the convective numerical flux on the interfaces of $z_{i+1/2}$, which is defined according to the upwinding principle and m^{κ}_i is the approximation of the interaction term (see below). Note that the step Δz should be small enough to capture the division of small cells, if any.

We can use formula (2.2.1) to check that the numerical procedure preserves the eigen-function of the growth division equation when m is replaced by 0 and using the eigen-function as initial data.

The effector cytotoxic cells displacement equation. The computational domain is the ball $\Omega = \{x = (x_1, x_2) \in \mathbb{R}^2, |x| = \sqrt{x_1^2 + x_2^2} < R\}$. We work with a tessellation made of triangles, that form an admissible mesh of Ω, see [21, Definition 3.1, sp. (iv)]. Let K be a control volume of the mesh τ_Ω. The set of the edges of the mesh is noted ξ. We distinguish the edges on $\partial\Omega$ and the internal edges : $\xi = \xi^{\text{ext}} \cup \xi^{\text{int}}$. We also denote $\xi_K = \{\varsigma \in \xi \cap \partial K\}$, $d_{K\varsigma}$ the distance from the point x_K to the edge ς and $|K|$ stands for the two dimensional measure of the control volume K, $|\varsigma|$ for the length of an edge $\varsigma \in \xi$. If $\varsigma \in \xi^{\text{int}}$, then $\varsigma = K|L$ and the distance d_{KL} between x_K and x_L is equal to $d_{K\varsigma} + d_{L\varsigma}$.

The chemotactic convection can be very strong and impact severely the stability condition of a scheme that would be explicit on the transport part of the equation. For this reason, we use an implicit approach defined by

$$|K|\frac{c_K^{\kappa+1} - c_K^k}{\Delta t} = \left(- \sum_{\varsigma \in \xi_K} \mathcal{F}_{K\varsigma}(c^{\kappa+1}_{\tau_\Omega}, \phi^{\kappa}_{\tau_\Omega}) - \sum_{\varsigma \in \xi_K} \mathcal{G}_{K\varsigma}(D, c^{\kappa+1}_{\tau_\Omega}) \right) + |K| p \mu_1^{\kappa} S_K - |K| \gamma c_K^{\kappa+1}, \tag{2.32}$$

and then we update the chemotactic potential by

$$- \sum_{\varsigma \in \xi_K} \mathcal{G}_{K\varsigma}(\mathcal{K}, \phi^{\kappa+1}_{\tau_\Omega}) = |K| \mu_1 \langle \sigma \rangle_K. \tag{2.33}$$

In (2.32)-(2.33), we have used the following notations :

— for the diffusive flux of a quantity w, with the diffusion matrix A, we set

$$\mathcal{G}_{K\varsigma}(A, w_{\tau_\Omega}) = A_\varsigma \frac{|\varsigma|}{d_{KL}}(w_K - w_L) \quad \text{if } \varsigma \in \xi^{\text{int}}$$

with the necessary adaptation on the boundary, according to the boundary condition (Dirichlet or Neumann),

— for the convective flux, we set

$$\mathcal{F}_{K\varsigma}(c_{\tau_\Omega}, \phi_{\tau_\Omega}) = \frac{|\varsigma|}{d_{KL}}(\chi c_K (\phi_L - \phi_K)^+ - \chi c_L (\phi_L - \phi_K)^-) \quad \text{for } \varsigma \in \xi^{\text{int}},$$

and $\mathcal{F}_{K\varsigma}(c_{\tau_\Omega}, \phi_{\tau_\Omega}) = 0$ if $\varsigma \in \xi^{\text{ext}}$.

The expression of the interaction term in (2.31) depends on the details on the death term; for instance when it depends linearly on c and n, it reads

$$m^{\kappa}_i = n^{\kappa}_i \sum_{K \in \tau_\Omega} |K| \delta_K c^{\kappa}_K.$$

The time step Δt is determined in order to preserve the positivity of the solution, namely we assume the following CFL stability condition :

$$\Delta t \leq \min\Big(\frac{\Delta z}{\max_{0\leq z\leq z_\star} V(z)}, \frac{1}{\max_{0\leq z\leq z_\star} a(z)}, \frac{1}{\sum_{K\in\tau_\Omega} |K|\delta_K c_K^\kappa}\Big).$$

2.5.4 Incorporating saturation effects in the model

Non-saturated interactions and saturated conversion of effector cells

In this Section, we discuss the saturation effect taken into account in the conversion from non activated immune cells to effector cytotoxic cells. Namely, in the evolution equation for c, we take $\mu_1 \mapsto g(\mu_1)$ as in (2.12), with $\beta = 5000$. The other parameters are still as in Table 2.1. The saturation effect accounts for the fact that the activation process of immune cells is limited. We can expect that as the threshold decreases, the immune system is less efficient in controlling the tumor growth.

On the simulations, we still observe the asymptotic trend towards an equilibrium, as predicted by the theoretical results. However, the tumor mass is considerably higher than for the saturation-free model, see Fig. 2.20. With an homogeneous source of immune cells, the control still occurs as the death rate γ of the cytotoxic effector cells increases, but the high asymptotic tumor mass reveals a loss of efficiency of the immune system, see Fig. 2.21. When the source of immune cells is heterogeneous (we work with the same distribution as in Fig. 2.12), the control is lost as γ increases, see Fig. 2.22. The saturation effect can be discussed also by making the steepness parameter β vary. As β is reduced, the control is not lost, but the asymptotic mass of the tumor becomes higher, see Fig. 2.23 and 2.24.

Saturated interactions and non-saturated conversion of effector cells

In this section, let us briefly discuss the saturation effect taken into account in the interaction between the effector cells and the tumor cells. Namely, in the tumor growth equation, the interaction term becomes

$$m(c,n)(t,z) = \int_\Omega \delta(y)c(t,y)\,\mathrm{d}y \times \frac{n(t,z)}{\alpha + n(t,z)},$$

as in (2.21), with $\alpha\alpha' = 1$. For the numerical tests, we set $\alpha = 3000$. The other parameters are as in Table 2.1. This expression traduces the fact that the tumor antigen-specific cytotoxic effector cells have access to a limited amount of tumor cells. We point out that our analysis by means of eigen-elements does not apply here since we have introduced non linearities with respect to n in the tumor growth equation. Nevertheless, we can investigate on numerical grounds whether or not the immune system can control the tumor growth in this case. We observe, see Fig. 2.25 (homogeneous source of immune cells), an effective control of the tumor evolution, at least when the tumor is not too agressive, with a moderate division rate a. When a becomes larger, the tumor mass grows exponentially fast. Similar features are observed with a non homogeneous source of immune cells. As we make α vary, we observe two phenomena : when α increases, both

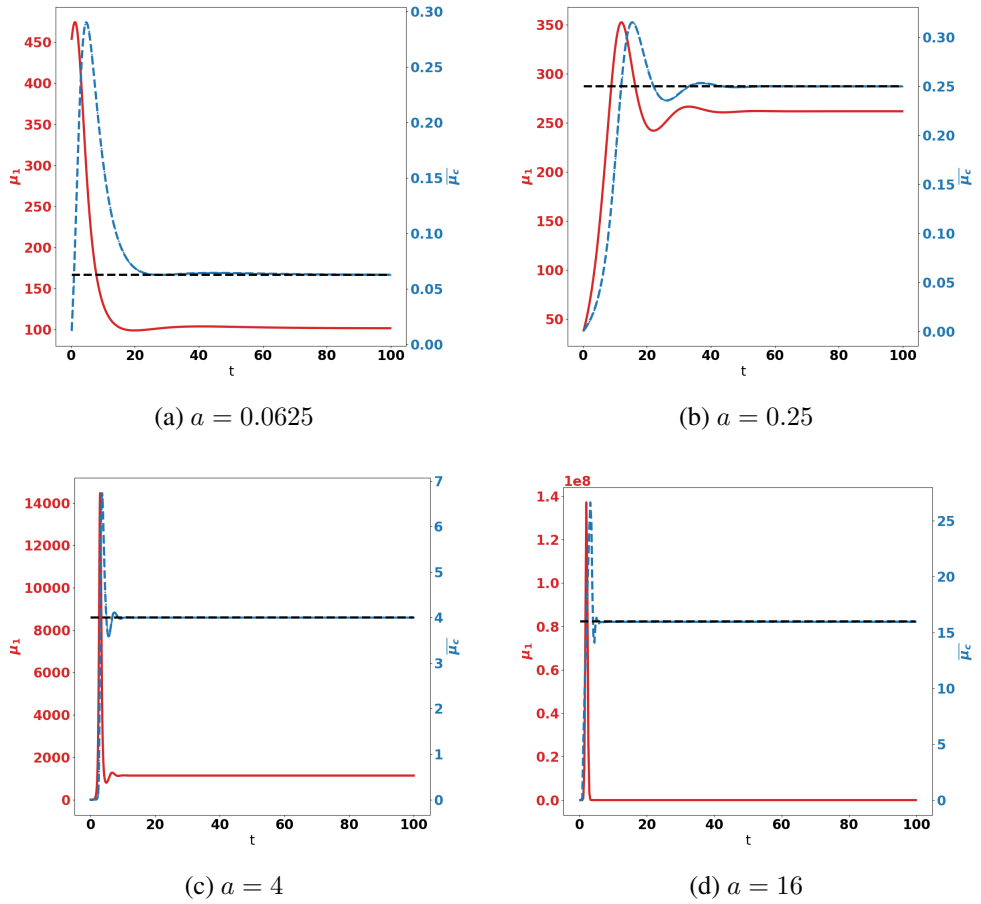

(a) $a = 0.0625$ (b) $a = 0.25$

(c) $a = 4$ (d) $a = 16$

FIGURE 2.20 – Saturated conversion, homogeneous source of immune cells. Evolution of the tumor mass μ_1 (red curves, left axis), and of $\bar{\mu}_c$ (blue curve, right axis) for several values of a.

the frequency of oscillations is higher and the damping is stronger, see Fig. 2.26 (homogeneous source of immune cells). We get a similar behavior by playing with A_σ. Surprisingly, with an heterogeneous source of immune cells, the periodic behavior observed in the saturation-less case reappears when α (or A_σ) is small, see Fig. 2.27. (In Fig. 2.27-(a) the behavior is also periodic but the period is higher than the represented simulation time.)

2.5.5 Multiple tumor sites

The model can be adapted to consider the relevant situation where there are many tumor sites. With q the number of tumor sites, we can consider possibly different parameters governing the growth and the immune interactions. Let

— n_i be the size-structured distribution of tumor cells in the site $i \in \{1, ..., q\}$;

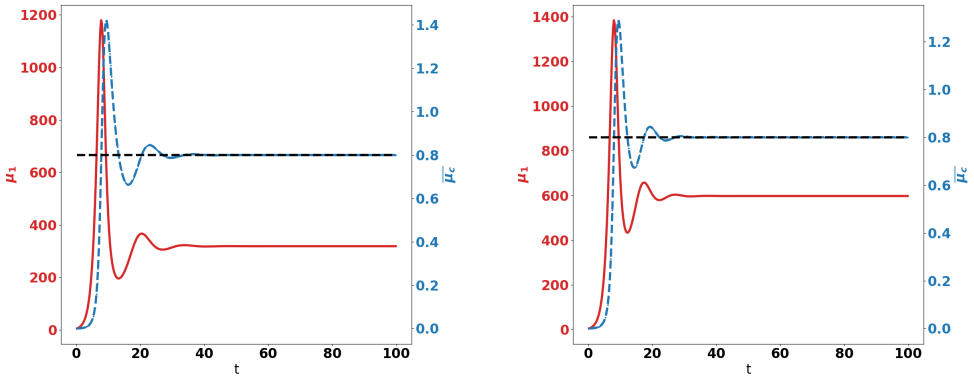

(a) $\gamma = 0.0625$

(b) $\gamma = 0.25$

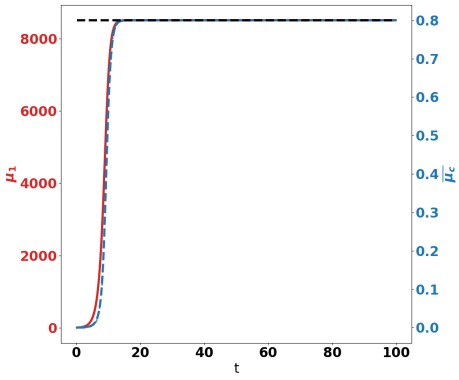

(c) $\gamma = 4$

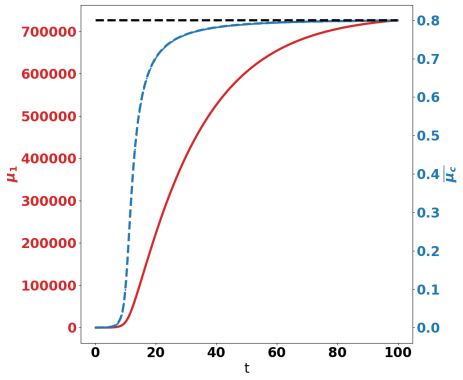

(d) $\gamma = 16$

FIGURE 2.21 – Saturated conversion, homogeneous source of immune cells. Evolution of the tumor mass μ_1 (red curves, left axis), and of $\bar{\mu}_c$ (blue curve, right axis) for several values of γ.

— V_i, a_i and δ_i be the corresponding growth rate, division rate and immune strengths, respectively ;

— σ_i be the form function describing the signal emitted by each tumor.

The model becomes

$$\begin{cases} \partial_t n_i + \partial_z(V_i n_i) = Q_i(n_i) - n_i \int_\Omega \delta_i(x) c(t,x)\,\mathrm{d}x \\ \partial_t c + \nabla_x \cdot (\chi c \nabla_x \phi - D\nabla_x c) = pS \sum_{i=1}^q \int_0^\infty z n_i(t,z)\,\mathrm{d}z - \gamma c, \\ -\nabla_x \cdot (\mathcal{K}\nabla_x \phi) = \sum_{i=1}^q \int_0^\infty z n_i(t,z)\,\mathrm{d}z \langle \sigma_i \rangle, \end{cases} \tag{2.34}$$

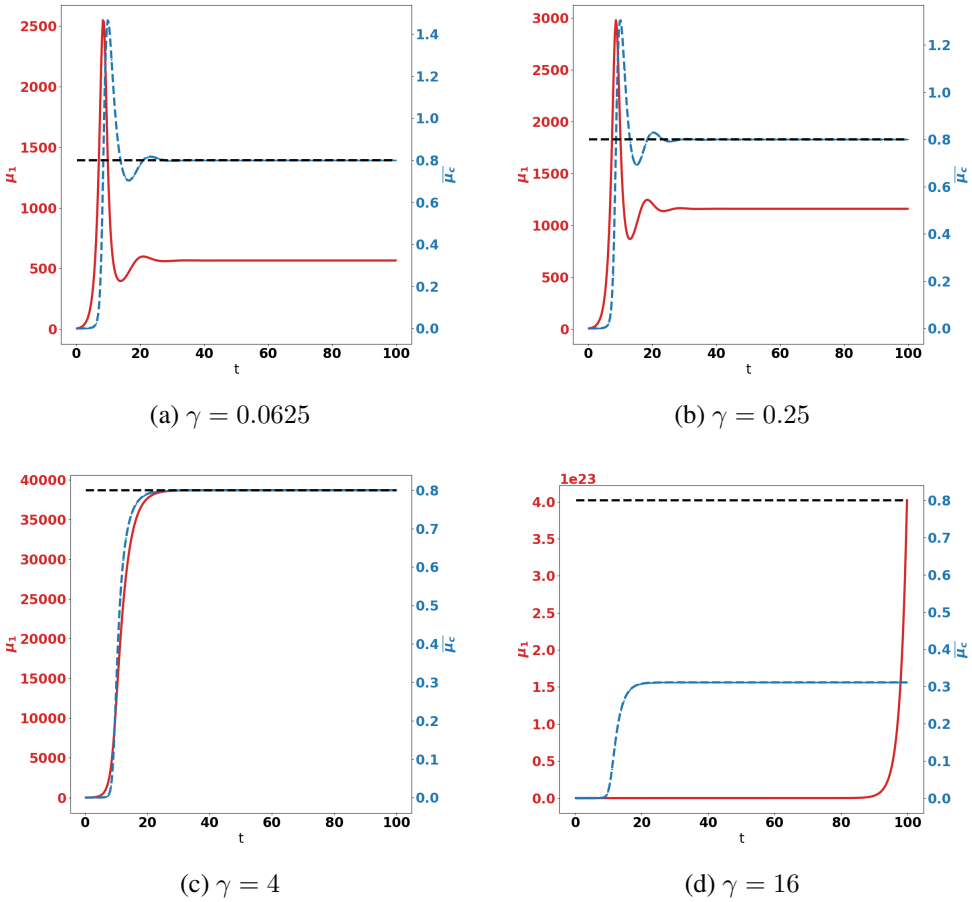

(a) $\gamma = 0.0625$ (b) $\gamma = 0.25$

(c) $\gamma = 4$ (d) $\gamma = 16$

FIGURE 2.22 – Saturated conversion, heterogeneous source of immune cells. Evolution of the tumor mass μ_1 (red curves, left axis), and of $\bar{\mu}_c$ (blue curve, right axis) for several values of γ.

endowed with initial and boundary conditions. For the numerical test, we deal with $q = 3$ tumor sites, located at the positions

$$x_1 = (0, -0.30), \qquad x_2 = (0.5, 0.3), \qquad x_3 = (-0.5, 0.3).$$

We assume that the tumor sites have the same constant growth rate V, immune strength δ and form function σ, but distinct division rates, $a, 2a, 1.5a$. The parameters are defined as in Table 2.1. We work with the heterogeneous source of immune cells illustrated in Fig. 2.12. The behavior of the tumor mass and immune cells mass has the same features as in the single site case, see Fig. 2.29.

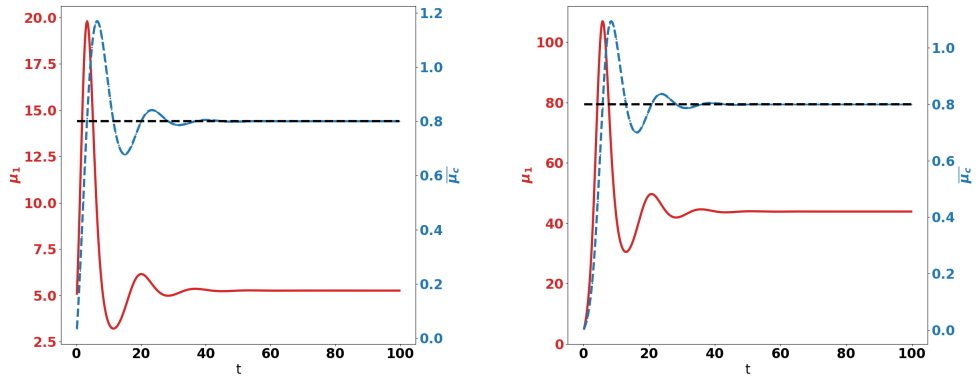

(a) $\beta = 10$

(b) $\beta = 100$

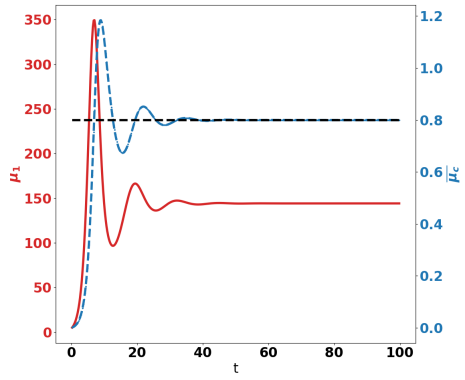

(c) $\beta = 500$

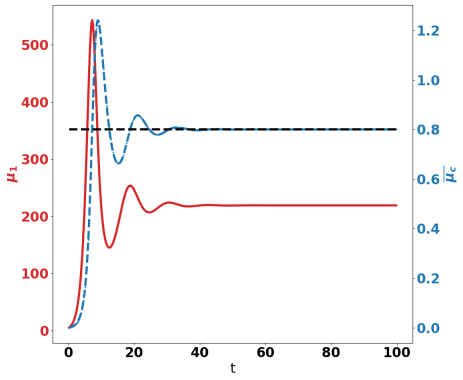

(d) $\beta = 1000$

FIGURE 2.23 – Saturated conversion, homogeneous source of immune cells. Evolution of the tumor mass μ_1 (red curves, left axis), and of $\bar{\mu}_c$ (blue curve, right axis) for several values of β.

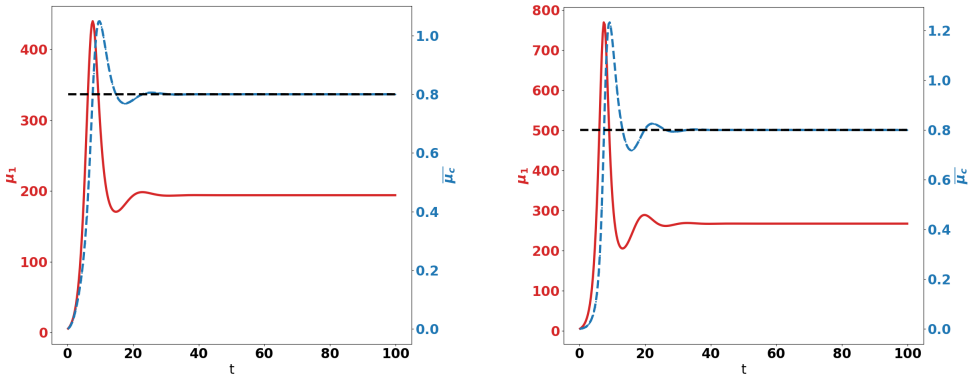

(a) $\beta = 10$

(b) $\beta = 100$

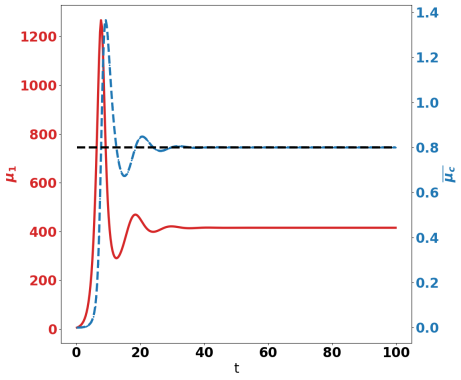

(c) $\beta = 500$

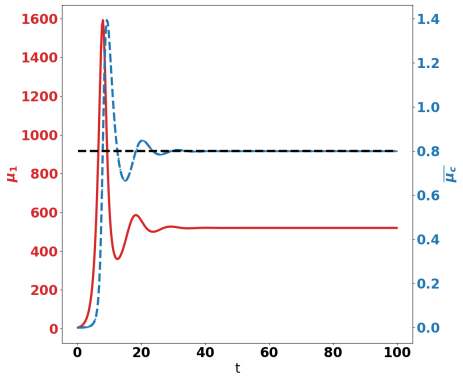

(d) $\beta = 1000$

FIGURE 2.24 – Saturated conversion, heterogeneous source of immune cells. Evolution of the tumor mass μ_1 (red curves, left axis), and of $\bar{\mu}_c$ (blue curve, right axis) for several values of β.

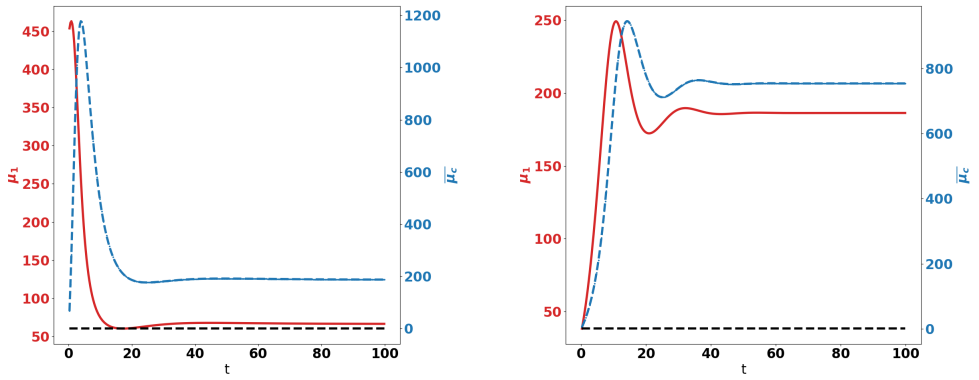

(a) $a = 0.0625$ (b) $a = 0.25$

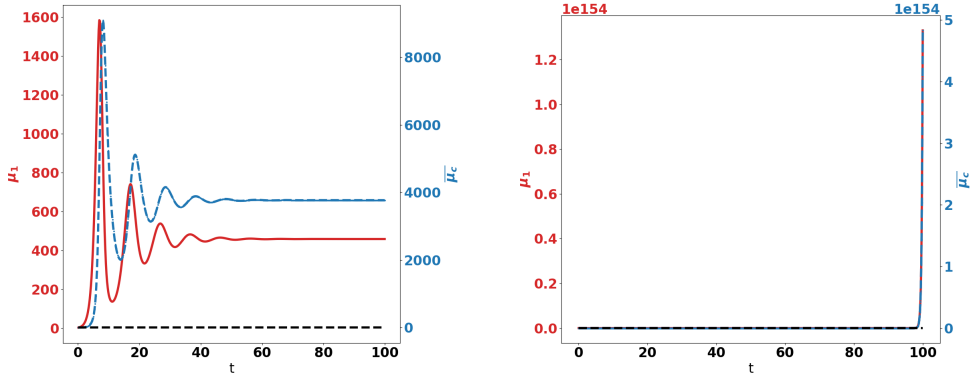

(c) $a = 1$ (d) $a = 4$

FIGURE 2.25 – Saturated interactions, homogeneous source of immune cells. Evolution of the tumor mass μ_1 (red curves, left axis), and of $\bar{\mu}_c$ (blue curve, right axis) for several values of a.

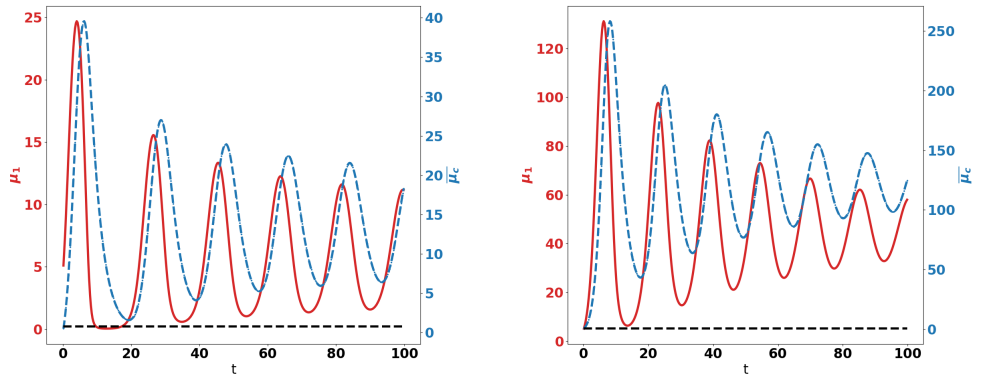

(a) $\alpha = 10$

(b) $\alpha = 100$

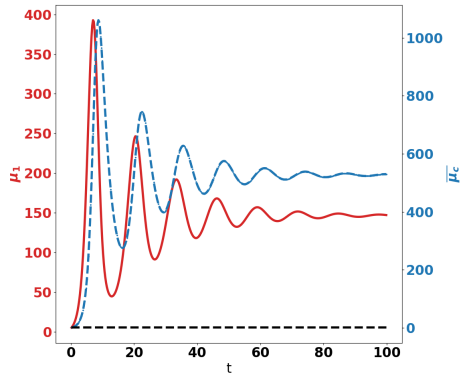

(c) $\alpha = 500$

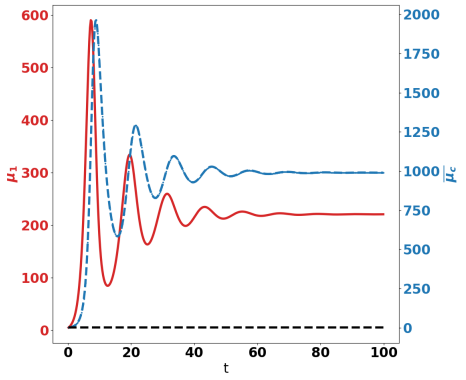

(d) $\alpha = 1000$

FIGURE 2.26 – Saturated interactions, homogeneous source of immune cells. Evolution of the tumor mass μ_1 (red curves, left axis), and of $\bar{\mu}_c$ (blue curve, right axis) for several values of α.

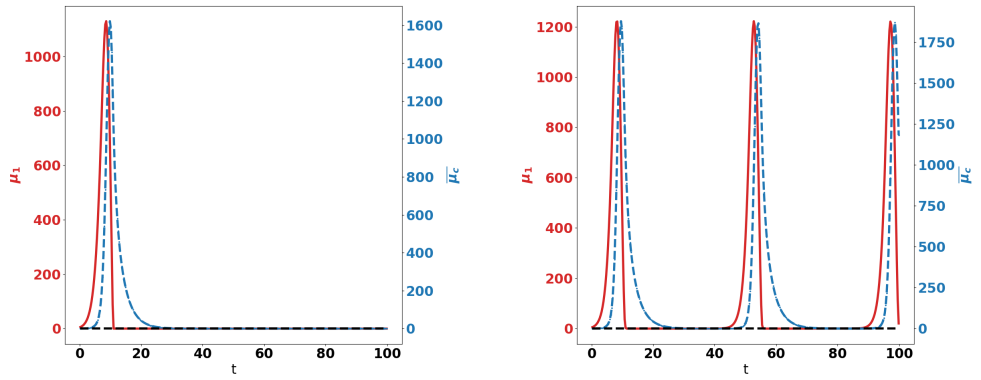

(a) $\alpha = 10$

(b) $\alpha = 100$

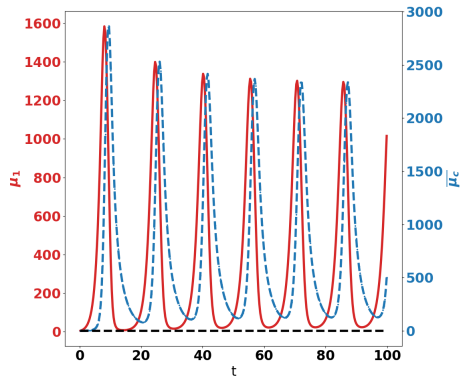

(c) $\alpha = 500$

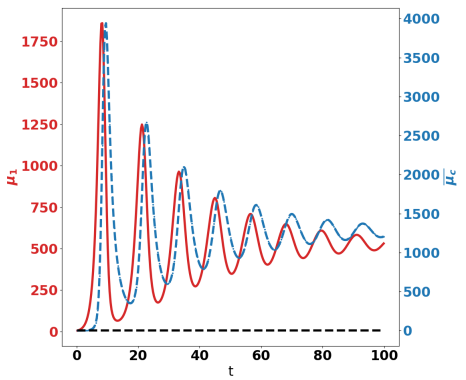

(d) $\alpha = 1000$

FIGURE 2.27 – Saturated interactions, heterogeneous source of immune cells. Evolution of the tumor mass μ_1 (red curves, left axis), and of $\bar{\mu}_c$ (blue curve, right axis) for several values of α.

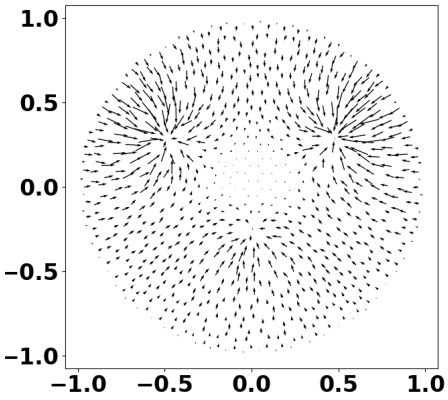

FIGURE 2.28 – Chemotactic potential at $t = 0.12$ in the case of multiple tumor sites with different division rates

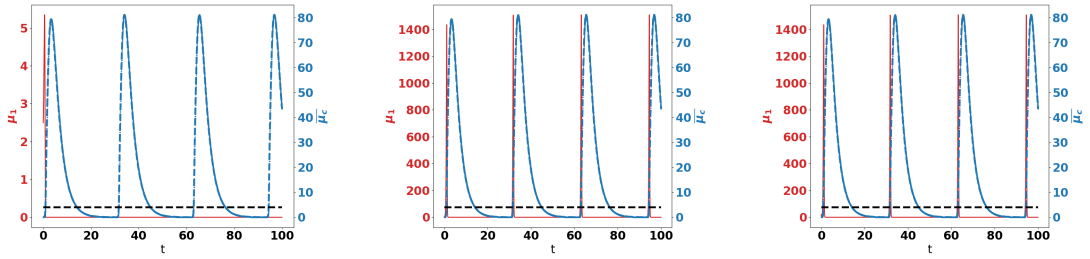

(a) a (b) $2a$ (c) $1.5a$

FIGURE 2.29 – Evolution of the tumor masses μ_1 (red curves, left axis), and of $\bar{\mu}_c$ (blue curve, right axis) for three different tumor sites.

Bibliographie

[1] Z. Agur, K. Halevi-Tobias, Y. Kogan, and O. Shlagman. Employing dynamical computational models for personalizing cancer immunotherapy. *Expert Opinion on Biological Therapy*, 16(11) :1373–1385, 2016.

[2] N. André, D. Barbolosi, F. Billy, G. Chapuisat, F. Hubert, E. Grenier, and A. Rovini. Mathematical model of cancer growth controled by metronomic chemotherapies. *ESAIM :ProcS*, 41 :77–94, 2013.

[3] F. Baccelli, D. McDonald, and J. Reynier. A mean field model for multiple TCP connections through a buffer implementing RED. *Performance Evaluation*, 49(1-4) :77–97, 2002.

[4] B. Basse, B. C. Baguley, E. Marshall, W. R. Joseph, B. van Brunt, G. Wake, and D. J. N. Wall. A mathematical model for analysis of the cell cycle in cell lines derived from human tumors. *J. Math. Biol.*, 47(4) :295–312, 2003.

[5] F. Bekkal Brikci, J. Clairambault, B. Ribba, and B. Perthame. An age-and-cyclin-structured cell population model for healthy and tumoral tissues. *J. Math. Biol.*, 57(1) :91–110, 2008.

[6] P. Bi, S. Ruan, and X. Zhang. Periodic and chaotic oscillations in a tumor and immune system interactionmodel with three delays. *Chaos*, 24 :023101, 2014.

[7] G. Caravagna, A. d'Onofrio, P. Milazzo, and R. Barbuti. Tumour suppression by immune system through stochastic oscillations. *J. Theor. Biol.*, 265(3) :336–345, 2010.

[8] D. A. Chen and I. Mellman. Oncology meets immunology : The cancer immunity cycle. *Immunity*, 39(1) :1–10, 2013.

[9] D. A. Chen and I. Mellman. Elements of cancer immunity and the cancer-immune set point. *Nature*, 541 :321–330, 2017.

[10] A. K. Cooper and P. S. Kim. A cellular automata and a partial differential equation model of tumor–immune dynamics and chemotaxis. In A. Eladdadi, P. Kim, and D. Mallet, editors, *Mathematical Models of Tumor-Immune System Dynamics*, pages 21–46, New York, NY, 2014. Springer New York.

[11] L. G. de Pillis, A. E. Radunskaya, and C. L. Wiseman. A validated mathematical model of cell-mediated immune response to tumor growth. *Cancer Res.*, 65(17) :7950–7958, 2005.

[12] U. Del Monte. Does the cell number 109 still really fit one gram of tumor tissue ? *Cell Cycle*, 8(3) :505–506, 2009. PMID : 19176997.

[13] A. Devys, T. Goudon, and P. Lafitte. A model describing the growth and size distribution of multiple metastatic tumors. *Disc. Cont. Dyn. Syst.-B*, 12 :731–767, 2009.

[14] A. d'Onofrio. A general framework for modeling tumor-immune system competition and immunotherapy : mathematical analysis and biomedical inferences. *Physica D*, 208(3-4) :220–235, 2005.

[15] A. d'Onofrio, G. F., P. Cerrai, and L. Fresch. Delay-induced oscillatory dynamics of tumour-immune system interaction. *Math. Comput. Model.*, 51 :572–591, 2010.

[16] M. Doumic. *Growth-fragmentation equations in biology*. Habilitation à diriger des recherches, Université Pierre et Marie Curie - Paris VI, June 2013.

[17] M. Doumic-Jauffret and P. Gabriel. Eigenelements of a general aggregation-fragmentation model. *Math. Models Methods Appl. Sci.*, 20(5) :757–783, 2010.

[18] G. P. Dunn, A. T. Bruce, H. Ikeda, L. J. Old, and R. D. Schreiber. Cancer immunoediting : from immunosurveillance to tumor escape. *Nat. Immunol.*, 3 :991–998, 2002.

[19] R. Eftimie, J. L. Bramson, and D. J. D. Earn. Interactions between the immune system and cancer : A brief review of non-spatial mathematical models. *Bull. Math. Biol.*, 73(1) :2–32, Jan 2011.

[20] R. Eftimie, J. J. Gillard, and D. A. Cantrell. Mathematical models for immunology : Current stateof the art and future research directions. *Bull. Math. Biol.*, 78 :2091–2134, 2017.

[21] R. Eymard, T. Gallouët, and R. Herbin. Finite volume methods. In P. Ciarlet and J.-L. Lions, editors, *Handbook of Numerical Analysis, Vol. VII*, volume VII of *Handb. Numer. Anal.*, pages 715–1022. North-Holland, 2000.

[22] J. Faget, S. Groeneveld, G. Boivin, M. Sankar, N. Zangger, M. Garcia, N. Guex, I. Zlobec, L. Steiner, A. Piersigilli, I. Xenarios, and E. Meylan. Neutrophils and snail orchestrate the establishmentof a pro-tumor microenvironment in lung cancer. *Cell Report*, 21 :3190–3204, 2017.

[23] J. D. Farrar, K. H. Katz, J. Windsor, G. Thrush, R. H. Scheuermann, J. W. Uhr, and N. E. Street. Cancer dormancy. VII. a regulatory role for $CD8+$ t-cells and $IFN - \gamma$ in establishing and maintaining the tumor-dormant state. *J. Immunol.*, 162(5) :2842–2849, 1999.

[24] B. E. Farrell, R. P. Daniele, and D. A. Lauffenburger. Quantitative relationships between single-cell and cell-population model parameters for chemosensory migration responses of alveolar macrophages to C5a. *Cell Motility*, 16(4) :279–293, 1990.

[25] A. Friedman and W. Hao. The role of exosomes in pancreatic cancer microenvironment. *Bull. Math. Biol.*, 80(5) :1111–1133, May 2018.

[26] P. Gabriel. *Transport-fragmentation equations and applications to prion diseases*. Phd thesis, Université Pierre et Marie Curie - Paris VI, June 2011.

[27] N. Glodde, T. Bald, D. van den Boorn-Konijnenberg, K. Nakamura, J. S. O'Donnell, S. Szczepanski, M. Brandes, S. Eickhoff, I. Das, N. Shridhar, D. Hinze, M. Rogava, T. C. van der Sluis, J. J. Ruotsalainen, G. E., J. Landsberg, K. U. Ludwig, C. Wilhelm, M. Riek-Burchardt, A. J. Müller, C. Gebhardt, R. A. Scolyer, G. V. Long, V. Janzen, M. W. L. Teng,

W. Kastenmüller, M. Mazzone, M. J. Smyth, T. Tüting, and M. Hölzel. Reactive neutrophil responses dependent on the receptor tyrosine kinase $c-MET$ limit cancer immunotherapy. *Immunity*, 47(4) :789 – 802.e9, 2017.

[28] D. Hanahan and R. A. Weinberg. The hallmarks of cancer. *Cell*, 100(1) :57 – 70, 2000.

[29] T. Hillen and K. J. Painter. A user's guide to PDE models for chemotaxis. *Journal of Mathematical Biology*, 58(1) :183, Jul 2008.

[30] D. Horstmann. From 1970 until present : the Keller-Segel model in chemotaxis and its consequences. I. *Jahresber. Deutsch. Math.-Verein.*, 105 :103–165, 2003.

[31] D. Horstmann. From 1970 until present : the Keller-Segel model in chemotaxis and its consequences. II. *Jahresber. Deutsch. Math.-Verein.*, 106 :51–69, 2003.

[32] E. Itakura, R.-R. Huang, D.-R. Wen, E. Paul, P. H. Wünsch, and A. J. Cochran. IL-10 expression by primary tumor cells correlates with melanoma progression from radial to vertical growth phase and development of metastatic competence. *Mod. Pathol.*, 24(6) :801–809, 2011.

[33] Y. Iwai, M. Ishida, Y. Tanaka, T. Okazaki, T. Honjo, and N. Minato. Involvement of PD-L1 on tumor cells in the escape from host immune system and tumorimmunotherapy by PD-L1 blockade. *Proc. Natl. Acad. Sci.*, 99(19) :12293–12297, 2002.

[34] J. N. Kather, J. Poleszczuk, M. Suarez-Carmona, J. Krisam, P. Charoentong, N. A. Valous, C.-A. Weis, L. Tavernar, F. Leiss, E. Herpel, F. . Klupp, A. Ulrich, M. Schneider, A. Marx, D. Jäger, and N. Halama. *In Silico* modeling of immunotherapy and stroma-targeting therapies in human colorectal cancer. *Cancer Res.*, 77(22) :6442–6452, 2017.

[35] E. F. Keller and L. A. Segel. Model for chemotaxis. *J. Theor. Biol.*, 30(2) :225 – 234, 1971.

[36] D. Kirschner and J. C. Panetta. Modeling immunotherapy of the tumor-immune interaction. *J. Math. Biol.*, 37 :235–252, 1998.

[37] C. M. Koebel, W. Vermi, J. B. Swann, N. Zerafa, S. J. Rodig, L. J. Old, M. J. Smyth, and R. D. Schreiber. Adaptive immunity maintains occult cancer in an equilibrium state. *Nature*, 450 :903–908, 2007.

[38] V. A. Kuznetsov, I. A. Makalkin, M. A. Taylor, and A. S. Perelson. Nonlinear dynamics of immunogenic tumors : Parameter estimation and global bifurcation analysis. *Bull. Math. Biol.*, 56(2) :295–321, Mar 1994.

[39] A. Matzavinos, M. A. J. Chaplain, and V. A. Kuznetsov. Mathematical modelling of the spatio-temporal response of cytotoxic T-lymphocytes to a solid tumour. *Mathematical Medicine and Biology*, 21(1) :1–34, 2004.

[40] E. D. McGrady and R. M. Ziff. "shattering" transition in fragmentation. *Phys. Rev. Lett.*, 58 :892–895, Mar 1987.

[41] P. Michel. Existence of a solution to the cell division eigenproblem. *Models Math. Meth. App. Sci.*, 16(Suppl. issue 1) :1125–1153, 2006.

[42] P. Michel, S. Mischler, and B. Perthame. General relative entropy inequality : an illustration on growth models. *J. Math. Pures et Appl.*, 84(9) :1235–1260, 2005.

[43] M. Müller, F. Gounari, S. Prifti, H. J. Hacker, V. Schirrmacher, and K. Khazaie. Eblacz tumor dormancy in bone marrow and lymph nodes : Active control of proliferating tumor cells by $CD8+$ immune t-cells. *Cancer Res.*, 58(23) :5439–5446, 1998.

[44] N. Nagarsteth, M. S. Wicha, and W. Zou. Chemokines in the cancer microenvironment and their relevance in cancer immunotherapy. *Nat. Rev. Immunol.*, 17 :559–572, 2017.

[45] S. Olver, P. . Groves, K. Buttigieg, E. S. Morris, M. L. Janas, A. Kelso, and N. Kienzle. Tumor-derived Interleukin-4 reduces tumor clearance and deviates the cytokine and granzyme profile of tumor-induced $CD8^+$ T-cells. *Cancer Res.*, 66(1) :571–580, 2009.

[46] B. Perthame. *Transport equations in biology*. Frontiers in Math. Birkhauser, 2007.

[47] B. Perthame and L. Ryzhik. Exponential decay for the fragmentation or cell-division equation. *J. Differ. Eq.*, 210 :155–177, 2005.

[48] G. A. Rabinovich, D. Gabrilovich, and E. M. Sotomayor. Immunosuppressive strategies that are mediated by tumor cells. *Ann. Rev. Immunol.*, 25(1) :267–296, 2007. PMID : 17134371.

[49] M. Robertson-Tessi, A. El-Kareh, and A. Goriely. A mathematical model of tumor–immune interactions. *J. Theor. Biol.*, 294 :56 – 73, 2012.

[50] H. Salmon, K. Franciszkiewicz, D. Damotte, P. Validire, A. Trautmann, F. Mami-Chouaib, and E. Donnadieu. Matrix architecture defines the preferential localization and migration of T-cells into the stroma of human lung tumors. *J. Clinical Investigation*, 122(3) :899–910, 2012.

[51] J. Shimizu, S. Yamazaki, and S. Sakaguchi. Induction of tumor immunity by removing $CD25^+$ $CD4^+$ t-cells : A common basis between tumor immunity and autoimmunity. *J. Immunol.*, 163 :5211–5218, 1999.

[52] C. Y. Slaney, M. H. Kershaw, and P. K. Darcy. Trafficking of t-cells into tumors. *Cancer Res.*, 74 :7168–7174, 2014.

[53] M. J. Smyth, D. I. Godfrey, and J. A. Trapani. A fresh look at tumor immunosurveillance and immunotherapy. *Nat. Immunol.*, 2, 2001.

[54] T. H. Stewart. Immune mechanisms and tumor dormancy. *Medicina (B Aires)*, 56(Suppl. 1) :74–82, 1996.

[55] A. Talkington and R. Durrett. Estimating tumor growth rates *in vivo*. *Bull. Math. Biol.*, 77(10) :1934–1954, 2015.

[56] T. A. Traina, U. Dugan, B. Higgins, K. Kolinsky, M. Theodoulou, C. A. Hudis, and L. Norton. Optimizing chemotherapy dose and schedule by Norton-Simon mathematical modeling. *Breast disease*, 131 :7–18, 2010.

[57] K. P. Wilkie and P. Hahnfeldt. Modeling the dichotomy of the immune response to cancer : Cytotoxic effects and tumor-promoting inflammation. *Bull. Math. Biol.*, 79 :1426–1448, 2017.

CHAPITRE. 3

Analysis of the equilibrium phase in immune-controlled tumor

Contents

Abstract : Extensive research and clinical trials have improved our understanding of tumor immunology but despite considerable clinical benefits, current immunotherapies only provide durable responses in a minority of patients with cancer. The challenge is to identify key biological parameters maintaining an equilibrium state and preventing immune escape. Based on a previously described space and size structured partial differential equation model, we developed numerical methods to predict the parameters of the equilibrium without running simulations of the evolution problem. By using global sensitivity analysis methods, we investigated the influence of the immune response and tumor growth parameters of the model and identified the elimination rate of tumor cells by immune cells as the leading parameter on the equilibrium size of the tumor. Our findings support the use of combinations of drugs which sustain and strengthen the immune response in order to control the tumor mass. Applied to relevant biological parameters for each type of cancer analyzed, such numerical investigation can provide hints for the design and optimization of cancer treatments.
Significance : Based on a space and size structured PDE model, the analyses of the equilibrium phase in immune surveillance of cancer provide numerical methods to evaluate the influence of immune response and tumor growth parameters and hints for the design and optimization of cancer treatments.

3.1 Introduction

The immune system plays a major role in the control of tumor growth. This has led to the concept of immune surveillance and cancer immunoediting composed of three phases [18, 19] : the elimination, where tumors are rapidly eradicated by the immune system, the equilibrium, a latency period where tumors can survive but remain on a controlled state, and the escape, the final outgrowth of tumors that have outstripped immunological restraints. In this later phase, immune suppression is prevailing and immune cells are also subverted to promote tumor growth. Numerous cancer immunotherapy strategies have been designed and assessed to counteract cancer immune evasion and restore effective and durable elimination of tumors [6, 17, 30, 54, 62, 67, 70]. They show improved efficacy over conventional anticancer treatments but only a minority of patients respond. The challenge to face now is to identify key biological parameters which will convert a fatal outcome into a chronic, manageable state, the durable maintenance of cancer in a viable equilibrium phase controlled by immunity. Reaching an equilibrium stage in immune-controlled tumors is indeed the first key step for successful control of tumor growth and a goal for immunotherapy. Mathematical modeling of the tumor-immune system interactions can provide useful hints about the features of the equilibrium phase during primary tumor development, and guide the design of therapies to boost the immune response [37, 36, 38, 42, 53, 69].

In the previous chapter we introduced a specific mathematical model based on partial differential equations, intended to describe the earliest stages of this interaction. The originality of the model was to introduce size-space structured quantities, providing new perspectives compared to mere ordinary differential systems [14, 20, 37, 56, 68]. The model thus accounted for both the growth of the tumor, by natural cell growth and cell divisions, and the displacement of the immune cells towards the tumor, by means of activation processes and chemotaxis effects. The

most notable finding was that an equilibrium state can be observed, with residual tumor and active immune cells. Mathematical analysis provided a basis for the explanation of the possible formation of the equilibrium, which was indeed observed in numerical experiments. However, even if the model is able to reproduce, in the long-time range, cancer-persistent equilibrium, the theory is not yet complete to fully understand this phenomena, and the circumstances on which the equilibrium establishes. We therefore further investigated on numerical grounds the features of the equilibrium formation. Our purpose was two-fold. First, as far as we know, the total mass of the residual tumor – which is certainly a critical property of the equilibrium – was obtained in an implicit way. Hence, we wished to design a complete numerical procedure in order to compute the final mass, for a given set of biological parameters of the model. Second, it is relevant to address the question of the sensitivity of the residual mass to the parameters. This information can be decisive to design further clinical experiments and therapeutic strategies. this work therefore provides a tool for cancer treatment management.

3.1.1 Quick guide to equations : A coupled PDE model for tumor-immune system interactions

The principles of the modeling adopted in chapter 2 led to couple an evolution equation for the size-distribution of the tumor cells, and a convection-diffusion equation for the activated immune cells. The two-way coupling arose by the death term induced by the action of the immune cells on the tumor cells, and by the activation and the attraction of immune cells towards the tumor, which are determined by the total mass of the tumor. The unknowns are

— the size density of tumor cells $(t, z) \mapsto n(t, z)$ so that the integral $\int_a^b zn(t, z)\,\mathrm{d}z$ gives the volume of the tumor occupied at time t by cells having their size z in the interval (a, b) ;

— the concentration of activated immune cells which are fighting against the tumor $(t, x) \mapsto c(t, x)$;

— the concentration of chemical signal that attracts the immune cells towards the tumor micro-environment $(t, x) \mapsto \phi(t, x)$.

The model assumes that the tumor is located at the center of a domain Ω, and it distinguishes two distinct length scales. The size of the tumor cells $z \geq 0$ is considered as “infinitely small” compared to the scale of displacement of the immune cells, described by the space variable $x \in \Omega$. Immune cells, once activated, are subjected to natural diffusion and to a chemotactic drift, induced by the presence of the tumor. The strength of this drift, as well as the activation of immune cells, directly depends on the total mass of the tumor, proportional to the quantity

$$\mu_1(t) = \int_0^\infty zn(t, z)\,\mathrm{d}z.$$

The immune system-tumor competition is described by the following system of PDEs

$$\partial_t n + \partial_z(Vn) = Q(n) - m(n,c), \tag{3.1a}$$

$$\partial_t c + \nabla_x \cdot (c\chi\nabla_x\phi - D\nabla_x c) = \mu_1 R - \gamma c, \tag{3.1b}$$

$$-\mathcal{K}\Delta_x\phi = \mu_1\left(\sigma(x) - \int_\Omega \sigma(y)\,\mathrm{d}y\right), \tag{3.1c}$$

$$n(t,0) = 0,\ c|_{\partial\Omega} = 0,\ \mathcal{K}\nabla_x\phi\cdot\nu(\cdot)|_{\partial\Omega} = 0, \tag{3.1d}$$

$$n(t=0,z) = n_0(z),\ c(t=0,x) = c_0(x). \tag{3.1e}$$

The growth-division dynamics for the tumor cells (3.1a) involves the (possibly size-dependent) growth rate $z \mapsto V(z) \geq 0$ and the cell division mechanism is embodied into the operator $Q(n)$. What is crucial for modeling purposes is the principle that cell-division does not change the total mass : the operator Q satisfies $\int_0^\infty zQ(n)\,\mathrm{d}z = 0$. However, the total number of cells in the tumor increases since $\int_0^\infty Q(n)\,\mathrm{d}z \geq 0$ (we refer the reader to chapter 2 for further details). In what follows, we restrict to the mere symmetric binary division operator

$$Q(n)(t,z) = a(4n(t,2z) - n(t,z)), \tag{3.2}$$

with $a > 0$ the division rate. Further relevant examples of division operators can be found in [16]. The boundary condition for n in (3.1d) means that no tumor cells are created with size 0.

In the right hand side of (3.1b), $(t,x) \mapsto R(t,x)$ stands for the space distribution of the influx rate of activated tumor antigen specific effector immune cells. It takes into account the sources of naive immune cells, namely T-cells and NK cells, that can be activated in the tumor microenvironment or in the draining lymph nodes into cells fighting the tumor. The rate of the activation process is supposed to be directly proportional to μ_1. The Dirichlet boundary condition for c in (3.1d) means that the immune cells far from the tumor are non-activated. Immune cells are directed towards the tumor by a chemo-attractive potential ϕ, induced by the presence of the tumor cells. Through (3.1c), the strength of the signal is proportional to the total mass of the tumor, and it is shaped by a form function $x \mapsto \sigma(x)$. Finally, the activated immune cells are able to destroy tumor cells, as described by the death term in (3.1a)

$$m(c,n)(t,z) = \int_\Omega \delta(y)c(t,y)\,\mathrm{d}y \times n(t,z), \tag{3.3}$$

where $\delta \geq 0$ is another form function. For the numerical experiments, we shall work with the Gaussian profiles

$$\delta(x) = \frac{A}{\theta\sqrt{2\pi}}\exp\left(-\frac{|x|^2}{2\theta^2}\right), \qquad \sigma(x) = \frac{A_\sigma}{\theta_\sigma\sqrt{2\pi}}\exp\left(-\frac{|x|^2}{2\theta_\sigma^2}\right). \tag{3.4}$$

We refer the reader to chapter 2 for further details and comments about the model.

3.2 Materials and Methods

Mice FVB/N wild-type (WT) mice (Charles River Laboratories, St Germain Nuelles, France) were bred and housed in specific-pathogen-free conditions. Experiments were performed using 6-7 week-old female FVB/N, in compliance with institutional guidelines and have been approved by the regional committee for animal experimentation (reference MESR 2016112515599520; CIEPAL, Nice Côte d'Azur, France).

In vivo tumor growth mSCC38 tumor cell line was established from DMBA/PMA induced sSCCs and maintained in DMEM (Gibco-ThermoFisher Scientific, Courtaboeuf, France) supplemented with 10% heat-inactivated fetal bovine serum (FBS) (GE Healthcare, Chicago, Illinois, USA) penicillin (100 U/ml) and streptomycin (100 $\mu g/ml$) (Gibco-ThermoFisher Scientific, Courtaboeuf, France). 5×10^5 mSCC38 were intradermally injected in anesthetized mice after dorsal skin shaving. Tumor volume was measured manually using a ruler and calculated according to the ellipsoid formula : Volume=Length $(mm) \times$ Width $(mm) \times$ Height $(mm) \times \pi/6$.

Tissue preparation and cell count mSCC38 were excised and enzymatically treated twice with collagenase IV (0.6 mg/ml) (Sigma-Aldrich, St Quentin Fallavier, France), dispase II (2.5 mg/ml) and DNase I (0.2 mg/ml) (Roche Diagnostic, Meylan, France) for 20 minutes at 37° C. Total cell count was obtained on a Casy cell counter (Ovni Life Science, Bremen, Germany). Immune cell count was determined from flow cytometry analysis. Cell suspensions were incubated with anti-CD16/32 (2.4G2) to block Fc receptors and stained with antiCD45 (30-F11).

Mathematical and statistical analysis Computations were realized in `Python` and we made use of dedicated libraries, in particular the packages `stats` (linear regression), `optimize` (for the Levenberg-Marquard mean square algorithm; similar results have been obtained with the CMA-ES algorithm of the library `cma`) from the library `scipy`, the library `Pygpc` for the generalized Polynomial Chaos approximation [66] and the library `Salib` for the sensitivity analysis [33]. We also performed numerical experiments with the library `Ray` for parallelization methods [49].

3.3 Results

3.3.1 Identification of biological parameters

The PDE system is governed by the set of parameters collected in Table 3.1 : most parameter values were retrieved from previously published experimental results.

Symbol	Description	Value and unit	References
χ	chemotactic coefficient	$8.64 \times 10^1 - 8.64 \times 10^6$ $mm^2 \cdot mmol^{-1} \cdot day^{-1}$	(Macrophages) [24]
D	natural space diffusion coef. of the cytotoxic effector cells population	$8.64 \times 10^{-5} - 10^{-3}$ $mm^2 \cdot day^{-1}$	(CD8+ T-cells) [25], [45]
R	the normal rate of influx of effector immune cells	$6.11 \times 10^{-7}, 9.74 \times 10^{-7}$ $\frac{cell_c \cdot mm^{-3}}{\mu m^3} \cdot day^{-1}$	estimated
γ	natural death rate of the tumor antigen-specific cytotoxic effector cells	$2 \times 10^{-2} - 1 \quad day^{-1}$	[1], [10], [14], [40]
A	strength of the immune response	$2 - 57.6\ cell_c^{-1} \cdot day^{-1}$	[5], [8], [31], [50]
$\mathcal{K}$	natural space diffusion of the attractive potential ϕ	$10^{-2} - 1\ mm^2 \cdot day^{-1}$	[41], [45]
A_σ	strength of the chemical signal induced by each tumor cell	$5 \cdot 10^{-17} - 0.625 \times 10^{-16}$ $mmol \cdot^{-1} \mu m^3 \cdot day^{-1}$	[7]
a	division rate of the tumor cells	$0.103 - 0.351\ day^{-1}$	estimated
V	growth rate of the tumor cells	$308.526 - 2521.975$ $\mu m^3 \cdot day^{-1}$	estimated

TABLE 3.1 – Key model parameters and their biophysical meaning

To estimate the parameter R, we used a simple linear regression, by using 34 data points from an in vivo experimental cutaneous squamous cell carcinoma (cSCC) tumor growth mouse model [35] : R is predicted from the "influx rate of effector immune cell", denoted by Y and expressed in $cell_c \cdot day^{-1}$, given as a function, assumed to be linear, of the volume of the tumor μ_1 in μm^3, see Fig. 3.1-(a). The determination coefficient and the p-value are respectively, $r^2 = 0.705$ and $p = 2.84 \cdot 10^{-10}$, the slope of the regression line is $R = 7.92 \cdot 10^{-7}$. It is measured in $\frac{cell_c \cdot mm^{-3}}{\mu m^3} \cdot day^{-1}$ assuming homogeneity with respect to the unit mm^3. Table 3.1 gives the 95% confidence interval. This interval is quite small, but it already shows a sensitive impact of variations of this parameter; since the variability due to the biological model is likely important and we wished to investigate the impact of treatments that directly affect this parameter, we also

made some simulations with a larger range of values.

We turn to the determination of the tumor growth parameters a and V. Neglecting the immune response, the tumor growth is driven by

$$\partial_t n + \partial_z(Vn) = Q(n). \tag{3.5}$$

As explained below, this leads to an exponential growth of the tumor mass, see [16, 26, 46, 47, 51, 52]. Let $t \mapsto \mu_0 = \int_0^\infty n(t,z)\,\mathrm{d}z$ and $t \mapsto \mu_1(t) = \int_0^\infty zn(t,z)\,\mathrm{d}z$. We thus get

$$\frac{\mathrm{d}}{\mathrm{d}t}\mu_0 = a\mu_0, \qquad \frac{\mathrm{d}}{\mathrm{d}t}\mu_1 = V\mu_0. \tag{3.6}$$

We now aim at estimating the division rate a and the growth rate V from the experimental data. We denote $\Theta = (a, V)$ the parameters to be identified. We have at hand some experimental noisy data $(Y_1^{(0)}, \cdots, Y_n^{(0)})$, $(Y_1^{(1)}, \cdots, Y_n^{(1)})$ representing respectively μ_0 and μ_1 at several times. Hence, we have

$$Y_i^{(j)} = \mu_{j,\Theta}(t_i) + \epsilon_i, \quad i \in \{1, \cdots, n\}, \quad j \in \{0, 1\} \tag{3.7}$$

where $t \mapsto (\mu_{0,\Theta}, \mu_{1,\Theta})(t)$ stands for the solution of (3.6) defined with the parameters Θ. Forgetting for a while the discreteness of the observed data, the approach can be expressed as a cost minimization problem where the cost function is defined by

$$C_\lambda^{(j)}(\Theta) = \int_0^T |\mu_{j,\Theta}(t) - Y^{(j)}(t)|^2\,\mathrm{d}t. \tag{3.8}$$

We finally set

$$\widehat{\Theta} = \mathrm{argmin}\{C_\lambda^{(j)}(\Theta),\ \Theta = (a, V),\ a > 0,\ V > 0\}. \tag{3.9}$$

We fit the data that give the number of cells in the tumor and the volume of the tumor for several times by using a non-linear least square algorithm, the Levenberg-Marquardt algorithm [48], [55], Fig. 3.1.

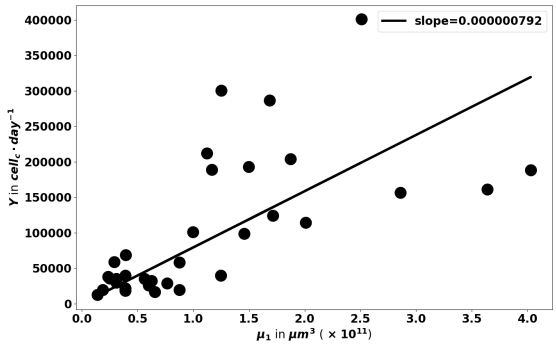

(a) rate of effector immune cell

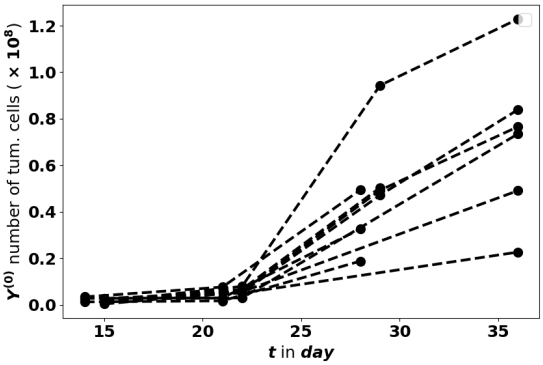

(b) tumor cell number

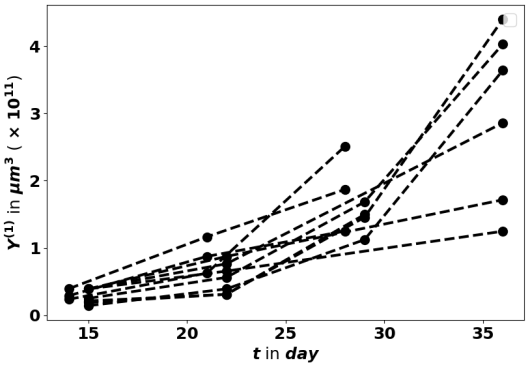

(c) tumor volume

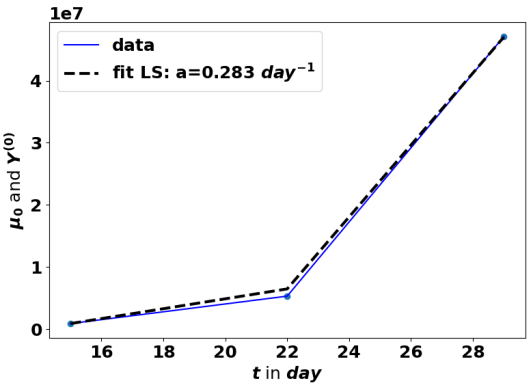

(d) curve fit of tumor cell number

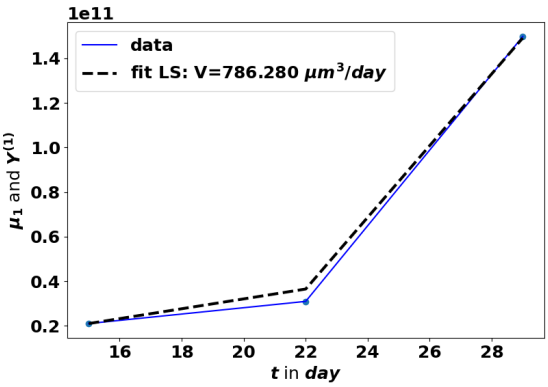

(e) curve fit of tumor volume

FIGURE 3.1 – Top : Regression on the "rate of effector immune cell" in $cell_c \cdot day^{-1}$ denoted by Y, as a function of the tumor volume μ_1 in μm^3 Middle : Tumor evolution kinetics kinetics from in vivo experimental cSCC tumor growth in mice. Bottom : Illustration of the estimation of the parameters a and V. Here, we found $a = 0.283\ day^{-1}$ and $V = 786.280\ \mu m^3 \cdot day^{-1}$ using 3 data points of a typical tumor evolution kinetic, from the dataset depicted in (b) and (c)

3.3.2 Development of numerical methods predicting parameters of the equilibrium in immune-controlled tumors

Based on the space and size structured PDE model (3.1a)-(3.1e), we study the equilibrium phase in immune-controlled tumors. We wish to predict, for given biological parameters, see Table 3.1, the total mass of the residual tumor and its size distribution. To this end, we developed specific numerical procedures based on the mathematical interpretation of the equilibrium.

Equilibrium states

The definition of the equilibrium relies on the following arguments. The cell-division equation admits a positive eigenstate : in absence of immune response, see (3.5), the tumor population grows exponentially fast, with a rate $\lambda > 0$, and its size repartition obeys a certain profile $\overline{N}$. The equilibrium occurs when the immune response counterbalances the growth rate of this equation. To be more specific, we look for $\lambda > 0$ and a non negative function $z \geq 0 \mapsto \overline{N}(z)$ satisfying

$$\begin{cases} \partial_z(V\overline{N}) - Q(\overline{N}) + \lambda\overline{N} = 0 \text{ for } z \geq 0 \\ \overline{N}(0) = 0, \qquad \overline{N}(z) > 0 \text{ for } z > 0, \qquad \int_0^{+\infty} \overline{N}(z)\,\mathrm{d}z = 1. \end{cases} \tag{3.10}$$

The existence-uniqueness of the eigenpair $(\lambda, \overline{N})$ can be found in [16, 46, 51]. When the tumor does not interact with the immune system, the large time behavior is precisely driven by the eigenpair : the solution of (3.5) behaves likes $n(t,z) \sim_{t\to\infty} \nu_0 e^{\lambda t}\overline{N}(z)$ where ν_0 is a constant determined by the initial condition, see [15, 46, 47]. In the specific case where V is constant and Q is the binary division operator (3.2), we have $\lambda = a$ and the profile $\overline{N}$ is explicitly known, [3, 51, 52]. However, for general growth rates and division kernels the solution should be determined by numerical approximations.

Coming back to the coupled model, we infer that the equilibrium phase corresponds to the situation where the death rate precisely counterbalances the natural exponential growth of the tumor cell population. In other words, the equilibrium is defined by the stationary equation

$$\gamma C - \nabla_x \cdot (D\nabla_x C) - \mu_1 \nabla_x \cdot (\chi C \nabla_x \Phi) = g(\mu_1) pS, \qquad C|_{\partial\Omega=0} = 0, \tag{3.11}$$

where Φ is the solution of

$$-\Delta_x \Phi = \sigma - \frac{1}{|\Omega|}\int_\Omega \sigma(y)\,\mathrm{d}y,$$

endowed with the homogeneous Neumann boundary condition, together with the constraint

$$\int_\Omega \delta(x) C(x)\,\mathrm{d}x = \lambda. \tag{3.12}$$

This can be interpreted as an implicit definition of the total mass μ_1, to be the value such that the solution of the boundary value problem (3.11) satisfies (3.12). The existence of an equilibrium state defined in this way is rigorously justified in chapter 2, Theorem 2.2.2. Fig. 3.2 illustrates how the equilibrium establishes in time : as time becomes large, the concentration of active immune cells in the neighborhood of the tumor tends to the eigenvalue of the cell-division equation, the total mass tends to a constant and the size distribution of tumor cells takes the profile of the corresponding

eigenstate. This result has been obtained by using the lower bounds of the parameters in Table 3.1 for the immune system and $(a, V) = (0.351, 713.608)$ for the tumor growth, We observe a non symmetric shape, peaked about a diameter of 13 μm, which is consistent with observational data reporting the mean size distribution of cancer cells [60].

Numerical experiments show that the model (3.1a)–(3.1e) is able to reproduce, in the long-time range, cancer-persistent equilibrium, but the features of the equilibrium, and its ability to establish, are highly sensitive to the parameters in Table 3.1 . To discuss this issue further, we focus here on the mass at equilibrium considered as a critical quantity that evaluates the efficacy of the immune response. Indeed, it is known that a tumor gains in malignancy when its mass reaches certain thresholds [23, 44], see also chapter 4 and the references therein. The smaller the tumor mass at equilibrium, the better the vital prognosis of the patient. In doing so, we do not consider transient states and time necessary for the equilibrium to establish (see Fig. 3.4-(a-c) below).

The determination, on numerical grounds, of the equilibrium state relies on a two-step process. First, we compute the normalized eigenstate of the tumor cell equation, second, we find the tumor mass which makes the coupled death rate fit with the eigenvalue. To this end, we have developed a specific numerical approach.

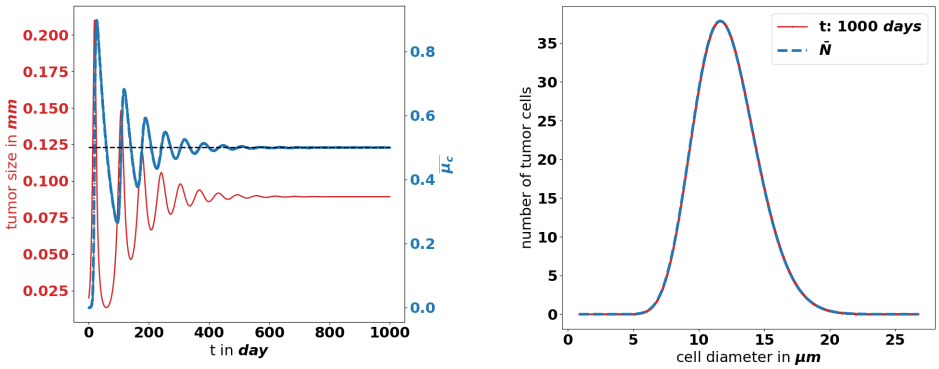

(a) Time evolution of the diameter of the tumor (red) and concentration of active immune cells (blue)

(b) Eigenstate $\bar{N}$ of (3.10) and the equilibrium profile from the evolution equation

FIGURE 3.2 – Left : evolution of the mean concentration of active immune cells in the neighborhood of the tumor (blue), and evolution of the total mass of the tumor (red). Right : Comparison of the tumor cell-size distribution at $T = 1000\ days$ with the positive eigenstate of the cell division equation (x-axis : size of the tumor cells, y-axis : number of tumor cells at the final time)

The eigen-elements of the growth-division equation

The numerical procedure is inspired from the spectral analysis of the equation : λ is found as the leading eigenvalue of a conveniently shifted version of the growth-division operator. In

practice, we work with a problem where the size variable is both truncated and discretized. Hence, the problem recasts as finding the leading eigenvalue of a shifted version of the underlying matrix, which can be addressed by using the inverse power method [29, Section 1.2.5]. We refer the reader to [11, 12] for a thorough analysis of the approximation of eigenproblems for differential and integral operators, which provides a rigorous basis to this approach. It is also important to check a priori, based on the analysis of the equation [16], how large the shift should be, and that it remains independent on the numerical parameters, see Appendix-Section 3.5.3. For some specific fragmentation kernels and growth rates, the eigenpair (λ, N) is explicitly known, see [16]. We used these formula to validate the ability of the algorithm to find the expected values and profiles, see Appendix-Section 3.5.3.

Computation of the equilibrium mass

Having at hand the eigenvalue λ, we go back to the convection-diffusion equation (3.11) and the constraint (3.12) that determine implicitly the total mass μ_1 of the residual tumor. For a given value of μ_1, we numerically solve (3.11) by using a finite volume scheme, see chapter 2, section 2.5.3. Then, we use the dichotomy algorithm to fit the constraint :

— The chemo-attractive potential Φ is computed once for all.

— Pick two reference values $0 < \mu_a < \mu_b$; the mass we are searching for is expected to belong to (μ_a, μ_b).

— Set $\mu_1 = \dfrac{\mu_a + \mu_b}{2}$ and compute the associated solution C_{μ_1} of (3.11). Evaluate the discrete version of $I = \int \delta C_{\mu_1} \, \mathrm{d}x - \lambda$.

— If $I < 0$, then replace μ_a by μ_1, otherwise replace μ_b by μ_1.

— We stop the algorithm when the relative error $\frac{\mu_b - \mu_a}{\mu_a} < \epsilon$ is small enough.

It is also possible to design an algorithm based on the Newton method. However, this approach is much more numerically demanding (it requires to solve more convection-diffusion equations) and does not provide better results.

For the evaluation of the residual mass, we do not know explicit solutions, even for the simplest model. Nevertheless, we can compare the results of the inverse power-dichotomy procedure that predicts the residual mass, to the large time simulations as performed in chapter 2.

Therefore, we adopt the same framework as in chapter 2 : the tumor is located at the origin of the computational domain Ω, which is the two-dimensional unit disk. We work with the lower bound of the parameters collected in Table 3.1 . We compare the asymptotic value of the total mass μ_1^f given by the large time simulation of the evolution problem (and checking that the variation of the total mass has become negligible) to the total mass μ_1^{pd} predicted by the power-dichotomy procedure; let

$$E_{\mu_1} = \frac{|\mu_1^f - \mu_1^{pd}|}{\mu_1^f}.$$

The results for several cell division rates a are collected in Table 3.2 : the numerical procedures finds the same equilibrium mass as the resolution of the evolution problem, which is another validation of the method.

a	μ_1^f (mm^3) at final time $T = 500$	μ_1^{pd} (mm^3)	E_{μ_1}
0.103	$7.67271875 \times 10^{-5}$	$7.67271872 \times 10^{-5}$	4.10×10^{-9}
0.15	$1.11701535 \times 10^{-4}$	$1.11701543 \times 10^{-4}$	7.97×10^{-8}
0.20	$1.48924575 \times 10^{-4}$	$1.48924641 \times 10^{-4}$	4.40×10^{-7}
0.3	$2.23420663 \times 10^{-4}$	$2.23420562 \times 10^{-4}$	4.53×10^{-7}
0.351	$2.61368442 \times 10^{-4}$	$2.61367974 \times 10^{-4}$	1.80×10^{-6}

TABLE 3.2 – Comparison of the large time tumor mass and the predicted tumor mass for several values of a

3.3.3 Numerical simulations show how parameters influence equilibrium

The numerical methods were used to assess how the parameters influence the equilibrium. In particular, we wish to assess the evolution of the tumor mass at equilibrium according to immune response and tumor growth parameters.

For the numerical simulations presented here, we thus work on the eigenproblem (3.10) and on the constrained system (3.11)-(3.12). Unless precisely stated, the immune response parameters are fixed to the lower bounds in Table 3.1. The tumor growth parameters are set to $a = 0.3\ day^{-1}$ and $V = 469.545\ \mu m^3 \cdot day^{-1}$. When necessary, the initial values of the unknowns are respectively $\mu_0(0) = 1\ cell_n$, $\mu_1(0) = 4188\ \mu m^3$, $c(0, x) = 0$.

The main features of the solutions follow the observations made in chapter 2, which were performed with arbitrary "academic" values for the parameters. We observe that $\int_\Omega \delta(y)c(t, y)\,\mathrm{d}y$ tends to the division rate a, which in this case corresponds to the leading eigenvalue of the cell-division equation. It is remarkable that the predicted diameter of the tumor at equilibrium — see Fig. 3.2 — is significantly below modern clinical PET scanners resolution limit, which could detect tumors with a diameter larger than 7 mm [21].

The aggressiveness of the tumor is characterized by the division rate, the variations of which impact the size of the tumor at equilibrium : the larger a, the larger the residual tumor, see Fig. 3.3-(a). Increasing the immune strength A increases the efficacy of the immune response, reducing the size of the residual tumor see Fig. 3.3-(b). Similarly, increasing the mean rate of influx of effector immune cells in the tumor microenvironment R, decreases the tumor size at equilibrium, see Fig. 3.3-(c). On the contrary, increasing the diffusion coefficient D reduces the efficacy of the immune response and increases the equilibrium tumor size see Fig. 3.3-(d).

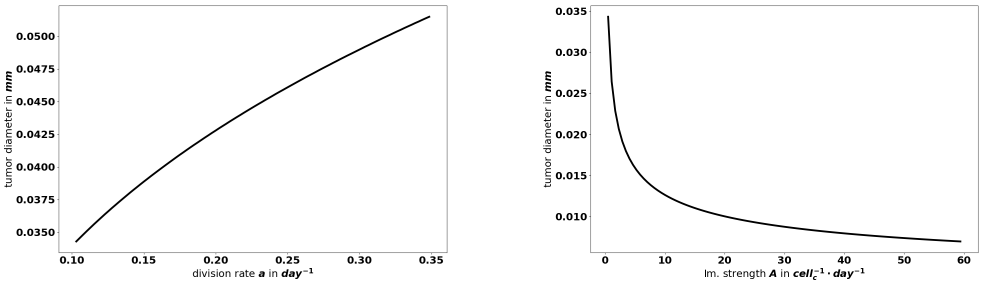

(a) division rate a

(b) immune strength A

(c) influx rate R

(d) death rate γ of the effector cells

FIGURE 3.3 – Evolution of the tumor diameter at equilibrium, with respect to the division rate a, the strength of the effector immune cells A, the influx rate of effector immune cells R, the natural death rate γ of the effector cells

Moreover, as mentioned above, not only the parameters determine the equilibrium mass, but they also impact how the equilibrium establishes. Fig. 3.4-(a-c) shows what happens by making the tumor cell division rate a vary. There are more oscillations along time, with larger amplitude, as a increases. Similar observations can be made by playing with the strength of the immune system. Fig 3.4-(d-f) shows several scenario, which illustrate that the relevance of the equilibrium can be questionable depending on the value of the parameters. Here, we make the strength of the immune system A vary (likely out of its realistic range). The smaller A, the smaller the damping of the oscillations and the longer the periods. We notice that the decay of the maximal tumor radius holds at a polynomial rate. In extreme situations, the equilibrium does not establish on reasonable observation times, and the evolution can be confounded with a periodic alternance of growing and remission phases. In what follows, we focus on the details of the equilibrium itself, rather than on the transient states.

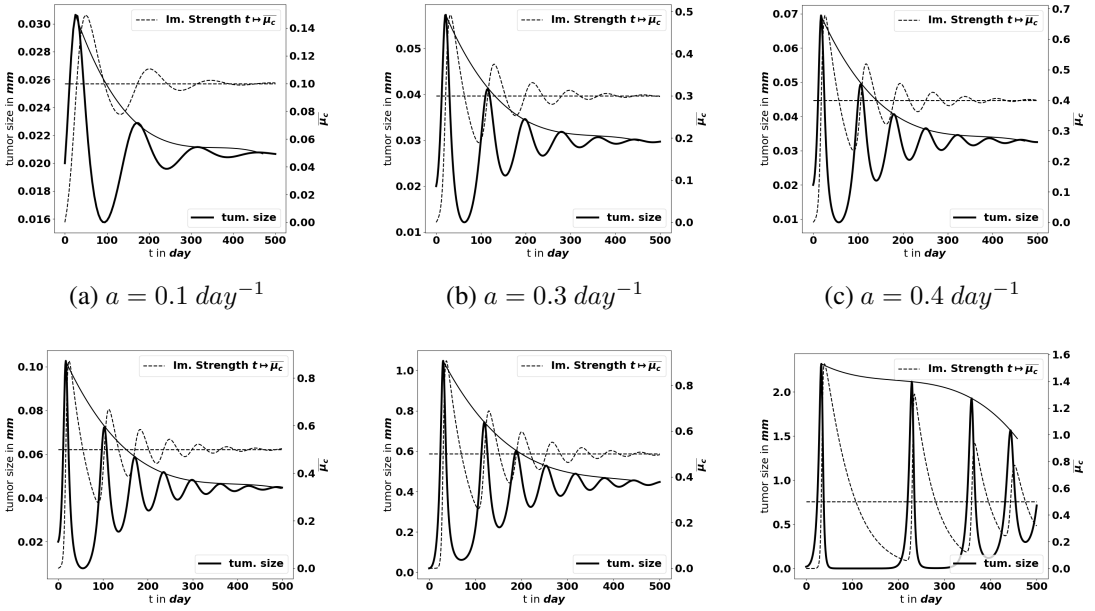

(a) $a = 0.1\ day^{-1}$ (b) $a = 0.3\ day^{-1}$ (c) $a = 0.4\ day^{-1}$

(d) $A = 1\ cell_c^{-1} \cdot day^{-1}$ (e) $A = 1 \cdot 10^{-3}\ cell_c^{-1} \cdot day^{-1}$ (f) $A = 5 \cdot 10^{-5}\ cell_c^{-1} \cdot day^{-1}$

FIGURE 3.4 – Large-time simulation of the PDE system : evolution of the tumor diameter (red curves, left axis), and of the concentration of immune cells $\bar{\mu}_c$ (blue curve, right axis), for several values of the division rate a (top) and for several values of the immune strength A (bottom). The equilibrium needs more time to establish as the strength of the immune system decreases

3.3.4 Global sensitivity analysis on the equilibrium mass identifies the key parameters to target in cancer therapy

Since we are able to predict for a reduced numerical cost the residual mass of the equilibrium phase, we can discuss in further details the influence of the parameters on this criterion, by means of a global sensitivity analysis. Details on the applied methods for the sensitivity analysis can be found in the Appendix-Section 3.5.4. Among the parameters, we distinguish :

— the tumor cell division rate a which drives the tumor aggressiveness,

— the efficacy of the immune system, governed by the mean influx rate of activated effector immune cells R, the strength of the immune response A, the chemotactic sensitivity χ, the death rate γ of the immune cells, and the strength of the chemical signal induced by each tumor cell A_σ

— environmental parameters such as the diffusion coefficients D (for the immune cells) and $\mathcal{K}$ (for the chemokine concentration).

We assume that the input parameters are independent random variables. Due to the lack of knowledge on the specific distribution of these parameters and according to the constraints on

the parameter bounds (Table 3.1), the most suitable probability distribution is the one which maximizes the continuous entropy ([32]), more precisely, the uniform distribution. Therefore, the uncertainty in the parameter values is represented by uniform distributions $\mathcal{U}(p_{min}, p_{max})$ where p_{min} and p_{max} are respectively the lower and upper bound of each uncertain input parameter (see Table 3.1). In what follows, the total mass at equilibrium, μ_1, given by the power-dichotomy algorithm, is seen as a function of the uncertain parameters :

$$\mu_1 = f(a, A, R, \chi, D, A_\sigma, \gamma, \mathcal{K}). \tag{3.13}$$

To measure how the total variance of the output μ_1 of the algorithm is influenced by some subsets $i_1 \cdots i_p$ of the input parameters $i_1 \cdots i_k$ ($k \geq p$ being the number of uncertain input parameters), we compute the so-called Sobol's sensitivity indices. The total effect of a specific input parameter i is evaluated by the total sensitivity index $S_T^{(i)}$, the sum of the sensitivity indices which contain the parameter i. (Details on the computed Sobol indices can be found in Suppl. Material). The computation of these indices is usually based on a Monte Carlo (MC) method (see [57, 63]) which requires a large number of evaluations of the model due to its slow convergence rate ($O(1/\sqrt{N})$ where N is the size of the experimental sample). To reduce the number of model evaluations, we use instead the so-called generalized Polynomial Chaos (gPC) method (see [13]). The backbone of the method is based on building a surrogate of the original model by decomposing the quantity of interest on a basis of orthonormal polynomials depending on the distribution of the uncertain input parameters $\theta(\omega) = (a, A, R, \chi, D, A_\sigma, \gamma, \mathcal{K})$, where ω represents an element of the set of possible outcomes. Further details on the method can be found in [65]. For uniform distributions, the most suitable orthonomal polynomial basis is the Legendre polynomials. The analysis of the distribution of μ_1 after a suitable sampling of the parameters space indicates that μ_1 follows a log-normal distribution. This distribution is not uniquely determined by its moments (the Hamburger moment problem) and consequently can not be expanded in a gPC (see [22]). Based on this observation, to obtain a better convergence in the mean square sense, we apply the gPC algorithm on the natural logarithm of the output μ_1. Typically, $\ln(\mu_1)$ is decomposed as follows :

$$\ln(\mu_1(\omega)) = \sum_{\alpha \in \mathcal{I}_{k,p}} q_\alpha L_\alpha(\theta(\omega)) + \varepsilon, \tag{3.14}$$

where ε corresponds to the approximation error, $\mathcal{I}_{k,p} = \{\alpha \in \mathbb{N}^k : \sum_{i=1}^k \alpha_i \leq p\}$ and p represents the highest degree of the expansion. Hence, the dimension of the polynomial basis is given by $\frac{(k+p)!}{k!p!}$. We reduce the number of model evaluations to 642 runs by constraining also the parameters interaction order to 2. For our purpose, a degree $p = 5$ gives a better fit (see Fig. 3.5) to the original model and the goodness of fit of the gPC algorithm is measured by a Leave One Out Cross Validation (LOOCV) technique [43]. The resulting LOO error indicates 0.4% prediction error. The Sobol's sensitivity indices are then computed from the exponential of the surrogate model (3.14) by using Monte Carlo simulations combined with a careful space-filling sampling of the parameters space (see [57, 58]). For the computations, a sample with $N = 1.8 \times 10^6$ points has been used in order to get stable second order Sobol indices. Indeed, the sensitivity indices that are needed to discriminate the impact of the input parameters are the first and total Sobol' sensitivity indices. Here, the analysis revealed a significant difference between some first order Sobol' indices

and their corresponding total Sobol indices, which indicated the importance of computing also the second order Sobol' indices.

It is important to stress that the obtained results, and the associated conclusions, could be highly dependent on the range of the parameters value. This observation makes the measurement / estimation of the parameters a crucial issue which can be dependent on the type of cancer analyzed.

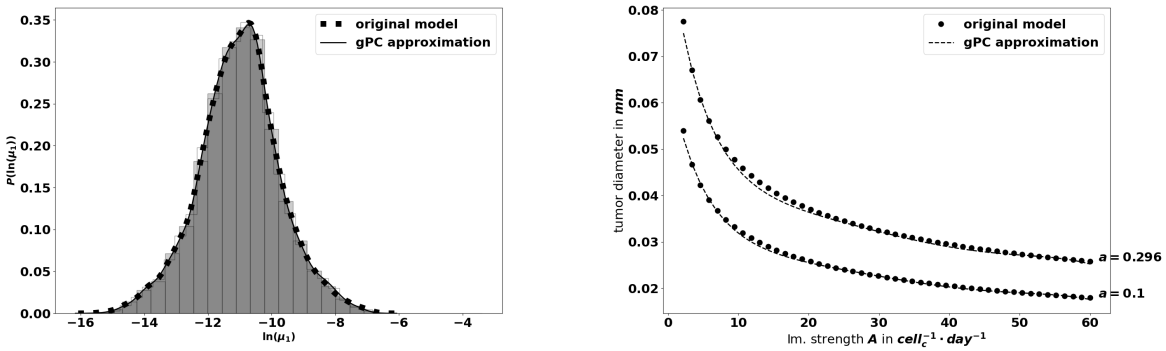

FIGURE 3.5 – Left : comparison between the pdf of $\ln(\mu_1)$ from the gPC approximation and the pdf from the original model . Right : Comparison between the value of μ_1 generated by the power-dichotomy algorithm and the gPC approximation.

Efficacy of the immune response The first order Sobol indices represented in Fig. 3.6 indicate that the parameters which impact the most the variability of the immune-controlled tumor mass at equilibrium are respectively,

— the strength of the lethal action of the immune cells on the tumor cells A,

— the natural death rate γ of the effector immune cells,

— the division rate a of the tumor cells,

— the influx rate of activated effector immune cells into the tumor microenvironment R.

This is consistent with the observations made from the numerical experiments above and in [2] : the immune response is enhanced by increasing either A or R and decreasing γ. Surprisingly, the chemotactic sensitivity χ, like the strength of the chemical signal induced by each tumor cell A_σ, the space diffusion coefficient of the effector immune cells D and the diffusion coefficient of the chemokines $\mathcal{K}$, have a negligible influence on the immune-controlled tumor mass, see Fig. 3.6-left, whether individually or in combination with other parameters. This result can be explained by the fact that despite the capacity of the cells of the immune system to infiltrate the tumor, this ability has a reduced effect when these cells are not able to effectively kill the tumor cells.

The second order Sobol' indices indicate that the leading interactions are the pairs (A, γ), (a, A), (a, γ) and (A, R). Accordingly, in order to enhance the immune response, an efficient strategy can be to act simultaneously on the immune to act simultaneously on the immune strength A together with the natural death rate γ or together with the tumor division rate a. Increasing the

influx rate of activated effector immune cells into the tumor microenvironment R by enhancing the activation / recruitment processes leading to the conversion of naive immune cells into tumor antigen specific effector immune cells can also be efficient when combined with A.

The tumor aggressiveness The tumor aggressiveness is mainly described by the cell division rate a. The first order Sobol indice indicates that a influences significantly the tumor mass at equilibrium, and we observe that the total Sobol index of a is higher than the individual one. This indicates that this parameter has strong interactions with the others. By taking a look at Fig. 3.6 we remark that a interacts significantly with the parameters A, γ. However, the most significant interaction is the one with A. This is consistent with recent successes of combined therapies targeting tumor and immune cells [4].

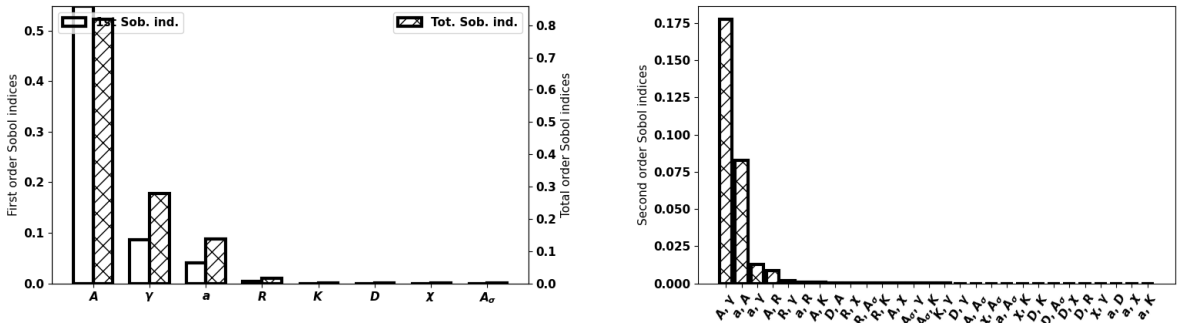

FIGURE 3.6 – Left : First (empty) and total (dashed) order Sobol indices for μ_1. Right : Second order Sobol indices for μ_1.

Towards optimized treatments It is worthwhile to try to bring these findings closer to therapeutic decision-making. Fig. 3.7 illustrates how the equilibrium mass is impacted when combining variations of two parameters, namely the immune strength A combined to the tumor cell division rate a or the mean rate of influx of effector immune cells R and the tumor cell division rate a combined to the death rate of effector immune cells γ. Interestingly, a reduction of the tumor mass at equilibrium can be obtained significantly more easily by acting on two parameters than on a single one. This observation highlights the interest of combined treatments having such complementary actions.

3.4 Conclusion and Discussion

Controlling parameters that maintain cancer-immune equilibrium is key to the successful development of novel cancer therapies. To understand how equilibrium establishes and how it is influenced by immune, environmental and tumor-related parameters, we evaluated the tumor mass which tends to a constant at equilibrium (while the size-distribution of tumor cells tends

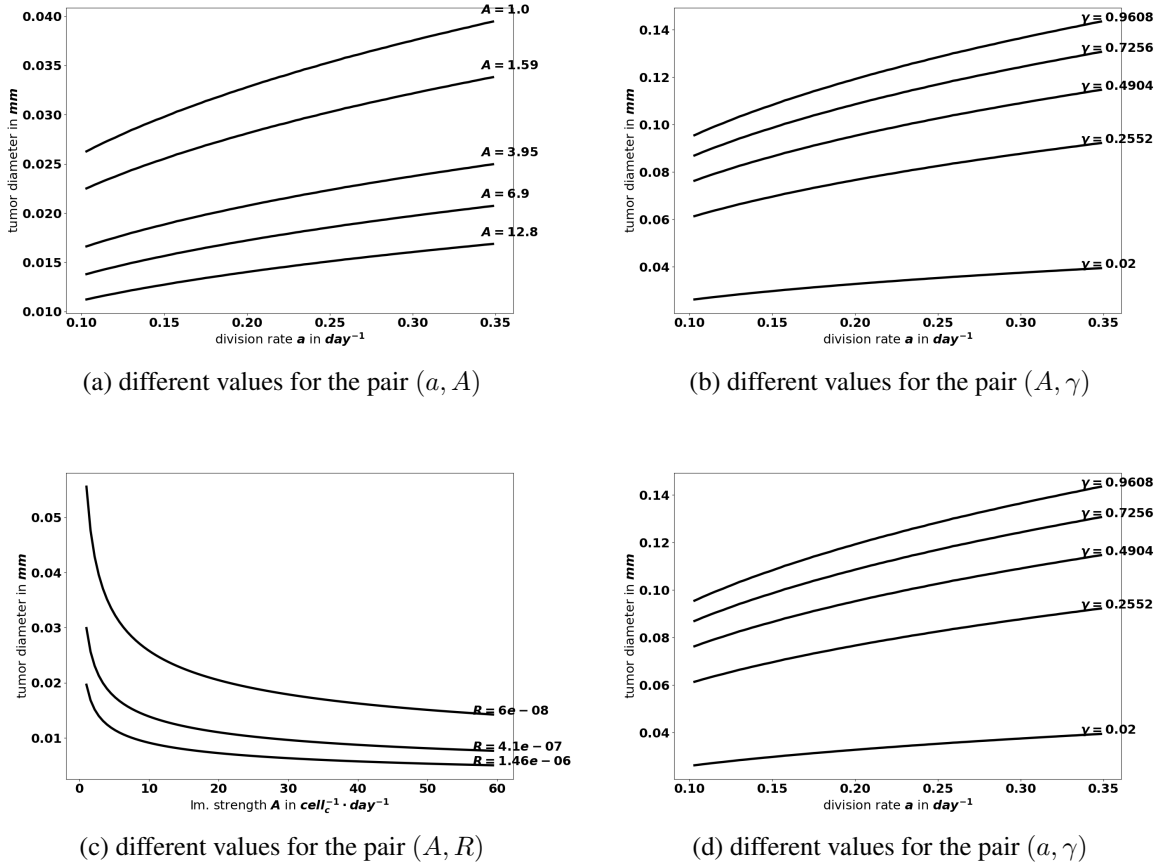

(a) different values for the pair (a, A)

(b) different values for the pair (A, γ)

(c) different values for the pair (A, R)

(d) different values for the pair (a, γ)

FIGURE 3.7 – Evolution of the tumor diameter at equilibrium, with respect to the division rate a for several values of the immune strength A (top-left), with respect to immune strength A for several values of the death rate γ (top-right), and with respect to the immune strength A for several values of the influx rate of effector immune cells R (bottom).

to a specific profile). In this study, we made use of the space and size structured mathematical model developed in chapter 2 and we provide innovative, efficient methods to predict, at low numerical cost, the residual tumor mass at equilibrium. By means of numerical simulations and global sensitivity analysis, we identified the elimination rate A of tumor cells by immune cells as the most influential factor. Therefore, the most efficient therapeutic strategy is to act on the immune system rather than on the tumor itself. We also demonstrate the need to develop combined cancer treatments either by boosting the immune capacity to kill tumor cells (increase A) while reducing natural death rate of effector immune cells (decrease γ) or by boosting the conversion into effective immune cells (increase R) while reducing the ability of tumor cells to divide (decrease a). The combination of such strategy definitely outperforms the performances of a single action ; it permits to maintain the tumor in a long-lasting equilibrium state, likely far below the measurements capabilities.

Generally, therapeutic strategies are designed to target preformed, macroscopic cancers. Indeed, patients are diagnosed once their tumor is established and measurable, which likely corresponds to the escape phase of the cancer immunoediting process [18]. The goal of successful treatments is therefore to revert to the equilibrium phase and ultimately to tumor elimination. Experimental and clinical evidence indicate that equilibrium exists but is difficult to measure. In human, cancer recurrence after therapy and long period of remission or detection of low number of tumor cells in remission phases are suggestive of an equilibrium phase. Mathematical models can also be used to provide evidence of such state. The system of partial differential equations proposed in chapter 2 is precisely intended to describe the earliest stages of immune control of tumor growth. Remarkably, while being in the most favorable condition, only taking into account the tumor antigen-specific cytotoxic immune cells and no immunosuppressive mechanisms, the model reproduces the formation of an equilibrium phase rather than a complete elimination of tumor cells. Besides suggesting that elimination may be difficult to attain, this finding also emphasizes the importance to elaborate cancer therapy strategies that lead to this state of equilibrium.

To address this challenging issue and decipher tumor-immune system dynamics leading to equilibrium state, we have developed here computational tools to depict factors that influence equilibrium. The total mass of the tumor is a critical criterion of the equilibrium and was used to predict parameters that contribute the most to the establishment of the equilibrium. By means of global sensitivity analysis, we identified four parameters that affect the most the variability of the immune-controlled tumor mass. Three of them are related to immune cells, A, R and γ and one to tumor cells, a. Moreover, the influence of the leading parameters is significantly increased when they are paired. This observation might be particularly relevant and useful for the development of therapeutic treatments with reduced toxicity. Because the pair (a, A) is among the most influential, we predict that therapeutic strategies combining drugs enhancing anti-tumor immune response with drugs diminishing tumor aggressiveness will be the most efficient. This is consistent with clinical benefit obtained when combining chemotherapies reducing the tumor cell division rate a with immunotherapies increasing A and R [4]. The parameter A which governs the efficacy of the immune system to eliminate tumor cells, is the most influential. This finding correlates with the observation that “hot” tumors infiltrated with immune cells have better prognostic than “cold” tumors [27] and that the immune cells with the strongest positive impact on patient’s survival are the cytotoxic $CD8^+$ T cells [28]. Thus, the present study predicts that any therapy that increases the efficiency of the anti-tumor immune response should be considered. This is the case for immune

checkpoint blockade therapies which contribute to revert immune tolerance, adoptive T and NK cell therapies with T/NK cell engineering resulting in enhanced killing, immunomodulating antibody therapies or cancer vaccines which boost the anti-tumor immune response [4, 9, 61]. More precisely, to enhance the immune response, it is more efficient to increase the rate of influx and conversion of naive immune cells into effector cells (parameter R) or to increase the lifespan of immune effectors (parameter γ) than to increase chemotaxis as a whole (parameters χ, A_σ , $\mathcal{K}$). The leading influence of the parameters A, R and γ stresses the importance of having functional immune cells infiltrating tumors. On the contrary, the lack of influence of chemotaxis emphasizes that the localization of immune cells within tumors is necessary but not sufficient. This point may explain the low percentage of responders among patients receiving immune checkpoint inhibitors. Indeed these patients may have a default of relocation to the tumor site of immune cells that have been successfully reactivated by the treatment [61, 64].

In conclusion, clinical trials have been undertaken quite often based on the assumption and knowledge of tumor development and immune response to cancer cells, but without tools to help the decision-making. The numerical methods developed here provide valuable hints for the design and the optimization of anti-tumor therapies that are quite in line with clinical evidence obtained so far, thus validating the approach By adapting the range of the parameters to the biological values, one can more precisely adapt the therapeutic strategies to specific type of tumors. We thus conclude that mathematical modelling combined with numerical validation provide valuable information that could contribute to better stratify the patients eligible for treatments and consequently save time and lives. In addition, it could also help to decrease the burden of treatment cost providing hints on optimized therapeutic strategies

3.5 Appendix

3.5.1 Cell division operator

The binary divsion operator (3.2) is a particular case, and for applications it is relevant to deal with more general expressions. Namely, we have

$$Q(n)(t,z) = -a(z)n(t,z) + \int_z^\infty a(z')k(z|z')n(t,z')\,\mathrm{d}z'. \tag{3.15}$$

In (3.15), $a(z')$ is the frequency of division of cells having size z', and $k(z|z')$ gives the size-distribution that results from the division of a tumor cell with size z'. What is crucial for modeling purposes is the requirement

$$\int_0^z z'k(z'|z)\,\mathrm{d}z' = z,$$

which is related to the principle that cell-division does not change the total mass

$$\int_0^\infty zQ(n)\,\mathrm{d}z = 0.$$

We refer the reader to [16] for examples of such cell-division operators.

3.5.2 Equilibrium states

The equilibrium state is characterized by means of an eigenproblem : we look for $\lambda > 0$ and a non negative function $z \geq 0 \mapsto N(z)$ satisfying (3.10) The analysis of the existence-uniqueness of the eigenpair (λ, N) can be found in [46], the textbook [51, Theorem 4.6], and, for extension to cases with non constant growth rate V, in [16].

Coming back to the coupled model, we infer that the equilibrium phase corresponds to the situation where the death rate precisely counterbalances the natural exponential growth of the tumor cells population. Let Φ be the solution of

$$-\Delta_x \Phi = \sigma - \frac{1}{|\Omega|} \int_\Omega \sigma(y)\, \mathrm{d}y,$$

endowed with the homogeneous Neumann boundary condition. Note that this quantity is a priori defined; it does not depend on the coupling between tumor cells and immune cells. In a computational perspective, it can thus be pre-computed once for all. The equilibrium mass μ_1 is implicitely defined by the fact that the solution of the stationary equation (3.11) satisfies the constraint (3.12). This implicit definition is clarified by the following statement, see chapter 2.

Theorem 3.5.1. *Let $g : [0, \infty) \to [0, \infty]$ be a non decreasing function such that $g(0) = 0$, and let $x \mapsto pS(x) \in L^2(\Omega)$ be a non negative function. If $\ell > 0$ is small enough, there exists a unique $\bar{\mu}_1(\ell) > 0$ such that $C_{\bar{\mu}_1(\ell)}$, solution of the stationary equation (3.11) satisfies $\int_\Omega \delta C \, \mathrm{d}x = \ell$.*

Theorem 3.5.1 requires a smallness assumption; for (3.2) with a constant division rate a, this is a smallness assumption on a. Numerical experiments have shown different large time behaviors for the evolution problem (3.1a)-(3.1e) :

— when the source term S is space-homogeneous, the expected behavior seems to be very robust. The immune cells concentration tends to fulfill the constraint (3.12) as time becomes large, and the size repartition of tumor cells tends to the eigenfunction N. The total mass μ_1 tends to a constant; however the asymptotic value cannot be predicted easily. We again refer the reader to Fig. 3.2 for an illustration of these facts.

— When S has spacial variations, the asymptotic behavior seems to be much more sensitive to the smallness condition. On short time scale of simulations, we observe alternance of growth and remission phases, and the damping to the equilibrium could be very slow.

These observations bring out the complementary roles of different type of cytotoxic cells [23]. The NK cells could be seen as a space-homogenous source of immune cells, immediately available to fight against the tumor, at the early stage of tumor growth. In contrast, T-cells need an efficient priming which occurs in the draining lymph nodes, and their sources is therefore non-homogeneously distributed. Eventually, NK and $CD8^+$ T-cells cooperate to the anti-tumor immune response.

3.5.3 Computation of the eigen-elements of the growth-fragmentation equation

It is important to bear in mind the main arguments of the proof of the existence-uniqueness of the eigenpair (λ, N) for the growth-fragmentation equation. Namely, for Λ large enough we

consider the *shifted* operator

$$\mathscr{T}_\Lambda N = \Lambda N + \partial_z(VN) + aN - \int_z^\infty a(z')k(z|z')N(z')\,\mathrm{d}z'.$$

Then, we check that the operator $\mathscr{S}_\Lambda$ which associates to a function f the solution n of $\mathscr{T}_\Lambda n = f$ fulfills the requirements of the Krein-Rutman theorem (roughly speaking, positivity and compactness), see [39]. Accordingly, the quantity of interest λ is related to the leading eigenvalue of $\mathscr{S}_\Lambda$. In fact, this reasoning should be applied to a somehow truncated and regularized version of the operator, and the conclusion needs further compactness arguments; nevertheless this is the essence of the proof. In terms of numerical method, this suggests to appeal to the inverse power algorithm, applied to a discretized version of the equation. However, we need to define appropriately the shift parameter Λ. As far as the continuous problem is considered, Λ can be estimated by the parameters of the model [16], but it is critical for practical issues to check whether or not this condition is impacted by the discretization procedure. This information will be used to apply the inverse power method to the discretized and shifted version of the problem.

Analysis of the discrete problem

The computational domain for the size variable is the interval $[0, R]$ where R is chosen large enough : due to the division processes, we expect that the support of the solution remains essentially on a bounded interval, and the cut-off should not perturb too much the solution. In what follows, the size step $h = z_{i+1} - z_i$ is assumed to be constant. The discrete unknowns N_i, with $i \in \{1, ..., I\}$ and $h = R/I$, are intended to approximate $N(z_i)$ where $z_i = ih$. The integral that defines the gain term of the division operator is approximated by a simple quadrature rule. For the operator (3.2) the kernel involves Dirac masses which can be approached by peaked Gaussian. We introduce the operator $\mathscr{T}^h_\Lambda : \mathbb{R}^I \to \mathbb{R}^I$ defined by

$$\begin{cases} (\mathscr{T}^h_\Lambda N)_i = F_i - F_{i-1} + h(\Lambda + a_i)N_i - h^2 \sum_{j=i}^I a(z_j)k(z_i|z_j)N_j, \\ N_1 = 0 \end{cases} \tag{3.16}$$

where $F_i = V_{i+1/2}N_i$ represents the convective numerical flux on the grid point $z_{i+1/2} = (i + 1/2)h$, $i \in \{1, ..., I\}$. This definition takes into account that the growth rate is non negative, and applies the upwinding principles. Note that the step size h should be small enough to capture the division of small cells, if any. The following statement provides the a priori estimate which allows us to determine the shift for the discrete problem.

Theorem 3.5.2. *We suppose that*

i) $z \mapsto V(z)$ *is a continuous function which lies in* L^∞ *and it is bounded from below by a positive constant,*

ii) $h \sum_{j=1}^I a(z_j)k(z_i|z_j)$ *remains bounded uniformly with respect to* h*,*

iii) for any $i \in \{1, ..., I-1\}$*, there exists* $j \in \{i+1, ..., I\}$ *such that* $a(z_j)k(z_i|z_j) > 0$*,*

iv) there exists $Z_0 \in (0, \infty)$ *such that, setting* $\bar{\mathcal{N}}(z) = h \sum_{j=2}^I k(z_j|z)$*, we have* $a(z)(\bar{\mathcal{N}}(z) - 1) \geq \nu_0 > 0$ *for any* $z \geq Z_0$*.*

Let

$$\Lambda > \frac{\|V\|_{L^\infty}}{\min_{j\in\{1,\dots,I\}} |V_{j+1/2}|} \max_{k\in\{1,\dots,I\}} \Big(h \sum_{j=k}^{I} a_j k(z_k|z_j)\Big) - \min_{j\in\{1,\dots,I\}} |a_j|, \tag{3.17}$$

and we suppose that $R > Z_0$ is large enough. Then, $\mathscr{T}_\Lambda^h$ is invertible and there exists a pair $\mu > 0$, $N \in \mathbb{R}^I$ with positive components, such that $\mathrm{Ker}((\mathscr{T}_\Lambda^h)^{-1} - \mu) = \mathrm{Span}\{N\}$. *Moreover* $\lambda = \Lambda - \frac{1}{\mu} > 0$.

Note that the sum that defines $\bar{\mathcal{N}}(z)$ is actually reduced over the indices such that $jh \le z$; this quantity is interpreted as the expected number of cells produced from the division of a cell with size z so that the forth assumption is quite natural.

Proof. Let $f \in \mathbb{R}^I$. We consider the equation

$$\mathscr{T}_\Lambda^h N = f.$$

We denote $N = \mathscr{S}_\Lambda^h f$ the solution. We are going to show that $\mathscr{S}_\Lambda^h$ is well defined and satisfies the assumptions of the Perron-Frobenius theorem, see e. g. [29, Theorem 1.37 & Corollary 1.39] or [59, Chapter 5].

It is convenient to introduce the change of unknown $U_i = N_i V_{i+1/2}$, $\forall i \in \{1, \cdots, I\}$. The problem recasts as

$$\begin{cases} (\widetilde{\mathscr{T}}_\Lambda^h U)_i = h\dfrac{f_i}{V_{i+1/2}}, \text{ with} \\ (\widetilde{\mathscr{T}}_\Lambda^h U)_i = U_i - U_{i-1} + h\dfrac{\Lambda + a_i}{V_{i+1/2}} U_i - h^2 \sum_{j=i}^{I} \dfrac{a_j}{V_{j+1/2}} k(z_i|z_j) U_j, \\ U_1 = 0. \end{cases} \tag{3.18}$$

The solution is interpreted as the fixed point of the mapping

$$\xi \longmapsto U = A^h \xi$$

where U is given by $U_1 = 0$ and

$$U_i = U_{i-1} + h^2 \sum_{j=i}^{I} \frac{a_j}{V_{j+1/2}} k(z_i|z_j)\xi_j + h\frac{f_i}{V_{i+1/2}}.$$

We are going to show that A^h is a contraction : $\|A^h\xi\|_{\ell^\infty} \le k\|\xi\|_{\ell^\infty}$ for some $k < 1$. Multiplying (3.18) by $\mathrm{sign}(U_i)$, we obtain

$$\begin{aligned} \left(1 + h\frac{\Lambda + a_i}{V_i}\right) \mathrm{sign}(U_i) U_i &= \left(1 + h\frac{\Lambda + a_i}{V_i}\right) |U_i| \\ &= \mathrm{sign}(U_i) U_{i-1} + h^2 \textstyle\sum_{j=i}^{I} \dfrac{a_j}{V_{j+1/2}} k(z_i|z_j) \mathrm{sign}(U_i) \xi_j \\ &\le |U_{i-1}| + h^2 \textstyle\sum_{j=i}^{I} \dfrac{a_j}{V_{j+1/2}} k(z_i|z_j) |\xi_j|. \end{aligned}$$

We multiply this by the weight $\prod_{l=1}^{i-1}\left[1+h\frac{\Lambda+a_l}{V_{l+1/2}}\right]$, where all factors are ≥ 1. We get

$$\begin{aligned}
&|U_i|\prod_{l=1}^{i}\left[1+h\frac{\Lambda+a_l}{V_{l+1/2}}\right]\\
&\quad\leq |U_{i-1}|\prod_{l=1}^{i-1}\left[1+h\frac{\Lambda+a_l}{V_{l+1/2}}\right]+h^2\prod_{l=1}^{i}\left[1+h\frac{\Lambda+a_l}{V_{l+1/2}}\right]\sum_{j=i}^{I}\frac{a_j}{V_{j+1/2}}k(z_i|z_j)|\xi_j|.
\end{aligned}$$

Then, summing over $i\in\{2,...,m\}$ yields

$$\begin{aligned}
&|U_m|\prod_{l=1}^{m}\left[1+h\frac{\Lambda+a_l}{V_{l+1/2}}\right]\\
&\quad\leq |U_1|\left[1+h\frac{\Lambda+a_1}{V_{3/2}}\right]+h^2\sum_{i=2}^{m}\prod_{l=1}^{i}\left[1+h\frac{\Lambda+a_l}{V_{l+1/2}}\right]\sum_{j=i}^{I}\frac{a_j}{V_{j+1/2}}k(z_i|z_j)|\xi_j|
\end{aligned}$$

where actually $U_1=0$. It follows that

$$\begin{aligned}
|U_m| &\leq h^2\sum_{i=2}^{m}\prod_{l=i}^{m}\left[1+h\frac{\Lambda+a_l}{V_{l+1/2}}\right]^{-1}\sum_{j=i}^{I}\frac{a_j}{V_{j+1/2}}k(z_i|z_j)|\xi_j|\\
&\leq \frac{h^2\|\xi\|_{\ell^\infty}}{\min_{j\in\{1,...,I\}}V_{j+1/2}}\sum_{i=2}^{m}\prod_{l=i}^{m}\left[1+h\frac{\Lambda+a_l}{V_{l+1/2}}\right]^{-1}\sum_{j=i}^{I}a_jk(z_i|z_j)\\
&\leq \frac{h^2\|\xi\|_{\ell^\infty}}{\min_{j\in\{1,...,I\}}V_{j+1/2}}\left\|\sum_{j=i}^{I}a_jk(z_i|z_j)\right\|_{\ell^\infty}\sum_{i=2}^{m}\left[1+h\frac{\Lambda+\min_{l\in\{1,...,I\}}a_l}{\|V\|_{L^\infty}}\right]^{i-m+1}\\
&\leq \frac{h\|\xi\|_{\ell^\infty}}{\min_{j\in\{1,...,I\}}V_{j+1/2}}\left\|\sum_{j=i}^{I}a_jk(z_i|z_j)\right\|_{\ell^\infty}\left[\frac{\Lambda+\min_{l\in\{1,...,I\}}a_l}{\|V\|_{L^\infty}}\right]^{-1}.
\end{aligned}$$

Therefore, A^h is a contraction provided (3.17) holds. This estimate is similar to the condition obtained for the continuous problem, see [16, Proof of Theorem 2, Appendix B]; the discretization does not introduce further constraints.

We are now going to show that $\mathscr{T}_\Lambda^h$ is a M-matrix when (3.17) holds. Let $f\in\mathbb{R}^I\setminus\{0\}$ with non negative components. Let $U\in\mathbb{R}^I$ satisfy $(\widetilde{\mathscr{T}}_\Lambda^h U)_i=h\frac{f_i}{V_{i+1/2}}$. Let i_0 be the index such that $U_{i_0}=\min\{U_i,\ i\in\{2,...,I\}\}$. We have

$$\begin{aligned}
U_{i_0}\left(1+h\frac{\Lambda+a_{i_0}}{V_{i_0+1/2}}\right) &= U_{i_0-1}+h^2\sum_{j=i_0}^{I}\frac{a_j}{V_{j+1/2}}k(z_{i_0}|z_j)U_j+h\frac{f_{i_0}}{V_{i_0+1/2}}\\
&\geq U_{i_0}\left(1+h^2\sum_{j=i_0}^{I}\frac{a_j}{V_{j+1/2}}k(z_{i_0}|z_j)\right)+h\frac{f_{i_0}}{V_{i_0+1/2}}.
\end{aligned}\tag{3.19}$$

Since $f_{i_0}\geq 0$, we get

$$U_{i_0}\underbrace{\left(\frac{\Lambda+a_{i_0}}{V_{i_0+1/2}}-h\sum_{j=i_0}^{I}\frac{a_j}{V_{j+1/2}}k(z_{i_0}|z_j)\right)}_{>0 \text{ by (3.17)}}\geq 0,$$

which tells us that $U_{i_0} \geq 0$. Suppose $U_{i_0} = 0$ for some $i_0 > 1$. Coming back to (3.19), we deduce that U_{i_0-1} vanishes too, and so on and so forth, we obtain $U_1 = ... = U_{i_0} = 0$. Finally, we use the irreductibility assumption iii) : we can find $j_0 > i_0$ such that $\frac{a_{j_0}}{V_{j_0+1/2}} k(z_{i_0}|z_{j_0}) > 0$ and (3.19) implies $\frac{a_{j_0}}{V_{j_0+1/2}} k(z_{i_0}|z_{j_0}) U_{j_0} = 0$, so that $U_{j_0} = 0$. We deduce that $U = 0$, which contradicts $f \neq 0$. Therefore the components of U are positive, but U_1.

We conclude by applying the Perron-Froebenius theorem to $(\mathscr{T}_\Lambda^h)^{-1}$, [59, Chapter 5]. It remains to prove that $\lambda = \Lambda - \frac{1}{\mu}$ is positive, with μ the spectral radius of $(\mathscr{T}_\Lambda^h)^{-1}$. To this end, we make use of assumption iv). We set $Z_0 = i_0 h$. We argue by contradiction, supposing that $\lambda = \Lambda - 1/\mu < 0$. We consider the eigenvector with positive components and normalized by the condition $h \sum_{i=1}^I U_i = 1$. We have

$$(\widetilde{\mathscr{T}}_0^h U)_i = U_i - U_{i-1} + \frac{a_i}{V_{i+1/2}} h U_i - h^2 \sum_{j=i}^I \frac{a_j}{V_{j+1/2}} k(z_i|z_j) U_j = -\lambda U_i \geq 0.$$

It follows that, for $m \geq i_0$,

$$\begin{aligned}
U_m &\geq -h \textstyle\sum_{i=2}^m \frac{a_i}{V_{i+1/2}} U_i + h^2 \sum_{i=2}^m \sum_{j=i}^I \frac{a_j}{V_{j+1/2}} k(z_i|z_j) U_j \\
&\geq -h \textstyle\sum_{i=2}^m \frac{a_i}{V_{i+1/2}} U_i + h \sum_{j=2}^m \left(h \sum_{i=2}^j k(z_i|z_j) \right) \frac{a_j}{V_{j+1/2}} U_j \\
&\geq -h \textstyle\sum_{i=2}^m \frac{a_i}{V_{i+1/2}} U_i + h \sum_{j=2}^m \bar{\mathcal{N}}(z_j) \frac{a_j}{V_{j+1/2}} U_j \\
&\geq h \textstyle\sum_{i=2}^m (\bar{\mathcal{N}}(z_i) - 1) \frac{a_i}{V_{i+1/2}} U_i \\
&\geq h \textstyle\sum_{i=i_0}^m (\bar{\mathcal{N}}(z_i) - 1) \frac{a_i}{V_{i+1/2}} U_i \geq \frac{\nu_0}{\|V\|_{L^\infty}} h \sum_{i=i_0}^m U_i.
\end{aligned}$$

It implies

$$1 = h \sum_{m=1}^I U_m \geq h \sum_{m=i_0}^I U_m \geq h(I - i_0) \frac{\nu_0}{\|V\|_{L^\infty}} h \sum_{i=i_0}^m U_i.$$

We arrive at

$$1 \geq (R - Z_0) \frac{\nu_0}{\|V\|_{L^\infty}},$$

a contradiction when R is chosen large enough (but how large R should be does not depend on h). Therefore, we conclude that $\lambda > 0$

■

Numerical approximation of (λ, N)

We compute (an approximation of) the eigenpair (λ, N) by using the inverse power method which finds the eigenvalue of $(\mathscr{T}_\Lambda^h)^{-1}$ with largest modulus :

— We pick Λ verifying (3.17).

— We compute once for all the LU decomposition of the matrix $\mathscr{T}_\Lambda^h$.

— We choose a threshold $0 < \epsilon \ll 1$.

— We start from a random vector $N^{(0)}$ and we construct the iterations

  — $LUq^{(k+1)} = N^{(k)}$,

  — $N^{(k+1)} = \frac{q^{(k+1)}}{\|q^{(k+1)}\|}$

  until the relative error $\frac{\|N^{(k+1)}-N^{(k)}\|}{\|N^{(k)}\|} \leq \epsilon$ is small enough. Then, given the last iterate $N^{(K)}$, we set $LUq = N^{(K)}$, $\tilde{\mu} = \frac{q \cdot N^{(K)}}{N^{(K)} \cdot N^{(K)}}$, and $\tilde{\lambda} = \Lambda - 1/\tilde{\mu}$.

This approach relies on the ability to approximate correctly the eigenpair of the growth-fragmentation operator. In particular, it is important to preserve the algebraic multiplicity. This issue is quite subtle and it is known that the pointwise convergence of the operator is not enough to guarantee the convergence of the eigenelements and the consistency of the invariant subspaces, see [11] for relevant examples. This question has been thoroughly investigated in [11, 12] which introduced a suitable notion of stability. It turns out that one needs a uniform convergence of the operators. Namely, here, we should check that $\|(\mathscr{T}_\Lambda^I)^{-1} - (\mathscr{T}_\Lambda)^{-1}\| \longrightarrow 0$ as $I \longrightarrow \infty$. In the present framework, a difficulty relies on the fact that the size variable lies in an unbounded domain, which prevents for using usual compactness arguments. For this reason, we introduce a truncated version of the problem, which has also to be suitably regularized. Let us denote by $\mathscr{T}_\Lambda^{R,\epsilon}$ the corresponding operator, where ϵ represents the regularization parameter. This truncated and regularized operator appeared already in [16]. Indeed, we know from [16] that $\|\mathscr{T}_\Lambda^{R,\epsilon} - \mathscr{T}_\Lambda\| \longrightarrow 0$ as $R \longrightarrow \infty$ and $\epsilon \longrightarrow 0$, hence, this implies that $\|(\mathscr{T}_\Lambda^{R,\epsilon})^{-1} - (\mathscr{T}_\Lambda)^{-1}\| \longrightarrow 0$ as $R \longrightarrow \infty$ and $\epsilon \longrightarrow 0$ by continuity of the map $\Pi : \mathscr{T}_\Lambda \mapsto (\mathscr{T}_\Lambda)^{-1}$. Moreover, $(\mathscr{T}_\Lambda^{R,\epsilon})^{-1}$ is well-defined, continuous and compact, see [16, Appendix. B]. The discrete operators $(\mathscr{T}_\Lambda^I)^{-1}$ converge pointwise to $(\mathscr{T}_\Lambda^{R,\epsilon})^{-1}$, and the compactness of $(\mathscr{T}_\Lambda^{R,\epsilon})^{-1}$ ensures that the discrete operator converges uniformly to $(\mathscr{T}_\Lambda^{R,\epsilon})^{-1}$, for $0 < R < \epsilon$ and $0 < \epsilon < 1$ fixed (see [12] for more details on this fact). Following [12], we deduce that the numerical eigenelements (λ^I, N^I) converges to $(\lambda^{R,\epsilon}, N^{R,\epsilon})$, the eigenelements of $(\mathscr{T}_\Lambda^{R,\epsilon})^{-1}$, while preserving their algebraic multiplicity. Finally the uniform convergence $\|(\mathscr{T}_\Lambda^{R,\epsilon})^{-1} - (\mathscr{T}_\Lambda)^{-1}\| \longrightarrow 0$ as $R \longrightarrow \infty$ and $\epsilon \longrightarrow 0$ ensures the convergence of $(\lambda^{R,\epsilon}, N^{R,\epsilon})$ to (λ, N), [16].

Numerical results

For some specific fragmentation kernels and growth rates, the eigenpair (λ, N) is explicitly known, see [16]. We can use these formula to check that the algorithm is able to find the expected values and profiles. To this end, we introduce the relative errors

$$E_\lambda^h = \frac{|\lambda - \tilde{\lambda}|}{\tilde{\lambda}} \quad \text{and} \quad E_V^h = h \sum_{i=1}^{I} |N_i^{(K)} - N(ih)|$$

where $N^{(K)}$ and N are both normalized by $h\sum_{i=1}^I N_i^{(K)} = h\sum_{i=1}^I N(ih) = 1$.

Mitosis fragmentation kernel. We start with the binary division kernel :

$$k(z|z') = \delta_{z'=2z}. \tag{3.20}$$

The associated division operator is described by (3.2). We assume that a and V are constant. In this specific case the eigenpair is given by

$$\lambda = a, \qquad N(z) = \bar{N} \sum_{n=0}^{\infty} (-1)^n \alpha_n \exp\left(-2^{n+1} \frac{a}{V} z\right), \tag{3.21}$$

with $\bar{N} > 0$ an appropriate normalizing constant and $(\alpha_n)_{n\in\mathbb{N}}$ is the sequence defined by the recursion

$$\alpha_0 = 1, \qquad \alpha_n = \frac{2}{2^n - 1} \alpha_{n-1}.$$

In practice we shall use a truncated version of the series that defines N. For the numerical tests, we use the parameters collected in Table 3.3

a	V	R	ϵ
4	0.6	5	10^{-6}

TABLE 3.3 – Data for the numerical tests : binary division kernel

Number of cells	E_λ	E_V
1000	3.73×10^{-5}	3.83×10^{-2}
2000	5.68×10^{-8}	1.93×10^{-2}
4000	6.77×10^{-7}	9.69×10^{-3}
8000	6.84×10^{-7}	4.85×10^{-3}

TABLE 3.4 – Binary division kernel : errors for several number of grid points

With this threshold ϵ, the approached eigenpair is reached in 43 iterations, independently of the size step. Fig. 3.8 represents the evolution of the error E_V^h as a function of h in a log-log scale : $N^{(K)}$ approaches N at order 1. The rate improves when using a quadrature rule with a better accuracy. For this test, the approximation of the eigenvalue is already accurate with a coarse grid ; it is simply driven by the threshold ϵ and E_L^h does not significantly change with h.

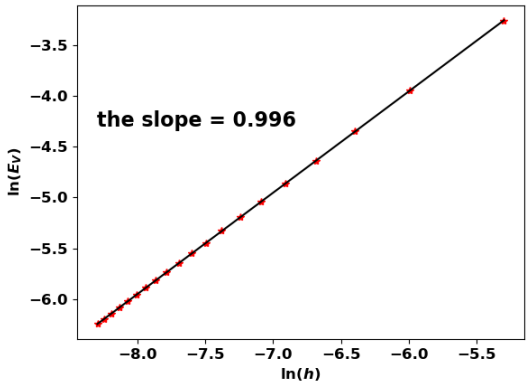

(a) The rate of convergence to the exact eigenfunction with respect to h

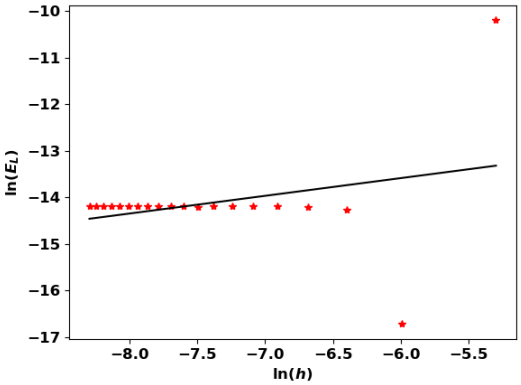

(b) The rate of convergence to the exact eigenvalue with respect to h

FIGURE 3.8 – Binary division kernel : convergence rates of $(\lambda^{(K)}, N^{(K)})$ with respect to h

Uniform fragmentation. The uniform fragmentation kernel is defined by :

$$k(z|z') = \frac{1}{z'}\mathbb{1}_{0\leq z\leq z'}.$$

We apply the algorithm for the following two cases :

1. $V(z) = V_0$ and $a(z) = a_0 z$. We have :

$$\lambda = \sqrt{a_0 V_0}, \qquad N(z) = 2\sqrt{\frac{a_0}{V_0}}\left(Z + \frac{Z^2}{2}\right)\exp\left(-Z - \frac{Z^2}{2}\right).$$

We still use the values in Table 3.3 (especially, $a_0 = a$ and $V_0 = V$). The approximated eigenpair is obtained in 84 iterations and, as in the previous test, it does not change with the size step. In this case, both the eigenvalue and the eigenfunction are approached at order 1, see Table 3.5 and Fig. 3.9.

Number of cells	E_λ	E_V
1000	1.30×10^{-2}	8.89×10^{-3}
2000	6.43×10^{-3}	4.50×10^{-3}
4000	3.23×10^{-3}	2.24×10^{-3}
8000	1.62×10^{-3}	1.13×10^{-3}

TABLE 3.5 – Uniform fragmentation, ex. 1 : errors for several number of grid points

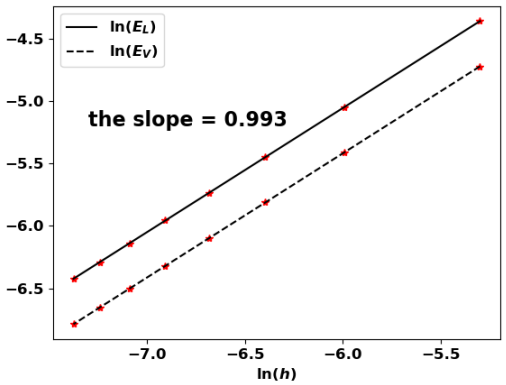

FIGURE 3.9 – Uniform fragmentation, ex. 1 : rate of convergence to the exact eigenpair with respect to h

2. $V(z) = V_0 z$ and $a(z) = a_0 z^n$ with $n \in \mathbb{N} \setminus \{0\}$. The eigenpair is defined by the following formula :

$n = 1$	$\lambda = V_0$	$N(z) = \frac{a_0}{V_0} \exp\left(-\frac{a_0}{V_0} z\right)$
$n = 2$	$\lambda = V_0$	$N(z) = \frac{2a_0}{\pi V_0} \exp\left(-\frac{a_0}{2V_0} z^2\right)$
n	$\lambda = V_0$	$N(z) = \left(\frac{a_0}{nV_0}\right)^{\frac{1}{n}} \frac{n}{\Gamma(\frac{1}{n})} \exp\left(-\frac{a_0}{nV_0} z^n\right)$

Note that the growth rate V vanishes and Theorem 3.5.2 does not apply as such. Nonetheless, the algorithm works well and still captures the eigenpair. We perform the test for $n = 1$ and $n = 2$ and the results are recorded in Table 3.6, Fig. 3.10 and Table 3.7, Fig. 3.11, respectively.

Number of cells	E_λ	E_V
1000	4.70×10^{-2}	2×10^{-2}
2000	2.43×10^{-2}	1.06×10^{-2}
4000	1.25×10^{-2}	5.5×10^{-3}
8000	6.39×10^{-3}	2.81×10^{-3}

TABLE 3.6 – Uniform fragmentation, ex. 2, case $n = 1$: errors for different number of cells

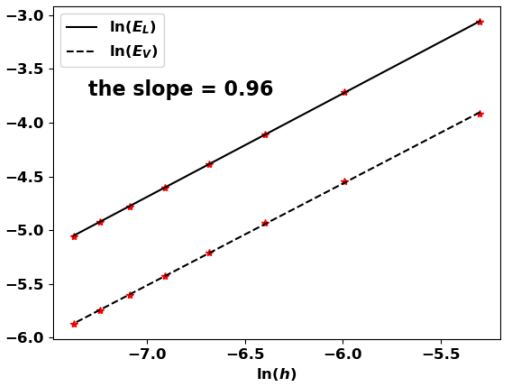

FIGURE 3.10 – Uniform fragmentation, ex. 2 case $n = 1$: rate of convergence to the exact eigenpair with respect to h

Number of cells	E_λ	E_V
1000	2.39×10^{-2}	8.81×10^{-2}
2000	1.23×10^{-3}	4.53×10^{-3}
4000	6.41×10^{-3}	2.35×10^{-3}
8000	3.41×10^{-3}	1.24×10^{-3}

TABLE 3.7 – Uniform fragmentation, ex. 2, case $n = 2$: errors for different number of cells

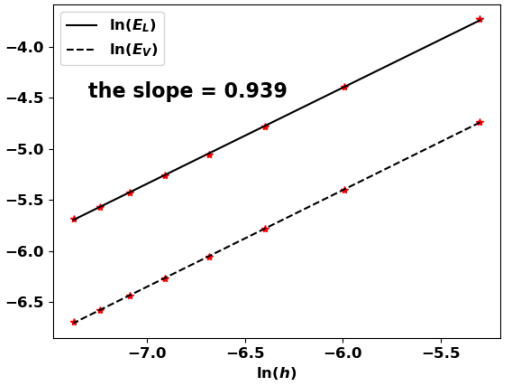

FIGURE 3.11 – Uniform fragmentation, ex. 2 : rate of convergence to the exact eigenpair with respect to h

3.5.4 Sensitivity analysis on the equilibrium mass

Having an efficient procedure to predict the residual mass of the equilibrium phase also opens perspectives to discuss the influence of the parameters. This can provide useful hints for the design and the optimization of anti-tumor therapies. We address this issue by performing a global sensitivity analysis on the immune-controlled tumor mass. Sensitivity analysis also provides information on the quantification of uncertainty in the model output with respect to the uncertainties in the input parameters. We remind the reader that the equilbrium mass is seen as a function of the parameters in Table 3.1 :

$$\mu_1 = f(a, A, R, \chi, D, A_\sigma, \gamma, \mathcal{K}). \tag{3.22}$$

We consider that the input parameters are independent random variables uniformly distributed in an interval $[x_1, x_2] \subset (0, \infty)$:

$$M = (a, A, R, \chi, D, A_\sigma, \gamma, \mathcal{K}) \text{ with } M_i \sim U(x_1, x_2). \tag{3.23}$$

The pillar of the Sobol sensitivity analysis is the decomposition of f into $2^n - 1$ summands of increasing dimensions :

$$f(M) = f_0 + \sum_{i=1}^{n} f_i(M_i) + \sum_{1 \le i < j \le n} f_{ij}(M_i, M_j) + \cdots + f_{1\cdots n}(M_1, \cdots, M_n), \tag{3.24}$$

where

$$\frac{1}{x_2 - x_1} \int_{[x_1,x_2]} f_{i_1\cdots i_p}(M_{i_1\cdots i_p})\, \mathrm{d}M_{i_k} = 0 \quad \text{for } k \in \{1, ..., p\}, \tag{3.25}$$

$$f_0 = \frac{1}{(x_2 - x_1)^n} \int_{[x_1,x_2]^n} f(M)\, \mathrm{d}M, \tag{3.26}$$

$$\int_{[x_1,x_2]^n} f_{i_1\cdots i_p}(M_{i_1\cdots i_p}) f_{j_1\cdots j_p}(M_{j_1\cdots j_p})\, \mathrm{d}M = 0, \tag{3.27}$$

and $M_{i_1\cdots i_p} = (M_{i_1}, \cdots M_{i_p})$. The existence and uniqueness of the above decomposition has been proven in [63], given f a square integrable function. Owing to the orthogonality condition (3.27), the total variance of f reads :

$$\mathcal{V} = \mathrm{Var}(f(M)) = \frac{1}{(x_2 - x_1)^n} \int_{[x_1,x_2]^n} f(M)^2\, \mathrm{d}M - f_0^2. \tag{3.28}$$

Given (3.24), $\mathcal{V}$ can be decomposed as follows :

$$\mathcal{V} = \sum_{i=1}^{n} \mathcal{V}_i + \sum_{1 \le i < j \le n} \mathcal{V}_{ij} + \cdots + \mathcal{V}_{1\cdots n}, \tag{3.29}$$

where the terms $\mathcal{V}_{i_1\cdots i_p}$, called partial variances read :

$$\mathcal{V}_{i_1\cdots i_p} = \frac{1}{(x_2 - x_1)^n} \int_{[x_1,x_2]^n} f_{i_1\cdots i_p}^2\, \mathrm{d}M_{i_1} \cdots \mathrm{d}M_{i_p}. \tag{3.30}$$

Following the description in [63], the Sobol' sensitivity indices are defined as follows :

$$S_{i_1\cdots i_p} = \frac{\mathcal{V}_{i_1\cdots i_p}}{V}. \tag{3.31}$$

They verify

$$\sum_{i=1}^{n} S_i + \sum_{1\le i<j\le n} S_{ij} + \cdots + S_{1\cdots n} = 1. \tag{3.32}$$

Each index $S_{i_1\cdots i_p}$ measures how the total variance of f is affected by uncertainties in the set of input parameters $i_1\cdots i_p$. An equivalent definition of the above indices is given by (see [57]) :

$$\mathcal{V}_i = \mathrm{Var}(\mathbb{E}(Y|M_i)), \quad \mathcal{V}_{ij} = \mathrm{Var}(\mathbb{E}(Y|M_i, M_j)) - \mathcal{V}_i - \mathcal{V}_j, ... \tag{3.33}$$

The total effect of a specific input parameter i is evaluated by the so-called total sensitivity index $S_T^{(i)}$, the sum of the sensitivity indices which contain i :

$$S_T^{(i)} = \sum_{C_i} S_{i_1\cdots i_p} \tag{3.34}$$

where $C_i = \{(i_1\cdots i_p) : \exists m \in \{1, ..., p\},\ i_m = i\}$. In practice, the sensitivity indices that are needed to discriminate the impact of the parameters are the first, second and total Sobol' sensitivity indices. The above indices are computed using Monte Carlo simulations combined with a careful sampling of the parameters space in order to reduce the computational load and the number of model evaluations. For this purpose, the following estimators can be derived using two different N samples A and B, see [57, 58],

$$\hat{f}_0 = \frac{1}{N}\sum_{l=1}^{N} f(M_l), \tag{3.35}$$

$$\hat{\mathcal{V}} = \frac{1}{N}\sum_{l=1}^{N} f^2(M_l) - \hat{f}_0^2, \tag{3.36}$$

$$\hat{\mathcal{V}}_i = \frac{1}{N}\sum_{l=1}^{N} f(M^{(A)}_{(-i)l}, M^{(A)}_{il}) f(M^{(B)}_{(-i)l}, M^{(A)}_{il}) - \hat{f}_0^2, \tag{3.37}$$

$$\hat{\mathcal{V}}_{ij} = \frac{1}{N}\sum_{l=1}^{N} f(M^{(A)}_{-(i,j)l}, M^{(A)}_{il}, M^{(A)}_{jl}) f(M^{(B)}_{-(i,j)l}, M^{(A)}_{il}, M^{(A)}_{jl}) - \hat{f}_0^2 - \hat{\mathcal{V}}_i - \hat{\mathcal{V}}_j. \tag{3.38}$$

Here the notation $M_{-(i_1\cdots i_p)l}$ stands for the l-th sample line where we get rid of the points corresponding to the indices $i_1, \cdots, i_p$. The total sensitivity [34] is given by :

$$S_{T_i} = 1 - S_{-i} \tag{3.39}$$

where S_{-i} is the sum of all the sensitivity indices that do not contain the index i. Hence, the total sensitivity index estimator reads :

$$\hat{S}_{T_i} = 1 - \frac{\hat{\mathcal{V}}_{-i}}{\hat{\mathcal{V}}} \tag{3.40}$$

where

$$\hat{\mathcal{V}}_{-i} = \frac{1}{N}\sum_{l=1}^{N} f(M^{(A)}_{(-i)l}, M^{(A)}_{il}) f(M^{(A)}_{(-i)l}, M^{(B)}_{il}) - \hat{f}_0^2.$$

Bibliographie

[1] Y. Andrew and C. Robin. Cell death and the maintenance of immunological memory. *Disc. Cont. Dyn. Syst.-B*, 1, 2001.

[2] K. Atsou, F. Anjuère, V. M. Braud, and T. Goudon. A size and space structured model describing interactions of tumor cells with immune cells reveals cancer persistent equilibrium states in tumorigenesis. *J. Theor. Biol.*, 490 :110163, 2020.

[3] F. Baccelli, D. McDonald, and J. Reynier. A mean field model for multiple TCP connections through a buffer implementing RED. *Performance Evaluation*, 49(1-4) :77–97, 2002.

[4] C. Bailly, X. Thuru, and B. Quesnel. Combined cytotoxic chemotherapy and immunotherapy of cancer : modern times. *NAR Cancer*, 2(1) :1–20, 2020.

[5] R. J. Beck, M. Slagter, and J. B. Beltman. Contact-dependent killing by cytotoxic t lymphocytes is insufficient for el4 tumor regression in vivo. *Cancer Research*, 79(13) :3406–3416, 2019.

[6] T. Boon, P. G. Coulie, B. J. V. den Eynde, and P. van der Bruggen. Human T-cell responses against melanoma. *Annual Review of Immunology*, 24(1) :175–208, 2006. PMID : 16551247.

[7] C. M. Cairns, J. R. Gordon, F. Li, M. E. Baca-Estrada, T. Moyana, and J. Xiang. Lymphotactin Expression by Engineered Myeloma Cells Drives Tumor Regression : Mediation by $CD4$+ and $CD8$+ T-Cells and Neutrophils Expressing $XCR1$ Receptor. *J. Immun.*, 167(1) :57–65, 2001.

[8] M. Cazaux, C. L. Grandjean, F. Lemaître, Z. Garcia, R. J. Beck, I. Milo, J. Postat, J. B. Beltman, E. J. Cheadle, and P. Bousso. Single-cell imaging of CAR T-cell activity in vivo reveals extensive functional and anatomical heterogeneity. *J. Experimental Medicine*, 216(5) :1038–1049, 2019.

[9] S. Champiat, L. Tselikas, S. Farhane, T. Raoult, M. Texier, E. Lanoy, C. Massard, C. Robert, S. Ammari, T. de Baere, and A. Marabelle. Intratumoral immunotherapy : from trial design to clinical practice. *Clin. Cancer Res.*, 2020.

[10] M. A. Chaplain, V. A. Kuznetsov, Z. H. James, F. Davidson, and L. A. Stepanova. Spatio-temporal dynamics of the immune system response to cancer. In M. A. Horn, S. Gieri, and G. F. Webb, editors, *Mathematical models in medical and health science*. Vanderbilt

University Press, 1998. International Conference on Mathematical Models in Medical and Health Sciences.

[11] F. Chatelin. Convergence of approximation methods to compute eigenelements of linear operations. *SIAM J. Numer. Anal.*, 10(5) :939–948, 1973.

[12] F. Chatelin. The spectral approximation of linear operators with applications to the computation of eigenelements of differential and integral operators. *SIAM Rev.*, 23(4) :495–522, 1981.

[13] T. Crestaux, O. Le Maître, and J.-M. Martinez. Polynomial chaos expansion for sensitivity analysis. *Reliability Engineering and System Safety*, 94(7) :1161–1172, 2009.

[14] L. G. de Pillis, A. E. Radunskaya, and C. L. Wiseman. A validated mathematical model of cell-mediated immune response to tumor growth. *Cancer Res.*, 65(17) :7950–7958, 2005.

[15] A. Devys, T. Goudon, and P. Lafitte. A model describing the growth and size distribution of multiple metastatic tumors. *Disc. Cont. Dyn. Syst.-B*, 12 :731–767, 2009.

[16] M. Doumic-Jauffret and P. Gabriel. Eigenelements of a general aggregation-fragmentation model. *Math. Models Methods Appl. Sci.*, 20(5) :757–783, 2010.

[17] G. Dranoff. Cytokines in cancer pathogenesis and cancer therapy. *Nature Reviews Cancer*, 2004.

[18] G. P. Dunn, A. T. Bruce, H. Ikeda, L. J. Old, and R. D. Schreiber. Cancer immunoediting : from immunosurveillance to tumor escape. *Nat. Immunol.*, 3 :991–998, 2002.

[19] G. P. Dunn, L. J. Old, and R. D. Schreiber. The immunobiology review of cancer immunosurveillance and immunoediting. *Immunity*, 21 :137–148, 2004.

[20] R. Eftimie, J. L. Bramson, and D. J. D. Earn. Interactions between the immune system and cancer : A brief review of non-spatial mathematical models. *Bull. Math. Biol.*, 73(1) :2–32, Jan 2011.

[21] Y. E. Erdi. Limits of tumor detectability in nuclear medicine and PET. *Molecular imaging and radionuclide therapy*, 21(1) :23–28, 2012.

[22] O. G. Ernst, A. Mugler, H. J. Starkloff, and E. Ullmann. On the convergence of generalized polynomial chaos expansions. *ESAIM : Mathematica Modelling and Numerical Analysis*, 46(2) :317–339, 2012.

[23] J. Faget, S. Groeneveld, G. Boivin, M. Sankar, N. Zangger, M. Garcia, N. Guex, I. Zlobec, L. Steiner, A. Piersigilli, I. Xenarios, and E. Meylan. Neutrophils and snail orchestrate the establishmentof a pro-tumor microenvironment in lung cancer. *Cell Report*, 21 :3190–3204, 2017.

[24] B. E. Farrell, R. P. Daniele, and D. A. Lauffenburger. Quantitative relationships between single-cell and cell-population model parameters for chemosensory migration responses of alveolar macrophages to C5a. *Cell Motility*, 16(4) :279–293, 1990.

[25] A. Friedman and W. Hao. The role of exosomes in pancreatic cancer microenvironment. *Bull. Math. Biol.*, 80(5) :1111–1133, May 2018.

[26] P. Gabriel. *Transport-fragmentation equations and applications to prion diseases*. Phd thesis, Université Pierre et Marie Curie - Paris VI, June 2011.

[27] J. Galon and D. Bruni. Approaches to treat immune hot, altered and cold tumours with combination immunotherapies. *Nature Reviews Drug Discovery*, 18 :197–218, 2019.

[28] J. Galon, A. Costes, F. Sanchez-Cabo, A. Kirilovsky, B. Mlecnik, C. Lagorce-Pagès, M. Tosolini, M. Camus, A. Berger, P. Wind, F. Zinzindohoué, P. Bruneval, P.-H. Cugnenc, Z. Trajanoski, W.-H. Fridman, and F. Pagès. Type, density, and location of immune cells within human colorectal tumors predict clinical outcome. *Science*, 313(5795) :1960–1964, 2006.

[29] T. Goudon. *Mathematics for Modeling and Scientific Computing*. Mathematics and Statistics. Wiley-ISTE, 2016.

[30] H. L. H. and K. M. B. Cell cycle control and cancer. *Science*, 1994.

[31] H. L. . Hanson, D. L. Donermeyer, H. Ikeda, J. M. White, V. Shankaran, L. J. Old, H. Shiku, R. D. Schreiber, and P. M. Allen. Eradication of established tumors by $CD8+$ T-cell adoptive immonutherapy. *Cell Press*, 13 :265–276, 2000.

[32] D. Harenberg, S. Marelli, B. Sudret, and V. Winschel. Uncertainty quantification and global sensitivity analysis for economic models. *Quantitative Economics*, 10(1) :1–41, 2019.

[33] J. Herman and W. Usher. SALib : An open-source python library for sensitivity analysis. *The Journal of Open Source Software*, 2(9), jan 2017.

[34] T. Homma and A. Saltelli. Importance measures in global sensitivity analysis of nonlinear models. *Reliability Engineering & System Safety*, 52(1) :1 – 17, 1996.

[35] S. Khou, A. Popa, C. Luci, F. Bihl, A. Meghraoui-Kheddar, P. Bourdely, E. Salavagione, E. Cosson, A. Rubod, J. Cazareth, P. Barbry, B. Mari, R. Rezzonico, F. Anjuère, and V. M. Braud. Tumor-associated neutrophils dampen adaptive immunity and promote cutaneous squamous cell carcinoma development. *Cancers*, 10-12(7) :E1860, 2020.

[36] D. Kirschner, T. Jackson, and J. Arciero. A mathematical model of tumor-immune evasion and siRNA treatment. *Disc. Cont. Dyn. Syst.-B*, 4(1) :39–58, 2008.

[37] D. Kirschner and J. C. Panetta. Modeling immunotherapy of the tumor-immune interaction. *J. Math. Biol.*, 37 :235–252, 1998.

[38] A. Konstorum, A. T. Vella, A. J. Adler, and R. C. Laubenbacher. Addressing current challenges in cancer immunotherapy with mathematical and computational modelling. *J. Royal Soc. Interface*, 14(131), 2017.

[39] M. Krein and M. Rutman. Linear operator leaving invariant a cone in a Banach space. *Amer. Math. Soc. Translation*, 10 :199–325, 1962.

[40] V. A. Kuznetsov, I. A. Makalkin, M. A. Taylor, and A. S. Perelson. Nonlinear dynamics of immunogenic tumors : Parameter estimation and global bifurcation analysis. *Bull. Math. Biol.*, 56(2) :295–321, Mar 1994.

[41] C. S. Kwok, S. E. Cole, and S.-K. Liao. Uptake kinetics of monoclonal antibodies by human malignant melanoma multicell spheroids. *Cancer Res.*, 48(7) :1856–1863, 1988.

[42] X. Lai, W. E. Carson, A. Stiff, A. Friedman, R. Wesolowski, and M. Duggan. Modeling combination therapy for breast cancer with BET and immune checkpoint inhibitors. *Proc. Nat. Acad. Sc.*, 115(21) :5534–5539, 2018.

[43] L. Le Gratiet, S. Marelli, and B. Sudret. *Metamodel-Based Sensitivity Analysis : Polynomial Chaos Expansions and Gaussian Processes*, pages 1289–1325. Springer International Publishing, Cham, 2017.

[44] C.-Y. Li, S. Shan, Q. Huang, R. D. Braun, J. Lanzen, K. Hu, P. Lin, and M. W. Dewhirst. Initial stages of tumor cell-induced angiogenesis : evaluation via skin window chambers in rodent models. *J. Nat. Cancer Institute*, 92(2) :143–147, 01 2000.

[45] A. Matzavinos, M. A. J. Chaplain, and V. A. Kuznetsov. Mathematical modelling of the spatio-temporal response of cytotoxic T-lymphocytes to a solid tumour. *Math. Medicine and Biology*, 21(1) :1–34, 03 2004.

[46] P. Michel. Existence of a solution to the cell division eigenproblem. *Models Math. Meth. App. Sci.*, 16(Suppl. issue 1) :1125–1153, 2006.

[47] P. Michel, S. Mischler, and B. Perthame. General relative entropy inequality : an illustration on growth models. *J. Math. Pures et Appl.*, 84(9) :1235–1260, 2005.

[48] J. J. Moré. The Levenberg-Marquardt algorithm : Implementation and theory. In G. A. Watson, editor, *Numerical Analysis*, pages 105–116, Berlin, Heidelberg, 1978. Springer Berlin Heidelberg.

[49] P. Moritz, R. Nishihara, S. Wang, A. Tumanov, R. Liaw, E. Liang, M. Elibol, Z. Yang, W. Paul, M. I. Jordan, and I. Stoica. Ray : A distributed framework for emerging ai applications, 2018.

[50] J. C. Nolz and A. B. Hill. Strength in numbers : Visualizing CTL-mediated killing in vivo. *Immunity*, 44(2) :207 – 208, 2016.

[51] B. Perthame. *Transport equations in biology*. Frontiers in Math. Birkhauser, 2007.

[52] B. Perthame and L. Ryzhik. Exponential decay for the fragmentation or cell-division equation. *J. Differ. Eq.*, 210 :155–177, 2005.

[53] M. Qomlaqi, F. Bahrami, M. Ajami, and J. Hajati. An extended mathematical model of tumor growth and its interaction with the immune system, to be used for developing an optimized immunotherapy treatment protocol. *Mathematical Biosciences*, 292 :1–9, 2017.

[54] G. A. Rabinovich, D. Gabrilovich, and E. M. Sotomayor. Immunosuppressive strategies that are mediated by tumor cells. *Ann. Rev. Immunol.*, 25(1) :267–296, 2007. PMID : 17134371.

[55] D. Ramadasan, M. Chevaldonné, and T. Chateau. LMA : A generic and efficient implementation of the Levenberg-Marquardt algorithm. *Software : Practice and Experience*, 47(11) :1707–1727, 2017.

[56] M. Robertson-Tessi, A. El-Kareh, and A. Goriely. A mathematical model of tumor–immune interactions. *J. Theor. Biol.*, 294 :56 – 73, 2012.

[57] A. Saltelli. Sensitivity analysis of model output. An investigation of new techniques. *Computational Statistics and Data Analysis*, 15(2) :211–238, 1993.

[58] A. Saltelli. Making best use of model evaluations to compute sensitivity indices. *Computer Physics Comm.*, 145(2) :280 – 297, 2002.

[59] D. Serre. *Matrices : theory and applications*, volume 216 of *Graduate Texts in Math.* Springer, 2002.

[60] B. Shashni, S. Ariyasu, R. Takeda, T. Suzuki, S. Shiina, K. Akimoto, T. Maeda, N. Aikawa, R. Abe, T. Osaki, N. Itoh, and S. Aoki. Size-based differentiation of cancer and normal cells by a particle size analyzer assisted by a cell-recognition pc software. *Biological and Pharmaceutical Bulletin*, 41(4) :487–503, 2018.

[61] T. Shekarian, S. Valsesia-Wittmann, C. Caux, and A. Marabelle. Paradigm shift in oncology : targeting the immune system rather than cancer cells. *Mutagenesis*, 30 :205–211, 2015.

[62] M. J. Smyth, D. I. Godfrey, and J. A. Trapani. A fresh look at tumor immunosurveillance and immunotherapy. *Nat. Immunol.*, 2, 2001.

[63] I. Sosol'. Sensitivity estimates for nonlinear mathematical models. *Math. Modell. Comput.*, 1 :407–414, 1993.

[64] S. Spranger, A. Sivan, L. Corrales, and T. F. Gajewski. *Tumor and host factors controlling antitumor immunity and efficacy of cancer immunotherapy*, volume 130, chapter 3, pages 75–93. Elsevier, 2016.

[65] B. Sudret. Global sensitivity analysis using polynomial chaos expansions. *Reliability Engineering and System Safety*, 93(7) :964–979, 2008.

[66] K. Weise, L. Poßner, E. Müller, R. Gast, and T. R. Knösche. Pygpc : A sensitivity and uncertainty analysis toolbox for Python. *SoftwareX*, 11 :100450, 2020.

[67] T. L. Whiteside. Immune suppression in cancer : Effects on immune cells, mechanisms and future therapeutic intervention. *Seminars in Cancer Biology*, 16(1) :3–15, 2006. The Inflammation-Cancer Linkage : A Double-Edged Sword ?

[68] K. P. Wilkie and P. Hahnfeldt. Modeling the dichotomy of the immune response to cancer : Cytotoxic effects and tumor-promoting inflammation. *Bull. Math. Biol.*, 79 :1426–1448, 2017.

[69] J.-L. Yu and S. R.-J. Jang. A mathematical model of tumor-immune interactions with an immune checkpoint inhibitor. *Appl. Math. Comput.*, 362 :124523, 2019.

[70] G. Zhou, C. G. Drake, and H. I. Levitsky. Amplification of tumor-specific regulatory t cells following therapeutic cancer vaccines. *Blood*, 107(2) :628–636, 2006.

CHAPITRE. 4

A size an space structured model for tumors, effector and pro-tumor T cells interactions

Contents

Abstract : We introduce a mathematical model intended to describe the interactions between the immune system and tumors. The model is based on partial differential equations, describing the displacement of immune cells subjected to both diffusion and chemotactic mechanisms, the strength of which is driven by the development of the tumors. In this chapter we discuss the dual nature of the immune response, with the activation of both anti-tumor and pro-tumor mechanisms. The competition between these antagonistic effects leads to either equilibrium or escape phases.

Keywords. Tumor growth. Immune system. Equilibrium phase. Escape phase.

4.1 Introduction

The immune system can both constrain and promote tumor development through several complex processes, encompassed in the concept of cancer immunoediting. The antagonistic and competing effects of the immune response to tumor growth shape the different phases that have been identified to characterize this interaction : elimination, where the immune system is able to detect and eradicate the developing tumors, equilibrium, where the immune system is able to maintain the tumor expansion in a cancer-persistent state, and escape, where the tumor develops in an uncontrolled manner (see Fig. 1.1 or[11, 12]). Mathematical modeling might shed some light on these interactions and provide some tools to design efficient treatments by enhancing the immune response (immunotherapy).

The cancer immunity response is characterized by the activation of T-cells, and their migration towards the tumor micro-environment where they can eliminate tumor cells. However, the immune system might fail in this controling the tumor growth. One reason comes from the effects immunosupressive mechanisms that break the anti-tumor activity [8, 9, 25, 28, 31]. Those mechanisms involve the recruitment and shift of immune cells towards pro-tumor functions. While the anti-tumor immune response can be expected to eliminate early-stage tumors, or at least to control in a viable equilibrium developing tumors, later phases where tumor growth proceeds unrestrained are characterized by the inhibition of the protective functions of the immune system, and effects that favor the tumor development, as described by [11, 12]. Among others, the ratio effector immune cells/pro-tumor immune cells is considered as a relevant indicator of patient survival [29], the higher the ratio, the better the patient vital prognostics. The ratio evolves dynamically : tumor cells can produce inhibitory factors (anti-inflammatory cytokines) such as IL-10, IL-4 (Interleukin 10 or Interleukin 4), TGF-β (Transforming Growth Factor-beta) which favor the polarization of anti-tumor immune cells into pro-tumor ones. For instance, neutrophils N1 and classically-activated macrophages (M1), which are identified for their contribution to anti-tumor immunity, together with effector T-cells and Natural Killer (NK) cells, are converted into Tumor-Associated Neutrophils (TAN) N2 and Tumor-Associated Macrophages (TAM) M2 which have pro-tumor activities [15]. They are part of a pool of myeloid suppressor cells which can also be directly recruited from the bone marrow [16]. Moreover, DCs become tolerogenic which leads to anergic and tolerant T-cells, in addition to the priming and proliferation of regulatory T-cells (Tregs). The Tregs come into play in the mechanism of balancing or annihilating the anti-tumor immune response [24]. Besides the immunosuppressive mechanisms, the immune cells with pro-

tumor functions also contribute directly to the growth of the tumor, notably by their contribution to angiogenesis : under the pressure of hypoxia, Vascular Endothelial Growth Factors (VEGF) are secreted, which induce angiogenesis.

In the chapter 2, we proposed a system of partial differential equations describing the earliest stages of the tumor/immune system interactions. This model, which only considers the anti-tumor actions of the immune system, is able to reproduce the equilibrium phase : the large time behavior of this PDEs system is a state where residual tumor cells and positive concentration of active immune cells exist in equilibrium with rate of proliferation and death resulting in no increase of tumor size. The equilibrium can be mathematically characterized by means of an eigenvalue problem which allows us to evaluate a priori the main features of the residual state, in particular the total mass of the residual tumor (see chapter 3). By using adapted numerical procedures, this viewpoint has also permitted to identify the leading effects that shape the equilibrium state. However, the simple model of chapter 2 and 3 does not consider the contribution of immune cells with pro-tumor functions and the establishment of numerous mechanisms of immunosuppression. This is the issue addressed in this work. In the mathematical model we develop, we see that the pro-tumor immune response can break the equilibrium and lead to an escape phase characterized by the uncontrolled growth of the tumor. Also, thresholds that govern the activation of the pro-tumor mechanisms are critical in the transient phase. Moreover, we also challenge on numerical grounds the effect of various therapeutic strategies that can either restore the effector role of anti-tumor anergic cells or limit the pro-tumor activities. The investigation demonstrates the interest of combining both approaches.

4.2 Mathematical Model

4.2.1 Modeling Assumptions

We take into account three populations of interacting cells :

— the tumor antigen-specific cytotoxic effector cells including $CD8^+$ T-cells and NK cells as well as the myeloid effector cells (neutrophils N1 and macrophages M1) that will be referred to as the "anti-tumor" immune cells ;

— the "pro-tumor" immune cells, including regulatory T-cells –Treg –, myeloid-derived suppressor cells (MDSCs), tumor-associated neutrophils (TAN N2) and tumor-associated macrophages (TAM M2) favoring tumor growth ;

— the tumor cells.

The construction of the model uses the same basis as in chapter 2, to which we incorporate the "pro-tumor" immune cells. Let us collect the modeling assumptions.

A.1 the environmental constraints such as nutrient concentrations, temperature, etc. are assumed to be constant. Nevertheless, in late stages of tumor growth, some phenomena such as hypoxia or difficulties in accessing the nutrients can limit the tumor cells expansion ;

A.2 the state of the tumor cells is characterized by their size [1] ; the evolution of the tumor cells is driven by two phenomena : each tumor cell grows with a certain rate, possibly depending on its size, and it can divide into daughter cells ;

A.3 activated anti-tumor immune cells are able to destroy the targeted tumor cells ;

A.4 activated pro-tumor immune cells suppress the anti-tumor immune cells by direct contact or by the release of soluble substances (like immunosuppressive cytokines) ;

A.5 activated pro-tumor immune cells favor the tumor growth by enhancing the growth rate of the tumor cells and by favoring angiogenesis.

Moreover, the tumor cells produce several signals of chemical nature (cytokines and chemokines), related to the tumor antigenicity, which drive the immune response as follows :

A.6 a chemotactic signal, proportional to the tumor mass, induces a potential, the gradient of which drives the anti and pro-tumor cells towards the tumor micro-environment ;

A.7 the tumor antigen-specific $CD8^+$ T-cells are recruited and activated by APCs and the NK cells as well as the myeloid cells (N1,M1) are recruited and activated from a bath of non-activated immune cells. The signal that defines the recruitment/activation rate is directly related to the tumor mass ;

A.8 similarly, pro-tumor immune cells can be recruited from a bath of passive immune cells, which depends on a signal directly related to the tumor mass ;

A.9 the signal triggers the shift of certain anti-tumor immune cells into pro-tumor immune cells.

Assumptions **A.1**–**A.3** appeared in the chapter 2 where they are discussed in details. The pro-tumor effects become sensitive in a later stage of the tumor growth, and, as we shall see, play a central role in the transition to the escape phase. Assuming a constant growth rate of the tumor cells becomes questionable in this regime, and we shall now model it by means of a Gompertz law, which accounts for size-limitation mechanisms, see (4.1) below. Assumption **A.4** describes immunosuppression mechanisms mediated by pro-tumor immune cells. In addition to the contact-dependent suppression of anti-tumor immune cells, the secretion of immunosuppressive cytokines abrogates the effector functions of T-cells and NK and negatively modifies their proliferation. It triggers the reverse conditioning of DCs and can induce the apoptosis of effector T-cells through the depletion of IL-2 from the tumor micro-environment. It is worth bearing in mind that not all the anti-tumor immune cells are eliminated : they become anergic and cannot act against the tumor growth, however, they can be reactivated by the action of some treatment (i. e. anti-PD1 therapy). Assumption **A.5** corresponds to the overexpression of VEGF by pro-tumor immune cells favoring the accumulation of microvessels supplying the tumor in nutrients [14]. Assumption **A.6** already appeared in chapter 2 ; here the chemotactic mechanisms apply on both type of immune cells. Assumption **A.7** corresponds to a rough description of the complex activation mechanisms. Similarly, assumption **A.8** corresponds to the recruitment of MDSC coming from the bone marrow, and Tregs from the circulation [30]. Assumption **A.9** corresponds to the possible conversion of some immune cells that eliminate the tumor into pro-tumor immune cells (i. e. macrophages and neutrophils becoming TAN M2 and TAM N2, conventional T-cells becoming immunosuppressive

1. or, with a similar setting, their content of cyclins [5, 6]

Treg). The model takes into account different reactions of the immune system : the anti-tumor response is immediately sensitive to the tumor growth ; while the pro-tumor reactions are slightly delayed and are driven by certain critical thresholds on the total mass of the tumor.

4.2.2 Construction of the model

Following the skeleton of chapter 2, the model uses two distinct length scales :

— the length scale of the displacement of the immune cells,

— the length scale describing the size of the tumor cells.

The modeling assumes that the former is "infinitely large" compared to the latter. The interactions between the tumor and the immune system are described by the evolution of the following unknowns :

— *Tumor cell density.* The population of tumor cells is described by $(t,z) \mapsto n(t,z)$, the volumic density of tumor cells. Given $z_2 > z_1 > 0$, the integral $\int_{z_1}^{z_2} n(t,z)\,\mathrm{d}z$ gives the number of tumor cells having a size in the interval $[z_1, z_2]$ at time t.

— *Cytotoxic effector cell concentration.* The concentration of anti-tumor immune cells that are actively fighting against the tumor is $(t,x) \mapsto c(t,x)$.

— *Pro-tumor immune cell concentration.* Similarly, $(t,x) \mapsto c_r(t,x)$ stands for the concentration of the pro-tumor immune cells favoring tumor growth.

— *Chemoattractant potential.* We denote by $(t,x) \mapsto \phi(t,x)$ the concentration of the chemical signal (chemokines) that attracts the immune cells towards the tumor micro-environment.

— *Cytokine concentration.* Finally, let $t \mapsto I(t)$ be the concentration of cytokines in the overall tumor microenvironment.

The evolution of the population of tumor cells is governed by volume growth and cellular division. We add to these effects a death rate induced by the activated anti-tumor immune cells. Let $z \mapsto V(z) \geq 0$ stand for the tumor cell growth rate. We can assume it is a positive constant, but in the present context it is more appropriate to adopt a size dependent model, that incorporates size-limitation effects. We work with the Gompertz law

$$V(z) = rz\ln(b/z), \tag{4.1}$$

with $r > 0$ and $b > 0$, the maximal size. Accordingly the size variable z lies in the interval $[0,b]$. We refer the reader to [1, 17, 18, 20, 21] for derivation and use of this law in tumor growth modeling, in particular when taking into account the limited access to nutrients or necrotic mechanisms, see **A.1**, **A.2**. The cell division mechanism is described by the operator

$$Q(n)(t,z) = -a(z)n(t,z) + \int_z^b a(z')k(z|z')n(t,z')\,\mathrm{d}z'. \tag{4.2}$$

The gain term accounts for cells with size z produced by the division of larger cells, and the loss term is related to the division of cells with size z. The division process is governed by the frequency $a(z')$ of division of cells having size z', and the distribution in size $k(z|z')$ of products

from the division of a tumor cell with size z'. It is likely that the parameters of the division process depend on the size variable. For instance, division frequency might vanish for the smallest cells, which means $a(z) = 0$ for $0 \leq z \leq z_0$. What is crucial for modeling purposes is the requirement

$$\int_0^z z' k(z'|z)\,\mathrm{d}z' = z,$$

which is related to the principle of mass conservation. Indeed, it implies that cell-division does not change the total mass

$$\int_0^b zQ(n)\,\mathrm{d}z = 0.$$

However, the total number of cells increases since $\int_0^b (n)\,\mathrm{d}z \geq 0$. A relevant example is provided by the binary division operator

$$Q(n)(t,z) = 4a(2z)n(t,2z) - a(z)n(t,z), \tag{4.3}$$

which describes the situation where cells with size $2z$ splits into two daughter cells, both with size z. Further relevant examples of division kernels can be found in [10]. The equation will be completed by the boundary condition $n(t,0) = 0$, which means that there is no production of cells with size 0. For further purposes, let us introduce the following quantities

$$\text{total number of tumor cells : } \mu_0(t) = \int_0^b n(t,z)\,\mathrm{d}z, \tag{4.4}$$

$$\text{total mass of tumor cells : } \mu_1(t) = \int_0^b zn(t,z)\,\mathrm{d}z. \tag{4.5}$$

The displacement of the anti and pro-tumor immune cells is driven by convection and diffusion, over a domain $\Omega \subset \mathbb{R}^N$. For the sake of simplicity we assume they have the same diffusion coefficient D. We shall work with a constant coefficient, but it is likely that space-dependent and anisotropic coefficients are more relevant, for instance to take into account the presence of different tissues in which the diffusion is more or less efficient, which is certainly far from harmless, as pointed out in our study in chapter 3. The convection is defined by the chemotactic potential ϕ, which depends on the total mass of the tumor. It obeys the diffusion equation

$$-\nabla_x \cdot (\mathcal{K}\nabla_x \phi) = f(\mu_1)\sigma, \qquad \mathcal{K}\nabla_x \phi \cdot \nu\big|_{\partial\Omega} = 0 \tag{4.6}$$

endowed with the homogeneous Neumann boundary condition. In (4.6), $x \mapsto \sigma(x)$ is a given form function with zero-mean, $\mathcal{K} > 0$ is a positive coefficient (it could be matrix-valued as well). The strength of the potential depends on the total mass of the tumor through the function $\mu_1 \mapsto f(\mu_1) \geq 0$. It is natural to assume that $f(0) = 0$ and f is non decreasing. A typical example of f is the following Michealis-Menten functional response :

$$f(\mu_1) = \frac{\mu_1}{\beta + \mu_1}, \qquad \beta > 0. \tag{4.7}$$

We suppose that c and c_r have the same chemotactic sensitivity $\chi > 0$, and they both satisfy homogeneous Dirichlet boundary condition on $\partial\Omega$: the immune cells far from the tumor are non-activated.

Let us now describe the zeroth order terms of the equations, that differ depending on the considered type of cells. Both type of immune cells is subjected to a death rate $\gamma, \gamma_r > 0$. The anti-tumor immune cells are recruited from a source of naive immune cells $(t, x) \mapsto S(t, x)$. The activation process is described through a rate $\mu_1 \mapsto g(\mu_1) \geq 0$, which depends on the total mass of the tumor. Again, it is natural to assume $g(0) = 0$ and g is non decreasing. There are two other mechanisms that lead to a loss of anti-tumor immune cells. First, according to assumption **A.4**, the pro-tumor immune cells suppress effector cells ; this is traduced by a loss term

$$-k_c c c_r$$

where $k_c > 0$ is the rate of this reaction. Second, according to assumption **A.9**, certain activated effector cells can be converted into pro-tumor immune cells under the action of cytokines in the tumor micro-environment. This leads to the loss term

$$-k_r I \theta c$$

where $k_r > 0$ is the rate of this conversion, and $x \mapsto \theta(x)$ is a given form function, say a peaked Gaussian, indicating that such processes occur in the vicinity of the tumor. This loss of anti-tumor immune cells contributes to the gain term for the population of pro-tumor immune cells. Cytokines also activate at possibly space-dependent rate p_r pro-tumor immune response from a distant source of immune cells denoted by S_r according to assumption **A.8**.

The effector cells release cytotoxic substances in the tumor micro-environment. This effect is described by the death term

$$m(c, n)(t, z) = n(t, z) \times \int_\Omega \delta(y) c(t, y) \, \mathrm{d}y \tag{4.8}$$

in the tumor growth equation. It involves a non negative space-dependent weight $x \mapsto \delta(x)$, which incorporates both the strength of the immune response and a radius of interaction. According to assumption **A.5**, recruited pro-tumor immune cells favor the tumor growth. Therefore the growth rate of the tumor cells is enhanced by the presence of pro-tumor immune cells and it becomes

$$V(z) \left(1 + \int_\Omega b_1(y) c_r(t, y) \, \mathrm{d}y \right) \tag{4.9}$$

with a certain non negative, radially symmetric and compactly supported kernel b_1.

Finally, we turn to the evolution of the tumor-secreted cytokines, which promote the pro-tumor reactions. The production of such cytokines occurs beyond a certain critical mass, denoted by m. Moreover, the cytokine concentration is naturally damped with a constant rate $\tau > 0$. This leads to the ODE

$$\partial_t I = \psi(\mu_1) - \tau I \tag{4.10}$$

where ψ is a threshold function, non negative and non decreasing. For instance, given a constant $\bar{\psi} > 0$ and a constant $m > 0$, it can be defined by :

$$\psi(\mu_1) = \bar{\psi} \begin{cases} (\mu_1 - m), & \mu_1 > m \\ 0, & \mu_1 \leq m \end{cases} \tag{4.11}$$

We shall need the technical assumptions $\psi(0) = \psi'(0) = 0$, which clearly holds when $m > 0$. Eventually, we arrive at the following system describing the interactions between the tumor cells, the effector and pro-tumor immune cells :

$$\partial_t n + \partial_z \left(V(z) \left(1 + \int_\Omega b_1(y) c_r(t,y) \right) n \right) = Q(n) - m(n,c), \tag{4.12a}$$

$$\partial_t c + \nabla_x \cdot (c\chi \nabla_x \phi - D\nabla_x c) = g(\mu_1)S - \gamma c - k_r I \theta_1 c - k_c c c_r, \tag{4.12b}$$

$$\partial_t c_r + \nabla_x \cdot (c_r \chi \nabla_x \phi - D\nabla_x c_r) = I(p_r S_r + k_r \theta_1 c) - \gamma_r c_r, \tag{4.12c}$$

$$\partial_t I = \psi(\mu_1) - \tau I, \tag{4.12d}$$

$$-\nabla_x \cdot (\mathcal{K} \nabla_x \phi) = f(\mu_1)\sigma, \tag{4.12e}$$

$$n(t,0) = 0,\ c|_{\partial\Omega} = 0,\ c_r|_{\partial\Omega} = 0,\ \mathcal{K}\nabla_x \phi \cdot \nu(\cdot)|_{\partial\Omega} = 0, \tag{4.12f}$$

$$n(t=0,z) = n_0(z),\ c(t=0,x) = c_0(x),\ c(t=0,x) = c_r^0(x),\ I(t=0) = I_0. \tag{4.12g}$$

We remind the reader that the cell division operator $Q(n)$ and the immune cell-tumor interaction term $m(c,n)$ are defined in (4.2) and (4.8) respectively. The Table 4.1 recapitulates the biological meaning of the parameters of the model.

4.2.3 A few mathematical comments

In this section, we provide some hints on the behavior of the solutions of (4.12a)-(4.12g), based on mathematical arguments. First, we consider the ODEs system which is the closest to (4.12a)-(4.12g), by disregarding the space dependence of the unknowns and dealing with constant coefficients. The analysis of this simple system helps in understanding the role of the parameters of the model. Second, we adapt the identification of the equilibrium phase as discussed in chapter 2.

A simplified model : damping and escape

Let us consider the very specific case where

— V and a are constant,

— the source S of immune cell is constant,

— the source $S_r = 0$ vanishes and the other parameters D, $\mathcal{K}$ are constant and positive,

— the coupling function is linear : $g(\mu_1) = \mu_1$,

— the space variation of the concentrations of immune cells is neglected,

— we consider the binary division model (4.3) with a constant frequency a.

These assumptions clearly lack of biological relevance, but the simplified framework shed some light on the possible behavior of the solutions and the role of the parameters. In this simple situation, the dynamics is described by the following system of ordinary differential equations

for μ_0, μ_1, given by (4.4), (4.5), and the time-dependent concentrations of immune cells and of cytokines :

$$\begin{cases} \frac{\mathrm{d}}{\mathrm{d}t}\mu_0 = \mu_0\left(a - \delta c\right), \\ \frac{\mathrm{d}}{\mathrm{d}t}\mu_1 = V(1 + b_1 c_r)\mu_0 - \delta\mu_1 c, \\ \frac{\mathrm{d}}{\mathrm{d}t}c = \mu_1 S - \gamma c - k_r c I - k_c c c_r, \\ \frac{\mathrm{d}}{\mathrm{d}t}c_r = k_r c I - \gamma_r c_r, \\ \frac{\mathrm{d}}{\mathrm{d}t}I = \psi(\mu_1) - \tau I. \end{cases} \tag{4.13}$$

The state

$$\begin{pmatrix} \mu_0^H \\ \mu_1^H \\ c^H \\ c_r^H \\ I^H \end{pmatrix} = \begin{pmatrix} 0 \\ 0 \\ 0 \\ 0 \\ 0 \end{pmatrix}$$

is a trivial equilibrium solution to (4.13) which corresponds to a healthy state. However, we can also find equilibrium states with residual tumor cells, effector immune cells and even pro-tumor immune cells. Indeed, let

$$\begin{pmatrix} \mu_0^{NP} \\ \mu_1^{NP} \\ c^{NP} \\ c_r^{NP} \\ I^{NP} \end{pmatrix} = \begin{pmatrix} \frac{\gamma a^2}{\delta V S} \\ \frac{\gamma a}{\delta S} \\ \frac{a}{\delta} \\ 0 \\ 0 \end{pmatrix}.$$

If $\mu_1^{NP} \leq m$, the threshold for the activation of cytokines, this defines an equilibrium solution with a residual tumor and free of pro-tumor immune cells. Next, let us introduce

$$Q = \frac{k_r a \sigma_2}{\delta\tau},$$

and let

$$\mu_1^P = \frac{\frac{\gamma a}{\delta} - Qm - \frac{k_c a}{\gamma_r \delta} Qm}{S - Q - \frac{k_c a}{\gamma_r \delta} Q}. \tag{4.14}$$

be the tumor mass at equilibrium with the presence of pro-tumor immune cells. Indeed, if $\mu_1^P > m$ another equilibrium solution is given by

$$\begin{pmatrix} \mu_0^P \\ \mu_1^P \\ c^P \\ c_r^P \\ I^P \end{pmatrix} = \begin{pmatrix} \frac{a}{V(1+b_1 c_r^P)}\mu_1^P \\ \mu_1^P \\ \frac{a}{\delta} \\ Q\frac{\psi(\mu_1^P)}{\gamma_r} \\ \psi\left(\mu_1^P\right)\frac{\sigma_2}{\tau} \end{pmatrix}$$

That the definition of this unhealthy state makes sense requires that the right hand side in (4.14) is positive. It means that either

$$\begin{aligned} &S > Q\left(1+\frac{k_c a}{\gamma_r \delta}\right) > 0 \text{ and } \frac{\gamma a}{\delta} > Qm\left(1+\frac{k_c a}{\gamma_r \delta}\right) \\ &\text{or } S < Q\left(1+\frac{k_c a}{\gamma_r \delta}\right) \text{ and } \frac{\gamma a}{\delta} < Qm\left(1+\frac{k_c a}{\gamma_r \delta}\right), \end{aligned} \tag{4.15}$$

imposing constraints on the parameters. Let us discuss the possibility of obtaining the different equilibrium states μ_1^{NP}, μ_1^P, depending on the ratio $\frac{a}{\delta}$ between the tumor division rate a and the strength of the immune response δ. It measures the competitiveness between the tumor and the anti-tumor immune cells. We thus study respectively the sign of $\mu_1^{NP} - m$ and $\mu_1^P - m$. On the one hand,

$$\mu_1^{NP} - m < 0 \text{ if and only if } \frac{a}{\delta} < \frac{mS}{\gamma}, \tag{4.16}$$

and on the other hand

$$\mu_1^P - m = \frac{\gamma\frac{a}{\delta} - mS}{S - Q_1\frac{a}{\delta} - Q_2\left(\frac{a}{\delta}\right)^2}, \tag{4.17}$$

where

$$Q_1 = \frac{k_r \sigma_2}{\tau} \quad \text{and} \quad Q_2 = \frac{k_c k_r \sigma_2}{\gamma_r \tau}.$$

Let us denote by

$$X_2 = \frac{-\frac{Q_1}{Q_2} + \sqrt{\left(\frac{Q_1}{Q_2}\right)^2 + \frac{4S}{Q_2}}}{2}, \tag{4.18}$$

the non-negative root of the denominator in (4.17). By analyzing the sign of (4.17), we distinguish two cases

— if $m < \frac{\gamma X_2}{S}$ (relatively small critical mass),

$$\mu_1^P - m > 0 \text{ if and only if } \frac{a}{\delta} \in \left(\frac{mS}{\gamma}, X_2\right) \tag{4.19}$$

and

$$\mu_1^P - m < 0 \text{ if and only if } \frac{a}{\delta} \in \left(0, \frac{mS}{\gamma}\right) \cup (X_2, +\infty)\,. \tag{4.20}$$

This is summarized in the following table

$\frac{a}{\delta}$	0		$\frac{mS}{\gamma}$		X_2		$+\infty$
$\mu_1^P - m$	< 0		0	> 0		< 0	
			μ_1^P **admissible**				
$\mu_1^{NP} - m$	< 0		0	> 0		> 0	
	μ_1^{NP} **admissible**						

There is no admissible equilibrium when $\frac{a}{\delta} \in [X_2, +\infty)$: the aggressiveness of the tumor is strong and the tumor mass certainly blows up.

— if $m > \frac{\gamma X_2}{S}$, we have

$\frac{a}{\delta}$	0		X_2		$\frac{mS}{\gamma}$		$+\infty$
$\mu_1^P - m$	< 0		> 0		0	< 0	
			μ_1^P **admissible**				
$\mu_1^{NP} - m$	< 0		< 0		0	> 0	
	μ_1^{NP} **admissible**						

Discussion on the stability of the equilibrium points The Jacobian matrix evaluated at the healthy state (H) reads

$$J^H = \begin{pmatrix} a & 0 & 0 & 0 & 0 \\ V & 0 & 0 & 0 & 0 \\ 0 & S & -\gamma & 0 & 0 \\ 0 & 0 & 0 & -\gamma_r & 0 \\ 0 & 0 & 0 & 0 & -\tau \end{pmatrix}$$

Since $a > 0$, J^H has a positive eigenvalue and the healthy state is linearly unstable. The equilibrium state (NP) corresponds to the unhealthy state in chapter 2. The Jacobian matrix at this state reads

$$J^{NP} = \begin{pmatrix} 0 & 0 & -\frac{\gamma a^2}{VS} & 0 & 0 \\ V & -a & -\frac{\gamma a}{S} & 0 & 0 \\ 0 & S & -\gamma & 0 & -k_r \frac{a}{\delta} \\ 0 & 0 & 0 & -\gamma_r & k_r \frac{a}{\delta} \\ 0 & 0 & 0 & 0 & -\tau \end{pmatrix}$$

and its characteristic polynomial is

$$p(\lambda) = -(\gamma_r + \lambda)(\tau + \lambda)(\lambda^3 + (\gamma + a)\lambda^2 + 2a\gamma\lambda + \gamma a^2).$$

As in chapter 2, we distinguish two cases, which depends on the ratio $\frac{\gamma}{a}$. The ratio compares the death rate of the anti-tumor immune cells to the tumor cells division rate. We get

— if $\gamma > 4a$, the eigenvalues of J^{NP} are given by

$$\lambda_1 = -\gamma_r, \quad \lambda_2 = -\tau, \quad \lambda_3 = -a, \quad \lambda_4 = \frac{1}{2p}\left(-\sqrt{\gamma(\gamma - 4a)} - \gamma\right),$$

$$\lambda_5 = \frac{1}{2}\left(\sqrt{\gamma(\gamma - 4a)} - \gamma\right).$$

They are all real and negative.

— if $\gamma < 4a$, the eigenvalues are given by

$$\lambda_1 = -\gamma_r, \quad \lambda_2 = -\tau, \quad \lambda_3 = -a, \quad \lambda_4 = \frac{1}{2}\left(-i\sqrt{\gamma(\gamma - 4a)} - \gamma\right),$$

$$\lambda_5 = \frac{1}{2}\left(i\sqrt{\gamma(\gamma - 4a)} - \gamma\right).$$

They all have a negative real part.

Therefore, when admissible ($\mu_1^{NP} < m$), the unhealthy state with no pro-tumor immune cells is always linearly stable. In addition, the ratio γ/a discriminates between a damped behavior, and an oscillatory behavior. As observed in chapter 2, the greater the cell division, the faster the oscillations of the tumor mass μ_1. We observe on numerical grounds that in the case where the equilibrium states μ_1^{NP} and μ_1^P coexist ($X_2 < \frac{a}{\delta} < \frac{mS}{\gamma}$), there is either the formation of an equilibrium free of pro-tumor cells, namely the state referred to by the superscript NP, or the blow up of the tumor mass due to the activation of pro-tumor immune cells; when $\frac{a}{\delta} > \frac{mS}{\gamma}$, the tumor mass always blows up. Typical results are depicted in Fig. 4.1 : when the control occurs the concentration of anti-tumor immune cells tends to the equilibrium value a/δ (Fig. 4.1-a)); otherwise it reaches a constant state below the equilibrium value (Fig. 4.1-b)-d)). The simulations also show that the control of the tumor is very sensitive to the strength of the source of naive immune cells and to the division rate of the tumor cells. It is worth remarking that the damping

of the tumor mass towards an equilibrium can be restored by strengthening the activation law of effector immune cells for large tumor masses, for instance by using $g(\mu_1) = \mu_1^2$, see Fig. 4.2.

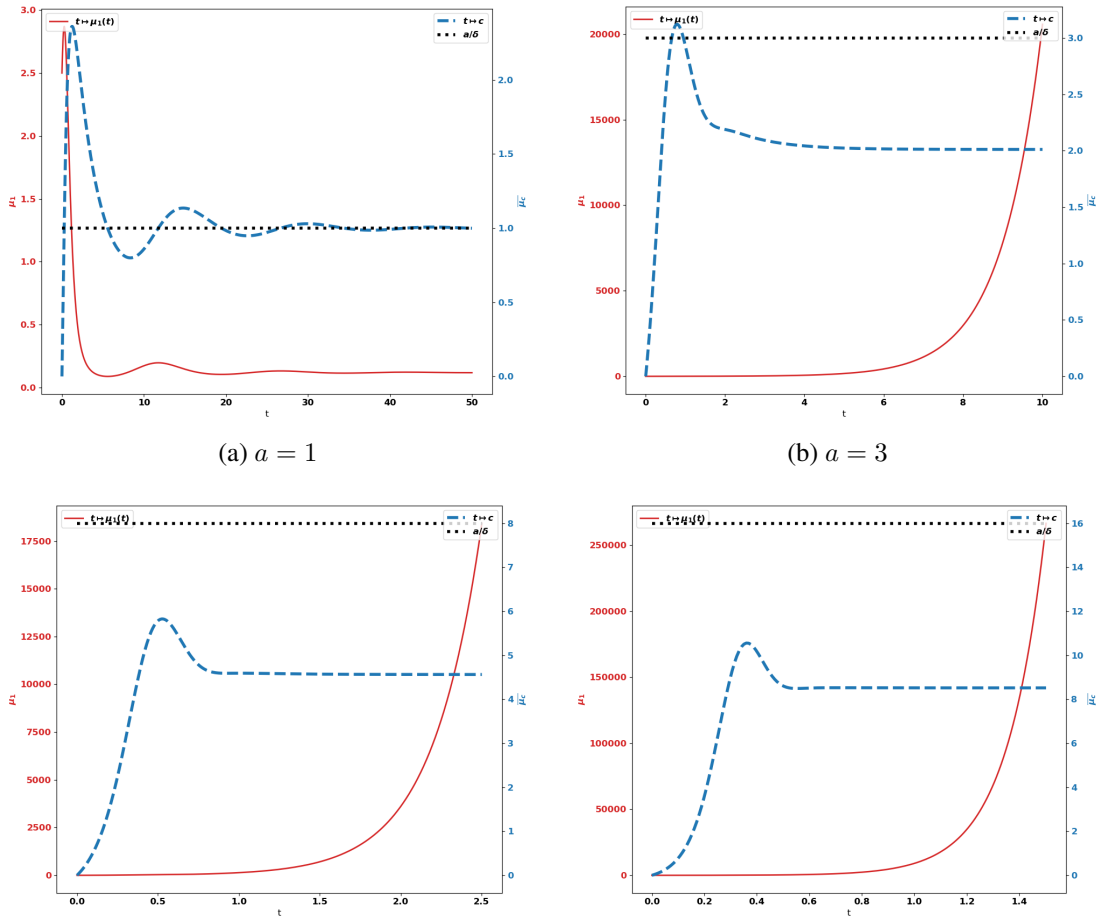

(a) $a = 1$ (b) $a = 3$

(c) $a = 8$ (d) $a = 16$

FIGURE 4.1 – Typical behavior of the solutions of (4.13). Data : $V = 0.616$, $\delta = 1.$, $S = 1.5$, $k_r = 1.25$, $k_c = 0.1$, $m = 2$. (x-axis : time, y-axis : μ_1, mass of the tumor in red, and $\mu_c = \delta c$, the strength of the active immune cells in blue, the tumor cells division rate a in black)

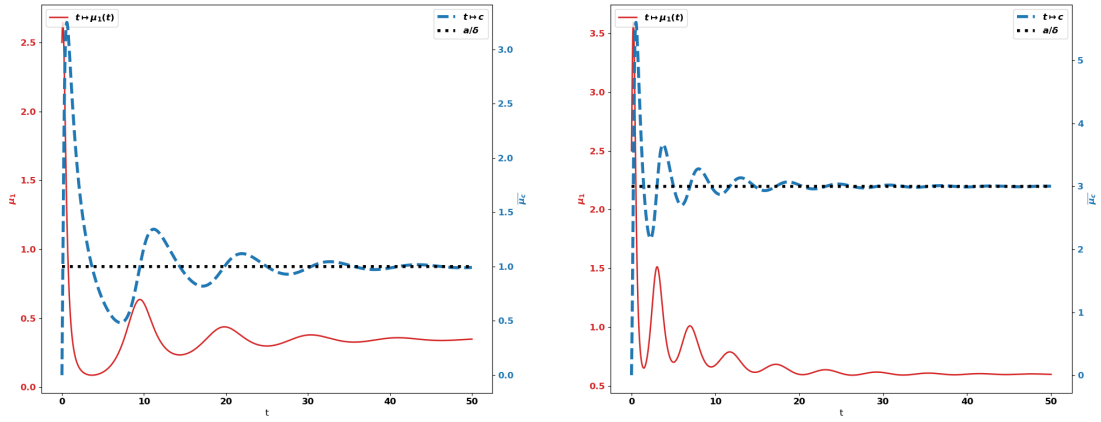

(a) $a = 1$

(b) $a = 3$

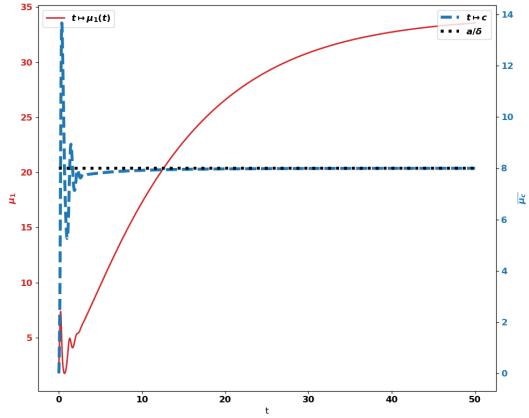

(c) $a = 8$

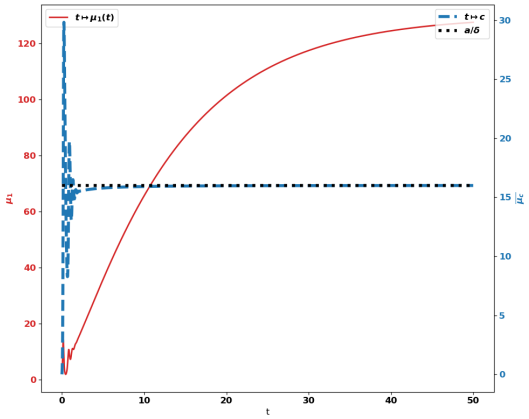

(d) $a = 16$

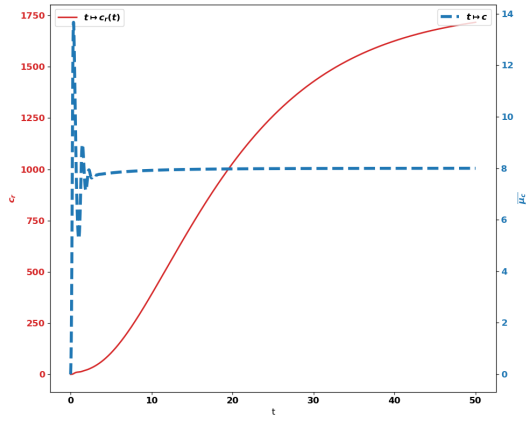

(e) $a = 8$, c_r in red and c in blue

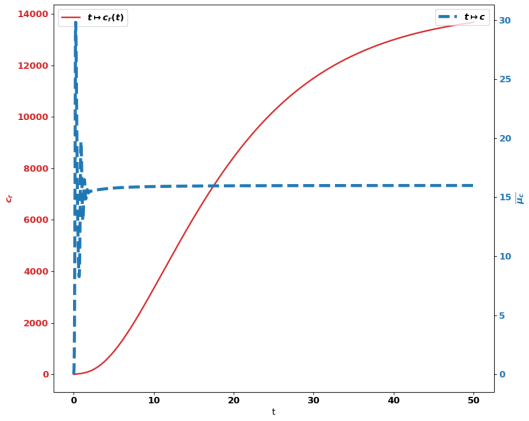

(f) $a = 16$, c_r in red and c in blue

FIGURE 4.2 – Typical behavior of the solutions of (4.13) with $g(\mu_1) = \mu_1^2$. Data : $V = 0.616$, $\delta = 1.$, $S = 1.5$, $k_r = 1.25$, $k_c = 0.1$, $m = 2$. (x-axis : time, y-axis : μ_1, mass of the tumor in red, and $\mu_c = \delta c$, the strength of the active immune cells in blue, the tumor cells division rate a in black)

Existence of equilibrium phases

The analysis and simulations carried out in chapter 2 for the model without pro-tumor immune cells reveal the existence and stability of a cancer-persistent equilibrium. In addition, further analysis of the equilibrium in chapter 3 reveals how the total mass of the tumor at equilibrium is influenced by the biological parameters. It turns out that the equilibrium phase corresponds to the situation where the death rate induced by the effector immune cells precisely counterbalances the natural exponential growth of the tumor cell population.

Indeed, it is known that the growth-fragmentation operator admits an eigenpair (λ, N) satisfying

$$\begin{cases} \partial_z(VN) - Q(N) + \lambda N = 0 \text{ for } z \geq 0, \\ N(0) = 0, \qquad N(z) > 0 \text{ for } z > 0, \qquad \int_0^{+\infty} N(z)\,\mathrm{d}z = 1, \qquad \lambda > 0. \end{cases}$$

We refer the reader to [10] for a detailed analysis of this eigenproblem. When the action of the immune system is neglected, namely $m(n,c) = 0$ and $b_1 = 0$ in (4.12a), the population of tumor cells grows exponentially fast and its size-distribution is governed by the eigenfunction : $n(t,z) \sim_{t\to\infty} e^{\lambda t} N(z)$, see [22, 23, 26]. Equilibrium occurs when the death rate due to the effector cells reaches the eigenvalue. Namely, the concentration C of cytotoxic effector cells at equilibrium should satisfy

$$\int_\Omega \delta(x) C(x)\,\mathrm{d}x = \lambda. \tag{4.21}$$

In turn, the definition of the concentration of activated immune cells by means of stationary convection-diffusion-reaction equations defines implicitly the total tumor mass at equilibrium. This intuition is made precise by the following statement.

Theorem 4.2.1. *Let Φ be the solution of*

$$\nabla_x \cdot (\mathcal{K} \nabla_x \Phi) = \sigma,$$

endowed with the homogeneous Neumann boundary condition. There exists $\ell_\star > 0$ such that for any $0 < \ell < \ell_\star$, there exists a unique $\bar{\mu}_1(\ell) > 0$ and $(C_{\bar{\mu}_1(\ell)}, C_{r,\bar{\mu}_1(\ell)}, I_{\bar{\mu}_1(\ell)})$, solution of the stationary equations

$$\gamma C + k_r I \theta_1 C + k_c C C_r - f(\bar{\mu_1}) \nabla_x \cdot (C \chi \nabla_x \phi) - \nabla_x \cdot (D \nabla_x C) = g(\bar{\mu_1}) S, \tag{4.22a}$$

$$\gamma_r C_r - f(\bar{\mu_1}) \nabla_x \cdot (C_r \chi \nabla_x \phi) - \nabla_x \cdot (D \nabla_x C_r) = I(S_r + k_r \theta_1 C), \tag{4.22b}$$

$$I = \frac{\psi(\bar{\mu_1})}{\tau}, \tag{4.22c}$$

$$C|_{\partial\Omega} = 0,\ C_r|_{\partial\Omega} = 0, \tag{4.22d}$$

satisfying $\int_\Omega \delta C\,\mathrm{d}x = \ell$.

Proof. We adapt the arguments from chapter 2. We start with introducing the mapping

$$\mathscr{F} : (\ell, \mu_1) \in [0,\infty) \times [0,\infty) \longmapsto \int_\Omega \delta C_{\mu_1}\,\mathrm{d}x - \ell$$

where C_{μ_1} is the solution of (4.22a) associated to μ_1. We are searching for the zeroes of $\mathscr{F}$. Clearly, when $\mu_1 = 0$, $C_0 = 0$, $I_0 = 0$, $C_{r,0} = 0$ satisfies (4.22a)-(4.22d), together with the constraint $\int \delta C_0 \, \mathrm{d}x = 0$, so that $\mathscr{F}(0,0) = 0$. Next, we have $\partial_{\mu_1}\mathscr{F}(\ell,\mu_1) = \int_\Omega \delta C'_{\mu_1} \, \mathrm{d}x$, where C'_{μ_1} is defined by the system

$$
\begin{aligned}
&(\gamma + k_r I\theta_1 + k_c C_r)C' + (k_r I'\theta_1 + k_c C'_r)C - \nabla_x \cdot (D\nabla_x C') - f(\mu_1)\nabla_x \cdot (C'\nabla_x \Phi) \\
&\qquad = g'(\mu_1)S + f'(\mu_1)\nabla_x \cdot (C_{\mu_1}\nabla_x \Phi) \\
&\gamma_r C'_r - \nabla_x \cdot (D\nabla_x C'_r) - f(\mu_1)\nabla_x \cdot (C'_r \nabla_x \Phi), \\
&\qquad = I'(S_r + k_r\theta_1 C) + I k_r \theta_1 C' + f'(\mu_1)\nabla_x \cdot (C_{\mu_1}\nabla_x \Phi), \\
&I' = \frac{\psi'(\mu_1)}{\tau}.
\end{aligned}
$$

With $\mu_1 = 0$, the right hand side of the equation for C'_r vanishes and we get $C'_r = 0$. In the right hand side of the equation for C', $g'(0)S \neq 0$ is non negative and the maximum principle for elliptic equations tells us that $C'_0 > 0$. It follows that $\partial_{\mu_1}\mathscr{F}(0,0) = \int_\Omega \delta C'_0 \, \mathrm{d}x > 0$. We can thus apply the implicit function theorem : there exists $\ell_\star > 0$ and a mapping $\bar{\mu}_1 : \ell \in [0,\ell_\star) \mapsto \bar{\mu}_1(\ell)$ such that $\mathscr{F}(\ell, \bar{\mu}_1(\ell)) = 0$ holds for any $\ell \in [0,\ell_\star)$. We have

$$
\partial_\ell \mathscr{F}(\ell,\bar{\mu}_1(\ell)) + \bar{\mu}'_1(\ell)\partial_{\mu_1}\mathscr{F}(\ell,\bar{\mu}_1(\ell)) = -1 + \bar{\mu}'_1(\ell)\partial_{\mu_1}\mathscr{F}(\ell,\bar{\mu}_1(\ell)) = 0
$$

with $\partial_{\mu_1}\mathscr{F}(0,0) > 0$. Hence, $\ell \mapsto \bar{\mu}_1(\ell)$ is increasing on the neighborhood of $\ell = 0$, and it thus takes positive values. ∎

Theorem 4.2.1 is at the basis of the interpretation of the equilibrium phase : it applies when the action of pro-tumor immune cells is neglected on the cell-division equation (namely assuming $b_1 = 0$). The statement involves a smallness assumption and it justifies the existence of equilibria with small tumor masses. In the case of the binary division model with a constant division rate a and a constant growth rate V, the smallness assumption is equivalent to a smallness assumption on the division rate a. The numerical simulations indicate a quite robust property (chapter 2 and chapter 3) and the smallness assumption could be only technical.

The analysis of the full model accounting for pro-tumor immune cells is much more involved because the tumor growth rate is modified by the action of the pro-tumor immune cells : $V(z)$ is multiplied by the factor $(1+\beta(t))$ with

$$
\beta(t) = \int b_1(y)c_r(t,y) \, \mathrm{d}y.
$$

As $t \to \infty$, we expect that $c_r(t,x)$ and $c(t,x)$ admits limits so that $\int \delta c(t,x) \, \mathrm{d}x$ tends to some $\lambda > 0$ and $\beta(t)$ tends to an asymptotic value β_∞ while the size-distribution of the tumor cells is described by an eigenpair (λ, N). However, in general the eigenvalue λ depends on the value of β_∞, which induces a stronger coupling between the unknowns. The case where both a and V are constant is specific and allows us to confort the intuition. In this case, the leading eigenvalue $\lambda = a$ does not change when V is replaced by $V(1+\beta_\infty)$; only the profile is rescaled into

$$
N_{\beta_\infty}(z) = N_1\Big(\frac{z}{1+\beta_\infty}\Big),
$$

where the profile N_1 is known. As β_∞ increases, the asymptotic size-distribution of tumor cells contains larger cells, see Fig. 4.3 and chapter 2, Fig. 2.3. For general coefficients, the leading eigenstate of the growth-fragmentation operator is not explicitly known but it can be computed numerically using the power method designed in chapter 3 (see Fig. 4.3).

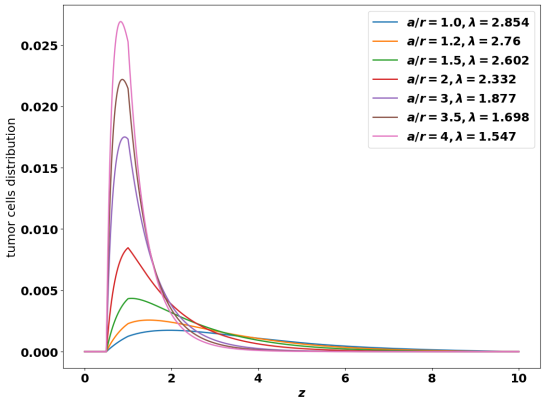

FIGURE 4.3 – Different shapes of the leading eigen-function of the growth-division equation for several values of $\frac{a}{r}$ where $r = (1 + \beta_\infty)$ is the intrinsic growth rate of the tumor cells. Here, the growth rate $z \mapsto V(z)$ follows the Gompertz law (4.1) and the division rate is given by $z \mapsto a(z) = a\mathbf{1}_{z_0 \leq z < \infty}$ for some $z_0 > 0$. (x-axis : z, size of the tumor cells, y-axis : number of tumor cells at the final time)

When the pro-tumor cells modify the growth rate of the tumor cells, we cannot use as such the power-dichotomy method designed in chapter 3 to predict the equilibrium state. Nevertheless, the numerical simulations of the evolution problem (see Section 4.3.2) highlight the following features :

— when the critical mass m is positive, either the steady state is free of pro-tumor immune cells ($c_r \equiv 0$) and the tumor is controlled by the anti-tumor immune cells or both the tumor mass μ_1 and the concentration of pro-tumor immune cells c_r blow up. The former occurs for small division rates, the latter is observed with more aggressive tumors. Furthermore, when the tumor growth is controlled, we can check that the asymptotic concentration of anti-tumor immune cells ($x \mapsto C(x)$) satisfies (4.21) (see Fig. 4.10, 4.11 and 4.12 below).

— when the critical mass is equal to zero ($m = 0$), either we observe an equilibrium state containing residual pro-tumor immune cells or the tumor mass μ_1 and the concentration of pro-tumor immune cells c_r blow up.

4.3 Results of the numerical experiments

We perform the numerical simulations considering the binary division operator (4.3) with a constant division rate $a > 0$. For details on the numerical methods we refer the reader to the chapter. 2 section 2.5.3 The case where the growth rate V is constant is less relevant biologically, but it can be used to check the properties of the model and of the numerical procedures since the eigenpair (λ, N) is explicitly known in this case, see [4, 27] and [26, Lemma 4.1] : in fact we have $\lambda = a$.

According to the framework in chapter 2, we assume that the tumor is located at the origin of the computational domain Ω, which here is the unit ball of $\mathbb{R}^2$, and we use the following definitions

$$\delta(x) = \frac{A}{\xi\sqrt{2\pi}} \exp\left(-\frac{|x|^2}{2\xi^2}\right), \quad b_1(x) = \frac{A_{b_1}}{\xi_{b_1}\sqrt{2\pi}} \exp\left(-\frac{|x|^2}{2\xi_{b_1}^2}\right). \tag{4.23}$$

For defining the source term of the chemoattractant potential and the form function θ_1 we also use the following Gaussian profiles :

$$\sigma(x) = \frac{A_\sigma}{\xi_\sigma\sqrt{2\pi}} \exp\left(-\frac{|x|^2}{2\xi_\sigma^2}\right), \quad \theta(x) = \frac{A_{\theta_1}}{\xi_{\theta_1}\sqrt{2\pi}} \exp\left(-\frac{|x|^2}{2\xi_{\theta_1}^2}\right) \tag{4.24}$$

In what follows, we set

$$f(\mu_1) = \frac{\mu_1}{\eta + \mu_1}, \ \eta > 0, \text{ and } g(\mu_1) = \mu_1.$$

For the simulations, we shall use the following data, otherwise explicitly stated : the initial data are $(c_0(x), c_{r,0}(x)) = (0, 0)$ and $n_0(z) = \mathbf{1}_{0.125 \le z \le 5}$. The parameters are given in Table 4.2. The source of naive immune cells S_r is represented by an heterogeneous bath of immune cells distant from the tumor site (see Fig. 4.4). This assumption describes the fact that pro-tumor cells are rather recruited and primed in specific sites, in contrast to anti-tumor cells, in particular NK cells, which can be considered as homogeneously distributed.

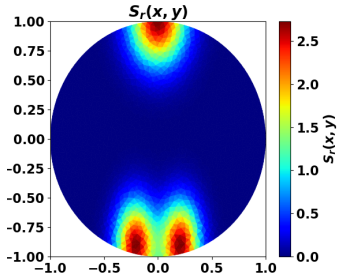

FIGURE 4.4 – Source S_r of pro-tumor cells

A	ξ^2	A_σ	ξ_σ^2	a	V	r	b	χ	S	γ
1	0.02	0.002	0.05	0.8	0.616	0.616	10	0.864	5	0.18

A_{b_1}	ξ_{b_1}	A_{θ_1}	ξ_{θ_1}	k_r	k_c	σ_2	τ	η	p_r	m
10^{-6}	0.03	0.2	0.3	1	1	1	1	1	0.20	2

TABLE 4.2 – Data for the simulations

4.3.1 Recruitment of pro-tumor immune cells without promotion of the tumor growth

Still with the purpose of assessing the model and the numerical method on simple basis, we start with simulations where the pro-tumor immune cells do not enhance the growth rate of the tumor cells ($b_1 = 0$).

We generically observe two behaviors : either an equilibrium state establishes, with a residual tumor and free of pro-tumor immune cells, or the immune system fails in controlling the tumor, with a significant concentration of pro-tumor immune cells at the center of the domain (like in Fig. 4.5 which also clearly illustrates how the anti-tumor resources is stemmed in the vicinity of the tumor) and the tumor mass blows up. This rough conclusion should be nuanced : the threshold m certainly plays a critical role. With $m = 0$, the worst situation since pro-tumor immune cells are immediately activated, we can find equilibria with the three phases. Such equilibria occur with quite small values of the cell division rate a ; increasing a leads to an escape phase. It is likely that similar phenomena occur with positive threshold m.

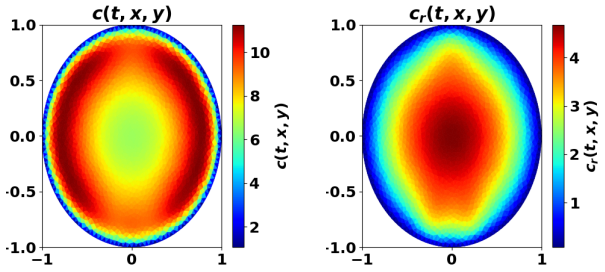

(a) c (b) c_r

FIGURE 4.5 – Space distribution c (left) and c_r (right) at time $t = 2.23$, with $a = 4$

We make the parameters vary in order to discuss the influence of their value on the behavior of the system. We only modify one quantity at a time, the others being kept as in Table. 4.2.

— *Tumor aggressiveness* As indicated in chapter 2, by increasing the division rate a, we make the tumor more aggressive. The results with the PDE system are consistent with this intuition and the observations made in Section 4.2.3 : for small division rates, the mass of

the tumor is rapidly damped, while the tumor escapes the control of the immune system as a increases, see Fig. 4.6. When control occurs, pro-tumor immune cells can be activated in the transient states, but insufficiently to counterbalance the effector immune response. Therefore, the concentration of pro-tumor immune cells decreases to zero, see Fig. 4.7. When the tumor is more aggressive, it recruits more pro-tumor immune cells : in turn, the action of these cells restrains the concentration of anti-tumor immune cells which remains below the expected equilibrium value, eventually favoring the tumor escape. The numerical simulations show that the bifurcation from a controlled tumor growth to the escape state happens for $a = 4$ keeping the other parameters fixed, see Fig. 4.6. However, this specific value depends on the critical mass m : the smaller the critical mass m, the smaller the critical division rate a.

— *Efficiency of the immune response* The immune response is enhanced by increasing A, that measures the strength of the immune cells against the tumor cells, see (4.23), or the source S of effector anti-tumor cells. For small values of these parameters, the tumor escapes the control of the immune response, see Fig. 4.8, 4.9.

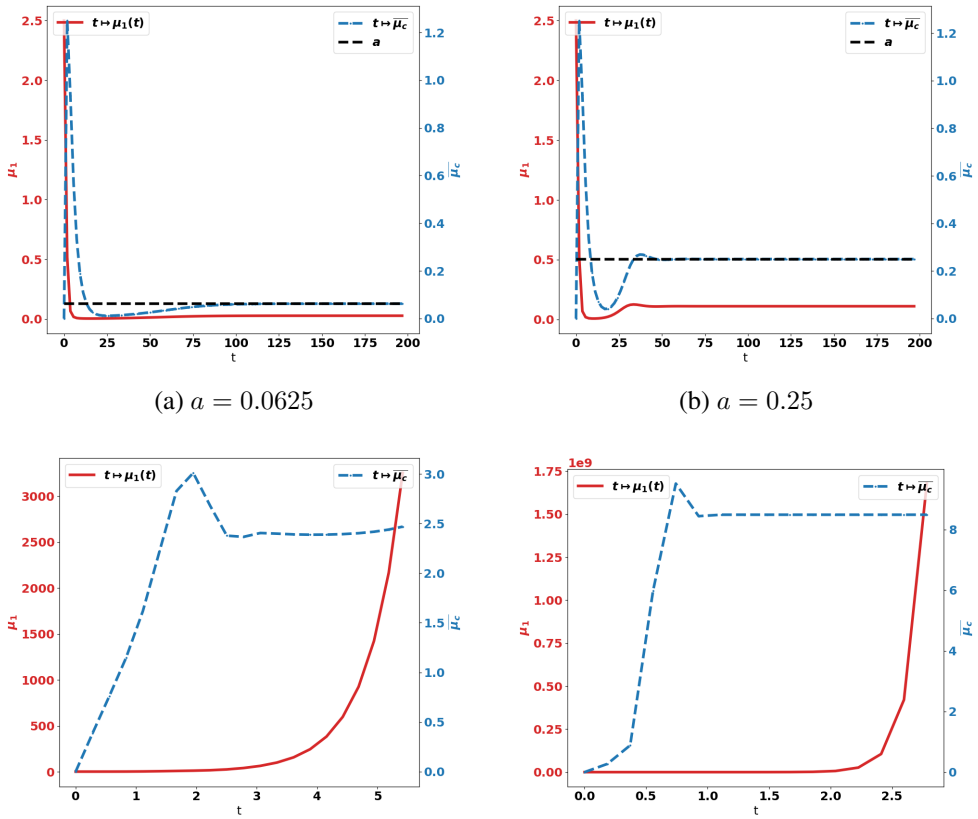

(a) $a = 0.0625$ (b) $a = 0.25$

(c) $a = 4$ (d) $a = 16$

FIGURE 4.6 – Evolution of the tumor mass μ_1 (red curves, left axis), and of the immune strength $\bar{\mu}_c$ (blue curve, right axis) for several values of the division rate a

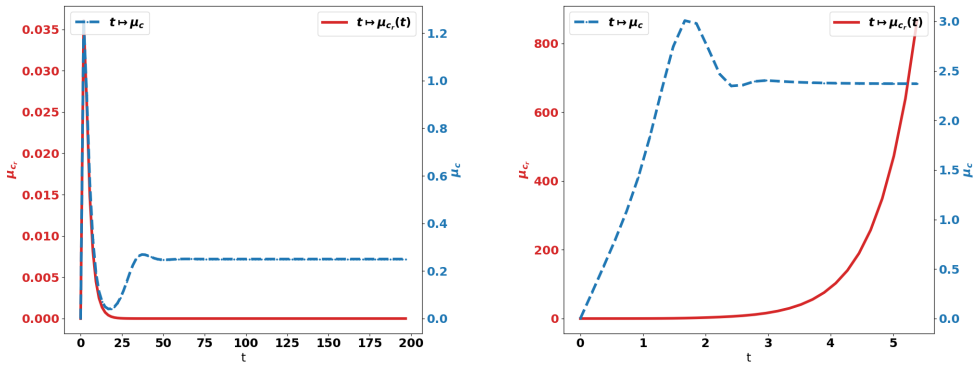

(a) $a = 0.25$ (b) $a = 4$

FIGURE 4.7 – Evolution of the pro-tumor immune cells concentration μ_{c_r} (red curves, left axis), and of the immune strength $\bar{\mu}_c$ (blue curve, right axis) for several values of the division rate a

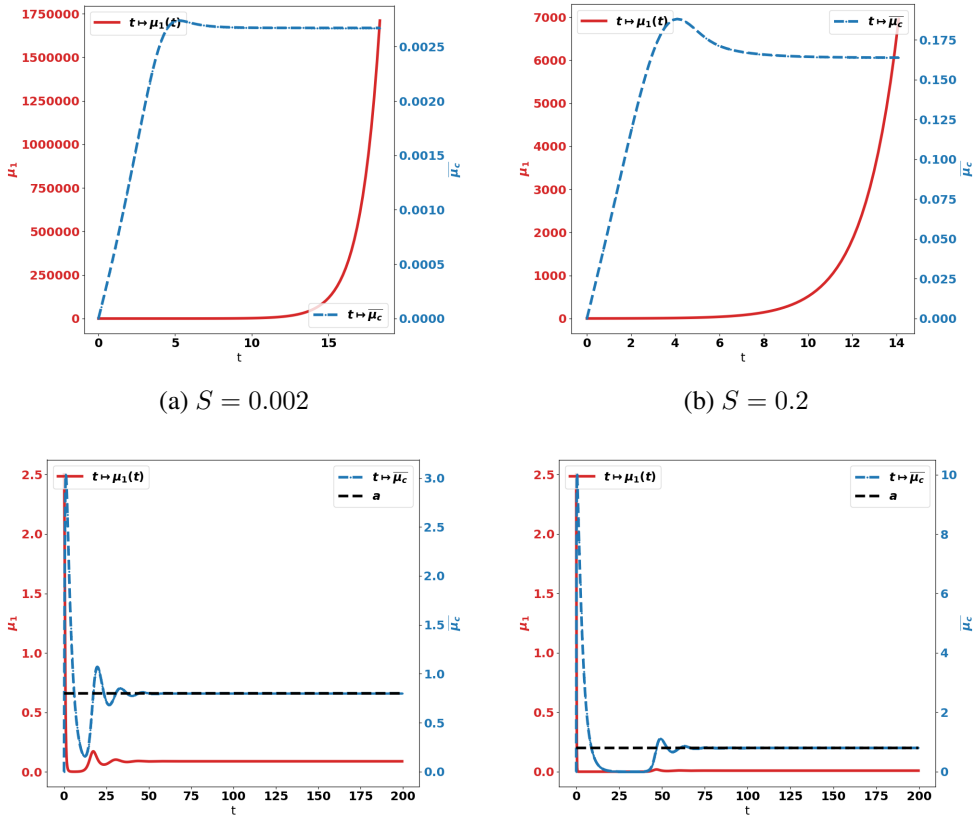

(a) $S = 0.002$ (b) $S = 0.2$

(c) $S = 20$ (d) $S = 200$

FIGURE 4.8 – Evolution of the tumor mass μ_1 (red curves, left axis), and of the immune strength $\bar{\mu}_c$ (blue curve, right axis) for several values of the source of immune cells S

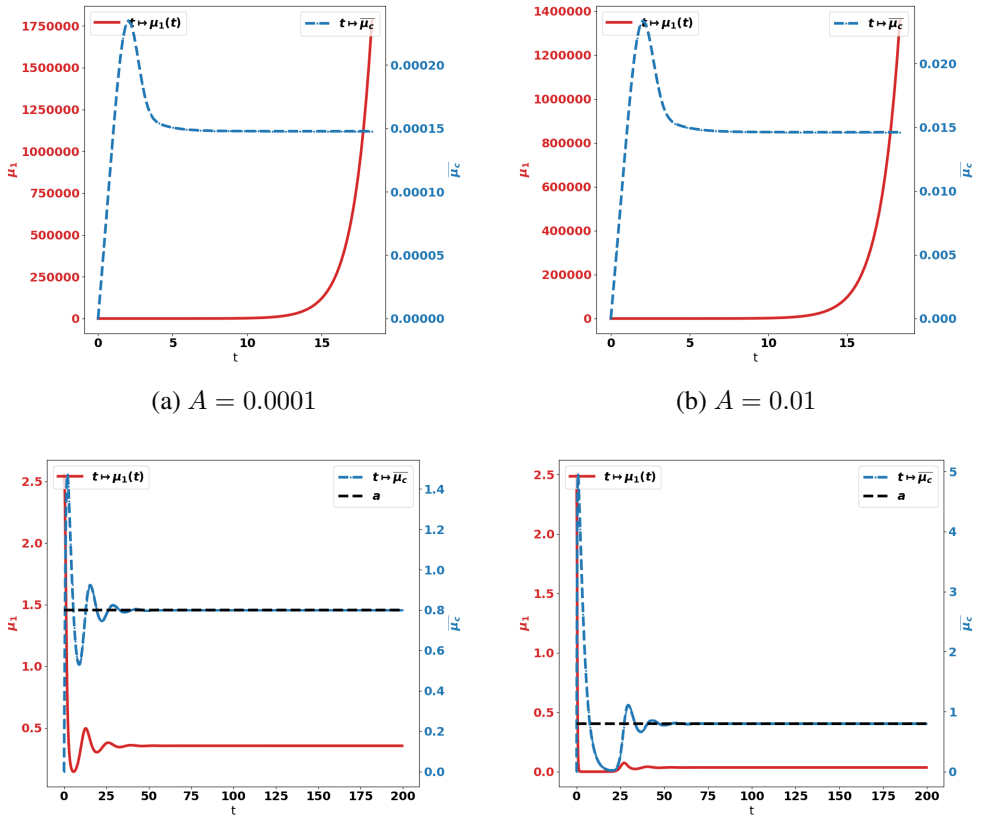

(a) $A = 0.0001$ (b) $A = 0.01$

(c) $A = 1$ (d) $A = 10$

FIGURE 4.9 – Evolution of the tumor mass μ_1 (red curves, left axis), and of the immune strength $\bar{\mu}_c$ (blue curve, right axis) for several values of the immune strength A

4.3.2 Recruitment of pro-tumor immune cells with the promotion of the tumor growth

In this section, we turn back to the full model (4.12a)-(4.12g). More precisely we perform a set of simulations with

— $z \mapsto V(z)$ obeys the Gompertz law (4.1);

— the division rate $z \mapsto a(z) = a\mathbf{1}_{z_0 \leq z < \infty}$ for some $z_0 > 0$ (for the numerical tests we set $z_0 = 1$.) vanishes for the smallest cells;

— the presence of the pro-tumor immune cells promotes tumor growth with $b_1 \neq 0$.

This model incorporates more biological phenomena and is likely more realistic.

Remarkably, the conclusions do not substantially change when comparing the results to the simpler situation dealt with in the previous Section : compare Fig. 4.10, 4.11, 4.12 to Fig. 4.6, 4.8, 4.9, respectively. This shows the robustness of the model in describing the equilibrium vs

escape phenomena and is very encouraging to perform further investigations with clinical data, as in chapter 3. In this direction, identifying the parameters of the equations is a critical issue. It can be interesting, based on the present observations, to neglect some phenomena which can only marginally affect the dynamics, while potentially introducing a set of unknown parameters.

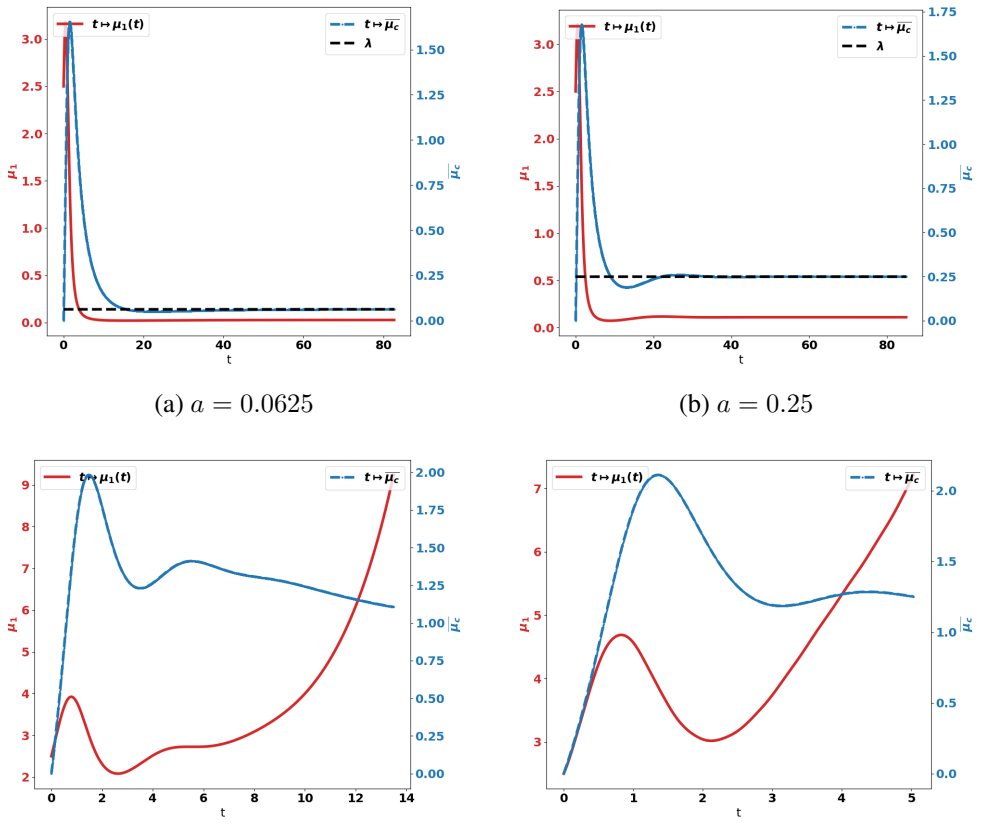

(a) $a = 0.0625$ (b) $a = 0.25$

(c) $a = 4$ (d) $a = 16$

FIGURE 4.10 – Evolution of the tumor mass μ_1 (red curves, left axis), and of the immune strength $\bar{\mu}_c$ (blue curve, right axis) for several values of the division rate a

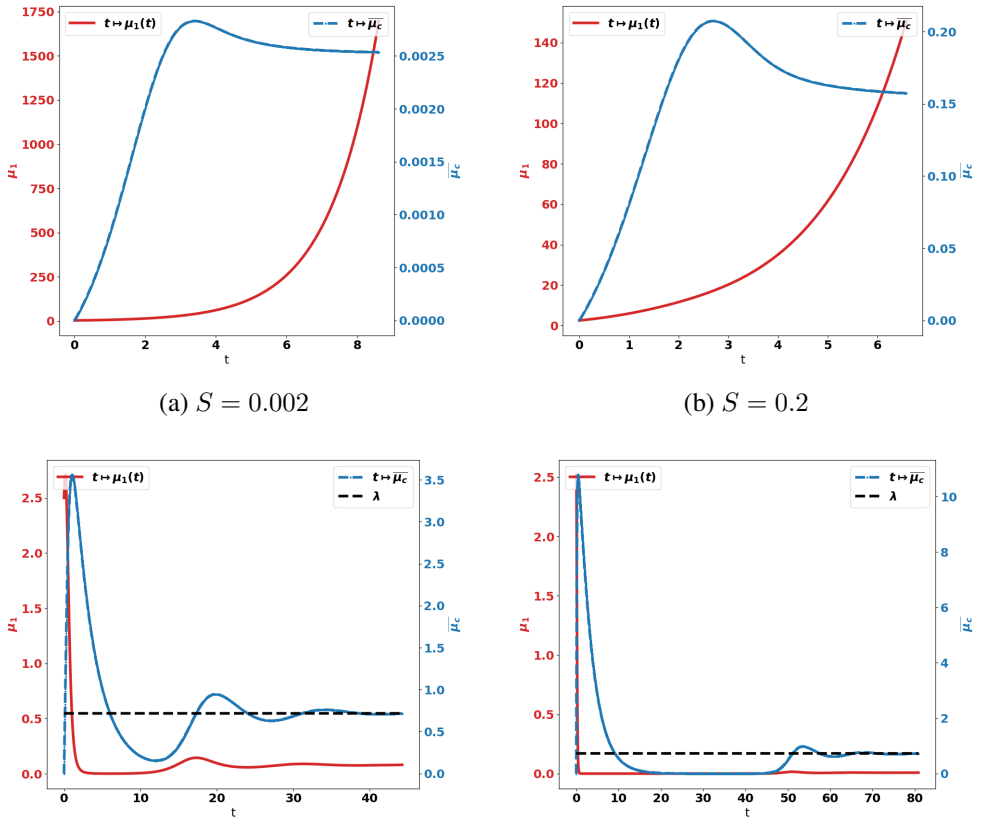

(a) $S = 0.002$ (b) $S = 0.2$

(c) $S = 20$ (d) $S = 200$

FIGURE 4.11 – Evolution of the tumor mass μ_1 (red curves, left axis), and of the immune strength $\bar{\mu}_c$ (blue curve, right axis) for several values of the source of effector immune cells S

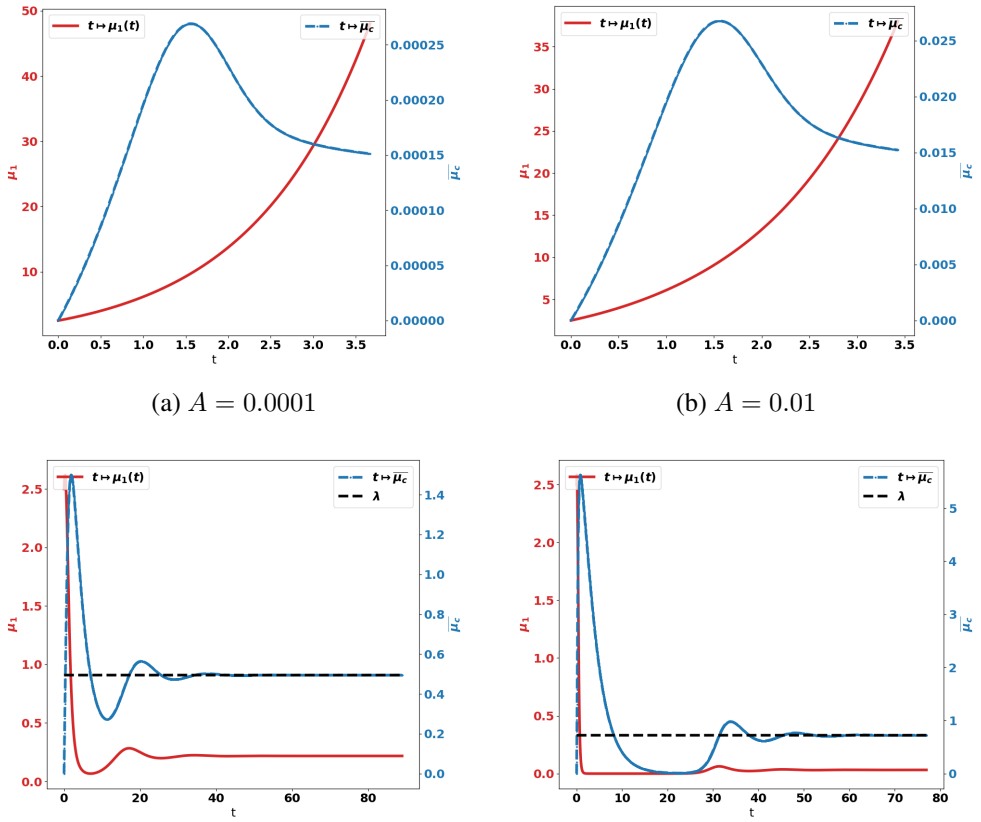

(a) $A = 0.0001$ (b) $A = 0.01$

(c) $A = 1$ (d) $A = 10$

FIGURE 4.12 – Evolution of the tumor mass μ_1 (red curves, left axis), and of the immune strength $\bar{\mu}_c$ (blue curve, right axis) for several values of the immune strength A

4.4 Effect of immunotherapy strategies

In this section we consider and compare the effects of two immunotherapy treatments. To this end, we bear in mind that a proportion of the effector cells are just inhibited by immunosuppressive mechanisms ; in other words they are not destroyed : they become anergic. However, they can be re-activated by specific treatments. The restoration of the anti-tumoral activity of effector T-cells can be obtained by using Immune Checkpoint Inhibitors, like anti-PD1 or anti-CTLA4 antibodies. Another strategy is based on the reduction of the recruitment of pro-tumor immune cells by blocking infiltration of MDSCs (anti-CXCR2, cMet) and Tregs (anti-CD25). We shall discuss the effect of these approaches independently and we shall also consider the combination of the two treatments in comparison to the mono-therapies.

4.4.1 Therapy based on the reactivation of anergic anti-tumor immune cells

In order to consider the action of treatments in boosting the immune response against the tumor, we introduce the concentration c_a of anergic cells. In order to describe the restoration mechanism, we add the following equation to the model :

$$\partial_t c_a + \nabla_x \cdot (c_a \chi \nabla_x \phi - D \nabla_x c_a) = \alpha k_c c c_r - \gamma c_a, \tag{4.25}$$

where the parameter $0 < \alpha < 1$ describes the proportion of effector T-cells that become anergic under the action of the pro-tumor cells (see (4.26a)).

Next, the effect of treatments able to restore the anti-tumor activity of the anergic immune cells is described by a time-dependent function $t \mapsto \mathcal{T}_1(t)$. It is assumed to be proportional to the drug concentration in the tumor microenvironment. Consequently, the dynamic is governed by the following system

$$\partial_t c + \nabla_x \cdot (c \chi \nabla_x \phi - D \nabla_x c) = g(\mu_1) S + \mathcal{T}_1 c_a - \gamma c - k_r I \theta_1 c - k_c c c_r, \tag{4.26a}$$

$$\partial_t c_r + \nabla_x \cdot (c_r \chi \nabla_x \phi - D \nabla_x c_r) = I(p_r S_r + k_r \theta_1 c) - \gamma_r c_r \tag{4.26b}$$

$$\partial_t c_a + \nabla_x \cdot (c_a \chi \nabla_x \phi - D \nabla_x c_a) = \alpha k_c c c_r - \gamma c_a - \mathcal{T}_1 c_a, \tag{4.26c}$$

$$\partial_t I = \psi(\mu_1) - \tau I \tag{4.26d}$$

$$-\nabla_x \cdot (\mathcal{K} \nabla_x \phi) = f(\mu_1)\sigma, \tag{4.26e}$$

$$c|_{\partial\Omega} = 0,\ c_r|_{\partial\Omega} = 0,\ \nabla_x \phi \cdot \nu(\cdot)|_{\partial\Omega} = 0, \tag{4.26f}$$

$$c(t=0,x) = c_0(x),\ c(t=0,x) = c_r^0(x),\ I(t=0) = I_0. \tag{4.26g}$$

The kinetic of the drug effect is described by the following equation

$$\partial_t \mathcal{T}_1 = \kappa(t) - d_{\mathcal{T}_1} \mathcal{T}_1, \tag{4.27}$$

where $t \mapsto \kappa(t)$ describes the drug administration protocol and $d_{\mathcal{T}_1}$ is the degradation rate of this drug. For the numerical tests, we set

$$\kappa(t) = \begin{cases} 0, & \forall 0 \le t \le t_0 \\ \sum_{k \ge 0} \kappa_k(t - kT_2), & \forall t \ge t_0 \end{cases} \tag{4.28}$$

where,

$$\kappa_k(t) = \begin{cases} q, & t_0 + kT_2 < t \le t_0 + kT_2 + T_1 \\ 0, & t_0 + kT_2 + T_1 \le t < t_0 + (k+1)T_2. \end{cases} \tag{4.29}$$

The model depends on

— the time t_0 when the treatment starts,

— the duration T_2 between two drug administrations,

— the duration T_1 of the drug administration,

— the administered drug concentration q.

For the numerical tests, we place ourselves in the same configuration as in Fig. 4.10-(c) where the tumor escapes the immune control due to the effects of pro-tumor immune cells. We fix α, the proportion of effector T-cells that become anergic to 0.5 and we keep the other parameters as in Table 4.2. We set

$$T_1 = 1, \qquad T_2 = 7, \qquad d_{\mathcal{T}_1} = 0.05$$

and we vary the parameters t_0 and q. We indeed observe that these parameters have a critical role on the treatment efficacy.

When the treatment is given early (for instance, when $0 \leq t_0 \leq 5$), the control of the tumor can be obtained with relatively low drug doses (see Fig. 4.13), in comparison to the cases where the treatment is administered later : the tumor growth is controlled with a residue of dormant tumor cells and activated effector immune cells. Reducing the treatment dose reduces the drug efficacy : smaller tumor masses are reached on longer times. For very small dose, the escape can occur.

Fig. 4.14 shows situations where the treatment is given later (for instance, when $10 \leq t_0 \leq 15$) : the tumor growth is slowed down by the treatment, but the tumor continues to grow exponentially fast. Increasing the drug dose increases the treatment efficacy. However, this observation raises the issue of the toxicity of the administered drug.

These observations are in line with those made in [19]. Indeed, [19] reports that Syngeneic CMS5 fibrosarcomas allowed to grow for 3 days in vivo were easily eradicated by adoptive transferred tumor-specific T-cells while a 100-fold larger transfer of tumor specific T-cell was mandatory to eradicate tumors that have been grown for an additional 48 hours. The same tumors that have been grown for 7 days before transferring adoptive tumor-specific T-cells were not eradicated.

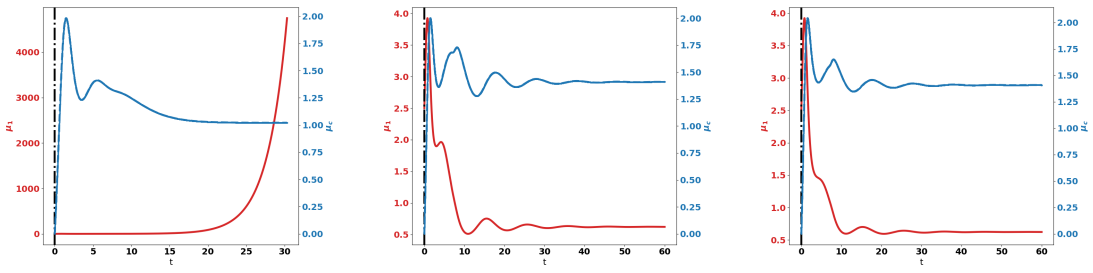

(a) $t_0 = 0$ and $q = 0.002$ (b) $t_0 = 0$ and $q = 0.5$ (c) $t_0 = 0$ and $q = 2$

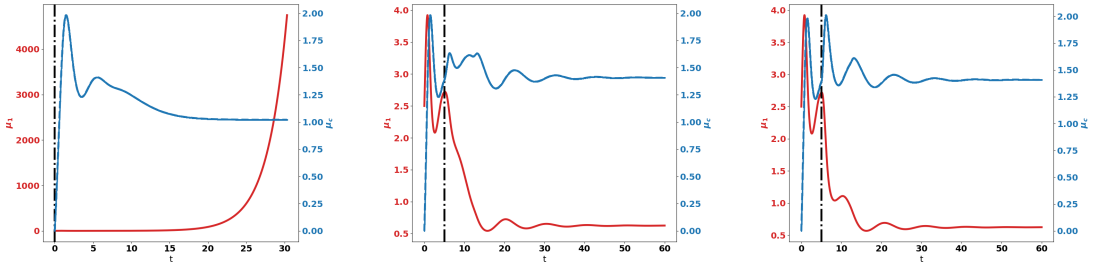

(d) $t_0 = 5$ and $q = 0.002$ (e) $t_0 = 5$ and $q = 0.5$ (f) $t_0 = 5$ and $q = 2$

FIGURE 4.13 – Early administration of the treatment. Evolution of the tumor mass μ_1 (red curves, left axis), and of the immune strength μ_c (blue curve, right axis) for some values the treatment dose q. The black dash-dotted line represents the time at which the treatment starts.

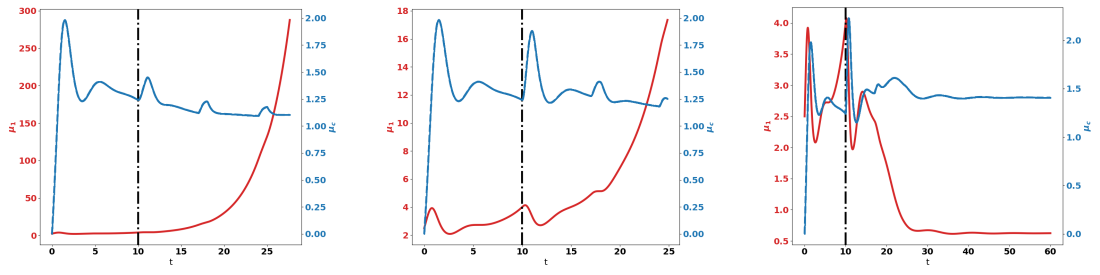

(a) $t_0 = 10$ and $q = 0.5$ (b) $t_0 = 10$ and $q = 2$ (c) $t_0 = 10$ and $q = 5$

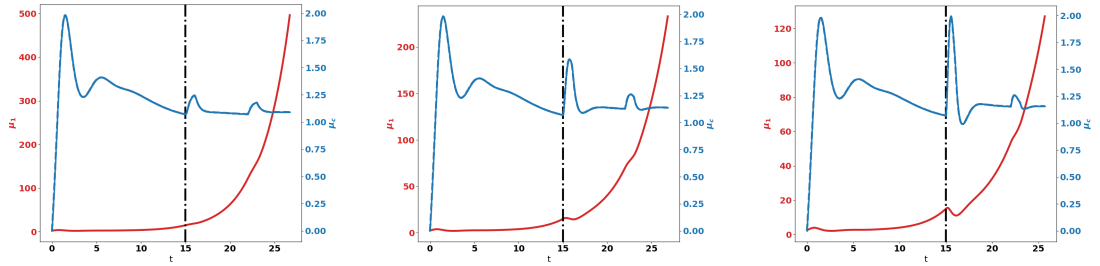

(d) $t_0 = 15$ and $q = 0.5$ (e) $t_0 = 15$ and $q = 2$ (f) $t_0 = 15$ and $q = 5$

FIGURE 4.14 – Late administration of the treatment. Evolution of the tumor mass μ_1 (red curves, left axis), and of μ_c (blue curve, right axis) for some values the treatment dose q. The black dash-dotted line represents the time at which the treatment starts.

4.4.2 Therapy based on reducing cytokines/chemokines recruiting pro-tumor immune cells

Treatments based on blocking cytokines and chemokines can help in reducing the recruitment of pro-tumor immune cells. A possible strategy uses cytokine traps [7], [13], by means of molecules that inhibit signal transduction from T-cells cytokine receptors. Therefore, the treatment acts by down-regulating the effect of the tumor induced cytokines. We denote by $\mathcal{T}_2$, the effect of treatments which are able to block those cytokines. It obeys a kinetic similar to (4.27)

$$\partial_t \mathcal{T}_2 = \kappa^{(2)}(t) - d_{\mathcal{T}_2}\mathcal{T}_2, \tag{4.30}$$

where

$$\kappa^{(2)}(t) = \begin{cases} 0, & \forall 0 \leq t \leq t_0 \\ \sum_{k\geq 0} \kappa_k^{(2)}(t - kT_2), & \forall t \geq t_0 \end{cases} \tag{4.31}$$

and

$$\kappa_k^{(2)}(t) = \begin{cases} q_2, & t_0 + kT_2 < t \leq t_0 + kT_2 + T_1 \\ 0, & t_0 + kT_2 + T_1 \leq t < t_0 + (k+1)T_2. \end{cases} \tag{4.32}$$

The effect on the cytokines is described by modifying in (4.12b), (4.12c) the terms related to the cytokine-dependent recruitment of pro-tumor immune cells. Therefore, the equations on the

immune response become

$$\partial_t c + \nabla_x \cdot (c\chi \nabla_x \phi - D\nabla_x c) = g(\mu_1)S - \gamma c - k_r I(1 - \mathcal{T}_2)\theta_1 c - k_c c c_r, \tag{4.33a}$$

$$\partial_t c_r + \nabla_x \cdot (c_r \chi \nabla_x \phi - D\nabla_x c_r) = I[1 - \mathcal{T}_2]_+(p_r S_r + k_r \theta_1 c) - \gamma_r c_r \tag{4.33b}$$

$$\partial_t c_a + \nabla_x \cdot (c_a \chi \nabla_x \phi - D\nabla_x c_a) = \alpha k_c c c_r - \gamma c_a, \tag{4.33c}$$

$$\partial_t I = \psi(\mu_1) - \tau I \tag{4.33d}$$

$$-\nabla_x \cdot (\mathcal{K}\nabla_x \phi) = f(\mu_1)\sigma, \tag{4.33e}$$

$$c|_{\partial\Omega} = 0,\ c_r|_{\partial\Omega} = 0,\ \nabla_x \phi \cdot \nu(\cdot)|_{\partial\Omega} = 0, \tag{4.33f}$$

$$c(t = 0, x) = c_0(x),\ c(t = 0, x) = c_r^0(x),\ I(t = 0) = I_0. \tag{4.33g}$$

For the numerical tests, we set

$$T_1 = 1, \qquad T_2 = 7, \qquad d_{\mathcal{T}_2} = 0.0105.$$

For the cytokine/chemokine-blockade based treatment we observe a similar behavior as with the treatment based on the reactivation of the anergic immune cells. The efficacy of the treatment is particularly sensitive to the starting time t_0, see Fig. 4.15

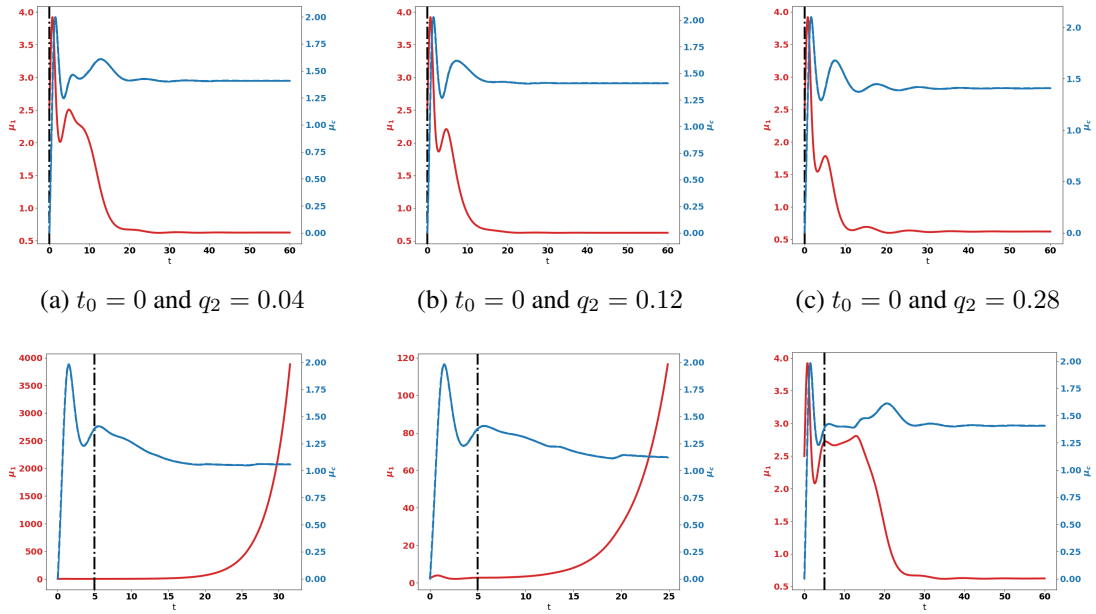

(a) $t_0 = 0$ and $q_2 = 0.04$ (b) $t_0 = 0$ and $q_2 = 0.12$ (c) $t_0 = 0$ and $q_2 = 0.28$

(d) $t_0 = 5$ and $q_2 = 0.04$ (e) $t_0 = 5$ and $q_2 = 0.12$ (f) $t_0 = 5$ and $q_2 = 0.28$

FIGURE 4.15 – Early administration of the treatment. Evolution of the tumor mass μ_1 (red curves, left axis), and of the immune strength μ_c (blue curve, right axis) for some values the treatment dose q. The black dash-dotted line represents the time at which the treatment starts.

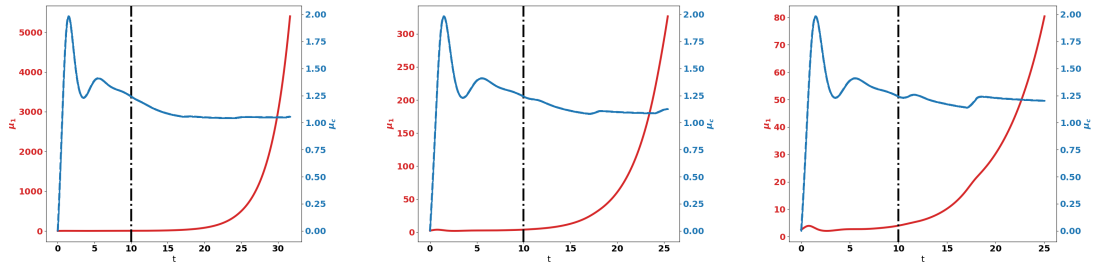

(a) $t_0 = 10$ and $q_2 = 0.04$ (b) $t_0 = 10$ and $q_2 = 0.12$ (c) $t_0 = 10$ and $q_2 = 0.28$

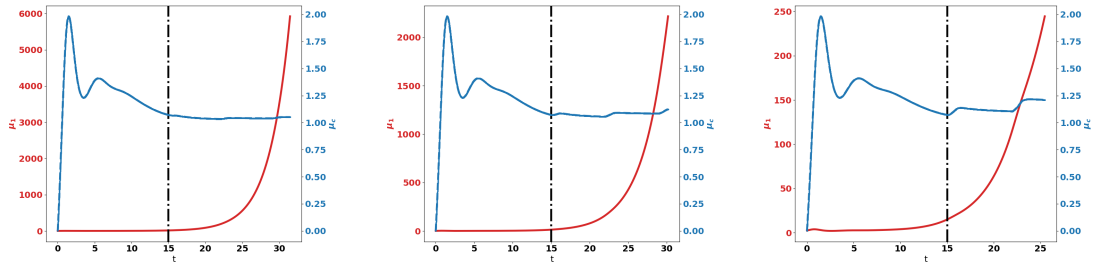

(d) $t_0 = 15$ and $q_2 = 0.04$ (e) $t_0 = 15$ and $q_2 = 0.12$ (f) $t_0 = 15$ and $q_2 = 0.28$

FIGURE 4.16 – Late administration of the treatment. Evolution of the tumor mass μ_1 (red curves, left axis), and of the immune strength μ_c (blue curve, right axis) for some values the treatment dose q. The black dash-dotted line represents the time at which the treatment starts.

4.4.3 Combination of two immunotherapy strategies

In this section, we combine the two treatments described above, acting on both the reactivation of anti-tumor immune cells and the blockade of the recruitment of pro-tumor immune cells. We observe that this combination is more efficient than the mono-therapies. Indeed a suitable combination of the treatment doses is able to control the tumor growth. For instance, the treatment based on the reactivation of anergic immune cells fails in controlling the tumor when given at $t_0 = 10$ with a dose $q = 2$ see Fig. 4.14-(b), and the treatment based on cytokine/chemokine blockade fails with a dose $q_2 = 0.12$ at $t_0 = 10$, see Fig. 4.16. However, the combination of the two treatments controls the tumor. Again, we observe that giving the treatments later requires to readjust the doses in order to control the tumor growth, see Fig. 4.18. We notice that the controlled state contains residual tumor cells and activated immune cells, see Fig. 4.17-(b) and (c).

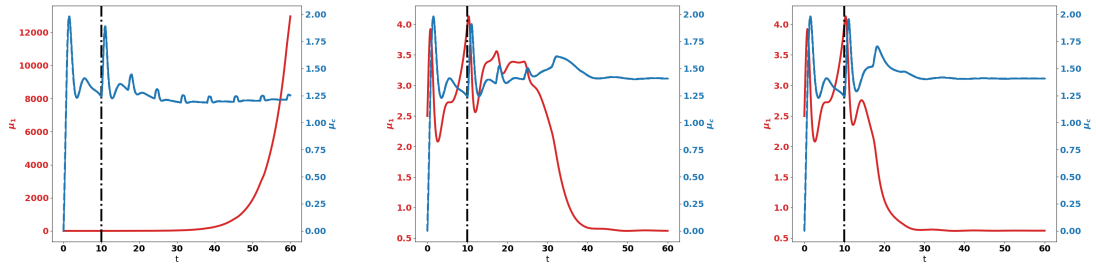

(a) $t_0 = 10$, $q = 2$ and $q_2 = 0.04$ (b) $t_0 = 10$, $q = 2$ and $q_2 = 0.12$ (c) $t_0 = 10$, $q = 2$ and $q_2 = 0.28$

FIGURE 4.17 – Administration of the combined treatments at $t_0 = 10$. Evolution of the tumor mass μ_1 (red curves, left axis), and of the immune strength μ_c (blue curve, right axis) for some values the treatment dose q. The black dash-dotted line represents the time at which the treatment starts.

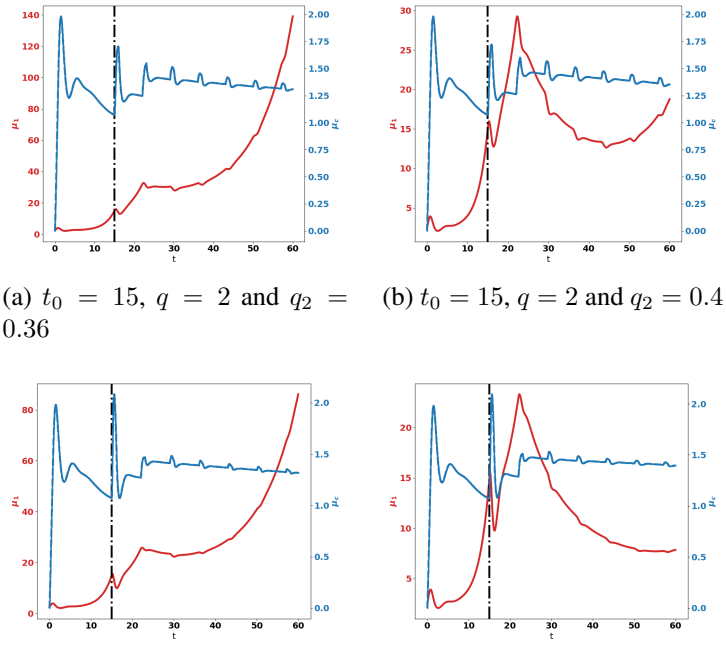

(a) $t_0 = 15$, $q = 2$ and $q_2 = 0.36$ (b) $t_0 = 15$, $q = 2$ and $q_2 = 0.4$

(c) $t_0 = 15$, $q = 5$ and $q_2 = 0.36$ (d) $t_0 = 15$, $q = 5$ and $q_2 = 0.4$

FIGURE 4.18 – Administration of the combined treatments at $t_0 = 15$. Evolution of the tumor mass μ_1 (red curves, left axis), and of the immune strength μ_c (blue curve, right axis) for some values the treatment dose q. The black dash-dotted line represents the time at which the treatment starts.

4.5 Conclusion

This work introduces a model describing the interactions between tumor cells and the immune system, taking into account the antagonistic effects of anti-tumor and pro-tumor immune cells induced by tumor growth. While the anti-tumor action aims at eliminating tumor cells, the pro-tumor effects can take different forms : elimination of anti-tumor cells, conversion of anti-tumor cells into pro-tumor cells, or enhancement of the tumor growth. Remarkably, the model is able to reproduce equilibrium and escape phases, depending on the value of the biological parameters.

Based on these findings, we study the effects of several therapeutic strategies – either by reactivation of anergic anti-tumor cells or by reduction of the recruitment of pro-tumor cells – that can be used to boost the immune response and restore the equilibrium that maintains the tumor in a viable state. The numerical investigation brings out the influence of the starting time of the treatment and of the administrated dose. We also show on numerical grounds that combining the two approaches clearly improves the efficacy of the treatment.

variable	description
z	volume of tumor cells
t	time variable
x	space variable
n	size-density of tumor cells with a volume z
V	tumor cells growth rate
a	tumor cells division rate
μ_0	total number of tumor cells
μ_1	total volume of tumor cells
c	concentration of anti-tumor cells
c_r	concentration of pro-tumor cells
χ	chemotactic coefficient
ϕ	chemotactic potential
D	diffusion coefficient of the immune cells
S	source of anti-tumor immune cells
S_r	source of pro-tumor immune cells
p_r	activation rate of pro-tumor cells
$\mathcal{K}$	diffusion coefficient of the chemotactic signal
σ	chemotactic signal
I	cytokine concentration
γ	death rate of the anti-tumor immune cells
γ_r	death rate of the pro-tumor immune cells
τ	damping rate of the cytokine concentration
k_c	suppression rate of anti-tumor cells by the pro-tumor cells
k_r	conversion rate of anti-tumor cells into pro-tumor cells
θ	form function of the conversion of anti-tumor cells into pro-tumor cells
δ	form function of the anti-tumor action in the tumor micro-environment
b_1	tumor growth rate induced by the pro-tumor cells
m	threshold on the tumor volume driving the cytokine activation

TABLE 4.1 – Recap of the main definitions and notations

Bibliographie

[1] E. O. Alzahrani and Y. Kuang. Nutrient limitations as an explanation of Gompertzian tumor growth. *Disc. Cont. Dyn. Syust. B*, 21(2) :357–372, 2016.

[2] K. Atsou, F. Anjuère, V. M. Braud, and T. Goudon. A size and space structured model describing interactions of tumor cells with immune cells reveals cancer persistent equilibrium states in tumorigenesis. *J. Theor. Biol.*, 490 :110163, 2020.

[3] K. Atsou, F. Anjuère, V. M. Braud, and T. Goudon. Analysis of the equilibrium phase in immune-controlled tumor predicts best strategies for anti-tumor therapies. Technical report, Univ. Côte d'Azur, Inria, CNRS, LJAD, 2020.

[4] F. Baccelli, D. McDonald, and J. Reynier. A mean field model for multiple TCP connections through a buffer implementing RED. *Performance Evaluation*, 49(1-4) :77–97, 2002.

[5] B. Basse, B. C. Baguley, E. Marshall, W. R. Joseph, B. van Brunt, G. Wake, and D. J. N. Wall. A mathematical model for analysis of the cell cycle in cell lines derived from human tumors. *J. Math. Biol.*, 47(4) :295–312, 2003.

[6] F. Bekkal Brikci, J. Clairambault, B. Ribba, and B. Perthame. An age-and-cyclin-structured cell population model for healthy and tumoral tissues. *J. Math. Biol.*, 57(1) :91–110, 2008.

[7] P. Berraondo, M. F. Sanmamed, M. C. Ochoa, I. Etxeberria, M. A. Aznar, J. L. Pérez-Gracia, M. E. Rodríguez-Ruiz, M. Ponz-Sarvise, E. Castañón, and I. Melero. Cytokines in clinical cancer immunotherapy. *British Journal of Cancer*, 120(1) :6–15, 2019.

[8] T. Boon, P. G. Coulie, B. J. V. den Eynde, and P. van der Bruggen. Human T-cell responses against melanoma. *Annual Review of Immunology*, 24(1) :175–208, 2006. PMID : 16551247.

[9] D. A. Chen and I. Mellman. Elements of cancer immunity and the cancer-immune set point. *Nature*, 541 :321–330, 2017.

[10] M. Doumic-Jauffret and P. Gabriel. Eigenelements of a general aggregation-fragmentation model. *Math. Models Methods Appl. Sci.*, 20(5) :757–783, 2010.

[11] G. P. Dunn, A. T. Bruce, H. Ikeda, L. J. Old, and R. D. Schreiber. Cancer immunoediting : from immunosurveillance to tumor escape. *Nat. Immunol.*, 3 :991–998, 2002.

[12] G. P. Dunn, L. J. Old, and R. D. Schreiber. The immunobiology review of cancer immunosurveillance and immunoediting. *Immunity*, 21 :137–148, 2004.

[13] A. N. Economides, L. R. Carpenter, J. S. Rudge, V. Wong, E. M. Koehler-Stec, C. Hartnett, E. A. Pyles, X. Xu, T. J. Daly, M. R. Young, J. P. Fandl, F. Lee, S. Carver, J. McNay, K. Bailey, S. Ramakanth, R. Hutabarat, T. T. Huang, C. Radziejewski, G. D. Yancopoulos, and N. Stahl. Cytokine traps : Multi-component, high-affinity blockers of cytokine action. *Nature Medicine*, 9(1) :47–52, 2003.

[14] A. Facciabene, G. T. Motz, and G. Coukos. T-regulatory cells : Key players in tumor immune escape and angiogenesis. *Cancer Research*, 72(9) :2162–2171, 2012.

[15] Z. G. Fridlender, J. Sun, S. Kim, V. Kapoor, G. Cheng, L. Ling, G. S. Worthen, and S. M. Albelda. Polarization of tumor-associated neutrophil phenotype by TGF-beta : "N1" versus "N2" TAN. *Cancer Cell*, 16(3) :183–194, 2009.

[16] D. Gabrilovich and S. Nagaraj. Myeloid-derived suppressor cells as regulators of the immune system. *Nat. Rev. Immunol.*, 9 :162–174, 2009.

[17] M. Gyllenberg and G. F. Webb. Quiescence as an explanation of Gompertzian tumor-growth. *Growth, Development, and Aging*, 53(1-2) :25–33, 1989.

[18] M. Gyllenberg and G. F. Webb. A nonlinear structred population model of tumor growth with quiescence. *J.Math. Biol.*, 28 :671–694, 1990.

[19] H. L. Hanson, D. L. Donermeyer, H. Ikeda, V. White, M.and Shankaran, L. J. Old, H. Shiku, D. Schreiber, and P. M. Allen. Eradication of established tumors by CD8+ T-cell adoptive immunotherapy. *Immunity*, 13 :265–276, 2000.

[20] K. Iwata, K. Kawasaki, and N. Shigesada. A dynamical model for the growth and size distribution of multiple metastatic tumors. *J. Theor. Biol.*, 203(2) :177–186, 2000.

[21] F. Kozusko and Z. Bajzer. Combining Gompertzian growth and cell population dynamics. *Math. Biosci*, 185(2) :153–167, 2003.

[22] P. Michel. Existence of a solution to the cell division eigenproblem. *Models Math. Meth. App. Sci.*, 16(Suppl. issue 1) :1125–1153, 2006.

[23] P. Michel, S. Mischler, and B. Perthame. General relative entropy inequality : an illustration on growth models. *J. Math. Pures et Appl.*, 84(9) :1235–1260, 2005.

[24] D. Mougiakakos, A. Choudhury, A. Lladser, R. Kiessling, and C. C. Johansson. Regulatory T Cells in Cancer. In G. F. V. Woude and G. Klein, editors, *Advances in Cancer Research*, volume 107, pages 57–117. Academic Press, 2010.

[25] K. J. O'Byrne, A. G. Dalgleish, M. J. Browning, W. P. Steward, and A. L. Harris. The relationship between angiogenesis and the immune response in carcinogenesis and the progression of malignant disease. *European J. Cancer*, 36(2) :151–169, Jan 2000.

[26] B. Perthame. *Transport equations in biology*. Frontiers in Math. Birkhauser, 2007.

[27] B. Perthame and L. Ryzhik. Exponential decay for the fragmentation or cell-division equation. *J. Differ. Eq.*, 210 :155–177, 2005.

[28] G. A. Rabinovich, D. Gabrilovich, and E. M. Sotomayor. Immunosuppressive strategies that are mediated by tumor cells. *Ann. Rev. Immunol.*, 25(1) :267–296, 2007. PMID : 17134371.

[29] E. Sato, S. H. Olson, J. Ahn, B. Bundy, H. Nishikawa, F. Qian, A. A. Jungbluth, D. Frosina, S. Gnjatic, C. Ambrosone, J. Kepner, T. Odunsi, G. Ritter, S. Lele, Y.-T. Chen, H. Ohtani, L. J. Old, and K. Odunsi. Intraepithelial CD8+ tumor-infiltrating lymphocytes and a high CD8+/regulatory T cell ratio are associated with favorable prognosis in ovarian cancer. *Proc. Nat. Acad. Sc.*, 102(51) :18538–18543, 2005.

[30] A. Tanaka and S. Sakaguchi. Regulatory t-cells in cancer immunotherapy. *Cell Res.*, 27 :109–118, 2017.

[31] K. P. Wilkie and P. Hahnfeldt. Modeling the dichotomy of the immune response to cancer : Cytotoxic effects and tumor-promoting inflammation. *Bull. Math. Biol.*, 79 :1426–1448, 2017.

Deuxième partie

Centre d'Été Mathématique de Recherche Avancée en Calcul Scientifique

...continue d'évoluer, d'apprendre, de découvrir, et ne t'enferme pas dans des habitudes qui sclérosent l'esprit, ni dans le confort engourdissant de ce que tu sais déjà faire.

Laurent Gounelle

CHAPITRE. 5

Phase transitions in a two-species model for cell segregation and logistic growth

Contents

Abstract : In this chapter, we study a model of cell segregation in a population composed of two cell types. Starting from a model initially proposed in [2], we aim to understand the impact of a cell division process on the system's segregation abilities. The original model describes a population of spherical cells subjected to a Brownian motion and interacting with their close neighbors by means of a repulsion potential. Here, we add a stochastic birth-death process in the agent-based model that approaches a logistic growth term in the continuum limit. We address the linear stability of the spatially homogeneous steady states of the macroscopic model and obtain a precise criterion for the phase transition, which links the system segregation ability to the model parameters. By comparing the criterion with the one obtained without logistic growth, we show that the system's segregation ability is the result of a complex interplay between logistic growth, diffusion and mechanical repulsive interactions. Numerical simulations are presented to illustrate the results obtained at the microscopic scale.

5.1 Introduction

The starting point of this work was the model previously proposed in [3, 4]. The authors provided a detailed multiscale analysis - from a microscopic model to a macroscopic description - of a system of particles interacting through a dynamical network. The model describes point particles with local cross-links modeled by springs that are randomly created and destructed. Each link between two particles generates a spring-like interaction potential, which depends on the link type (intra- or inter- species link). In the limit of large number of particles and links and assuming that the network remodelling rate is very large, the link density distribution becomes completely determined by the one-particle distribution function. The latter evolves on the slow time scale through an aggregation-diffusion equation, also known as the McKean-Vlasov equation. Their results have been extended and applied to the two-species case in order to study segregation mechanisms in tissue morphogenesis [2]. The ability of different cell types to segregate is known to be a key process in many biological phenomena, especially in embryogenesis or tumor metastasis. However, in their model, it was assumed that the cell population remains constant over time, which means that there is no growth process. The goal of this chapter is to investigate whether cell growth processes can enhance or knock out the system's segregation abilities, when cell segregation is otherwise driven by mechanical interactions between different types of cells. In this study, we investigate the effect of cell division on the segregation processes. To this aim, we derive a macroscopic logistic equation from the microscopic two-species model introduced in [2], modified to take into consideration density-saturated growth process at the microscopic scale. We will focus on the influence that homotypic/heterotypic repulsion has on the process of cell segregation and border sharpening, inspired from the results in [6]. After the derivation of the macroscopic model we carry out its stability analysis and we perform numerical simulations of the microscopic model.

5.2 The microscopic model

We describe the microscopic model for cells belonging to two distinct species with an additional growth process. The model introduced in [2], is a 2D individual based model which depicts two species of cells referred to as type A and type B cells. The cells are represented by 2D-spheres located by their centers and interacting with each others by creating and suppressing links via a random process with neighbouring cells located in a ball of radius R from their centers. The links creation and suppression are supposed to follow Poisson processes of frequencies $\nu_c^{AA}, \nu_c^{BB}, \nu_c^{AB}$ and $\nu_d^{AA}, \nu_d^{BB}, \nu_d^{AB}$, where the subscripts c and d denote respectively 'creation' and 'deletion' and the superscripts denote respectively the intraspecies links (AA, BB) and interspecies links (AB). Once created, the links generate a spring-like interaction potential which depends on the type of interactions (Figure 5.1). For instance in order to account for the effect of repulsion in the segregation phenomenon, the amplitude of the potential generated by inter-species (heterotypic) links might be greater than the one generated by intra-species(homotypic) links. Each cell is supposed to be animated by a two dimensional Brownian motion in order to describe its movement inside the tissue.

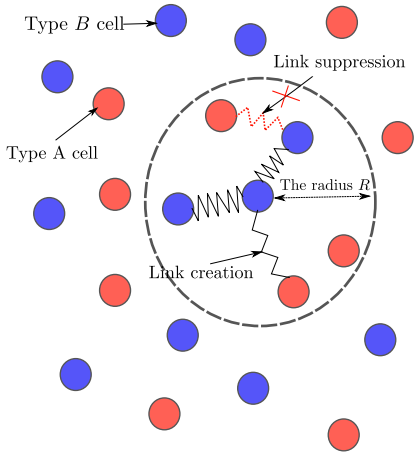

FIGURE 5.1 – Illustration of the cells interacting through the network of links

We stress the fact that the effects due to cell deformations are neglected. The description of the model is restricted to two spatial dimensions. The set of type A and type B cells contains respectively N_A and N_B individuals and the dynamic of their centers are described by points $(X_i^A, X_l^B) \in \mathbb{R}^2 \times \mathbb{R}^2, i \in \{1, \cdots, N_A\}, l \in \{1, \cdots, N_B\}$. The intra-species links generate potentials $\Phi^{AA}(X_i^A, X_j^A)$ and $\Phi^{BB}(X_l^B, X_m^B)$ and interspecies links generate potentials $\Phi^{AB}(X_i^A, X_l^B)$ and $\Phi^{BA}(X_l^B, X_i^A)$ not necessarily symmetric. Those potentials incorporate the fact that the two particle families act differently on each other. Hence, particle motion between two particles linking-unlinking events is supposed to occur in the steepest gradient descent of the

total mechanical potential :

$$\begin{cases} dX_i^A = -\mu \nabla_{X_i^A} W^A(X^A, X^B)dt + \sqrt{2D_A}dB_i, \quad \forall\, i \in \{1, \dots, N_A\} \\ dX_i^B = -\mu \nabla_{X_\ell^A} W^B(X^A, X^B)dt + \sqrt{2D_B}dB_\ell, \quad \forall\, \ell \in \{1, \dots, N_B\} \end{cases} \tag{5.1}$$

where $\mu > 0$ is the mobility coefficient considered to be given and B_i is a 2-dimensional Brownian motion $B_i = (B_i^1; B_i^2)$ with intensity $D_A > 0$ for specie A and $D_B > 0$ for specie B. We define W^S the total potential of the type-S particle, $S \in \{A, B\}$, as the sum over all pairwise link potentials acting on particles S :

$$W^S(X^S, X^T) = \sum_{k_1=1}^{K_{SS}} \Phi^{SS}(X^S_{i(k_1)}, X^S_{j(k_1)}) + \sum_{k_3=1}^{K_{ST}} \Phi^{ST}(X^S_{i(k_3)}, X^T_{j(k_3)}), \tag{5.2}$$

where k_1 and k_3 refer to indices of intra-species link and inter-species link, respectively, and where each link k_1 (resp. k_3) is associated with a unique pair of cell indices $(i(k_1), j(k_1))(m(k_3), l(k_3))$ resp.). The potential Φ^{ST} refers to the action a type T particle exerts on a type S particle while Φ^{TS} is the action a type S particle exerts on a particle of type T. All along the chapter, we will consider Hookean-type potentials of the form :

$$\Phi^{ST}(x_1, x_2) = \frac{\kappa^{ST}}{2} \left(|x_1 - x_2| - R\right)^2 .$$

We note that $(i(k_1), j(k_1))$ denote the indices of particles of type S connected by the intraspecies link k_1, and $(i(k_3), (k_3))$ the indices of particles of type S connected to particles of type T by link k_3.

The main extension in the model is the introduction of a cell birth and death process. Our modeling is based on the birth and death process proposed in [7]. The idea is that a cell of the type S population has a probability β_S to divide into two cells and a probability δ_S to die at each time step. To introduce the spatial logistic effect at the microscopic scale, we assume that the birth and death processes depend on the local density of individuals divided by the local carrying capacity of the population :

$$\beta_S(X_i^S) = b_0^S - (b_0^S - \theta_S)\left(\frac{\mathcal{N}_{R_0}(X_i^S)}{N^*}\right), \qquad \delta_S(X_i^S) = d_0^S + (\theta_S - d_0^S)\left(\frac{\mathcal{N}_{R_0}(X_i^S)}{N^*}\right) \tag{5.3}$$

where the coefficient $\mathcal{N}_{R_0}(X_i^S)$ is the number of cells (of both population) which centers are located at distance R_0 of X_i^S and N^* is the target number of cells in a ball of radius R_0 and is referred to as the local carrying capacity. The parameters b_0^S and d_0^S are respectively the intrinsic birth rate and death rate of an individual, the parameter θ_S is the turnover, which is equal to the birth and death probabilities when the population reaches its local population carrying capacity N^*. Note that θ_S must be taken in the range $d_0^S < \theta_S < b_0^S$. The probability for a cell to give birth or die within a small time step τ is respectively (see section 'Numerical results' for more details on the process) :

$$\tau\beta(X_i^S) \text{ or } \tau\delta(X_i^S). \tag{5.4}$$

Remark 5.2.1. *Such a birth and death process has been shown to approach (in the limit of large number of particles) a logistic equation, where the deterministic population growth rate is $b_0 - d_0$ (see [7] and references therein). Therefore, the condition $d_0 < b_0$ is introduced to ensure the positivity of the deterministic growth rate.*

5.3 The derivation of the macroscopic model

We study the main steps needed to perform the derivation of the macroscopic model from the microscopic dynamics. Following [2], we are interested in a regime of fast linking-unlinking of the particles. To this aim, we introduce an intermediate microscopic model in which the limit of fast linking/unlinking is considered for fixed number of cells, and then derive the PDE associated with this microscopic dynamics.

5.3.1 The microscopic dynamics in the limit of fast linking/unlinking processes

We denote by $A_{ij}(t)$, $B_{ij}(t)$, $C_{ij}(t)$ the adjacency matrices of particles A, B, and cross-links $A-B$ respectively. In particular, for $i,j \in \{1,\cdots,N_A\}$, $A_{ij}(t)$ (resp. $=0$) if particles of type A with indices i and j are connected at time t (resp. not connected). The definition of matrix B is similar. For $i \in \{1,\cdots,N_A\}$, $j \in \{1,\cdots,N_B\}$, $C_{ij}(t)=1$ (resp. $=0$) if particle i of type A and particle j of type B are connected at time t (resp. not connected). Here, A and B are square symmetric matrices, and C is an $N_A \times N_B$ rectangular matrix.

The derivation of the reduced microscopic model relies on averaging. The particles positions $X_i^A, X_i^B(t)$ are slow processes, and the links $A_{ij}(t), B_{ij}(t), C_{ij}(t)$ are fast processes : they quickly converge to stationary measures, which depend on the positions $X_i^{A,B}(t)$. We will then compute the evolution of $X_i^{A,B}$ by averaging the basic dynamical equation (5.1) over these stationary measures of the links processes. The processes for the links follow the following equations :

$$dA_{ij}(t) = -A_{ij}(t)dN_{ij}^{AA,d}(t) + [1-A_{ij}(t)]\,\chi_{|X_i^A(t)-X_j^A(t)|\le R}dN_{ij}^{AA,f}(t), \tag{5.5a}$$

$$dB_{ij}(t) = -B_{ij}(t)dN_{ij}^{BB,d}(t) + [1-B_{ij}(t)]\,\chi_{|X_i^B(t)-X_j^B(t)|\le R}dN_{ij}^{BB,f}(t), \tag{5.5b}$$

$$dC_{ij}(t) = -C_{ij}(t)dN_{ij}^{AB,d}(t) + [1-C_{ij}(t)]\,\chi_{|X_i^A(t)-X_j^B(t)|\le R}dN_{ij}^{AB,f}(t), \tag{5.5c}$$

where the $N_{ij}^{AA,d}, N_{ij}^{AA,f}, N_{ij}^{BB,d}, N_{ij}^{BB,f}, N_{ij}^{AB,d}, N_{ij}^{AB,f}$, are independent Poisson processes, with rates respectively

$$\nu_d^{AA} = \frac{\tilde\nu_d^{AA}}{\varepsilon^2}, \nu_c^{AA} = \frac{\tilde\nu_c^{AA}}{\varepsilon^2}, \nu_d^{BB} = \frac{\tilde\nu_d^{BB}}{\varepsilon^2}, \nu_c^{BB} = \frac{\tilde\nu_c^{BB}}{\varepsilon^2}, \nu_d^{AB} = \frac{\tilde\nu_d^{AB}}{\varepsilon^2}, \nu_c^{AB} = \frac{\tilde\nu_c^{AB}}{\varepsilon^2},$$

where $\varepsilon \ll 1$. Conditionally on the positions X_i^A, X_j^B, all the processes A_{ij}, B_{ij}, C_{ij} are independent. The stationary measures of (5.5a)-(5.5c), for fixed X_i^A, X_i^B are then simply product

of Bernoulli measures :

$$\mathcal{P}(A_{ij}=1)=\frac{\tilde{\nu}_c^{AA}\chi_{|X_i^A(t)-X_j^A(t)|\leq R}}{\tilde{\nu}_c^{AA}+\tilde{\nu}_d^{AA}},\quad \mathcal{P}(A_{ij}=0)=1-\mathcal{P}(A_{ij}=1)$$

$$\mathcal{P}(B_{ij}=1)=\frac{\tilde{\nu}_c^{BB}\chi_{|X_i^B(t)-X_j^B(t)|\leq R}}{\tilde{\nu}_c^{BB}+\tilde{\nu}_d^{BB}},\quad \mathcal{P}(B_{ij}=0)=1-\mathcal{P}(B_{ij}=1)$$

$$\mathcal{P}(C_{ij}=1)=\frac{\tilde{\nu}_c^{AB}\chi_{|X_i^A(t)-X_j^B(t)|\leq R}}{\tilde{\nu}_c^{AB}+\tilde{\nu}_d^{AB}},\quad \mathcal{P}(C_{ij}=0)=1-\mathcal{P}(C_{ij}=1).$$

Defining :

$$\tilde{\Phi}^{ST}(x)=\frac{\kappa^{ST}}{2}\begin{cases}(|x|-R)^2 & \text{for} |x|\leq R\\ 0 & \text{for} |x|>R\end{cases},$$

one can write the equations for the positions, averaged over the stationary measure for the links :

$$\begin{cases} dX_i^A=-\mu\left(\frac{\tilde{\nu}_c^{AA}}{\tilde{\nu}_c^{AA}+\tilde{\nu}_d^{AA}}\sum_{j=1}^{N_A}\nabla\tilde{\Phi}^{AA}(X_i^A-X_j^A)+\frac{\tilde{\nu}_c^{AB}}{\tilde{\nu}_c^{AB}+\tilde{\nu}_d^{AB}}\sum_{j=1}^{N_B}\nabla\tilde{\Phi}^{AB}(X_i^A-X_j^B)\right)dt \\ \qquad\qquad +\sqrt{2D_A}dB_i,\quad \forall\, i\in\{1,\dots,N_A\} \\ dX_i^B=-\mu\left(\frac{\tilde{\nu}_c^{AB}}{\tilde{\nu}_c^{AB}+\tilde{\nu}_d^{AB}}\sum_{j=1}^{N_A}\nabla\tilde{\Phi}^{BA}(X_i^B-X_j^A)+\frac{\tilde{\nu}_c^{BB}}{\tilde{\nu}_c^{BB}+\tilde{\nu}_d^{BB}}\sum_{j=1}^{N_B}\nabla\tilde{\Phi}^{BB}(X_i^B-X_j^B)\right)dt \\ \qquad\qquad +\sqrt{2D_B}dB_\ell,\quad \forall\,\ell\in\{1,\dots,N_B\}\end{cases} \tag{5.6}$$

Notice that in this limit a particle interacts with all its neighbors at distance smaller than R with intensity decreased by a factor $\frac{\tilde{\nu}_c^{ST}}{\tilde{\nu}_c^{ST}+\tilde{\nu}_d^{ST}}\leq 1$. Without loss of generality, we will now choose the time and space scales such that $\mu=1$.

5.3.2 Macroscopic description of the intermediate model

As we would like to analyze the microscopic dynamics from a macroscopic point of view, we aim to derive the PDE associated with the dynamics in (5.6). The standard method is to consider the so-called empirical distributions $f^A(x,t)$, $f^B(x,t)$ of the N_A type-A and N_B type-B cells respectively :

$$f^A(x,t)=\frac{1}{N_A}\sum_{i=1}^{N_A}\delta(x-X_i^A(t)),\quad f^B(x,t)=\frac{1}{N_B}\sum_{i=1}^{N_B}\delta(x-X_i^B(t)), \tag{5.7}$$

where $\{X_i^A(t),X_i^B(t)\}$ are solutions of the dynamical system (5.6). To find the equations satisfied by the empirical distributions, we integrate $f^A(x,t)$, $f^B(x,t)$ against a test function ϕ and take the

time derivatives. One deduces that if $b_0, d_0, \theta_S = 0$ (without growth terms), $f^A(x,t)$ and $f^B(x,t)$ satisfy (weakly) the following equations :

$$\begin{cases} \partial_t f^A = \nabla_x \cdot \left(f^A \nabla_x (\bar{\Phi}^{AA} * f^A) \right) + \nabla_x \cdot \left(f^A \nabla_x (\bar{\Phi}^{AB} * f^B) \right) + D_A \Delta_x f^A \\ \partial_t f^B = \nabla_x \cdot \left(f^B \nabla_x (\bar{\Phi}^{BB} * f^B) \right) + \nabla_x \cdot \left(f^B \nabla_x (\bar{\Phi}^{BA} * f^A) \right) + D_B \Delta_x f^B, \end{cases} \tag{5.8}$$

where the factors $\frac{\tilde{\nu}_c^{ST}}{\tilde{\nu}_c^{ST} + \tilde{\nu}_d^{ST}}$ have been included in the potential functions $\bar{\Phi}^{ST}$. Now, Eqs. (5.8) do not take into account growth phenomena. According to the description at the beginning of the paper, our model describes cell birth and death according to a logistic growth-like process : given a type-S cell (S being either A or B) at position x, its probability $P^S(x)$ to give birth to a new cell depends on the number of neighboring cells (type-A or type-B) contained in a ball of center x and radius R_0 :

$$P^S(x) = b_0^S - (b_0^S - \theta_S) \frac{\int_{B(x,R_0)} \left(f^A(y,t) + f^B(y,t) \right) dy}{N^*},$$

where N^* is the local population carrying capacity. Assuming that the detection radius is small, $R_0 \ll 1$, one can write :

$$\int_{B(x,R_0)} \left(f^A(y,t) + f^B(y,t) \right) dy = \pi R_0^2 \left(f^A(y,t) + f^B(y,t) \right) + O(R_0^6).$$

Therefore, ignoring the higher order terms in R_0, the number of new particles of type-S created at location x during a time dt can be approximated by :

$$f^S(x,t) \left(b_0^S - (b_0^S - \theta_S) \frac{f^A(y,t) + f^B(y,t)}{f^*} \right) dxdt.$$

where $f^* = \frac{N^*}{\pi R_0^2}$. Similarly for the death process, the number of type S particles which are destroyed during time dt can be approximated by :

$$f^S(x,t) \left(d_0^S - (d_0^S - \theta_S) \frac{f^A(y,t) + f^B(y,t)}{f^*} \right) dxdt.$$

Introducing these source terms into Eqs. (5.8) and dropping the bars, one obtains :

$$\begin{cases} \partial_t f^A = \nabla_x \cdot \left(f^A \nabla_x (\bar{\Phi}^{AA} * f^A) \right) + \nabla_x \cdot \left(f^A \nabla_x (\bar{\Phi}^{AB} * f^B) \right) + D_A \Delta_x f^A + \nu^A f^A \left(1 - \frac{f^A + f^B}{f^*} \right) \\ \partial_t f^B = \nabla_x \cdot \left(f^B \nabla_x (\bar{\Phi}^{BB} * f^B) \right) + \nabla_x \cdot \left(f^B \nabla_x (\bar{\Phi}^{BA} * f^A) \right) + D_B \Delta_x f^B + \nu^B f^B \left(1 - \frac{f^A + f^B}{f^*} \right), \end{cases} \tag{5.9}$$

where $\nu^S = b_0^S - d_0^S$.

Remarks :

— We do not normalize the cell distributions (5.7) by N_A, N_B in order to keep the information of the total number of cells. The total mass is essential at the cell level to determine the cell birth process. If one would like to study the asymptotic limit N_A, $N_B \longrightarrow \infty$, one would have to normalize the empirical distribution by the number of cells and consider the limit $R \longrightarrow 0$ (see [2]).

— It should be noted that the PDE model with non-normalized densities differs from the one derived in [2], in which the number of links had to be kept proportional to the number of cells to enable the limiting procedure to be well-defined. Here, because the PDE model is kept at the level of (large but) finite number of particles, such assumption is not needed for the derivation.

5.4 Stability analysis

We first note that the non-trivial constant (homogeneous) steady states $\bar{f}^A$, $\bar{f}^B$ such that

$$\bar{f}^A + \bar{f}^B = f^*, \tag{5.10}$$

are solutions of the macrocopic equation. In order to assess the stability of the homogeneous steady states, we will perform a linear stability analysis using a perturbative approach. We will briefly comment on the cases $\bar{f}^A = 0$ or $\bar{f}^B = 0$ (which are also steady-states of System (5.9)), but we will mostly focus on the non-extinction cases ($\bar{f}^A, \bar{f}^B \neq 0$)

5.4.1 Stability of homogeneous steady states

In order to perform a linear stability analysis, we use perturbation terms and Fourier transform as done in [2]. To this aim, we write :

$$f^A = \bar{f}^A + f^A_\varepsilon, \qquad f^B = \bar{f}^B + f^B_\varepsilon,$$

and will omit the ϵ for the sake of simplicity. Linearizing Eqs. (5.8) and taking the Fourier transform, we obtain :

$$\partial_t \begin{pmatrix} \hat{f}^A \\ \hat{f}^B \end{pmatrix}(y,t) = M(y) \begin{pmatrix} \hat{f}^A \\ \hat{f}^B \end{pmatrix}(y,t), \tag{5.11}$$

where M reads :

$$M(y) = \begin{pmatrix} -|y|^2(2\pi \bar{f}^A \hat{\Phi}^{AA}(y) + D_A) - \nu^A \frac{\bar{f}^A}{f^*} & -|y|^2 2\pi \bar{f}^A \hat{\Phi}^{AB}(y) - \nu^A \frac{\bar{f}^A}{f^*} \\ [15pt] - |y|^2 \bar{f}^B \hat{\Phi}^{BA}(y) - \nu^B \frac{\bar{f}^B}{f^*} & -|y|^2(2\pi \bar{f}^B \hat{\Phi}^{BB}(y) + D_B) - \nu^B \frac{\bar{f}^B}{f^*} \end{pmatrix}. \tag{5.12}$$

Note that system (5.11) has been obtained neglecting the perturbation terms of order two.

In the general case, the homogeneous steady states will be stable only if the real part of the eigenvalues of the matrix $M(y)$ are both negative, otherwise it will be unstable. Since we know that $det(M(y)) = \lambda_1 \cdot \lambda_2$ and $tr(M(y)) = \lambda_1 + \lambda_2$, with $\lambda_1(y), \lambda_2(y)$ eigenvalues, the stability occurs only if :

$$det(M(y)) > 0 \quad \text{and} \quad tr(M(y)) < 0.$$

We first compute the trace of matrix $M(y)$:

$$tr(M(y)) = -|y|^2(2\pi\bar{f}^A\hat{\Phi}^{AA}(y) + D_A) - \nu^A\frac{\bar{f}^A}{f^*} - |y|^2(2\pi\bar{f}^B\hat{\Phi}^{BB}(y) + D_B) - \nu^B\frac{\bar{f}^B}{f^*}. \quad (5.13)$$

We recall the fact that we consider the following assumption as in [2] for the parameters :

Hypothesis 1. *The intraspecies (or homotypic) links generate repulsive interactions, i.e* $\kappa^{AA} > 0$ *and* $\kappa^{BB} > 0$.

We can easily note that under hypothesis H1, the trace is always negative. Then we compute the determinant of matrix $M(y)$:

$$det(M(y)) = |y|^4\left[(\bar{f}^A 2\pi\hat{\Phi}^{AA} + D_A)(\bar{f}^B 2\pi\hat{\Phi}^{BB} + D_B) - \bar{f}^A\bar{f}^B 4\pi^2\hat{\Phi}^{AB}\hat{\Phi}^{BA}\right] +$$

$$+ |y|^2\left[\nu^B\frac{\bar{f}^B}{f^*}(\bar{f}^A 2\pi\hat{\Phi}^{AA} + D_A - \bar{f}^A 2\pi\hat{\Phi}^{AB}) + \nu^A\frac{\bar{f}^A}{f^*}(\bar{f}^B 2\pi\hat{\Phi}^{BB} + D_B - \bar{f}^B 2\pi\hat{\Phi}^{BA})\right]. \quad (5.14)$$

The first part with term in $|y|^4$ is exactly the determinant computed in [2] without logistic term. The contribution of the logistic growth is embodied into the second term.

As the trace of M is always negative under Hypothesis 1, one observes that the constant steady states will be unstable if $\Delta(M) < 0$ only. From Eq.(5.14), it is clear that the interspecies potential intensities controlled by parameters κ^{AB}, κ^{BA} must be large enough to allow the determinant to be negative. In order to quantify the relative importance of interspecies potential parameters compared to the others (diffusion intensities, growth rates, intraspecies potential intensities), we introduce $s \in \mathbb{R}^+$ such that $\kappa^{AB} = s\tilde{\kappa}^{AB}$, $\kappa^{BA} = s\tilde{\kappa}^{BA}$. We consider the following hypothesis on heterotypic interactions :

Hypothesis 2. *The interspecies (or heterotypic) links interactions are both repulsive , i.e* $\kappa^{AB} > 0$ *and* $\kappa^{BA} > 0$.

Following the same workflow and approach of [2], we can conclude that it exists a critical value s_L^* for s beyond which the homogeneous steady-states are unstable (corresponding to segregation between the two families) :

$$s_L^* = \frac{(24D_A + c^{AA}\bar{f}^A)\nu^B\bar{f}^B + (24D_B + c^{BB}\bar{f}^B)\nu^A\bar{f}^A}{\nu^B\bar{f}^B c^{AB}\bar{f}^A + \nu^A\bar{f}^A c^{BA}\bar{f}^B}, \quad (5.15)$$

with $c^{SS} = \frac{2\pi\kappa^{SS}\nu_c^{SS}R^4}{\nu_d^{SS}}$ and $c^{ST} = \frac{2\pi s\tilde{\kappa}^{ST}\nu_c^{ST}R^4}{\nu_d^{ST}}$, $S \neq T \in \{A, B\}$.

Note that in the case of extinction of one population ($\bar{f}^A = 0$ or $\bar{f}^B = 0$), the model reduces to a one-species diffusion equation, which converges in time towards a homogeneous distribution of the survivor species (stable homogeneous state). In what follows, the analysis is carried out outside of this particular regime (i.e for $\bar{f}^A \neq 0$ and $\bar{f}^B \neq 0$).

5.4.2 Characterization of the steady-states

It is noteworthy that the system's segregation ability depends on the mass ratio of the two families. Indeed, the critical values s_L^* for which the two-particle system departs from the homogeneous distributions $\bar{f}^A$, $\bar{f}^B$ depends on their initial relative ratio. Intuitively, this corresponds to the fact that the amount of mechanical forces exerted by a cell type on the other one must account for its relative mass compared to the other family, for the system to enable cell segregation. In order to give more insights into this phenomenon, we document the stability of the steady states as function of their mass distribution, by studying the influence of the value of s_L^* as function of the masses $\bar{f}^A$, $\bar{f}^B$.

Using $\bar{f}^B = f^* - \bar{f}^A$ we rewrite s_L^* as :

$$s_L^* = \frac{(\nu^B c^{AA} + \nu^A c^{BB})\bar{f}^A(f^* - \bar{f}^A) + (24D_B\nu^A - 24D_A\nu^B)\bar{f}^A + 24D_A\nu^B f^*}{\bar{f}^A(f^* - \bar{f}^A)(\nu^B c^{AB} + \nu^A c^{BA})}, \tag{5.16}$$

Moreover it is easy to check that under H1, H2, $\lim_{\bar{f}^A \to f^*} s_L^*(\bar{f}^A) = +\infty$ and $\lim_{\bar{f}^A \to 0} s_L^*(\bar{f}^A) = +\infty$, meaning that the states corresponding to one dominant population are always stable.

We are looking then for the minimum of function s_L^*, i.e the zero points of $\frac{\partial s_L^*(\bar{f}^A)}{\partial \bar{f}^A}$. After computation we find only one minimum $\bar{f}_m^A$ in $[0, f^*]$:

— If $D_A\nu^B - \nu^A D_B = 0$, the minimum is $\bar{f}_m^A = \frac{f^*}{2}$

— If $D_A\nu^B - \nu^A D_B \neq 0$, the minimum is given by :

$$\bar{f}_m^A = \frac{f^*(D_A\nu^B - \sqrt{D_A D_B \nu^B \nu^A})}{D_A\nu^B - \nu^A D_B}. \tag{5.17}$$

The minimum of function s_L^* corresponds to the less stable steady state, i.e the steady state which necessitates the least mechanical efforts to enable segregation between the two species. When the two population have the same ratio between diffusion and growth, the less stable configuration is the symmetric one. As a matter of fact, increasing parameter s corresponds to introduce asymmetry between the two populations, promoting an asymmetric steady state.

In Figure 5.2 we report the plot of s_L^* as a function of f^A in the case $D_A\nu^B - \nu^A D_B \neq 0$ (blue curve) and $D_A\nu^B - \nu^A D_B = 0$ (orange curve). As mentioned before, we can see that for given values of the parameters, there exist stable steady states corresponding to the case of a dominant population. For both set of parameters, we can observe a large plateau value meaning that a large number of steady states are unstable. Hence, we can observe a large plateau value meaning that a large number of steady states are unstable beyond the same of s.

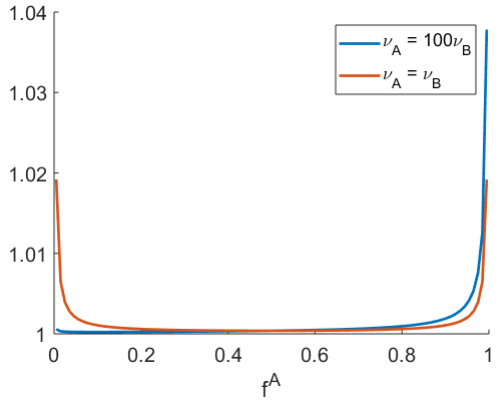

FIGURE 5.2 – value of s_L^* as function of $\bar{f}^A$, for $f^* = 1, D_A = D_B, \nu^A = 100\nu^B$.

5.4.3 Impact of the logistic growth on aggregation

It is noteworthy that in the model without logistic growth, mass is conserved, i.e the homogeneous state only depends on the initial condition, while with logistic growth, the equilibrium state is determined both by the initial condition and by birth/death parameters. Without the logistic growth, we report the following critical value s_C^* of s beyond which the system produces aggregates (see [2]) :

$$s_C^* = \left[\frac{576}{c^{AB} c^{BA} f^A f^B} \left(D_A + \frac{c^{AA} f^A}{24} \right) \left(D_B + \frac{c^{BB} f^B}{24} \right) \right]^{\frac{1}{2}}. \tag{5.18}$$

As previously noted, both critical values s_C^*, s_L^* are markers of instability and we will discuss some simulations to compare them. As remarked in [2], as diffusion and intraspecies repulsion tend to homogenize the system, then the interspecies repulsion forces must be large enough to compensate these phenomena and produce clustering/segregation. Thanks to the stability analysis, we can observe and conclude that the logistic growth can either support or repress aggregation, depending also on the choice of the parameters. The segregation is viewed as a breakdown of stability caused by changes in the parameters which characterize the system.

In the next section we will discuss some numerical simulations on the agent-based model to explore numerically the results provided by the stability anaysis. If not otherwise stated, the parameters of the simulations are the ones summarized in Table. 5.1. We will explore different parameter regimes :

— case $s_C^* < s_L^*$. If s is such that $s < s_C^*$, both model should converge towards a homogeneous state (mixing of the two families). if $s \in (s_C^*, s_L^*)$, the model without growth should segregate the two cell types (instability of the homogeneous state), while the model with logistic growth should maintain a homogeneous state. Finally for $s < s_L^*$, cell segregation should be observed for both models.

— case $s_C^* > s_L^*$. Values of s such that $s > s_C^*$ should produce segregation of the two families for both models, while for $s < s_L^*$, the system should converge towards homogeneous

steady states for both models. For s chosen in the range (s_L^*, s_C^*), the model without growth should create homogeneous state while the model with logistic growth should segregate the two families.

Parameters	Description	Values
L	Length related to periodic square demain	7.5
N_A	Number of A-type particles	500
N_B	Number of B-type particles	500
μ	Motility coefficient	1
D_S	Diffusion coefficient	10^{-4}
κ^{AB}	Interspecies (or heterotypic) interaction intensity	s
κ^{BA}		s
κ^{AA}	Intraspecies (or homotypic) interaction intensity	4
κ^{BB}		1
R	Radius of interaction (link repulsion)	1
R_0	Logistic radius	1.5
r	Maximal distance of a daughter cell to her parent	1.5
N^*	Local population carrying capacity	$\frac{500\pi R_0^2}{4L^2}$
ν^A	Logistic growth rate for the A cells	5.10^{-4}
ν^B	Logistic growth rate for the B cells	5.10^{-3}

TABLE 5.1 – Parameters and values used for the simulations of the microscopic model

5.5 Numerical scheme

We perform numerical simulations of the microscopic model as done in [2] following scheme in [1], on a $2D$ domain $[-L, L] \times [-L, L] = [-7.5, 7.5]^2$ with periodic boundary conditions. We set diffusion constants $D_A = D_B = 10^{-4}$ and investigate different values of inter- and intra-species intensities such as $\kappa^{AA}, \kappa^{BB}, \kappa^{AB} = s\tilde{\kappa}^{AB}, \kappa^{BA} = s\tilde{\kappa}^{BA}$. For each equation of system (5.1) we have the following time discretization :

$$X_i^{n+1} = X_i^n - \mu \nabla_{X_i} W(X^n) \Delta t^n + \sqrt{2D\Delta t^n}\mathcal{N}(0,1) \tag{5.19}$$

$\mathcal{N}(0,1)$ is the normal distribution with mean 0 and standard deviation 1.
The logistic growth is modelled via independent Poisson processes of position-dependent frequencies $\beta_S(X_i)$ and $\delta_S(X_i)$ for birth and death respectively. The probability of a cell to divide and/or die between time steps t and $t + \Delta t$ is given by :

$$\begin{cases} \mathcal{P}(\text{cell i divide}) & = 1 - \exp^{-\max(0, \beta_S(X_i)\Delta t)} \\ \\ \mathcal{P}(\text{cell i die}) & = 1 - \exp^{-\max(0, \delta_S(X_i))\Delta t}, \end{cases}$$

where the rates β_S and δ_S are computed thanks to (5.3). All simulations are performed with parameters $b_0^S = \frac{4\nu^S}{3}, d_0^S = \frac{\nu^S}{3}$ and $d_0^S < \theta^S = \nu^S < b_0^S$ for $S = A, B$. Note that these parameters are chosen such that the macroscopic logistic rate $\nu^S = b_0^S - d_0^S$. For each dividing 'parent' cell j, the 'daughter' cell is supposed to be born at a distance randomly chosen in $B(X_j, r)$, where we chose $r = 1.5$ from her parent.

Finally, we ensure that only one birth/death event happens between time t and $t + \Delta t$ by choosing the time step $\Delta t \ll \frac{1}{\max(\nu^A, \nu^B)N}$, where N is the maximal number of particles between family A and B.

We consider a periodic domain randomly filled with $N_A = N_B = 500$ cells initially and we fix κ^{ST} for S and T such as given in table 5.1. For such values, the critical value s_C^* of s beyond which the system without logistic growth aggregates is $s_C^* \approx 2.1$. We consider different logistic rates but we keep the ratio $\frac{\nu^B}{\nu^A} = 10$ such that the critical value s_L^* of s beyond which the model with logistic growth should produce aggregates is around $s_L^* \approx 3.8$. For each regime, we therefore explore the cases :

— s = 1.5 : both the original model and the one with logistic growth should produce homogeneous steady states

— s = 2.5 : the original model should produce an aggregated steady state while the one with logistic growth is expected to produce a homogeneous one.

— s = 4 : both the original model and the one with logistic growth should produce aggregated steady states.

In Fig. 5.3, we show the results of the simulations at time $t = 20000$, without logistic growth (left column) and with logistic growth for five different values of ν^B (keeping the ratio $\frac{\nu^B}{\nu^A} = 10$ constant, columns two to six : $\nu^B = 10^{-3},\ 2.10^{-3},\ 5.10^{-3},\ 10^{-2},\ 0.1$). For each regime, we consider the cases $s = 1.5, s = 2.5, s = 4$.

As one can observe in Fig. 5.3 column 1, the microscopic model without logistic growth is in good accordance with the predictions of the stability analysis of the macroscopic model since we observe aggregates for $s = 2.5, 4$ and a homogeneous steady-state for $s = 1.5$. When activating the logistic growth, one can observe a homogeneous steady-state for $s = 1.5$ and aggregated steady states for $s = 4$ provided the frequencies of the logistic growth are small enough (columns 2-4). For $s = 2.5$, a better mixing of the two populations seems to be observed compared to the case without logistic growth (compare line 2, columns 2-4 to column 1), but the system for $s = 2.5$ still shows aggregation abilities (compare lines 1 and 2). These observations are quantified below. It is noteworthy that for large values of ν^B (columns 5,6), one can observe at time $t = 20000$ the extinction of family B. This suggests that a fast logistic growth process can lead to the complete extinction of one specie. Note that this case was excluded from the stability analysis and the analysis close to this equilibrium state will be the subject of future work.

In order to quantify better the aggregation abilities of the system at equilibrium, we follow the steps of [2] and define a quantifier Q which measures the segregation amount between the two families using image processing tools. To this aim, given a RGB numerical image, we define the quantifier Q as the number of mixed red and green pixels (pixels which have non zero red and green components), normalized by $\min(P_g, P_r)$ where P_g, P_r are the total number of pixels with a non zero green component (resp. red component). Thus defined, $Q = 1$ describes a homogeneous

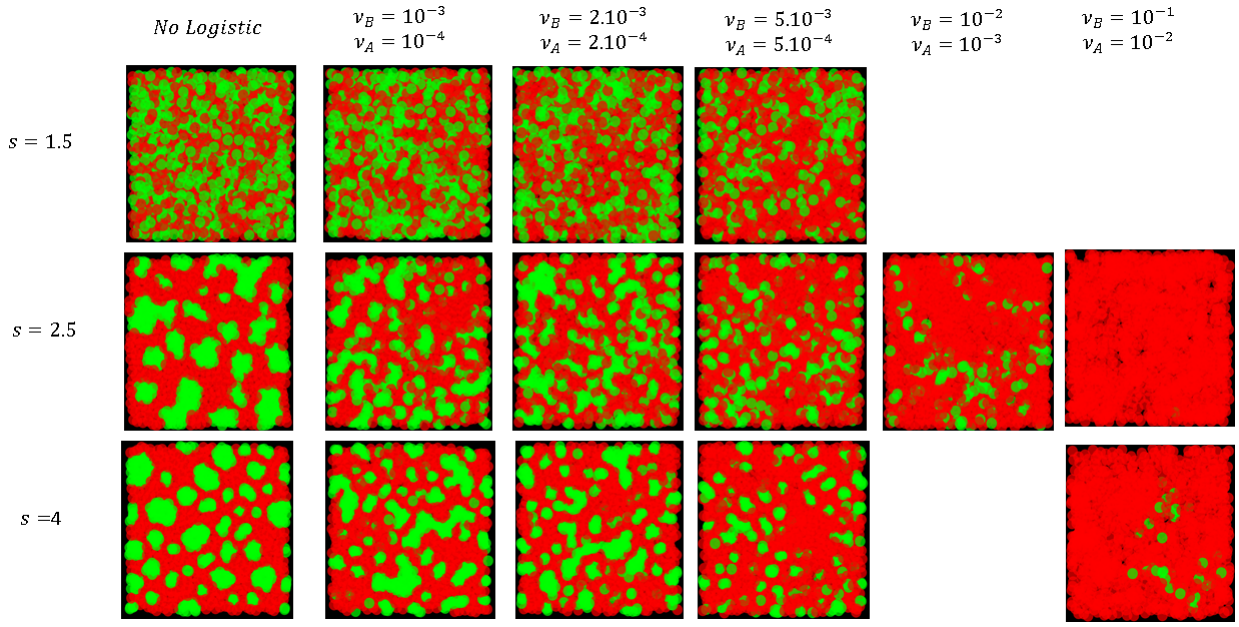

FIGURE 5.3 – Results of the microscopic model at time $t = 20000$, without logistic growth (left column) and with logistic growth for five different values of ν^B (keeping the ratio $\frac{\nu^B}{\nu\hat{\text{A}}} = 10$ constant, columns two to six : $\nu^B = 10^{-3},\ 2.10^{-3},\ 5.10^{-3},\ 10^{-2},\ 0.1$). For each regime, we consider the cases $s = 1.5, s = 2.5, s = 4$. Cells of family B are represented in green, cells of family A in red.

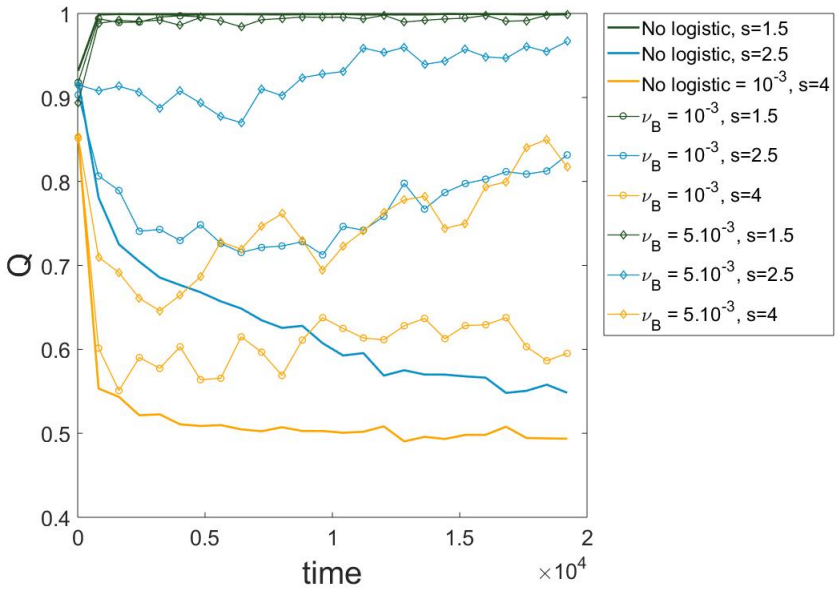

FIGURE 5.4 – Values of the quantifier Q as function of time for $N_A = N_B = 500$ cells initially, for three different values of the inter-species repulsion $s = 1.5$ (green curves), $s = 2.5$ (blue curves) and $s = 4$ (orange curve), for $N_A = N_B = 500$ initially. For each case, we consider the case with no logistic growth (continuous lines), with logistic growth for $\nu_B = 10^{-3}, \nu_A = 10^{-4}$ (round markers) and $\nu_B = 5.10^{-3}, \nu_A = 5.10^{-4}$ (diamond markers).

state (perfect mixing of the two families), while $Q \ll 1$ for separated phases. Note that because of the normalization, Q does not give a measure of the size/shape of the aggregates. This quantifier only enables to distinguish between mixed or separated phases.

In Fig. 5.4, we show the values of Q as function of time for three different values of the inter-species repulsion intensities $s = 1.5$ (green curves), $s = 2.5$ (blue curves) and $s = 4$ (orange curve), for $N_A = N_B = 500$ initially. For each case, we consider the case with no logistic growth (continuous lines), with logistic growth for $\nu_B = 10^{-3}, \nu_A = 10^{-4}$ (round markers) and $\nu_B = 5.10^{-3}, \nu_A = 5.10^{-4}$ (diamond markers). As one can observe, the value of Q decreases as s increases for all the regimes considered, with $Q \approx 1$ for $s = 1.5$ (green curves) and independently of the activation of the logistic growth. For $s = 2.5$ (blue curves), we observe that the value of Q increases as we increase the logistic growth rates, and we recover the predicted homogeneization of the logistic growth for sufficiently large values of ν_B, ν_A. If the logistic growth rate is too small ($\nu_B = 10^{-3}, \nu_A = 10^{-4}$), the system still shows some clustering for $s = 2.5$ and $N = 500$ (see the blue curve with round markers). For $s = 4$ (orange curves), the system produces segregated patterns independently on the logistic growth, as predicted by the stability analysis.

We note that increasing the total number of particles $N_A + N_B$ (and adapting the parameter N^* such that $N_A + N_B$ correspond to the equilibrium number of particles) leads to better correspondence between the numerical results and the states predicted by the stability analysis in

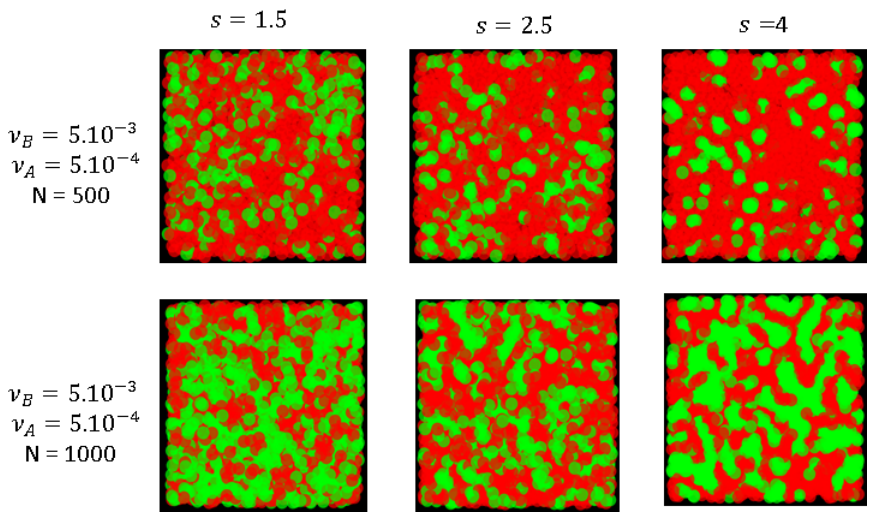

FIGURE 5.5 – Case $\nu^B = 5.10^{-3}$, $\nu^A = 5.10^{-4}$ for $N = 500$ (top line) and $N = 1000$ (bottom line

macroscopic model. As an illustration, we show in Fig. 5.5 the case $\nu^B = 5.10^{-3}$, $\nu^A = 5.10^{-4}$ for $N = 500$ and $N = 1000$, where the structures observed at $t = 20000$ for $s = 2.5$ seem to be closer to a homogeneous state for $N = 1000$ than for $N = 500$. In Fig. 5.6, we show the values of Q with $N_A = N_B = 1000$ particles initially, for three different values of s : $s = 1.5$ (green curves), $s = 2.5$ (blue curves), $s = 4$ (orange curves) as function of the time without logistic growth (continuous lines) and with logistic growth for $\nu_B = 5.10^{-3}, \nu_A = 5.10^{-3}$ (diamond). By comparing the diamond marked curves of Fig. 5.6 to the ones of Fig. 5.4, one can observe a better prediction and stability of the patterns in time for $N = 1000$ compared to $N = 500$.

Finally in Fig. 5.7, we show the evolution of the normalized number of cells $\frac{N_A}{N_A+N_B}$ (black curves) and $\frac{N_B}{N_A+N_B}$ (colored curves) as function of the time for $\nu_B = 10^{-3}$ and $\nu_A = 10^{-4}$, and different values of s : (I) for $s = 1.5$, (II) for $s = 2.5$ and (III) for $s = 4$. As one can observe in Fig. 5.7, in the stable cases $s = 1.5$ and $s = 2.5$, the fraction of cells reaches the equilibrium value corresponding to the predicted distribution given by Eq. (5.17). For $s = 1.5, 2.5$, the system stabilizes around 35% of type B cells and 65% of type A cells, while in the unstable case $s = 4$ the number of cells seems to oscillate around the initial ratio 50% for each family. Note that these large stochastic oscillations around the mean could be analogue to the ones reported in [5]. In [5], the authors report stochastic fluctuations in a non-spatial model of two competing species submitted to a logistic growth. They show that giant fluctuations (the variance being of order of the mean squared) in the number of individuals are obtained if the growth rates of the two families are of the same order, and that in this regime the deterministic equation must be abandoned and a stochastic treatment used instead. By introducing spatial mechanical interactions, we believe that the logistic regime for which fluctuations are expected is shifted and plays a role when the logistic growth balances the mechanical forces. Here, even for $\nu_B = 10\nu_A$, we still observe fluctuations in the number of cells when we are slightly after the transition value for the mechanical interactions.

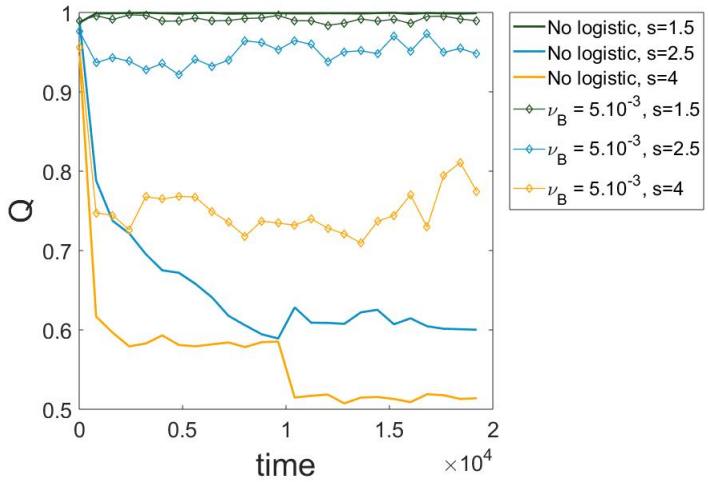

FIGURE 5.6 – Values of the quantifier Q as function of time for $N_A = N_B = 1000$ cells initially, for three different values of the inter-species repulsion $s = 1.5$ (green curves), $s = 2.5$ (blue curves) and $s = 4$ (orange curve), for $N_A = N_B = 500$ initially. For each case, we consider the case with no logistic growth (continuous lines), and with logistic growth for $\nu_B = 5.10^{-3}, \nu_A = 5.10^{-4}$ (diamond markers).

5.6 Conclusion

We have proposed a theoretical and numerical study of a cell division process in a cell aggregation model. The modeling is based on a multiscale approach, from a microscopic model to a macroscopic description of a system of particles interacting through a dynamical network. The model describes point particles with local cross-links modeled by springs that are randomly created and destructed. In the mean field limit, the link density distribution becomes a local function of the particle distribution density, evolving on a slow time scale through a McKean-Vlasov equation. We introduced the cell division process through a logistic growth on the macroscopic model and a birth-death process at the microscopic scale.

The linear stability analysis of the macroscopic model gives access to a criterion on the ratio between heterotypic and homotypic repulsion to ensure the formation of clusters. This criterion involves the logistic growth rate and it is compared to the case of a population with fixed size. Interestingly, the theoretical stability analysis of the macroscopic model showed that introducing a logistic growth term in this cell repulsion-diffusion model can either repress or promote segregation. Indeed, we have shown that the size of the parameter zone for which the homogeneous state is stable depends on the logistic growth parameters, and it can be increased or decreased by choosing the parameters appropriately. The mechanisms can be summarized as follows : consider a system of two types of particles where heterotypic repulsion forces dominate homotopic forces and diffusion, such that we observe the segregation of the two families in the case of populations of fixed sizes. Close to the transition zone (where the heterotypic forces are close to the critical value), the system can be homogenized by introducing a logistic term where

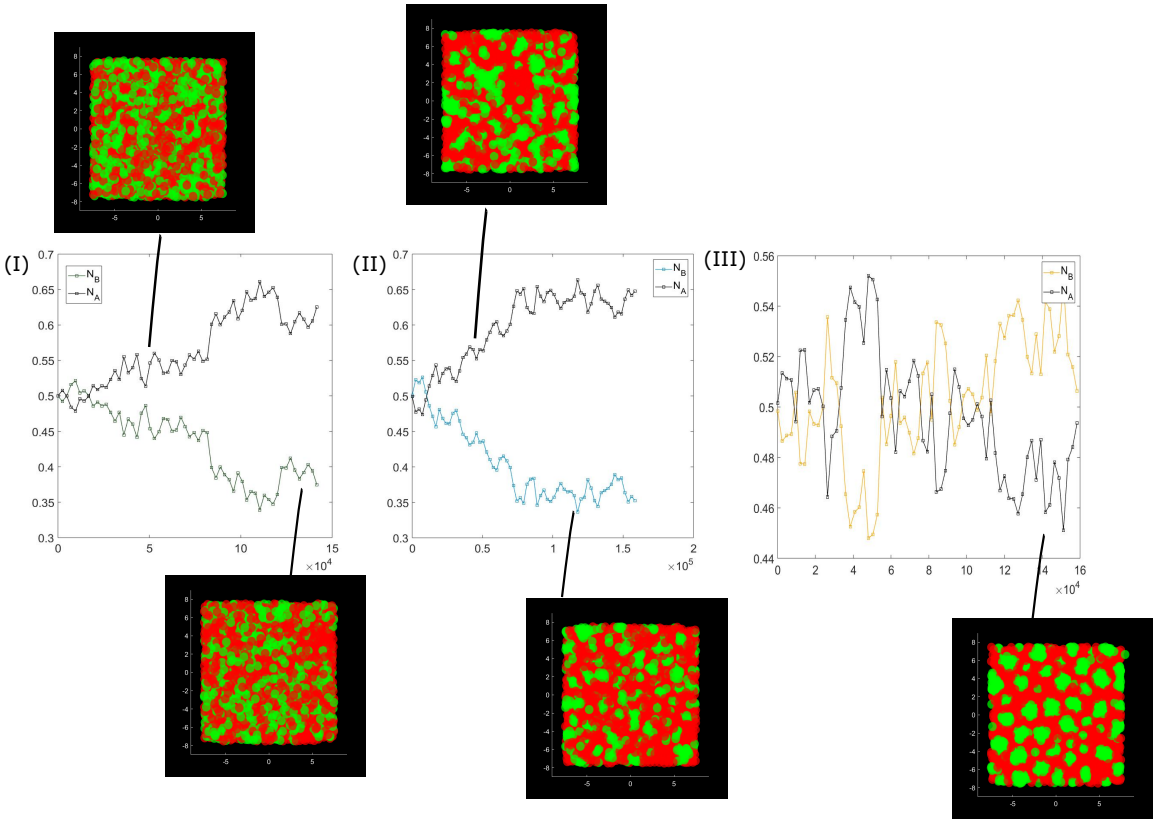

FIGURE 5.7 – Evolution of the normalized number of cells of each family $\frac{N_A}{N_A+N_B}$ (black curves) and $\frac{N_B}{N_A+N_B}$ (colored curves) as function of the time for $\nu_B = 10^{-3}$ and $\nu_A = 10^{-4}$ and different values of s : (I) for $s = 1.5$, (II) for $s = 2.5$ (stable cases) and (III) for $s = 4$ (unstable case).

the compressed family cell renewal is larger than the one of the predominant family. Enabling the clustered cells to be renewed at the border of the clusters faster than the compressing family leads to a spread out of the clustered family and the overall system converges towards a homogeneous (mixed) state.

In order to validate the theoretical analysis, we performed numerical simulations of the microscopic model which showed a good correspondence with the analysis of the macroscopic model, provided that the parameters are chosen in the right regime. The numerical results showed that for sufficiently large initial number of cells and sufficiently slow logistic growth compared to the time scale of the mechanical interactions, we could recover the homogenization via logistic growth as foreseen by the stability analysis. In time, the system converged towards the predicted value of cell distributions, which showed that the macroscopic model is a good approximation of the microscopic dynamics as the number of cells increases.

Since this work was a first attempt to introduce a logistic term -both at the microscopic/stochastic level and at the macroscopic one- in a system of mechanically interacting particles, several questions remain unanswered and require further investigations. For instance, from a theoretical viewpoint, the rigorous derivation of the macroscopic model is still an open problem. This will require precise estimates depending on the size and number of cells. On the numerical viewpoint, more work is needed to better understand the interplay between the mechanical interactions and the logistic growth in the regime of fast logistic growth. A deeper parametric analysis is needed to better capture the link between the stochastic growth process and its deterministic approximation. Future works will aim to perform the numerical comparison between the macroscopic and microscopic model.

Acknowledgements The work presented in this chapter is the result of a fruitful collaboration that took place during the CEMRACS 2018, organized by Vincent Calvez (Institut Camille Jordan, CNRS, Univ. Lyon 1) Celine Grandmont (Equipe projet Reo et LJLL, Inria Paris et Sorbonne Univ), Eva Locherbach (Departement de Mathematiques, Univ. de Cergy Pontoise), Clair Poignard (Equipe Projet Monc et IMB, Inria Bordeaux et Univ. de Bordeaux), Magali Ribot (Institut Denis Poisson, Univ. d'Orleans), Nicolas Vauchelet (Laga, Univ. Paris 13). This work was supported by the European Research Council (ERC) under the European Unions Horizon 2020 research and innovation program (grant agreement No 740623).

Bibliographie

[1] J. Barré, J. A. Carrillo, P. Degond, D. Peurichard, and E. Zatorska. Particle interactions mediated by dynamical networks : Assessment of macroscopic descriptions. *Journal of Nonlinear Science*, 28(1) :235–268, Aug 2017.

[2] J. Barré, P. Degond, D. Peurichard, and E. Zatorska. Modelling pattern formation through differential repulsion, 2019.

[3] J. Barré, P. Degond, and E. Zatorska. Kinetic theory of particle interactions mediated by dynamical networks, 2016.

[4] J. Barré, P. Degond, and E. Zatorska. Kinetic theory of particle interactions mediated by dynamical networks. *Multiscale Modeling & Simulation*, 15(3) :1294–1323, 2017.

[5] B. Houchmandzadeh. Giant fluctuations in logistic growth of two species competing for limited resources. *Physical Review E*, 98(4), Oct 2018.

[6] H. B. Taylor, A. Khuong, Z. Wu, Q. Xu, R. Morley, L. Gregory, A. Poliakov, W. R. Taylor, and D. G. Wilkinson. Cell segregation and border sharpening by eph receptor&#x2013 ;ephrin-mediated heterotypic repulsion. *Journal of The Royal Society Interface*, 14(132) :20170338, 2017.

[7] N. Tkachenko, J. D. Weissmann, W. P. Petersen, G. Lake, C. P. E. Zollikofer, and S. Callegari. Individual-based modelling of population growth and diffusion in discrete time. *PLOS ONE*, 12(4) :1–22, 04 2017.

CHAPITRE. 6

Numerical investigations of the compressible and barotropic Navier-Stokes equations

Contents

6.1 Introduction

In this chapter, we are interested in the simulation of the following Compressible Navier-Stokes system

$$\begin{aligned} \partial_t \rho + \partial_x(\rho u) &= 0, \\ \partial_t(\rho u) + \partial_x(\rho u^2) + \partial_x p - \partial_x(\mu \partial_x u) &= 0. \end{aligned} \tag{6.1}$$

In (6.1), the unknowns $(t,x) \mapsto \rho(t,x)$ and $(t,x) \mapsto u(t,x)$ stand respectively for the density and the velocity of a fluid. The quantity $\mu > 0$ is the viscosity of the fluid. We restrict to the isentropic case, where the pressure is a mere function of the density, namely we set $p(\rho) = a\rho^\gamma$, with $a > 0$ and $\gamma > 1$. Here we assume that the fluid is not subjected to external forces.

This contribution is particularly motivated by the pioneering work of D. Hoff [15]. Beyond the existence of weak solutions, [15] establishes several facts about *discontinuous solutions* of (6.1), which, at first glance, are quite surprising. Indeed, possible discontinuities of the initial velocity are instantaneously smoothed out : u becomes continuous, while the density ρ can present discontinuities, which are simply advected by the velocity field u, see [17, 26]. The velocity gradient has possible discontinuities, but cancellation occurs so that the mixed quantity $\mu\partial_x u - p$ is continuous. Moreover, the jump discontinuities of (6.1) tend to 0 exponentially fast as $t \to \infty$: the smaller the viscosity, the faster the decay. This form is not consistent with the discontinuous solutions of the Euler equations (obtained by replacing μ by 0 in (6.1)). Shock solutions for the Euler system can be obtained in the vanishing viscosity regime, but discontinuities of (6.1) do not produce discontinuities for the inviscid system ; instead the latter emerge in regular regions for the solutions of (6.1), see [11, 16]. For further results and references about the existence theory for the compressible Navier-Stokes system, we refer the reader to [6, 19] and the reference books [7, 22]. It is also worth mentioning the recent breakthrough [4] which deals with more intricate pressure laws and introduce new compactness arguments, and [5, 25, 27] for results on the case of density-dependent viscosities.

In terms of numerical methods, the basic idea consists in using an established method for the Euler equation, coupled to a suitable discretization of the diffusion term. In order to avoid non affordable time steps, it is quite natural to make the latter implicit. We will compare such schemes to approaches based on staggered discretizations, where the discrete densities and velocities are stored on dual locations ; such methods, strongly motivated by the simulation of low-Mach flows, are discussed for instance in [8, 10, 13, 14, 20] and in [1, 2, 3, 12, 24], with different viewpoints on the construction of the numerical fluxes. We will also perform simulations based on Lagrangian schemes, which are able to follow more accurately the discontinuities. Nevertheless, the convergence analysis of schemes for the compressible Navier-Stokes system is not that developed : we refer the reader to [9, 18] for recent results in this direction ; however, these papers investigate fully implicit schemes which could be very difficult to effectively implement (with the additional difficulties of using a Newton algorithm, which itself should be shown to converge in this context).

The chapter is organized as follows. In Section 6.2, we present the numerical schemes that we shall use for the simulation of (6.1). In Section 6.3, we discuss a Lax-Wendroff-like statement, which provides a rigorous basis to the most naive numerical strategy. Section 6.4 is devoted to the discussion of the numerical results.

6.2 Numerical methods

6.2.1 A splitting scheme for compressible Navier-Stokes equations

In this section, we propose a very simple scheme that consists in using a classical hyperbolic type scheme for the Euler system and adding, in a splitting procedure, the effect of the viscosity. To approximate the solution of the Euler system, we use the finite volume framework. The computational domain is the slab $(0,1)$, endowed with periodic boundary conditions for the sake of simplicity. It is discretized into I cells with equal length $C_i = (x_{i-1/2}, x_{i+1/2})$, and x_i being the center of the cell. This amounts to define, for $I \in \mathbb{N}^*$, $\Delta x = 1/I$, $x_{i+1/2} = i\Delta x$, $x_i = (i+1/2)\Delta x$ for $i = 0, \dots, I$. Note that we thus have $x_{I+1/2} = 1$, and we define also $x_{1/2} = 0$. For the time discretization, we discuss the schemes with the generic notation $\Delta t > 0$, but it has to be kept in mind that actually Δt will have to satisfy a local in time Courant-Friedrichs-Lewy type constraint. Therefore, in fact Δt may depend on the time step (and the local discrete time should be appropriately denoted $t^n = \sum_{k=1}^n \Delta t^k$ instead of $n\Delta t$). We denote by $X_i^n = (\rho_i^n, q_i^n)$ the approximate solution at time t_n on the cell C_i, where $q_i^n = \rho_i^n u_i^n$ is the discrete momentum : X_i^n is intended to be an approximation of $\frac{1}{\Delta x}\int_{C_i} X(t^n, x)\, dx$. The unknowns are updated as follows

$$X_i^{n+1} = X_i^n - \frac{\Delta t}{\Delta x}(\mathcal{F}_{i+1/2}^n - \mathcal{F}_{i-1/2}^n). \tag{6.2}$$

Here and below, we consider only first-order three points schemes where the flux $\mathcal{F}_{i+1/2}^n$ at the interface $x_{i+1/2}$ is defined as a function of the unknowns in the neighboring cells :

$$\mathcal{F}_{i+1/2}^n = \mathcal{F}(X_i^n, X_{i+1}^n).$$

There are many relevant choices for the numerical fluxes. Here, we shall use the Rusanov flux, given by

$$\mathcal{F}(X_i^n, X_{i+1}^n) = \frac{F(X_i^n) + F(X_{i+1}^n)}{2} - \max_{k\in\{1,2\}}\left(\lambda_k(X_i^n), \lambda_k(X_{i+1}^n)\right)\frac{X_{i+1}^n - X_i^n}{2}.$$

where

$$F(\rho, q) = \begin{pmatrix} [F(\rho,q)]_1 \\ [F(\rho,q)]_2 \end{pmatrix} = \begin{pmatrix} q \\ q^2/\rho + p(\rho) \end{pmatrix}$$

and

$$\lambda_1(X) = u - \sqrt{p'(\rho)} \qquad \lambda_2(X) = u + \sqrt{p'(\rho)}$$

are the eigenvalues of the Jacobian $\nabla_{\rho,q} F(\rho, q)$. We refer the reader for instance to the textbook [21] for further details about this classical scheme for conservation laws. What is crucial is the following consistency property

$$\mathcal{F} \text{ is continuous and satisfies } \mathcal{F}(X, X) = F(X). \tag{6.3}$$

In the convergence analysis made below, the details of the numerical fluxes are not important, except property (6.3). The "splitting" scheme for (6.1) reads

$$\frac{\rho_i^{n+1}-\rho_i^n}{\Delta t}+\frac{1}{\Delta x}\left[[\mathcal{F}_{i+1/2}^n]_1-[\mathcal{F}_{i-1/2}^n]_1\right]=0,\quad n\in\mathbb{N}, i=1,\dots,I, \tag{6.4}$$

$$\frac{\rho_i^{n+1}u_i^{n+1}-\rho_i^n u_i^n}{\Delta t}+\frac{1}{\Delta x}\left[[\mathcal{F}_{i+1/2}^n]_2-[\mathcal{F}_{i-1/2}^n]_2\right]-\frac{1}{\Delta x}(\mathcal{D}_{i+1/2}^{n+1}-\mathcal{D}_{i-1/2}^{n+1})=f_i^{n+1},$$
$$n\in\mathbb{N}, i=1,\dots,I, \tag{6.5}$$

where we have incorporated the diffusion flux at $x_{i+1/2}$, here defined by :

$$\mathcal{D}_{i+1/2}^{n+1}=\mu\frac{u_{i+1}^{n+1}-u_i^{n+1}}{\Delta x},\quad n\in\mathbb{N}, i=1,\dots,I-1. \tag{6.6}$$

Periodic boundary conditions are taken into account by setting

$$\mathcal{D}_{1/2}^{n+1}=\mu\frac{u_1^{n+1}-u_I^{n+1}}{\Delta x}=\mathcal{D}_{I+1/2}^{n+1},\quad n\in\mathbb{N}, \tag{6.7}$$

with

$$\rho_{1/2}^{n+1}=\frac{\rho_1^{n+1}+\rho_I^{n+1}}{2}=\rho_{I+1/2}^{n+1},\quad n\in\mathbb{N}. \tag{6.8}$$

Note that in the case where the viscosity depends on the density, (6.5)-(6.6) involves the density at time t^{n+1} : since it has been already updated by (6.4) it can be used without any extra cost to update the velocity.

6.2.2 An explicit scheme on staggered grids

We describe now a scheme on staggered grids : the velocity variables are stored on the cells $C_{i+1/2}=[x_i,x_{i+1}]$, while discrete densities and pressures are stored on $C_i=[x_{i-1/2},x_{i+1/2}]$. The discrete mass conservation equation reads

$$\frac{\rho_i^{n+1}-\rho_i^n}{\Delta t}+\frac{\mathcal{F}_{i+1/2}^n-\mathcal{F}_{i-1/2}^n}{\Delta x}=0 \tag{6.9}$$

where the mass flux $\mathcal{F}_{i+1/2}^n$ is defined from the velocity $u_{i+1/2}^n$ known at the interface $x_{i+1/2}$. Several definitions of the mass fluxes have been introduced, for instance by using the UpWind flux based on the material velocity [14], an idea reminiscent of the AUSM scheme [23]. Here we use instead the mass fluxes proposed in [2] which are constructed by using the characteristic speeds of the hyperbolic system. Denoting $c=\sqrt{p'(\rho)}$ the sound speed, we set

$$\mathcal{F}_{i+1/2}^n=\mathcal{F}^+(\rho_i^n,c_{i+1/2}^n,u_{i+1/2}^n)+\mathcal{F}^-(\rho_{i+1}^n,c_{i+1/2}^n,u_{i+1/2}^n),$$

with

$$\mathcal{F}^+(\rho,c,u)=\begin{cases}0 & \text{if } u\le -c,\\ \frac{\rho}{4c}(u+c)^2 & \text{if } |u|\le -c,\\ \rho u & \text{if } u\ge c,\end{cases}\qquad \mathcal{F}^-(\rho,c,u)=\begin{cases}\rho u & \text{if } u\le -c,\\ -\frac{\rho}{4c}(u-c)^2 & \text{if } |u|\le -c,\\ 0 & \text{if } u\ge c,\end{cases}$$

and

$$c_{i+1/2}^n = \sqrt{p'(\rho_{i+1/2}^n)}, \qquad \rho_{i+1/2}^n = \frac{\rho_i^n + \rho_{i+1}^n}{2}.$$

We note that $\mathcal{F}^{\pm} \gtrless 0$; the definition relies on the upwinding principles, according to the sign of the characteristic speeds $u \pm c$. For the momentum equation, we set

$$\frac{\rho_{i+1/2}^{n+1} u_{i+1/2}^{n+1} - \rho_{i+1/2}^n u_{i+1/2}^n}{\Delta t} + \frac{1}{\Delta x}(\mathcal{G}_{i+1}^n - \mathcal{G}_i^n) + \frac{1}{\Delta x}(\Pi_{i+1}^{n+1/2} - \Pi_i^{n+1/2}) = \frac{\mathcal{D}_{i+1}^{n+1} - \mathcal{D}_i^{n+1}}{\Delta x}. \tag{6.10}$$

In (6.10), a natural choice for the discretization of the pressure term would be $\Pi_i^{n+1/2} = p(\rho_i^n)$. However, it turns out that the semi-implicit formula $\Pi_i^{n+1/2} = \rho_i^n \Phi'(\rho_i^{n+1}) - \Phi(\rho_i^n)$ where $\rho\Phi'(\rho) - \Phi(\rho) = p(\rho)$, is a better choice, motivated by the consistency analysis of the scheme [2]. The convection fluxes are defined by

$$\begin{aligned} \mathcal{G}_i^n \quad = \quad & \frac{u_{i-1/2}^n}{2}(\mathcal{F}^+(\rho_{i-1}^n, c_{i-1/2}^n, u_{i-1/2}^n) + \mathcal{F}^+(\rho_i^n, c_{i+1/2}^n, u_{i+1/2}^n)) \\ & + \frac{u_{i+1/2}^n}{2}(\mathcal{F}^-(\rho_i^n, c_{i-1/2}^n, u_{i-1/2}^n) + \mathcal{F}^-(\rho_{i+1}^n, c_{i+1/2}^n, u_{i+1/2}^n)), \end{aligned}$$

which, again, rely on upwinding principles. Finally, for the diffusion term, the definition is quite similar to (6.6)

$$\mathcal{D}_i^{n+1} = \mu \frac{u_{i+1/2}^{n+1} - u_{i-1/2}^{n+1}}{\Delta x}.$$

Relations (6.9) and (6.10) hold for $i = 1, ..., I$, imposing furthermore $\rho_{I+1}^n = \rho_1^n$, $u_{1/2}^n = u_{I+1/2}^n$, $\mathcal{D}_{I+1}^{n+1} = \mu \frac{u_{3/2}^{n+1} - u_{I+1/2}^{n+1}}{\Delta x} = \mathcal{D}_1^{n+1}$.

In the following, this scheme will be referred to as *Eulerian staggered scheme 1*.

6.2.3 A staggered pseudo-Lagrangian scheme

In this section we propose a pseudo-Lagrangian scheme. We use the term "pseudo-Lagangrian" because although it approximates the solution in the Euler variables, it strongly uses the conservation of the quantities in material volumes. In this scheme, the density unknowns at time t^n, ρ_j^n, are *inside* the cells $(x_{j-1/2}^n, x_{j+1/2}^n)$, which are time-dependent, and the velocity unknowns $u_{j+1/2}^n$ are associated with the boundaries of the cells, the $x_{j+1/2}^n$'s. The latter are advected at velocity $u_{j+1/2}^n$. The discretization of the mass equation corresponds to the discretization of the relation

$$\frac{d}{dt}\int_{x(t)}^{y(t)} \rho(t,x)\, dx = 0,$$

with $x(t)$ and $y(t)$ moving at the fluid velocity. It expresses that the mass in every cell is constant in time. Namely, we obtain

$$\begin{cases} x_{j+1/2}^{n+1} = x_{j+1/2}^{n} + \Delta t u_{j+1/2}^{n}, \quad n \in \mathbb{N}, j = 1, \dots, J, \\ x_{1/2}^{n+1} = x_{J+1/2}^{n+1} - 1 \quad n = -1, \dots, +\infty, \\ \Delta x_{j}^{n+1} = x_{j+1/2}^{n+1} - x_{j-1/2}^{n+1}, \quad n = -1, \dots, +\infty, j = 1, \dots, J, \\ \rho_{j}^{n+1} = \rho_{j}^{n} \Delta x_{j}^{n} / \Delta x_{j}^{n+1}, \quad n \in \mathbb{N}, j \in 1, \dots, J. \end{cases} \tag{6.11}$$

The second equation in (6.11) accounts for the periodicity of the problem.

We turn to the momentum equation $\partial_t(\rho u) + \partial_x(\rho u^2) = \partial_x(\mu \partial_x u - p)$, which is interpreted as

$$\frac{d}{dt} \int_{x(t)}^{y(t)} \rho(t,x) u(t,x)\, dx = \mu \partial_x u(t, y(t)) - p(t, y(t)) - (\mu \partial_x u(t, x(t)) - p(t, x(t))).$$

It is approximated by

$$\begin{cases} \rho_{j+1/2}^{n+1} u_{j+1/2}^{n+1} \Delta x_{j+1/2}^{n+1} = \rho_{j+1/2}^{n} u_{j+1/2}^{n} \Delta x_{j+1/2}^{n} \\ \qquad - (p_{j+1}^{n+1} - p_{j}^{n+1}) + \mu \left(\dfrac{u_{j+3/2}^{n+1} - u_{j+1/2}^{n+1}}{\Delta x_{j+1}^{n+1}} - \dfrac{u_{j+1/2}^{n+1} - u_{j-1/2}^{n+1}}{\Delta x_{j}^{n+1}} \right), \quad n \in \mathbb{N}, j = 1, \dots J, \\ u_{1/2}^{n+1} = u_{J+1/2}^{n+1}, \quad n \in \mathbb{N}, \\ u_{J+3/2}^{n+1} = u_{3/2}^{n+1}, \quad n \in \mathbb{N}, \\ p_{J+1}^{n+1} = p_{1}^{n+1}, \quad n \in \mathbb{N}, \\ \Delta x_{J+1}^{n+1} = \Delta x_{1}^{n+1}, \quad n \in \mathbb{N}, \end{cases} \tag{6.12}$$

where the last four equations stand for the periodicity. In these formulae, we use the quantities $\rho_{j+1/2}^{n+1}$, $\Delta x_{j+1/2}^{n+1}$ and p_j^{n+1} that were not defined previously : we choose for them the following rather natural definition :

$$\begin{cases} \Delta x_{j+1/2}^{n+1} = (\Delta x_{j}^{n+1} + \Delta x_{j+1}^{n+1})/2, \quad n = -1, \dots, +\infty, j = 1, \dots, J, \\ \rho_{j+1/2}^{n+1} \Delta x_{j+1/2}^{n+1} = (\rho_{j}^{n+1} \Delta x_{j}^{n+1} + \rho_{j+1}^{n+1} \Delta x_{j+1}^{n+1})/2, \quad n = -1, \dots, +\infty, j = 1, \dots, J, \\ p_{j}^{n+1} = p(\rho_{j}^{n+1}), \quad n = -1, \dots, +\infty, j = 1, \dots, J. \end{cases} \tag{6.13}$$

Complemented with initial conditions ρ_j^0, $u_{j+1/2}^0$, $x_{j+1/2}^0$, the scheme is defined. Note that we have chosen an implicit approximation for the diffusion, in order to avoid any parabolic stability condition (and indeed we *observe* the stability of the algorithm).

6.2.4 A last staggered scheme

In this section we propose another staggered scheme, that can be viewed as a Eulerian version of the preceding pseudo-Lagrangian one. Here the cells are fixed and, starting from the pseudo-Lagrangian scheme, we have to take the transport into account. With the same notations, but now the length Δx of the cells is constant, the mass conservation is replaced with

$$\rho_j^{n+1} = \rho_j^n - \frac{\Delta t}{\Delta x}\left(\rho^n_{j+1/2,U} u^n_{j+1/2} - \rho^n_{j-1/2,U} u^n_{j-1/2}\right), \quad n \in \mathbb{N}, j \in 1, \dots, J, \tag{6.14}$$

where $\rho^n_{j+1/2,U}$ is upwinded, that is to say that it is ρ^n_j if $u^n_{j+1/2} \geq 0$ and $\rho^n_{j+1/2}$ if $u^n_{j+1/2} < 0$.

The momentum equation is approximated by

$$\left\{\begin{array}{l} \rho^{n+1}_{j+1/2} u^{n+1}_{j+1/2} = \rho^n_{j+1/2} u^n_{j+1/2} - \dfrac{\Delta t}{2\Delta x}\left(\rho^{n+1}_{j+3/2} |u^n_{j+3/2}|^2 - \rho^{n+1}_{j-1/2} |u^n_{j-1/2}|^2\right) \\ \qquad - \dfrac{\Delta t}{\Delta x}(p^{n+1}_{j+1} - p^{n+1}_j) + \mu \dfrac{\Delta t}{\Delta x^2}\left(u^{n+1}_{j+3/2} - 2u^{n+1}_{j+1/2} + u^{n+1}_{j-1/2}\right), \quad n \in \mathbb{N}, j = 1, \dots J, \\ u^{n+1}_{1/2} = u^{n+1}_{J+1/2}, \quad n \in \mathbb{N}, \\ u^{n+1}_{J+3/2} = u^{n+1}_{3/2}, \quad n \in \mathbb{N}, \\ p^{n+1}_{J+1} = p^{n+1}_1, \quad n \in \mathbb{N}, \\ \Delta x^{n+1}_{J+1} = \Delta x^{n+1}_1, \quad n \in \mathbb{N}, \end{array}\right. \tag{6.15}$$

where the last four equations stand for the periodicity. In these formulae, we use the quantities $\rho^{n+1}_{j+1/2}$ and p^{n+1}_j that were not defined previously : we choose for them the following rather natural definition :

$$\left\{\begin{array}{l} \rho^{n+1}_{j+1/2} = (\rho^{n+1}_j + \rho^{n+1}_{j+1})/2, \quad n = -1, \dots, +\infty, j = 1, \dots, J, \\ p^{n+1}_j = p(\rho^{n+1}_j), \quad n = -1, \dots, +\infty, j = 1, \dots, J. \end{array}\right. \tag{6.16}$$

Complemented with initial conditions ρ^0_j, $u^0_{j+1/2}$, $x^0_{j+1/2}$, the scheme is defined. Note that we have chosen an implicit approximation for the diffusion, in order to avoid any parabolic stability condition (and indeed we *observe* the stability of the algorithm). The convection term in the momentum equation is centered, but for fixed (not too small) viscosity coefficient, this does not make instabilities appear.

In the following, this scheme will be referred to as *Eulerian staggered scheme 2*.

6.3 Convergence analysis *à la* Lax-Wendroff

In this section, we investigate the convergence of the Rusanov scheme. For the sake of simplicity, we restrict the analysis to the case of uniform meshes : all cells have the same length.

We consider a sequence of meshes, parametrized by $k \in \mathbb{N}$, such that Δx_k and Δt_k both tend to 0, with $\frac{\Delta x_k}{\Delta t_k} = \lambda$ for some $\lambda > 0$ to ensure some stability property, for instance the positivity of the density.

The discrete initial data are given by

$$\rho_j^0 = \frac{1}{\Delta x_k} \int_{x_{j-1/2}}^{x_{j+1/2}} \rho^0(x)\, dx, \qquad u_j^0 = \frac{1}{\Delta x_k} \int_{x_{j-1/2}}^{x_{j+1/2}} u^0(x)\, dx \text{ for all } j \in \{1, ..., I\}.$$

The discrete approximation of ρ and u are denoted by

$$\rho_k(t,x) = \sum_{n=0}^{N-1} \sum_{j=1}^{I} \rho_j^n \mathbb{1}_{[t^n, t^{n+1})}(t) \mathbb{1}_{[x_{j-1/2}, x_{j+1/2})}(x),$$
$$u_k(t,x) = \sum_{n=0}^{N-1} \sum_{j=1}^{I} u_j^n \mathbb{1}_{[t^n, t^{n+1})}(t) \mathbb{1}_{[x_{j-1/2}, x_{j+1/2})}(x).$$

We bear in mind that ρ_j^n and u_j^n also depend on k but this dependency is omitted to simplify the notation. The following statement is in the same spirit as the standard Lax-Wendroff theorem for conservation laws, see [21, Section 12.10].

Theorem 6.3.1. *Suppose that*

— *there exists a constant* $C_\infty > 0$ *such that*

$$\sup_k \left(\|u_k\|_{L^\infty((0,T)\times(0,1))} + \|\rho_k\|_{L^\infty((0,T)\times(0,1))} \right) \leq C_\infty.$$

— *there exists* $(\rho, u) \in L^\infty((0,T) \times (0,1))^2$ *such that* (ρ_k, u_k) *converges to* (ρ, u) *in* $L^r((0,T) \times (0,1))^2$ *for any* $1 \leq r < +\infty$.

Then the pair (u, ρ) *is a weak solution of* (6.1).

Remark 6.3.2. *The statement remains true when* $\mu(\rho) = C\rho$ *at the price of assuming*

$$u \in L^r(0,T; W^{1,r}(0,1))$$

and

$$\frac{u_k(t, x + \Delta x_k) - u_k(t,x)}{\Delta x_k} \rightharpoonup \nabla u(t,x) \text{ weakly in } L^r((0,T) \times (0,1)).$$

It equally applies for a continuous function μ*, with the additional assumptions that the convergence of* (ρ_k, u_k) *to* (ρ, u) *holds almost everywhere.*

Proof. Consider a test function $\zeta = (\varphi, \chi) \in \mathcal{C}_0^\infty([0,T) \times (0,1); \mathbb{R}^2)$. We assume that Δt_k and Δx_k are small enough so that $\mathrm{supp}(\zeta) \subset [0, T - \Delta t_k) \times (2\Delta x_k, 1 - 2\Delta x_k)$. For $n \in \{0, ..., N-1\}$ and $j \in \{1, ..., I\}$, let us denote $\zeta_j^n = \zeta(t^n, x_j)$, and, for all $t \in (0,T)$, $x \in (0,1)$,

$$\zeta_{\Delta t_k, \Delta x_k}(t,x) = \sum_{n=0}^{N-1} \sum_{j=1}^{I} \zeta_j^n \mathbb{1}_{[t^n, t^{n+1})}(t) \mathbb{1}_{[x_{j-1/2}, x_{j+1/2})}(x), \qquad \zeta_k = \zeta_{\Delta t_k, \Delta x_k}.$$

We multiply the discrete mass conservation equation by $\Delta x_k \Delta t_k\, \varphi_j^n$, and we sum over j and n. We obtain

$$\Delta x_k \sum_{n=0}^{N-1}\sum_{j=1}^{I}(\rho_j^{n+1}-\rho_j^n)\varphi_j^n + \Delta t_k \sum_{n=0}^{N-1}\sum_{j=1}^{I}\Big[[\mathcal{F}_{j+1/2}^n]_1 - [\mathcal{F}_{j-1/2}^n]_1\Big]\,\varphi_j^n = 0.$$

The first term on the left hand side recasts as

$$\Delta x_k \sum_{n=0}^{N-2}\sum_{j=1}^{I}\rho_j^{n+1}(\varphi_j^n-\varphi_j^{n+1}) + \Delta x_k \underbrace{\sum_{j=1}^{I}\rho_j^N\varphi_j^N}_{=0} - \Delta x_k \sum_{j=1}^{I}\rho_j^0\varphi_j^0,$$

while the second term becomes

$$\Delta t_k \sum_{n=0}^{N-1}\sum_{j=1}^{I-1}[\mathcal{F}_{j+1/2}^n]_1(\varphi_j^n-\varphi_{j+1}^n) + \underbrace{\Delta t_k \sum_{n=0}^{N-1}[\mathcal{F}_{I+1/2}^n]_1\varphi_I^n - \Delta t_k \sum_{n=0}^{N-1}[\mathcal{F}_{1/2}^n]_1\varphi_{1/2}^n}_{=0}.$$

Hence we get

$$\Delta x_k \sum_{n=0}^{N-2}\sum_{j=1}^{I}\rho_j^{n+1}(\varphi_j^n-\varphi_j^{n+1}) + \Delta t_k \sum_{n=0}^{N-1}\sum_{j=1}^{I-1}[\mathcal{F}_{j+1/2}^n]_1(\varphi_j^n-\varphi_{j+1}^n) = \Delta x_k \sum_{j=1}^{I}\rho_j^0\varphi_j^0. \quad (6.17)$$

Using (6.3), the estimates and convergence assumed for (ρ_k, u_k), we obtain as $k\to\infty$

$$\begin{aligned}
&\Delta x_k \sum_{n=0}^{N-2}\sum_{j=1}^{I}\rho_j^{n+1}(\varphi_j^n-\varphi_j^{n+1}) \to \int_0^T\int_0^1 \rho\partial_t\varphi\,dx\,dt,\\
&\Delta t_k \sum_{n=0}^{N-1}\sum_{j=1}^{J-1}[F_{j+1/2}^n]_1(\varphi_j^n-\varphi_{j+1}^n) \to \int_0^T\int_0^1 \rho u\partial_x\varphi\,dx\,dt, \qquad (6.18)\\
&\Delta x_k \sum_{j=1}^{I}\rho_j^0\varphi_j^0 \to \int_0^1 \rho^0(x)\varphi(0,x)\,dx.
\end{aligned}$$

We turn to the momentum equation (6.5). Proceeding similarly, we obtain

$$\Delta x_k \sum_{n=0}^{N-1}\sum_{j=1}^{I}(\rho_j^{n+1}u_j^{n+1}-\rho_j^n u_j^n)\chi_j^n + \Delta t_k \sum_{n=0}^{N-1}\sum_{j=1}^{I}\Big[[\mathcal{F}_{j+1/2}^n]_2 - [\mathcal{F}_{j-1/2}^n]_2\Big]\,\chi_j^n$$

$$-\Delta t_k \sum_{n=0}^{N-1}\sum_{j=1}^{I}\left[\mu(\rho_{j+1/2}^{n+1})\frac{u_{j+1}^{n+1}-u_j^{n+1}}{\Delta x_k} - \mu(\rho_{j-1/2}^{n+1})\frac{u_j^{n+1}-u_{j-1}^{n+1}}{\Delta x_k}\right]\chi_j^n = 0.$$

The first two sums can be written as

$$\Delta x_k \sum_{n=0}^{N-2}\sum_{j=1}^{I-1}\rho_j^{n+1}u_j^{n+1}(\chi_j^n-\chi_j^{n+1}) + \Delta t_k \sum_{n=0}^{N-1}\sum_{j=1}^{I-1}[\mathcal{F}_{j+1}^n]_2(\chi_j^n-\chi_{j+1}^n),$$

which can be treated as for the mass conservation equation, by using that the product $\rho_k u_k$ still converges in $L^r((0,T)\times(0,1))$ for $1 \leq r < +\infty$. Let us study the viscous term

$$\Delta t_k \sum_{n=0}^{N-1}\sum_{j=1}^{I}\left[\mu(\rho_{j+1/2}^{n+1})\frac{u_{j+1}^{n+1}-u_j^{n+1}}{\Delta x_k} - \mu(\rho_{j-1/2}^{n+1})\frac{u_j^{n+1}-u_{j-1}^{n+1}}{\Delta x_k}\right]\chi_j^n. \tag{6.19}$$

The case where the viscosity μ is constant can be handled by using two summations by parts, which allow us to write (6.19) as

$$\Delta t_k \sum_{n=0}^{N-1}\sum_{j=2}^{I-1} u_j^{n+1}\frac{\chi_{j+1}^n - 2\chi_j^n + \chi_{j-1}^n}{\Delta x_k}.$$

This can be cast as

$$\int_0^{T-\Delta t_k}\int_{2\Delta x_k}^{1-2\Delta x_k} u_k(t+\Delta t_k,x)\frac{\chi_k(t,x+\Delta x_k)-2\chi_k(t,x)+\chi_k(t,x-\Delta x_k)}{\Delta x_k^2}\,dx\,dt,$$

and using the uniform convergence of χ_k and its derivatives, together with the convergence in L^r of u_k, we are able to pass to the limit : as $k\to\infty$, we obtain

$$\int_0^T\int_0^1 u(t,x)\partial_{xx}^2\chi(t,x)\,dx\,dt.$$

which completes the proof in the case of constant viscosity.

When μ depends on the density, we cannot proceed this way, and we need further assumptions. We start by writing (6.19) as

$$\begin{aligned}
&\Delta t_k \sum_{n=0}^{N-1}\sum_{j=1}^{I}\left[\mu(\rho_{j+1/2}^{n+1})\frac{u_{j+1}^{n+1}-u_j^{n+1}}{\Delta x_k} - \mu(\rho_{j-1/2}^{n+1})\frac{u_j^{n+1}-u_{j-1}^{n+1}}{\Delta x_k}\right]\chi_j^n \\
&= \int_{\Delta t_k}^T\int_0^1 \mu\left(\frac{\rho_k(t,x_k+\Delta x_k)+\rho_k(t,x)}{2}\right)\frac{u_k(t,x+\Delta x_k)-u_k(t,x)}{\Delta x_k} \\
&\qquad\times\frac{\chi_k(t-\Delta t_k,x)-\chi_k(t-\Delta t,x+\Delta x_k)}{\Delta x_k}\,dx\,dt.
\end{aligned} \tag{6.20}$$

To pass to the limit in the previous term we use a weak-strong convergence argument observing that

$$\begin{aligned}
&\mu\left(\frac{\rho_k(t,x_k+\Delta x_k)+\rho_k(t,x)}{2}\right)\frac{\chi_k(t-\Delta t_k,x)-\chi_k(t-\Delta t_k,x+\Delta x_k)}{\Delta x_k} \\
&\qquad\xrightarrow[k\to\infty]{} \mu(\rho(t,x))\partial_x\chi(t,x) \text{ in } L^{r'}((0,T)\times(0,1)).
\end{aligned}$$

This combines to the assumption that ∇u_k converges weakly in $L^r((0,T)\times(0,1))$ so that (6.20) tends to

$$\int_0^T\int_0^1 \mu(\rho(t,x))\partial_x u(t,x)\,\partial_x\chi(t,x)\,dx\,dt,$$

which concludes the proof.

6.4 Numerical results

Here, we present some numerical results that illustrate the behavior of the proposed schemes.

6.4.1 Comparisons

In this subsection, we compare the results obtained with the 4 different schemes that are dealt with in the chapter. The results here are obtained at time $t = 0.1$ with $\mu = 0.1$ for the initial condition $u^0(x) = 0$ and $\rho^0(x) = 0.125 + 1.875\chi_{[1/4,3/4]}(x)$.

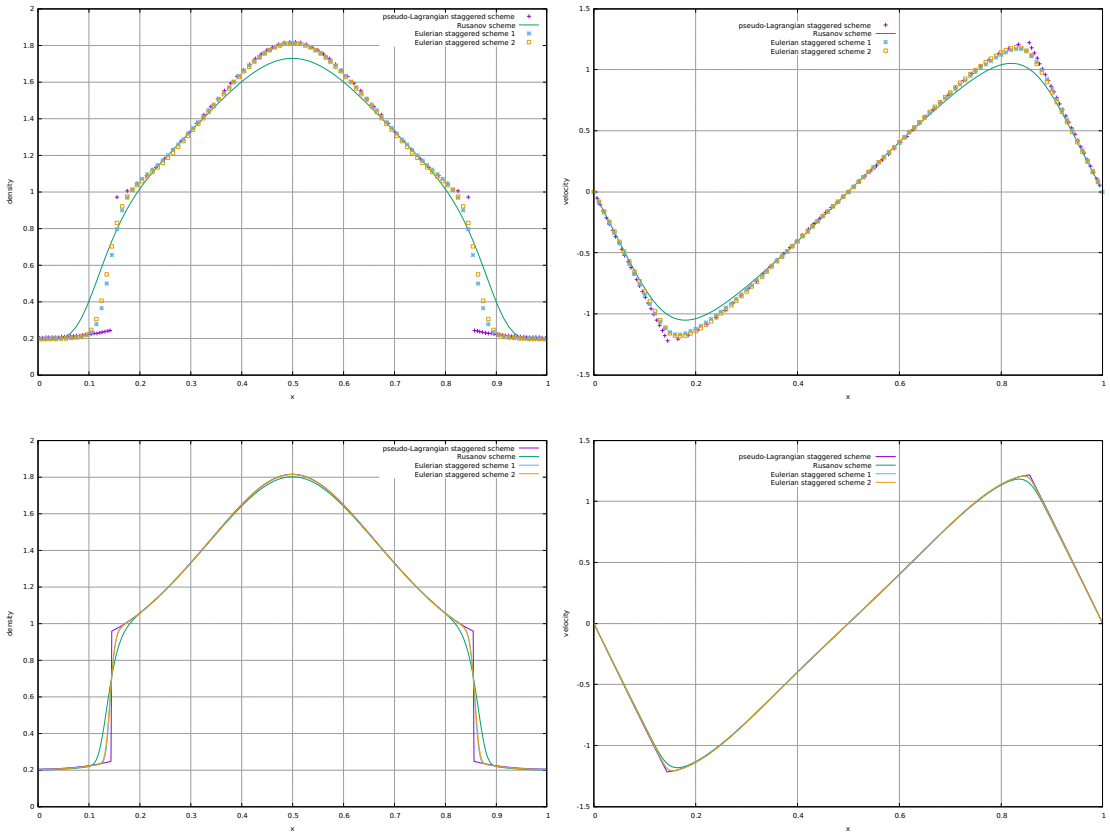

FIGURE 6.1 – Density and velocity solutions at time 0.1, with 100 cells (top) and 800 cells (bottom).

We see that the four schemes seem to converge to the same solution, and that the pseudo-Lagrange scheme is less diffusive (the scheme based on the Rusanov flux is the most diffusive). In particular, the pseudo-Lagrange scheme is able to maintain some discontinuities in the density and in the velocity derivative.

For the same test-case, we now more precisely compare these four schemes, in the velocity variable. In Table 6.1 we compare, for different numbers of cells, the non-diffusive pseudo-Lagrangian scheme from Section 6.2.3 and the Eulerian Rusanov scheme from Section 6.2.1. The difference between these schemes seems to be of order $1/2$, both in the L^1 and in the L^∞ norms. Note that the schemes are subject to some hyperbolic-typed Courant-Friedrichs-Lewy conditions, so that the time step is of the same order as the space step. Note also that to compare the solutions, as they are not obtained on the same meshes (the pseudo-Lagrange scheme is running on a moving mesh), we interpolate the difference of the two solutions on a mesh that is the intersection of the two and consider both solutions as constant-by-cell. In Table 6.2 we compare the pseudo-Lagrange and the Eulerian staggered scheme 1 presented in Section 6.2.2. In Table 6.4 we compare the pseudo-Lagrange and the Eulerian staggered scheme 2 form Section 6.2.4. We observe the same order of convergence.

Number of cells J	Difference in L^1 norm	Difference in L^∞ norm
100	0.734125	0.247230
200	0.038315	0.171206
400	0.019801	0.110994
800	0.010399	0.077385
1600	0.005710	0.052437
3200	0.003376	0.037031
6400	0.002201	0.251310
12800	0.001535	0.017738
25600	0.001090	0.012551

TABLE 6.1 – Difference between the pseudo-Lagrange scheme and the Rusanov scheme.

Number of cells J	Difference in L^1 norm	Difference in L^∞ norm
100	0.031244	0.116505
200	0.015694	0.076648
400	0.007999	0.048226
800	0.004164	0.033637
1600	0.002299	0.022405
3200	0.001393	0.015951
6400	0.000913	0.010339
12800	0.000629	0.007328
25600	0.000445	0.005201

TABLE 6.2 – Difference between the Pseudo-Lagrange scheme and the Euler staggered scheme 1.

Number of cells J	Difference in L^1 norm	Difference in L^∞ norm
100	0.022931	0.109549
200	0.012467	0.062358
400	0.007078	0.048725
800	0.004213	0.030653
1600	0.002638	0.023727
3200	0.001723	0.016027
6400	0.001159	0.011299
12800	0.000793	0.008065
25600	0.000549	0.005608

TABLE 6.3 – Difference between the Pseudo-Lagrange scheme and the Euler staggered scheme 2.

6.4.2 Behavior of the pseudo-Lagrange scheme on Hoff-type discontinuous solutions

In this section, we would like to illustrate a very interesting property of discontinuous solutions *à la* Hoff. These solutions, among which one finds the one illustrated in the previous section, have been studied by Hoff (see [15]). They consist in solutions with discontinuities in density, and thus in pressure and in the derivative of the velocity (because the effective flux $p-\mu\partial_x u$ is continuous in

space for almost every time). In [15] it is shown that the amplitude of the jump in $\log(\rho)$ decreases exponentially in time, with a rate that is at least some constant over the viscosity coefficient μ. We do not precise the result here because the constant depends on the maximum value of the density in the flow, and because actually the context of [15] is a bit different : it considers the Navier-Stokes system in Lagrange variables with a space variable ranging over $\mathbb{R}$, with a single discontinuity, while here we consider the Navier-Stokes system on the torus. We propose to analyse numerically the behavior of the jump of $\log(\rho)$. This is made possible thanks to the use of a pseudo-Lagrange scheme that does not smooth the discontinuity in ρ artificially. With the same initial condition as in the previous section, Figure 6.2 presents the amplitude of the jump in $\log(\rho)$ with respect to time, with 500 cells in space. We also present its best approximation as $\exp(a+bt)$ by computing a and b by the least square method. Note that it is not relevant to do this on a too large time interval (with a given cell size), because the amplitude of the jump decays exponentially fast and it rapidly becomes of the same order as the cell size so that it cannot be distinguished from the natural steps of the discrete solution in regular regions.

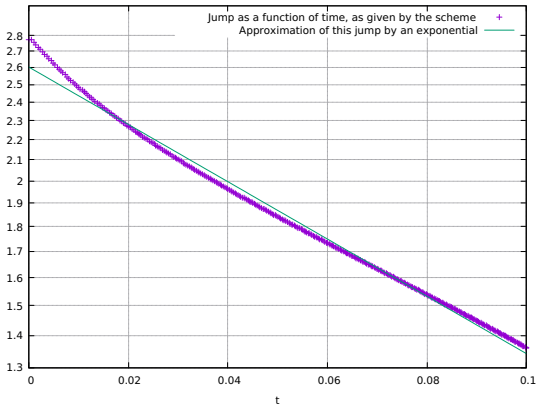

FIGURE 6.2 – Jump of the quantity $\log(\rho)$ as a function of time.

Now we want to evaluate the rate at which the jump decreases as a function of the viscosity coefficient. Table 6.4 provides the coefficient b computed by the least square method, for various values of μ.

Viscosity coefficient μ	Rate
0.1	-6.62
0.05	-11.05
0.025	-22.17
0.0125	-54.04
0.0675	-105.14

TABLE 6.4 – Rate for the (decreasing) amplitude of the jump of the logarithm of ρ.

We note in Table 6.4 that the jump $[\log(\rho)]$ (with usual notations for the jump of a quantity) seems to behave as $\exp(-Ct/\mu)$, which is exactly the majoration proved in [15]. Note that this is a very interesting phenomenon : as μ tends to 0, this kind of discontinuities do not persist at all (they disappear at time $t = 0^+$), what is a paradox, as for compressible inviscid gases discontinuities are expected (and they are called shocks). This result by Hoff thus proves that the shocks in inviscid gases are limits of smooth parts in the solutions of viscous gases, in which the amplitude of discontinuities tends to 0.

Bibliographie

[1] F. Berthelin, T. Goudon, and S. Minjeaud. Consistency analysis of a 1D finite volume scheme for barotropic Euler models. In J. Fuhrmann, M. Ohlberger, and C. Rohde, editors, *Finite Volumes for Complex Applications VII ; Methods, Theoretical Aspects, and Elliptic, Parabolic and Hyperbolic Problems, Berlin*, volume 77 and 78 of *Springer Proceedings in Mathematics & Statistics*, pages 97–106. Springer, 2014.

[2] F. Berthelin, T. Goudon, and S. Minjeaud. Kinetic schemes on staggered grids for barotropic Euler models : entropy-stability analysis. *Math. Comput.*, 84 :2221–2262, 2015.

[3] F. Berthelin, T. Goudon, and S. Minjeaud. Multifluid flows : a kinetic approach. *J. Sci. Comput.*, 66(2) :792–824, 2016.

[4] D. Bresch and P. E. Jabin. Global existence of weak solutions for compressible Navier-Stokes equations : thermodynamically unstable pressure and anisotropic viscous stress tensor. *Ann. Math.*, 188(2) :577–684, 2018.

[5] D. Bresch, A. Vasseur, and C. Yu. Global existence of entropy-weak solutions to the compressible Navier-Stokes equations with non-linear density dependent viscosities. Technical report, Univ. Texas Austin, 2019.

[6] G.-Q. Chen, D. Hoff, and K. Trivisa. Global solutions of the compressible Navier-Stokes equations with large discontinuous initial data. *Comm. Partial Differential Equations*, 25 :2233–2257, 2000.

[7] E. Feireisl. *Dynamics of viscous compressible fluids*, volume 26 of *Oxford Lecture Series in Mathematics and its Applications*. Oxford University Press, Oxford, 2004.

[8] T. Gallouët, R. Herbin, and J.-C. Latché. Kinetic energy control in explicit finite volume discretizations of the incompressible and compressible Navier-Stokes equations. *Int. J. Finite Vol.*, 7(2) :6, 2010.

[9] T. Gallouet, R. Herbin, D. Maltese, and A. Novotny. Error estimates for a numerical approximation to the compressible barotropic Navier-Stokes equations. *IMA J. Numer. Anal.*, 36(2) :543–592, 2016.

[10] L. Gastaldo, R. Herbin, W. Kheriji, C. Lapuerta, and J.-C. Latché. Staggered discretizations, pressure correction schemes and all speed barotropic flows. In *Finite Volumes for Complex*

Applications VI, Problems and Perspectives, Prague, Czech Republic, volume 4, pages 839–855, 2011.

[11] D. Gilbarg. The existence and limit behavior of the one-dimensional shock layer. *Amer. J. Math.*, 73 :256–274, 1951.

[12] T. Goudon, J. Llobell, and S. Minjeaud. An explicit MUSCL scheme on staggered grids with kinetic–like fluxes for the barotropic and full Euler system. *Comm. Comput. Phys.*, 2020. To appear.

[13] R. Herbin, W. Kheriji, and J.-C. Latché. Staggered schemes for all speed flows. *ESAIM :Proc*, 35 :122–150, 2012. Actes du Congrès National de Mathématiques Appliquées et Industrielles.

[14] R. Herbin, J.-C. Latché, and T. T. Nguyen. Explicit staggered schemes for the compressible Euler equations. In *Applied mathematics in Savoie—AMIS 2012 : Multiphase flow in industrial and environmental engineering*, volume 40 of *ESAIM Proc.*, pages 83–102. EDP Sci., Les Ulis, 2013.

[15] D. Hoff. Global existence for 1D, compressible, isentropic Navier-Stokes equations with large initial data. *Trans. Amer. Math. Soc.*, 303(1) :169–181, 1987.

[16] D. Hoff and T.-P. Liu. The inviscid limit for the Navier-Stokes equations of compressible, isentropic flow with shock data. *Indiana Univ. Math. J.*, 38(4) :861–915, 1989.

[17] D. Hoff and J. Smoller. Solutions in the large for certain nonlinear parabolic systems. *Ann. Inst. Henri Poincaré, Anal. Non lin.*, 2 :213–235, 1985.

[18] T. K. Karper. Convergent finite differences for 1D viscous isentropic flow in Eulerian coordinates. *Disc. Cont. Dyn. Syst.- S*, 7(5) :993–1023, 2014.

[19] A. V. Kazhikhov and V. V. Shelukhin. Unique global solution with respect to time of initial-boundary value problems for one-dimensional equations of a viscous gas. *Prikl. Mat. Meh.*, 41 :282–291, 1977.

[20] W. Kheriji, R. Herbin, and J.-C. Latché. Pressure correction staggered schemes for barotropic one-phase and two-phase flows. *Comput. & Fluids*, 88 :524 – 542, 2013.

[21] R. J. Leveque. *Finite Volume Methods for Hyperbolic Problems*. Cambridge Texts in Appl. Math. Cambridge Univ. Press, 2004.

[22] P.-L. Lions. *Mathematical topics in fluid mechanics. Vol. 2 : Compressible models*, volume 10 of *Oxford Lecture Series in Mathematics and its Applications*. The Clarendon Press, Oxford University Press, New York, 1998. Compressible models, Oxford Science Publications.

[23] M.-S. Liou and C. J. Steffen Jr. A new flux splitting scheme. *J. Comput. Phys.*, 107 :23–39, 1993.

[24] J. Llobell. *Schémas Volumes Finis à mailles décalées pour la dynamique des gaz*. PhD thesis, Université Côte d'Azur, 2018.

[25] A. Mellet and A. Vasseur. On the barotropic compressible Navier-Stokes equations. *Comm. PDE*, 32(3) :431–452, 2007.

[26] D. Serre. *Matrices : theory and applications*, volume 216 of *Graduate Texts in Math.* Springer, 2002.

[27] A. Vasseur and C. Yu. Existence of global weak solutions for 3D degenerate compressible Navier-Stokes equations. *Invent. Math.*, 206(3) :935–974, 2016.